CR 112176

TR - 3720289

Viking '75 Project

BALLOON LAUNCHED DECELERATOR TEST PROGRAM

POST-FLIGHT TEST REPORT

BLDT VEHICLE AV-1

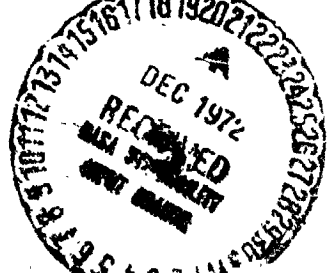

NAS1-9000

MARTIN MARIETTA

ABSTRACT

Four BLDT flights were conducted during the summer of 1972 over the White Sands Missile Range. The purpose of these tests was to qualify the Viking disk-gap band parachute system behind a full-scale simulator of the Viking Entry Vehicle over the maximum range of entry conditions anticipated in the Viking '75 soft landing on Mars. Test concerns centered on the ability of a minimum weight parachute system to operate without structural damage in the turbulent wake of the blunt-body entry vehicle (140°, 11.5' diameter cone). This is the first known instance of parachute operation at supersonic speeds in the wake of such a large blunt body. The flight tests utilized the largest successful balloon-payload weight combination known to get to high altitude (120kft) where rocket engines were employed to boost the test vehicle to supersonic speeds and dynamic pressures simulating the range of conditions on Mars.

This report presents the results of the first test in the series where the test conditions were the most severe expected at Mars; Mach number of 2.0 and dynamic pressure of 1.25 psf. The report also contains appendices describing the test vehicle, parachute performance analysis, and parachute dimensional description. The parachute sustained some fabric damage because test design load conditions were 60 percent rather than 23 percent greater than the design values. Parachute performance, however, was still adequate to permit the performance of a soft landing on mars. A retest successfully demonstrated prachute integrity at design load.

TR-3720289

11 September 1972

DRL Line Item No.: N3-T040

BALLOON LAUNCHED DECELERATOR TEST PROGRAM POST-TEST TEST REPORT

(45 day)

BLDT VEHICLE AV-1

prepared by:

D. Dickinson

J. Schlemmer

F. Hicks

F. Michel

R. D. Moog

PREPARED UNDER CONTACT NAS1-9000 by
MARTIN MARIETTA CORPORATION
DENVER DIVISION
P.O. Box 179
DENVER, COLORADO 80201

APPROVAL SHEET

R. J. Folutchko

Robert J. Folutchko
Project Engineer
Viking Vehicle Engineering

9/29/72
Date

R. J. Folutchko for

P. Donohue
Program Manager
BLDT Program

9/29/72
Date

TABLE OF CONTENTS

LIST OF ILLUSTRATIONS

LIST OF ILLUSTRATIONS (CONTINUED)

LIST OF ILLUSTRATIONS (CONTINUED)

LIST OF TABLES

I. PURPOSE OF REPORT

The purpose of this report is to document the pertinent events concerned with the launch, float and flight of Balloon Launched Decelerator Test Vehicle AV-1 and the performance of the Decelerator System installed therein. The report will describe and provide data pertinent to the flight trajectory and decelerator test points at the time of decelerator deployment as well as a description of the time history of vehicle events and anomalies encountered during the mission.

The final test reports for BLDT Vehicles AV-2, AV-3 and AV-4 are contained in the following MMC documents:

AV-2 - Document number TR-3720291

AV-3 - Document number TR-3720293

AV-4 - Document number TR-3720295

II. MISSION OBJECTIVES

The prime objective of the BLDT Vehicle AV-1 was to provide flight conditions such that satisfactory operation and performance of the full-scale Viking Decelerator System can be qualified in a simulated Mars environment and in the wake of a blunt body. The flight conditions as described in paragraph 3.3 of "Parachute Test Objectives and Requirements Document for BLDT Program", (RD-3720247) are:

Angle of Attack at Mortar Fire	$\leq 17^{\circ}$
Residual Spin Rate	$\leq 100^{\circ}$/sec
Parachute Temperature at Mortar Fire	$\leq 80^{\circ}$F
Mach Number/"q" Conditions - See Figure II-1	

It was a goal of this mission to separate the vehicle aeroshell following decelerator deployment in order to obtain a time/distance history of the separation function.

A description of the BLDT vehicle, which served as the qualification test bed, is included in Appendix A of this report. A description of the BLDT mission is provided in Appendix B.

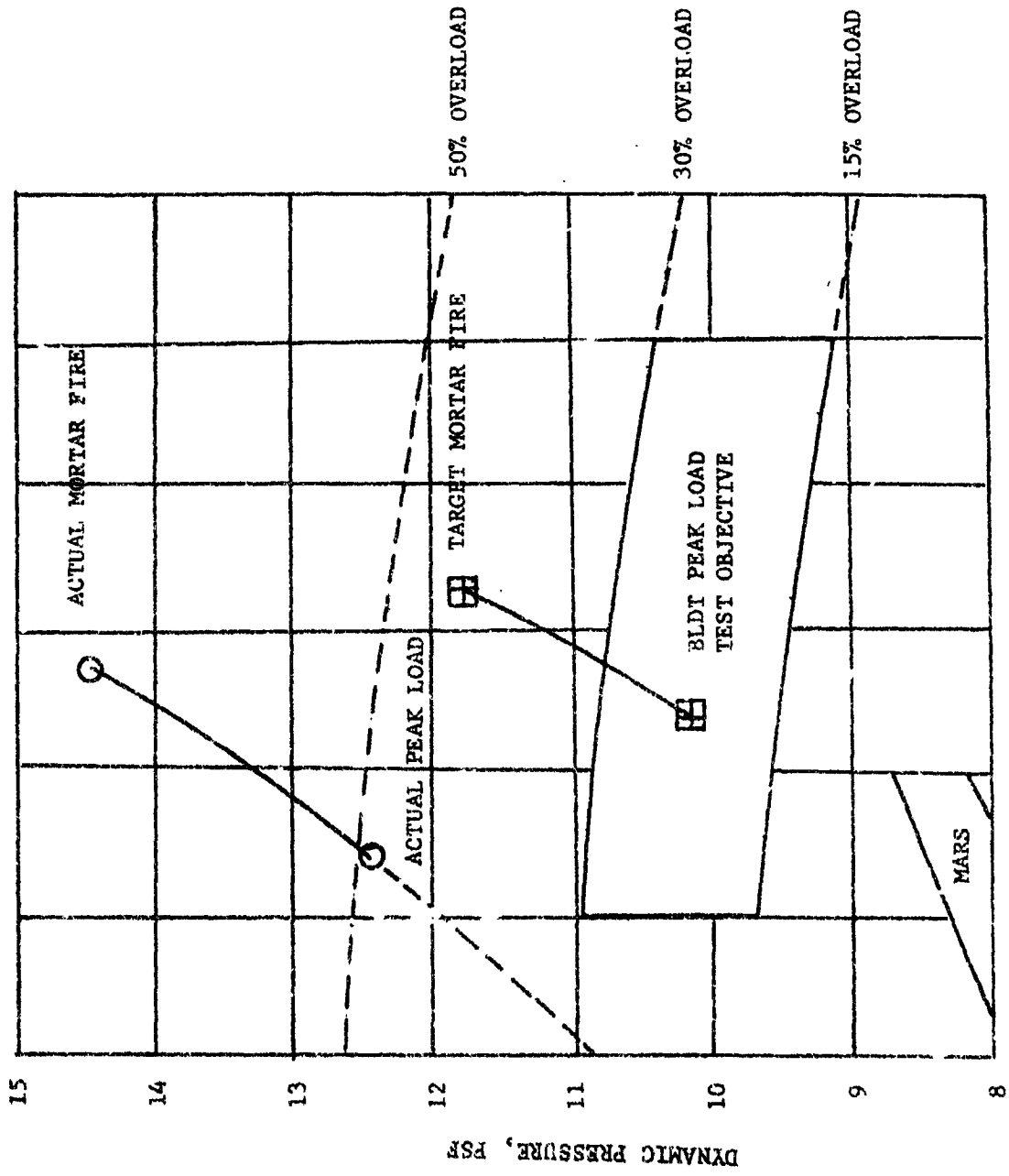

BLDT AV-1 TEST CONDITIONS

FIGURE II-1

III. DECELERATOR QUALIFICATION SUMMARY

The following is a summary of program events, pertinent to the decelerator system, occurring from the time of decelerator system installation in the BLDT vehicle through the recovery of the decelerator system at the point of payload impact.

A. Operations Summary

The decelerator system was installed in the base cover of vehicle AV-1 prior to final vehicle assembly for Flight Readiness Test. The system was Martin Marietta Corporation Serial Number 0000072 (GAC System S/N 12) with a system weight of 126.55# and an ejected pack weight of 90.1#.

During vehicle stand time while awaiting satisfactory meteorological conditions for launch, conditioned air was applied to the vehicle in order to maintain the vehicle interior, including the decelerator cannister, at a temperature below 80°F.

The decelerator system was subject to cooling during the ascent and float phases of the mission with pertinent decelerator temperatures just prior to release from the load bar as follows:

Sensor Location	Spec. Req'd (°F)	Actual Temp (°F)	
*Bridle #1	+210 to -90	+35	
*Bridle #2	+210 to -90	+40	
*Bridle #3	+210 to -90	+38	
Mortar Cannister #1	+80 (No Min)	+50	
Mortar Cannister #2	+80 (No Min)	+50	
Mortar Breach	+175 to +25	+50	(Automatic heater controlled)
Mortar Breach Flange	+74 to +25	+50	

*Temperature measured on the base cover interior beneath the bridle leg.

B. Vehicle Performance

The AV-1 vehicle performed normally and provided all anticipated functions with the exception that the vehicle did not attain the correct test altitude at mortar fire because of low float altitude when the vehicle was released from the load bar and decreased pitch attitude at drop due to vehicle damage sustained during launch. The damage to the aeroshell did not appear to effect the performance of the vehicle and the vehicle wake characteristics were a valid simulation of the Viking Lander Capsule. The mortar fire command, generated by the onboard programmers occurred at a dynamic pressure in excess of the required dynamic pressure (See Figure II-1) due to the low test altitude. The mortar fire conditions were:

	TARGET	ACTUAL
Mach Number	2.23	2.18
Dynamic Pressure (PSF)	11.8	14.63
Residual Spin Rate (Deg/Sec)	± 100	-28
Angle of Attack (Deg)	17	-13

During the flight of AV-1, it was anticipated that the solid rocket motors could create a heating condition on the base cover and bridle legs requiring thermal control. The base cover and bridle legs were protected with passive thermal control materials. The recovered base cover provided no evidence of base heating which would have been detrimental to the bridle legs.

C. Decelerator System Summary

Due to the previously discussed off test conditions, the parachute canopy sustained damage (described below) but despite the damage, the

parachute maintained structural integrity and produced sufficient drag and stability for a successful Mars Mission. Parachute drag was slightly less than nominal but within the acceptable range at terminal conditions. Supersonic drag was higher than anticipated when compared with wind tunnel test results.

Mortar performance was nominal and adequate despite the test dynamic pressure being 23% over the target dynamic pressure.

Parachute inflation time was normal and as a result of the canopy damage, the opening load was lower than expected. The parachute opening transient produced vehicle attitude rates as high as 148 degrees/second initially, which damped to less than 75 degrees/second in 10 seconds. The maximum rates were anticipated due to the degree of overtest compared with Mars conditions, but the damping characteristics of the parachute do not appear to be as good as expected.

Early in the inflation cycle, the parachute canopy sustained radial tears from the vent to the edge of the disk in two gore panels (See Appendix C - GAC Post-Test Failure Analysis). Analysis of the nature of the tears and the fact that the tears occurred much before peak canopy loading leads to the conclusion that the failed panels sustained frictional damage as the parachute emerged from the bag. The areas of frictional damage were then exposed to localized high pressure during an unsymmetrical canopy inflation which caused the damage to propagate.

Aeroshell separation was successfully demonstrated at a dynamic pressure of 2.39 psf and a Mach Number of 0.91. The separation distance of 197 feet in 3 seconds more than adequately fulfills the minimum system requirement of 50 feet in 3 seconds.

IV. MISSION OPERATION

The following is a description of the program events occurring from the time of vehicle Flight Readiness Test through Recovery Operations:

A. Flight Readiness Test and Launch

BLDT Vehicle AV-1 completed Flight Readiness Test #1 on June 6, 1972 with data review being completed on June 7. Launch schedules were delayed during the time period of June 7 through July 11 due to uncertain meteorological conditions at the launch site. A launch was initiated during the evening of June 15 for a June 16 launch. This countdown was aborted due to thunderstorms in the area with heavy rains during the morning hours. A second countdown was initiated June 22 for a launch attempt on June 23. This countdown was aborted due to thunderstorms in the launch area.

Launch readiness was cancelled on June 26 in order to replace the airborne batteries which were approaching the 30 day maximum activated life. Vehicle Flight Readiness Test #2 was completed on June 28 following installation of new batteries with data review completed on June 30.

The final launch countdown was initiated July 10 for a launch attempt on July 11. This launch attempt resulted in vehicle launch at 0835 hours on July 11.

Balloon winch up and system launch were complicated by gusty surface winds and steady state crosswinds which necessitated driving the launch crane off the paved runway. During the crane/system travel across the non-paved surface, the crane intersected a grated drainage depression just prior to system release. The resulting shock forces applied to the vehicle/

load bar interface structure resulted in damage to the structural interface and loss of vehicle drop attitude integrity.

B. Ascent and Float

The balloon ground track during ascent and float was as shown in Figure IV-1. The float track to range, range intersect point, float heading at range intersect and range intersect time were in general agreement with the preflight predictions for these parameters.

The ascent to float altitude was not completed until approximately 15 minutes prior to releasing the flight vehicle from the balloon load bar. Preflight prediction for the balloon ascent rate was 1000 feet/minute, which whould have provided approximately one hour at float altitude. The deviation in ascent time can be accounted for by the ascent rate less than 1000 feet/minute at altitudes above 60 K feet. Figure IV-2 presents the pressure altitude (Rosemont gauge) versus time for the AV-1 vehicle ascent.

Due to the slow ascent rate above 60 K feet and the ballast dumping activities late in the flight, an anticipated porpoising motion did not have sufficient time to damp out prior to vehicle release from the load bar. Figure IV-3 shows the geometric altitude (radar) versus time for final 18 minutes of float just prior to releasing the flight vehicle from the load bar. The porpoising shown on Figure IV-3 would normally damp out prior to vehicle drop.

During the ascent/float phase, at approximately 80 K feet, a command system checkout was completed to verify the ground station to flight vehicle communications links. The communications check verified system operations by transmitting commands which did not change vehicle status, (i.e.

vehicle safe, R. F. on) and monitoring command reception via the vehicle to ground T.M. link.

Vehicle azimuth pointing operations during the float phase just prior to vehicle drop are covered in Section VI - Vehicle Performance Analysis. The azimuth pointing system installation and operation was required as a range safety constraint in order to assure that the vehicle azimuth at drop would maximize the probability of vehicle impact on range in the event of a complete failure of the decelerator system.

C. Vehicle Flight

During the powered flight, all vehicle functions occurred as programmed with the exception that the ground mortar fire command was pre-empted by the issuance of the mortar fire command by the airborne programmers. The sequence of flight events and actual event times from vehicle drop to TM off are provided in Table IV-1.

The major mission anomaly occurred during this phase of the mission in that the flight vehicle did not attain the minimum predicted altitudes as a result of flying a low trajectory. The low trajectory resulted in higher dynamic pressures than predicted and the airborne programmers timed out and issued mortar fire before the dynamic pressures reached a value which would permit the ground computer to issue a ground mortar fire command based on dynamic pressure. The analysis of this flight anomaly is covered in Section VI-A - Flight Dynamics.

It was a requirement during this phase of the mission to separate the aeroshell from the BLDT vehicle, following decelerator deployment, in order to obtain a time-distance history of the separation. The analysis of the flight film for this function, covered in Section V of this report, reveals

that the aeroshell separation rate exceeded the minimum requirement of 50 feet in 3 seconds.

The analysis of the decelerator deployment is also covered in Section V.

Inspection of the recovered vehicle indicated:

1. All ordnance functions occurred with no damage to the vehicle due to separation processes or vehicle ordnance function.

2. Base recirculation or SRM exhaust products during the boost phase was minimal since there was no evidence of high temperature effect on the base cover ablator.

D. Recovery Operations

As can be seen on Figure IV-1, the payload and separated aeroshell impacted approximately 16 miles north-west of the vehicle drop point. The point of impact on the range was in mountainous terrain which contributed to extensive impact damage to the vehicle and difficulty in recovering the expended hardware. The recovery portion of the mission was completed on T+1 day with all subsystem parts being recovered except for the parachute bag and some minor structural metal and parachute material.

Discussion of the condition of the recovered hardware, including the decelerator, is covered in later appropriate paragraphs.

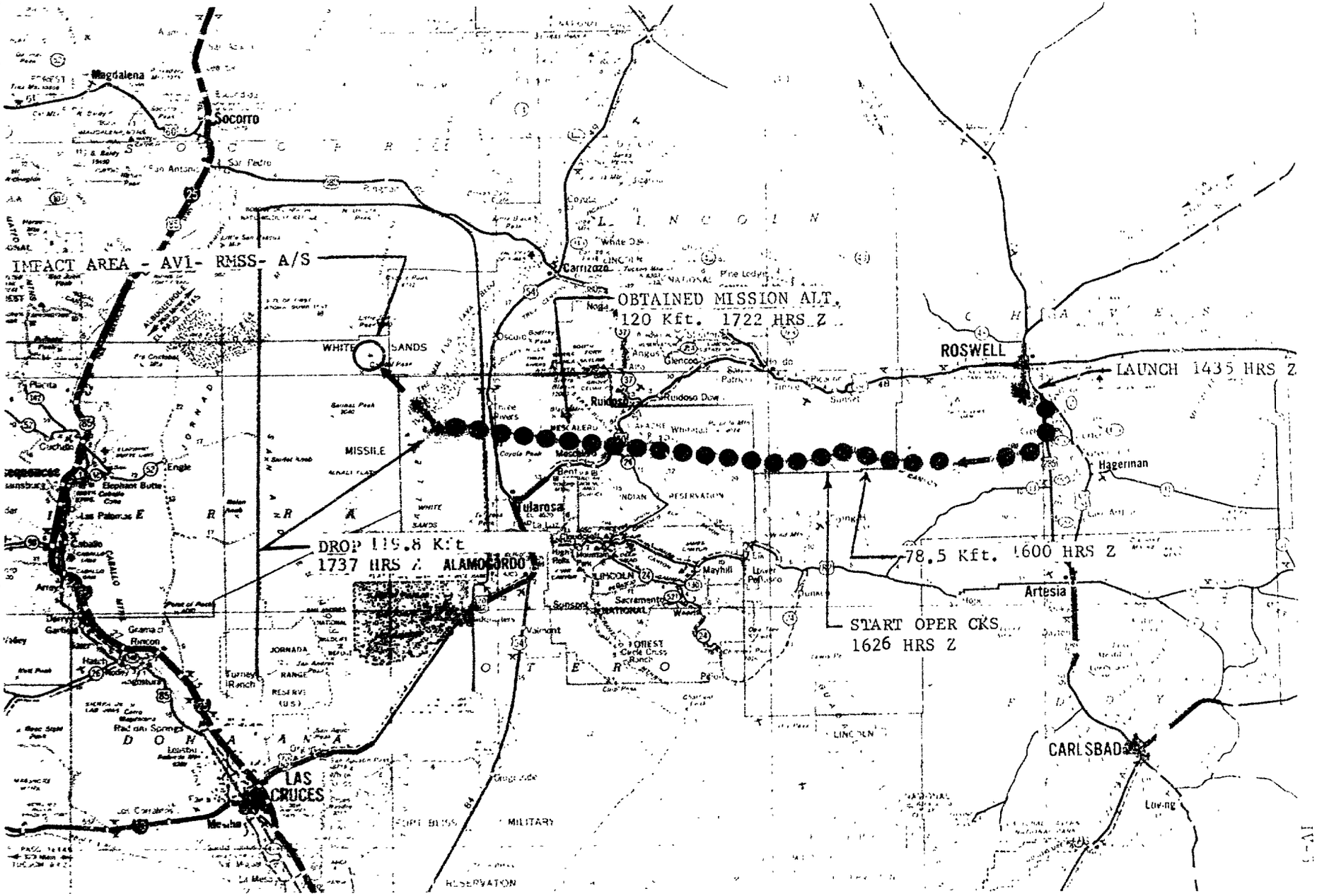

FIGURE IV-1

MISSION GROUND TRACK-AV1

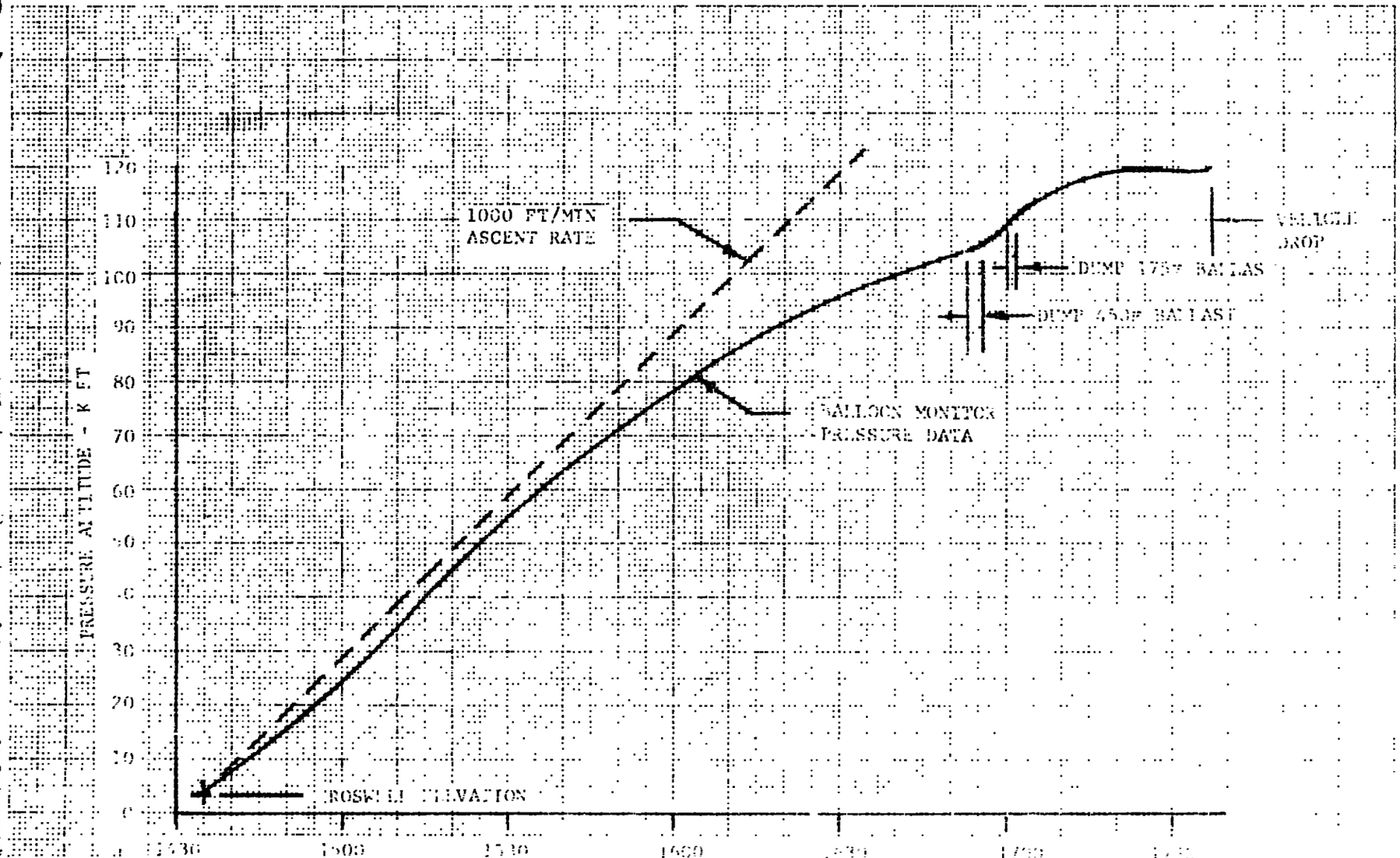

TIME OF DAY - HOURS MST

FIGURE IV-1 BALLOON ASCENT PROFILE

FIGURE IV-1 SYSTEM TROUBLESHOOTING TIMELINE

TABLE IV-1

AV-1 VEHICLE FLIGHT SEQUENCE OF EVENTS

	Programmed Time (Seconds)	Actual Time (Seconds)	Source
1. Drop from Load Bar/ Initiate A/B Programmer	0	0	Ground Command
2. Ignite Spin Motors/ Enable Boost Motors	+1	1.035	A/B Programmer
3. Ignite Boost Motors	+2	2.029	A/B Programmer
4. Ignite Despin Motors/ Release Camera Lens Covers/ Start Aft Milliken Camera	+33	33.252	A/B Programmer
5. Initiate Mortar Fire/ Start Aft Photosonics Camera/ Start Forward Milliken Camera	33.5 to 38.5	38.55	Ground Command
6. Initiate Mortar Fire Backup/ Start Aft Photosonics Camera B/O/ Start Forward Milliken Camera B/O	+38	38.312	A/B Programmer
7. Separate Aeroshell/ Start	47.6	47.992	A/B Programmer

V. DECELERATOR SYSTEM ANALYSIS

A. Mortar Fire Conditions

At mortar fire, the vehicle had a residual roll rate of 26 degrees/second and was coning about the velocity vector with a 3 - 4 degree angle. Plots of angle of attack and angle of sideslip in Figure V-1 show the mortar fire values to be -12 and -2 degrees respectively. Film data shows a total angle of attack of 13 degrees, i.e., 4.5 degrees away from the vehicle aerodynamic trim condition of 8.5 degrees. This deviation from trim is slightly higher than the 3 degree deviation expected on Mars (Reference 2) and is therefore a good qualification of this important variable. The pitch and yaw rates at mortar fire are shown in Figure V-2 to be 2 and -3 degrees/second, respectively.

A summary of the important mortar fire conditions compared with expected nominal values are tabulated below:

Mortar Fire Conditions	Nominal	Flight
Mach No.	2.229	2.18
Dynamics pressure, psf	11.759	14.63
Velocity, fps	2375	2314
Axial Acceleration, g's	-1.03	-1.18
Altitude, ft.	147,800	142,025
Angle of Attack	-8	-12
Angle of Sideslip	0	-2
Parachute Temperature at Mortar Fire	80°F	50°F

The objectives of this test as specified in Section II are all achieved by the above mortar fire conditions except the dynamic pressure which was 24 percent above the nominal value and fell outside the desired envelope of test conditions. Were it not for the damage sustained by the parachute, the high dynamic pressure would not have compromised the qualification of the parachute.

B. Mortar Performance

The mortar performance is evaluated by observing the bag stripping process from the on-board camera. The time at which the canopy first starts emerging from the bag (line stretch) can be clearly seen on the film data. The time from mortar fire to line stretch is observed to be 1.03 seconds. The actual distance the deployment bag must travel for the suspension lines to be pulled from the bag is defined by the length of the lines themselves. By simulating the mortar firing process with complete aerodynamic forces on the forebody and the deployment bag, the mortar velocity can be established. The AV-1 flight conditions of Mach number, dynamic pressure and flight path angle at mortar fire are used. Assumptions were used as follows where flight data was not available:

1. Deployment Bag $C_D S = 1.6$
2. Dynamic pressure gradient behind blunt body (Reference 3).
3. Forebody aerodynamic coefficients (Reference 4).
4. Line and canopy stripping forces of 2 and 6 lbs. respectively (Reference 5).

If the lines are assumed to follow a straight line path between forebody and the deployment bag, the mortar velocity would be 115 fps as seen in the simulation sequence shown below:

	Time - Seconds	Relative Vel - FPS
Mortar Fire	0	115
Line Stretch	1.03	74.6
Bag Strip	1.41	64.9

Observation of the suspension line geometry during line deployment (see picture sequence Figure V-3) shows that the lines are not in a straight line as assumed above but are bowed as a result of aerodynamic force on the lines. It is noted that mortar fire occurred when the vehicle was at an angle of attack of -13 degrees. It is typical of Mars type low dynamic pressure deployment for the deployment bag to proceed straight back relatively uninfluenced by the aerodynamic forces on it whereas the lines, being of less mass per unit area, begin to line up almost immediately with the relative wind. The extent of this line bowing effect shown in Figure V-4 has been incorporated in the simulation of the AV-1 stripping process. The results shown below indicate the mortar velocity was 112 FPS or very close to the middle of the expected nominal range of 112 $\pm$ 3 FPS.

	Time - Seconds	Relative Vel - FPS
Mortar Fire	0	112
Line Stretch	1.03	72
Bag Strip	1.40	71.5

The relative velocity between bag and vehicle dips to a low point of 62 FPS between line stretch and bag strip, but has increased to 71.5 FPS at

bag strip. This increase results from the bowed line force not being lined up with the bag relative motion direction and the fact that the bag mass is decreasing. In any case, the relative velocity at bag strip is considered to be more than adequate to have achieved positive bag strip.

C. Decelerator Inflation Sequence

The on-board Milliken and Photosonic camera films were examined in detail to establish event times and as a means of understanding the parachute panel tear mechanism. In the sequence of events shown below, certain events such as peak load were obtained from telemetry data: Good correlation of all three sources of data was achieved.

Sequence of Events	Time - Seconds
Mortar Fire	0
Line Stretch	1.030
Bag Strip	1.320
Bag Behind Canopy	1.365
Damage Evident	1.390
First Full Open	1.570
First Peak Load	1.690
Deployment Bag Separation	2.880
Aeroshell Separation	9.680

Selected frames from the Milliken aft viewing camera show in Figure V-3 some of the significant events during the inflation phase. The growth of the canopy from line stretch was obtained by tracing the projected area images from the Milliken camera and integrating these images with a planimeter. The open damaged gore area was consistently subtracted from

the total projected area. The resulting canopy growth parameter shown in Figure V-5 looks fairly typical of similar curves drawn for PEPP flights (Reference 6). What is significantly different, however, is the point where bag strip occurs on the curve. All LADT and PEPP flight tests of disk-gap-band parachutes showed bag strip occurring before the 50 percent point of the normalized filling time, T/T_{fill}. It is evident also in the visual inspection of the film data that a significant amount of band and disk inflation has occurred before bag strip.

A plot of the projected area ratio, $S_p/S_{p_{final}}$, versus time from line stretch is presented in Figure V-6. The area oscillations after first full inflation are typical for a DGB parachute deployed at this Mach number. No correction has been applied to the projected area ratio to account for variation in the canopy image plane under changing load conditions. The raw data is felt to be a better basic data source than one which might be based on a speculated amount of elongation under load.

Parachute inflation time from line stretch to first full inflation is seen in Figure V-6 to be .54 seconds. This value is plotted in Figure V-7 along with similar data from PEPP and LADT flight tests. The filling time for AV-1 falls toward the lower edge of but within the expected uncertainty in this parameter. The nominal and expected dispersion envelope shown will be re-established as a result of the total BLDT experience.

D. Opening Load

Figures V-8 and V-9 show the time-history of the total longitudinal parachute load recorded by the bridle attach point tensiometers for different time periods after mortar fire. The first peak opening load is seen to be 16,647 lbs. and occurs 1.69 seconds after mortar fire (.12

seconds after first full inflation). The actual maximum load of 17,393 occurs at 2.23 seconds. The individual tensiometer readings are recorded in Figures V-10, V-11 and V-12. By proper combination of the three tensiometer readings, the equivalent parachute pull angles in pitch and yaw are obtained and plotted in Figures V-13 and V-14. The large pull angles prior to load buildup (0. to 1.5 seconds from mortar fire) are influenced by line and swivel dynamics and do not reflect significant load conditions. The maximum pull angle at substantial but not peak load is 6 degrees. The peak load pull angle, combining pitch and yaw values is 3 degrees.

The peak load of 17,393 lbs. is lower than would be anticipated for the conditions experienced. Simulation of these conditions produced an opening load of 19,500 lbs. The difference between these values is atrributed in part to the canopy damage sustained prior to peak load.

The pull angles recorded in this test agree to within $\pm$ 1 degree of values shown for similar conditions in Reference 8.

Accelerometer readings in the X, Y and Z axis directions during the opening phase are presented in Figures V-15, V-16 and V-17. The peak longitudinal acceleration at 2.23 seconds is -11.2 g's which reflects a parchute opening load of 18,260 lbs. This is based upon subtracting out the aeroshell drag component using C_D of 1.6, a dynamic pressure of 11.0, and a payload mass of 55.8 slugs. The accelerometer reading, therefore, confirms the opening load recorded by the tensiometers.

E. Vehicle Stability

The BLDT vehicle was coning about the velocity vector with an angle of 3 - 4 degrees and a residual spin rate of 26 degrees/second at mortar fire. The vehicle rotation rate time histories in pitch, roll and yaw

thereafter are shown in Figures V-18, V-19 and V-20. The roll rate is seen to continue with little change in magnitude during the parachute deployment and deceleration phase. The maximum pitch rate of 148 degrees/second occurs 1.64 seconds after mortar fire or very nearly at the time of first peak load (1.69 seconds). The pitch rate oscillation damps to below 30 degrees/second in 10 seconds. Because of the residual roll rate, however, the energy of the transient is seen to transfer back and forth between pitch and yaw, each time reducing in magnitude. The maximum rate of 148 degrees/second being greater than the Mars specification limit of 100 degrees/second is not surprising when the degree of overtest from Mars conditions is considered (q = 14.4 PSF compared with q = 8.62 on Mars).

The rotation rate data generated on this flight probably is typical of what to expect on Mars. The damping characteristics of the parachute do not appear to be as good as predicted in Reference 2. There is reason to believe, however, that the damaged parachute generated a lift vector which may have influenced the damping behavior. These flight results will therefore have to be compared to undamaged parachute results and extrapolated to Mars before they are applied as requirements to Viking hardware.

F. Parachute Drag Performance

Parachute drag during the highly dynamic opening phase and deceleration is determined in two different ways using first the on-board longitudinal accelerometer and secondly the summation of tensiometer loads. The equations actually compute an axial force coefficient as indicated below:

$$C_{A_P} = A_x \cdot W_T/q \cdot S_P - C_{A_A} \cdot S_A/S_P$$

where: A_x = longidutinal accelerometer, g's

W_T = total weight of system, 1891 lbs.

q = dynamic pressure, psf

S_P = parachute reference area, 2206 ft^2

S_A = aeroshell reference area, 103.8 ft^2

C_{A_A} = aeroshell axial force coefficient, reference 4.

$$C_{A_P} = (F_x - 95 \cdot A_x)/q\ S_P$$

where: F_x = summation of tensiometers, os.

These parachute drag results, as plotted in Figures V-21 and V-22, are superimposed over the expected dispersion of parachute drag from wind tunnel results, (Reference 7). The supersonic drag coefficient is observed to be higher than anticipated, and there is little evidence of the typical drag reduction near Mach 1.0 that was experienced in the wind tunnel.

The quasi-steady state drag of the parachute plus base cover is determined from velocity and velocity differential data obtained from radar. The equation used is as follows:

$$C_{D_T} = \frac{m_T}{q\ S_P} \quad (\dot{V} + g \cdot \sin\gamma)$$

where: m_T = total mass of the system, 58.7 slugs.

$\dot{V} = \frac{dV}{dt}$ from radar

Since the drag coefficient of the base cover is nearly constant in this Mach number regime, it may be subtracted out of the total coefficient, C_{D_T}, leaving the parachute drag coefficient by itself:

$$C_{D_P} = C_{D_T} - C_{D_{B_C}} \cdot \frac{S_{BC}}{S_P} = C_{D_T} - .045$$

This data added to Figure V-22 in the low Mach No. range shows a steady state parachute drag that averages at 0.60 or just slightly below the nominal wind tunnel prediction of 0.61. The drag deduced in this manner neglects any lift from either the parachute or the vehicle.

The time-histories of Mach number and dynamic pressure from mortar fire are presented in Figures V-23 and V-24.

G. Aeroshell Separation

Aeroshell separation on this flight was intended to demonstrate satisfactory system operation at a Mach number of 1.18 and dynamic pressure of 2.8 psf. Higher than expected parachute drag, however, produced a separation Mach number of .92 and dynamic pressure of 2.42 psf. The objectives of the separation demonstration are: (1) to determine that there are no unpredictable aerodynamic disturbances at separation that would compromise the Viking mission and (2) to exercise the separation hardware and concept to insure that analytical evaluations of separation forces are valid, and (3) to determine that parachute drag is adequate to produce a minimum of 50 feet of separation between aeroshell and lander in 3 seconds.

Photographic evaluation of the forward viewing Milliken camera film indicated a well behaved separation with no tendency of the aeroshell to recontact the lander, no significant aerodynamic or mechanical perturbation imparted to the lander, little tendency of the aeroshell to move laterally at the instant of separation and a stable aeroshell trajectory after separation.

Separation distance versus time is obtained from the Milliken camera film by knowing the diameter of the aeroshell to be 11.5 feet, the horizontal field of view of the camera to be 54.9 degrees and the frame rate to be 32 frames per second. The separation distance may then be calculated by measuring the aeroshell image size on a specific horizontal field of view and correlating with the number of frames since separation.

Separation Distance = 11.5 x H.F.V./.958 x Image Diameter

The separation distance versus time plot in Figure V-25 shows 197 feet of separation in 3 seconds. Simulation of this separation using actual flight conditions including parachute drag shows excellent agreement with the AV-1 separation data. The early motion is faster than anticipated probably as a result of very high rigid body rail loads reflected in the simulation model which probably were significantly lower in the actual flexible body case. It is worth noting that aeroshell separation occurred at a time (9.68 seconds after mortar fire) when the vehicle was pitching at 69 degrees/second. This is more than twice the specification rate of 30 degrees/second which was a design criteria for the separation guide rail system design. The fast early separation motion is seen in the extensiometer in Figure V-26 also.

The geometry of the extensiometer units and the guide rail system shown in Figure V-27 is required to interpret and analyze the extensiometer data. From the geometry and the extensiometer readings, the relative angular rotation between aeroshell and lander is computed and plotted in Figure V-28. The amount of relative rotation while on the rails is surprising in view of the moment constraint applied to the two bodies by the guide rail system. In the ground test of the AV-1 separation system a peak relative angle of 1.53 degrees was recorded by the extensiometers when the system was subjected to a bending moment of 560 ft-lbs (.87 x design moment). This is about one-half of the 3.1 degree relative angle experienced on this flight at the point where total moment constraint is lost (.105 seconds from separation). Of this amount, approximately .5 to 1.0 degree is accounted for by known tolerances in the mating parts. Figure V-28 shows a plateau in the curve between .03 and .04 seconds that reflects a bottoming out of these tolerances at 0.5 degrees. The rest of the relative angle must be accounted for by elastic or permanent deformation.

Simulation of AV-1 aeroshell separation conditions using 69 degrees/second attitude rate at separation, indicates that guide rail loads were approximately twice as high as the Viking design values associated with 30 degree/second rates. This is consistent with the amount of deformation that is apparent from the extensiometer data. Based on the foregoing, it would be logical to conclude that the deformation in the guide rail system was all elastic were it not for one piece of evidence. The aeroshell ring frame was slightly buckled at diametrically opposite points near extensiometer No. 2 and the rail nearest the -Z axis (see Figure V-27). This damage was originally thought to have occurred at impact and this may still prove to be so. However, the abnormal deformation in the guide rail system

was an indication of a bending moment about an axis that was within 9 degrees of an axis between the buckled points. Since there was no noticeable permanent deformation in the rails, rollers or brackets, the rail bending moment would have been shared at least partially by the buckled ring frame. This information needs further review and structural analysis before being applied to the Viking hardware.

H. Parachute Recovery Assessment

A detailed assessment of parachute damage is presented in Appendix C and graphically documented in Attachment 1 therein. In summary, the parachute canopy sustained radial tears from the vent to the edge of the disk in gores 36 and 38 early in the inflation cycle. Analysis of the nature of the tears and the fact that they occurred much prior to peak canopy load, leads to the conclusion that the failed panels sustained frictional damage as they emerged from the deployment bag. An angle of attack of -13 degrees at mortar fire and excessive dynamic pressure which reduced the relative bag stripping velocities, allowed a significant amount of canopy inflation prior to bag strip. This behavior is felt to have caused the bag stripping damage. These areas were then exposed to localized high pressure during an unsymmetrical canopy inflation which caused the small initial damage to propagate into large tears.

In spite of the damage sustained to the canopy, the parachute maintained structural integrity and produced sufficient drag for a successful Mars mission.

A comparison of pre- and post-flight parachute dimensions is shown in Appendix D. The suspension line length increase ranges from 4 feet 3 inches on radial 39 to 5 feet 9 inches on radial 1. The disk radial dimension

increase ranged from 6 inches on radial 36 to one-half inch on radial 14. These dimension changes are indicative of significant asymmetrical loading. The bridle legs each gained 3/4 inch in length. All other dimensional changes are minor.

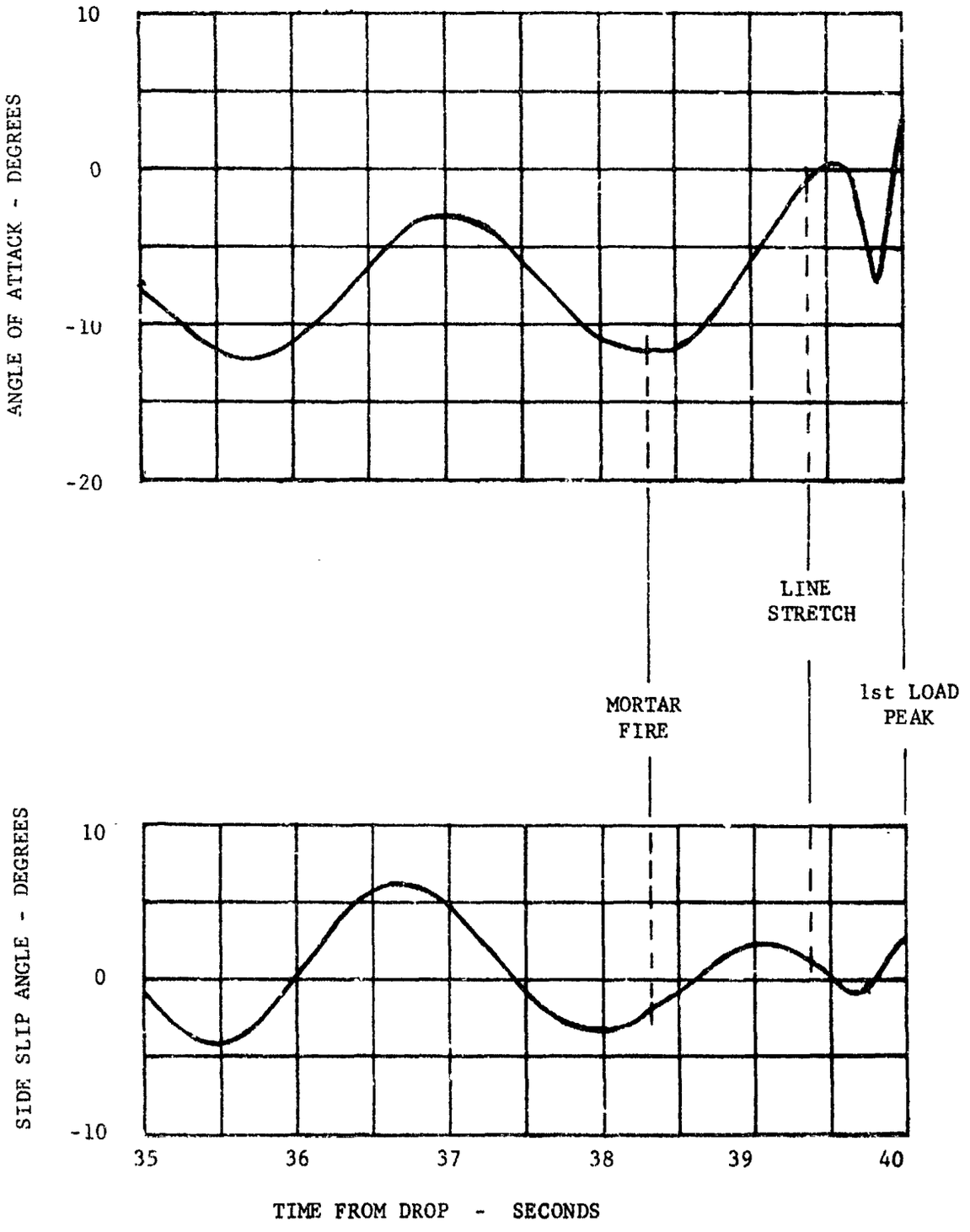

FIGURE V-1 ANGLE OF ATTACK AND SIDE SLIP AT DEPLOYMENT

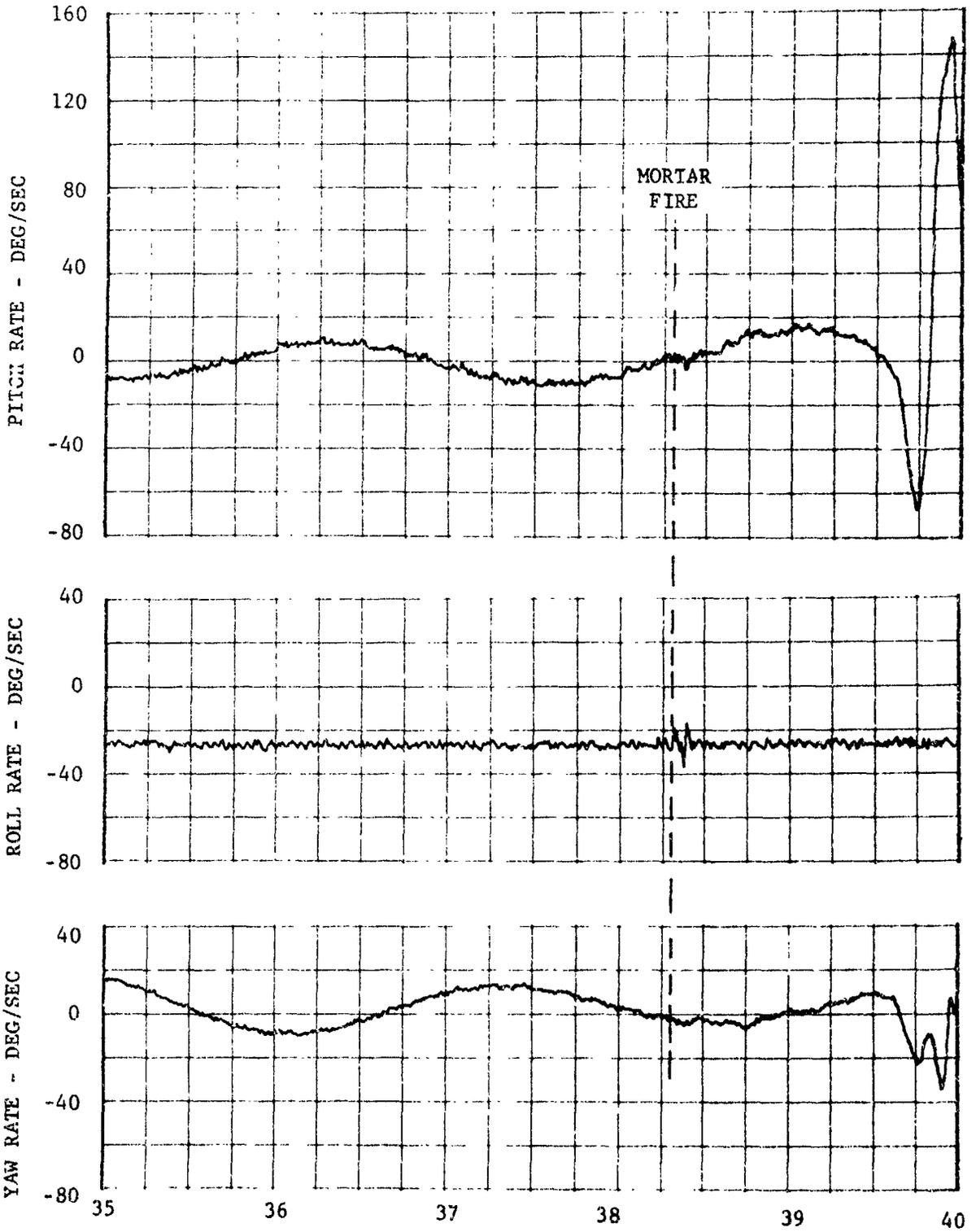

FIGURE V-2 VEHICLE ATTITUDE RATES AT DEPLOYMENT

t = .156

BAC DEFORMATION

t = .390

LINE BOWING

t = .546

LINE BOWING

t = .704

LINE BOWING

FIGURE V-3 ON-BOARD CAMERA PHOTOGRAPHS

t = 1.03

TIME STRETCH

t = 1.310

BAG STRIP

t = 1.420

FIRST DAMAGE

t = 1.500

C-SHAPED UNFOLD

FIGURE V-3 ON-BOARD CAMERA PHOTOGRAPHS (CONTINUED)

t = 1.593

FIRST FULL OPEN

t = 1.970

PARTIAL COLLAPSE

t = 2.095

OPEN AGAIN

t = 2.670

STILL OPEN

FIGURE V-3 ON-BOARD CAMERA PHOTOGRAPHS (CONTINUED)

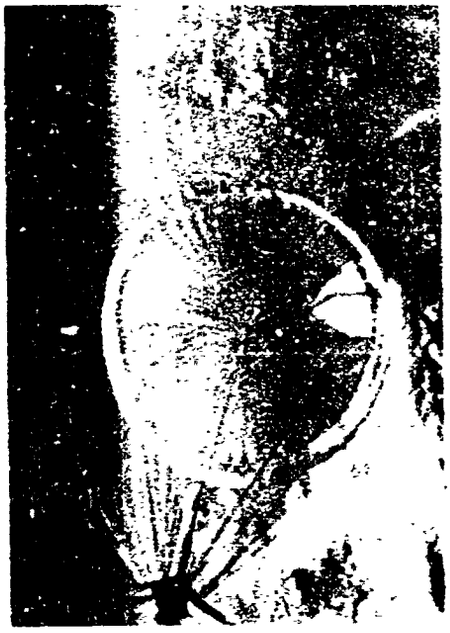

t = 3.110

BAG SEPARATING

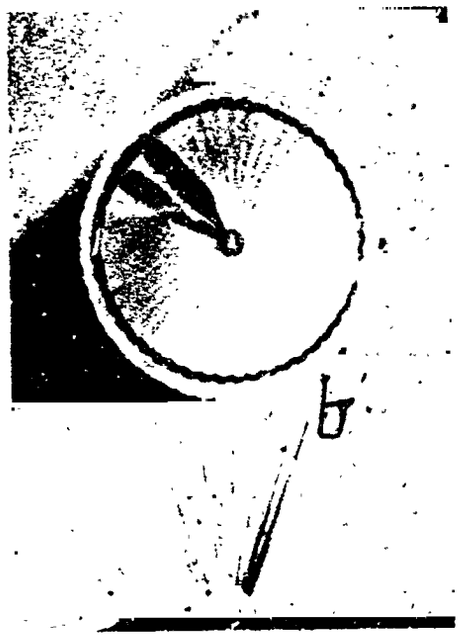

t = 7.72

NEAR APOGEE

t = 9.8

AFTER AEROSHELL SEPARATION

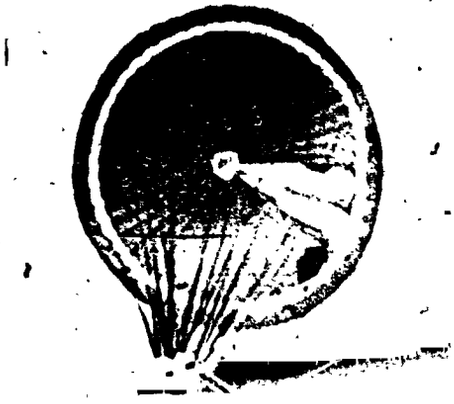

t = 12.35

FINAL VIEW

FIGURE V-3 ON-BOARD CAMERA PHOTOGRAPHS (CONTINUED)

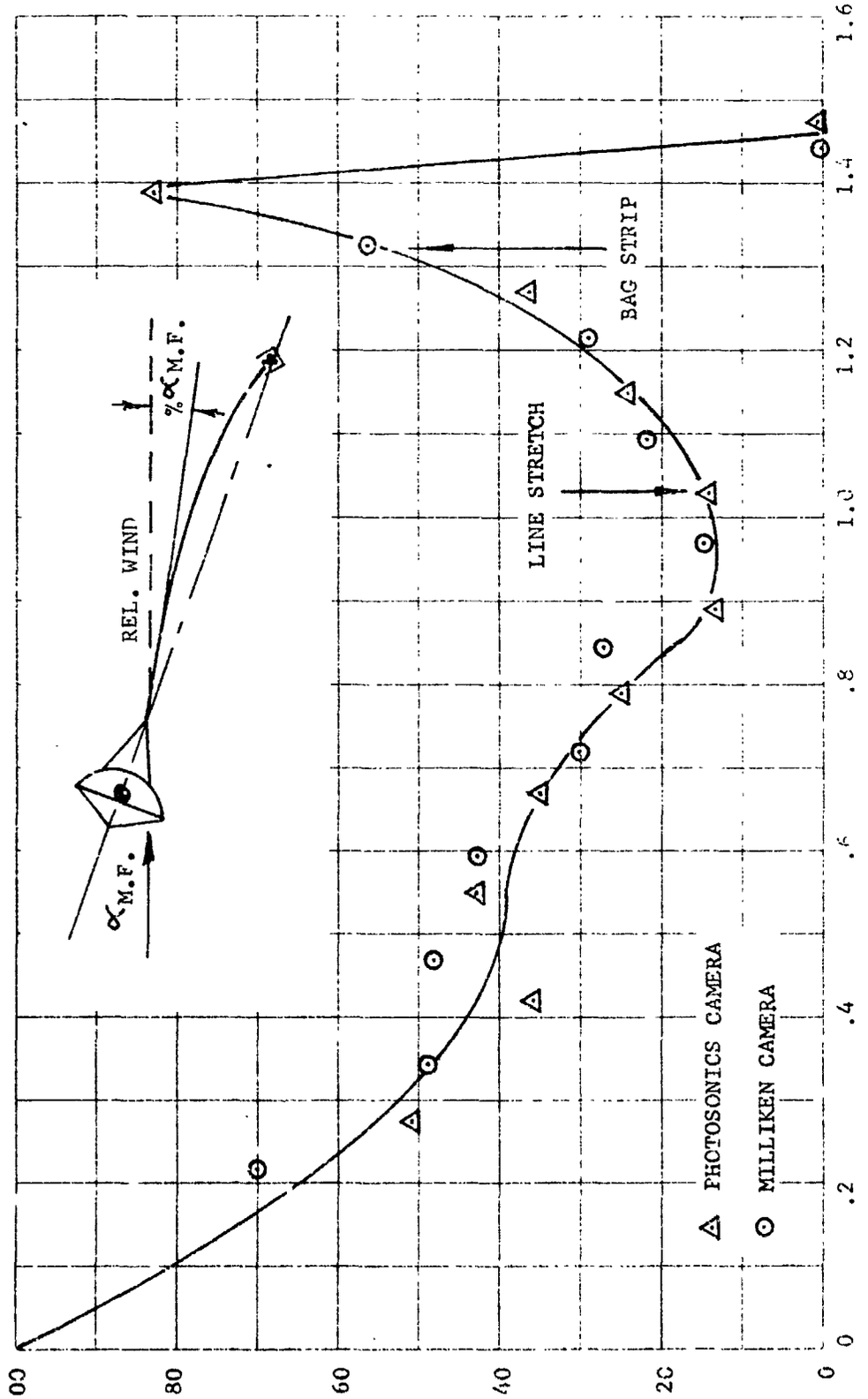

FIGURE V-4 ANGLE OF ATTACK LINE BOWING EFFECT

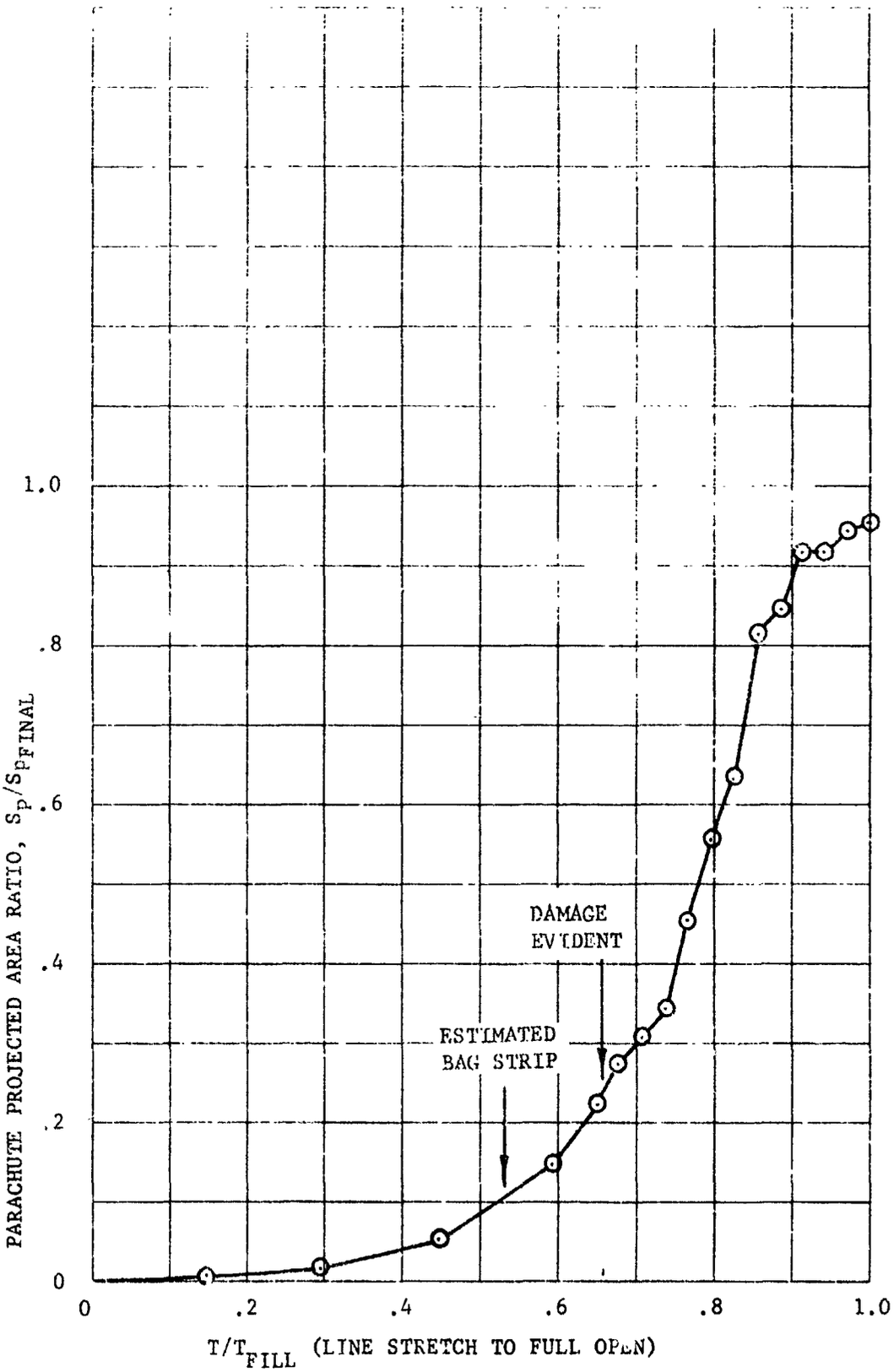

FIGURE V-5 CANOPY GROWTH PARAMETER

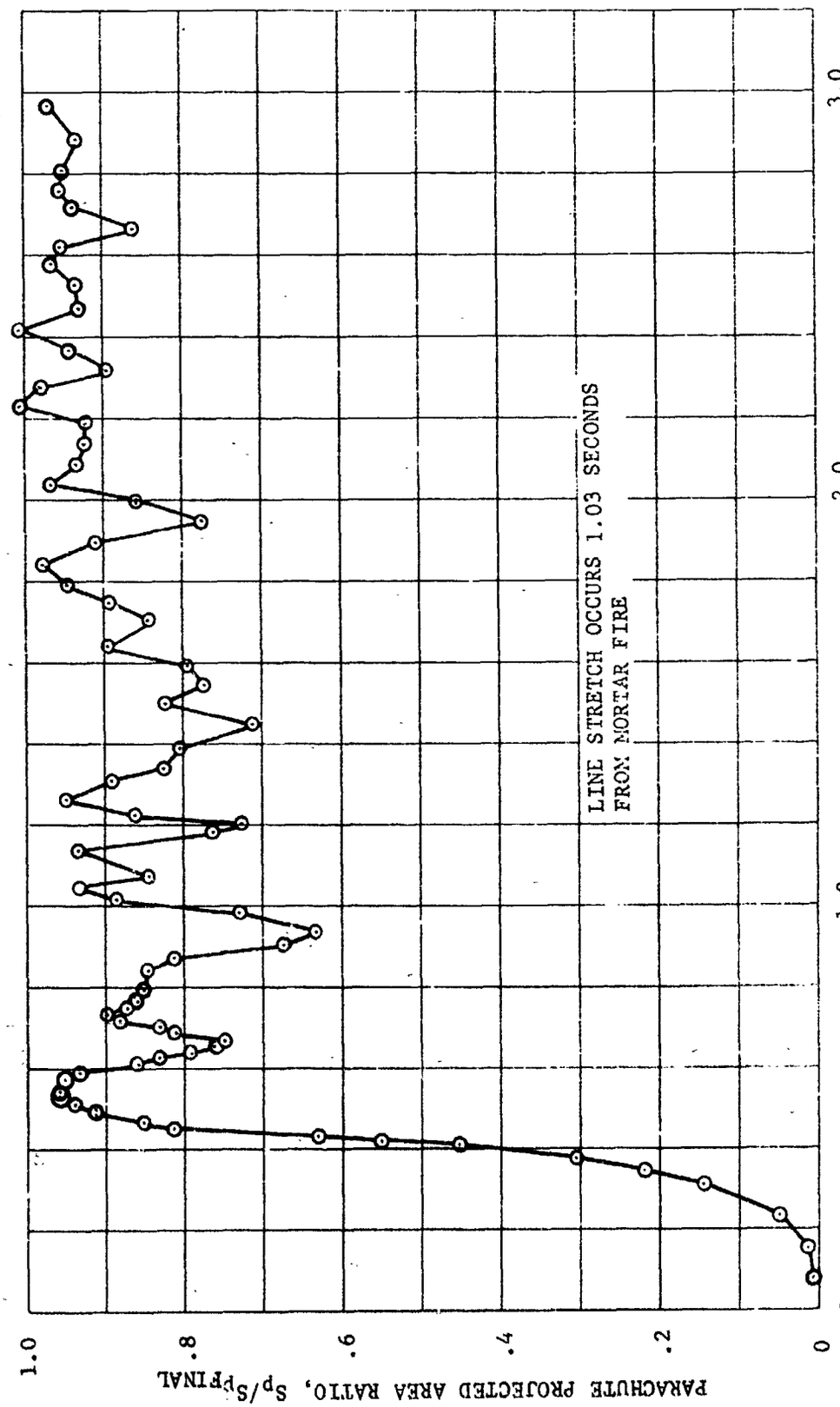

FIGURE V-6 CANOPY AREA OSCILLATIONS

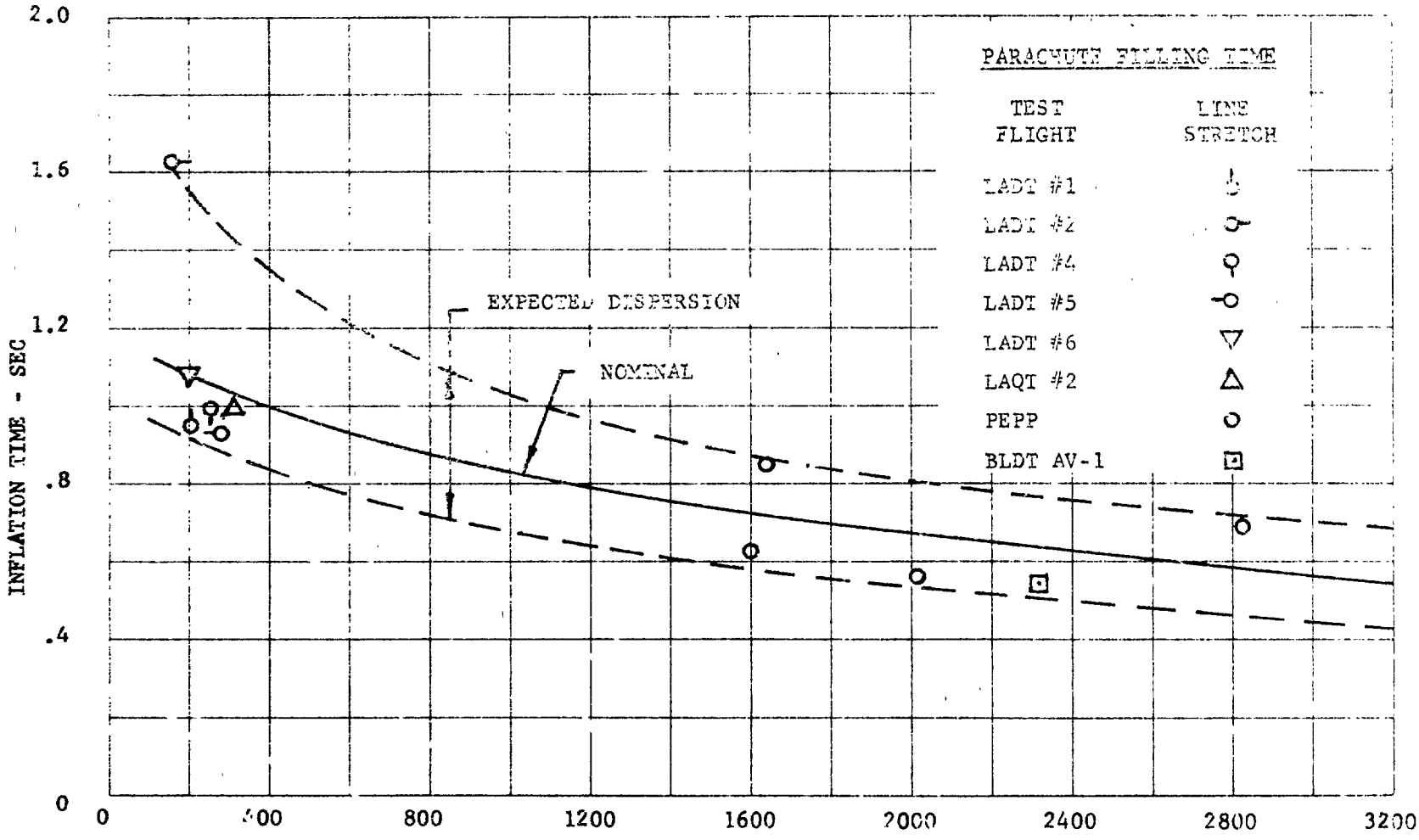

FIGURE V-7 PARACHUTE FILLING TIME

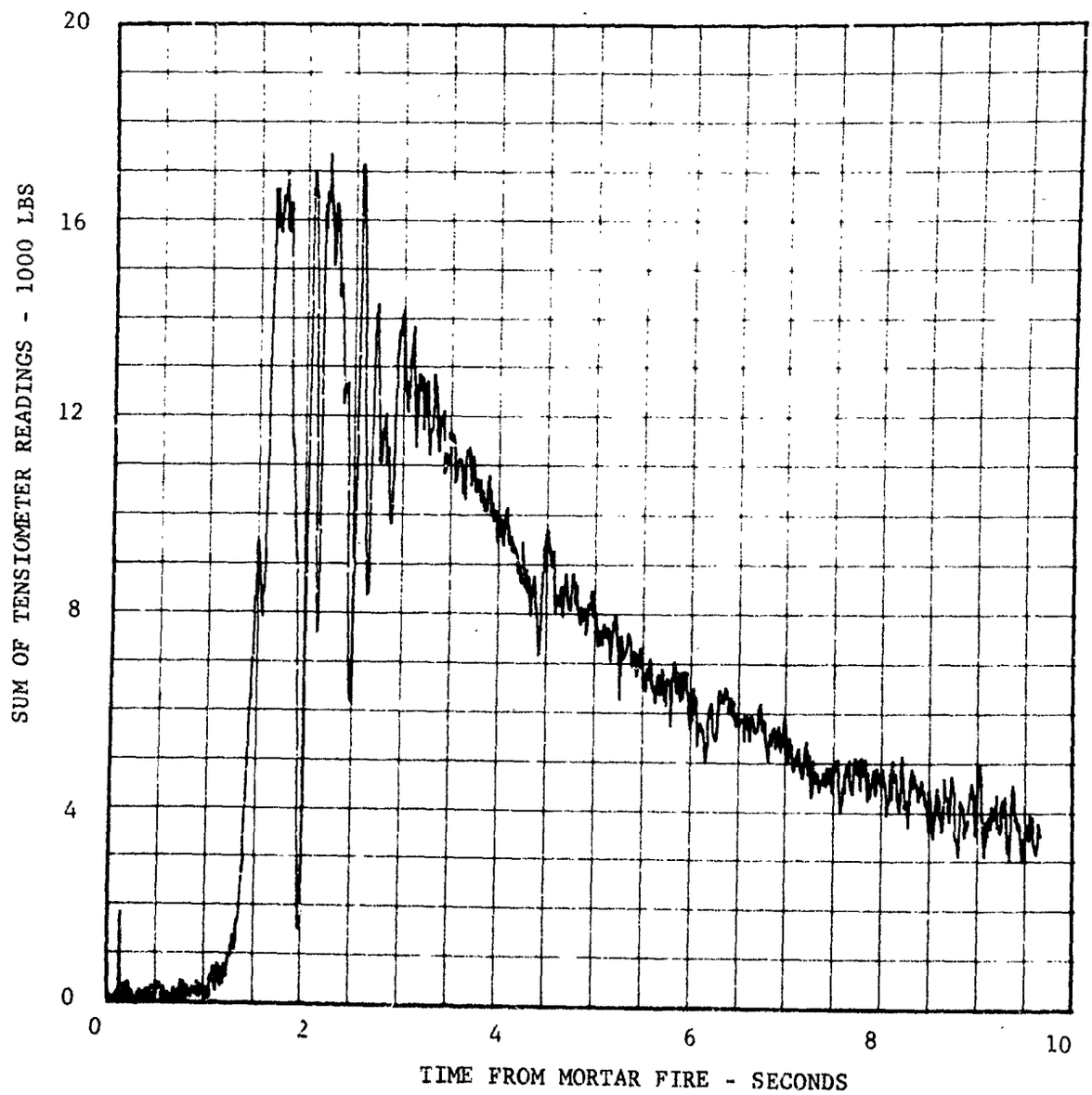

FIGURE V-3 PARACHUTE OPENING LOAD, 0-10 SECONDS

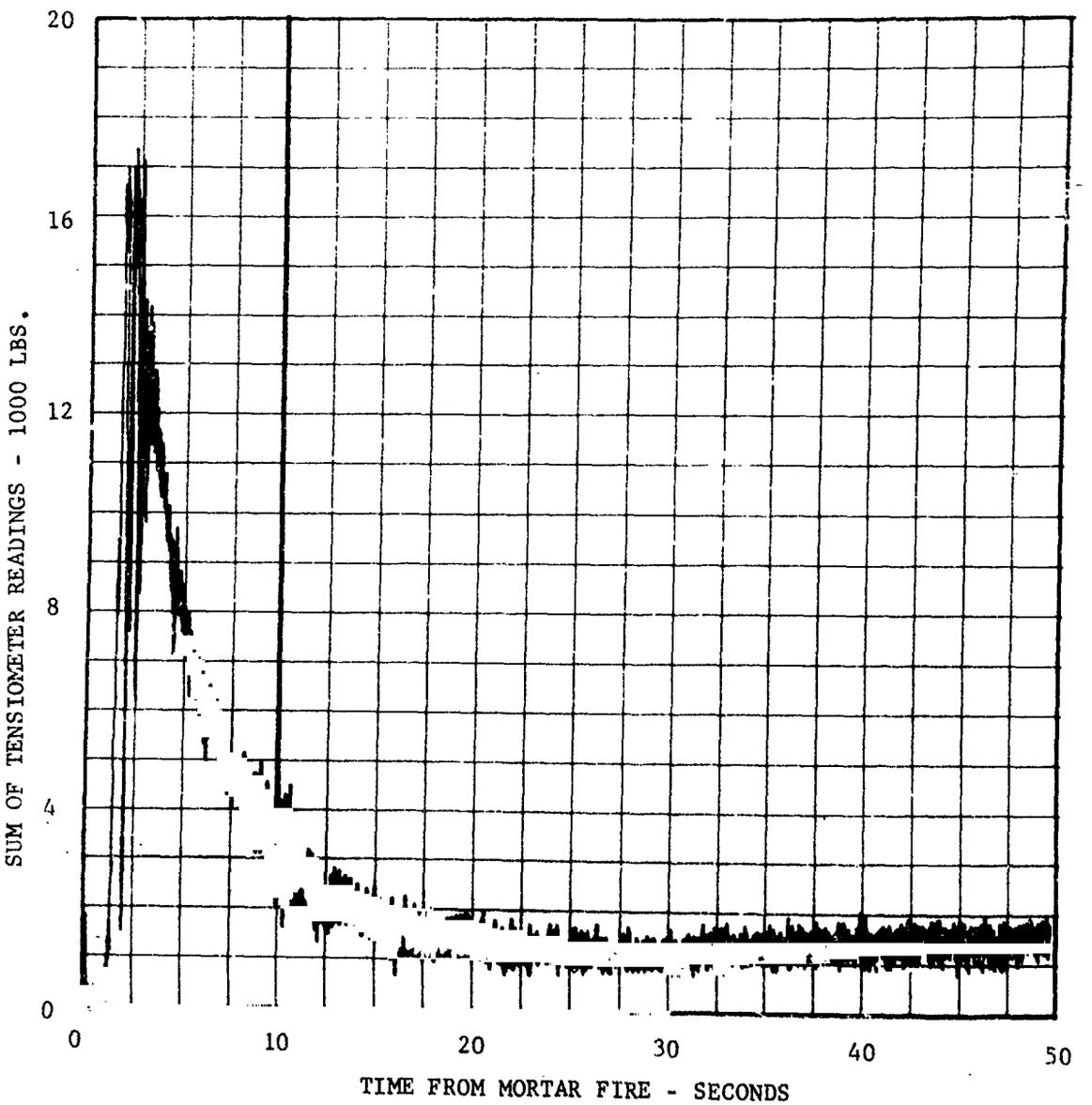

FIGURE V-9 PARACHUTE OPENING LOAD, 0-50 SECONDS

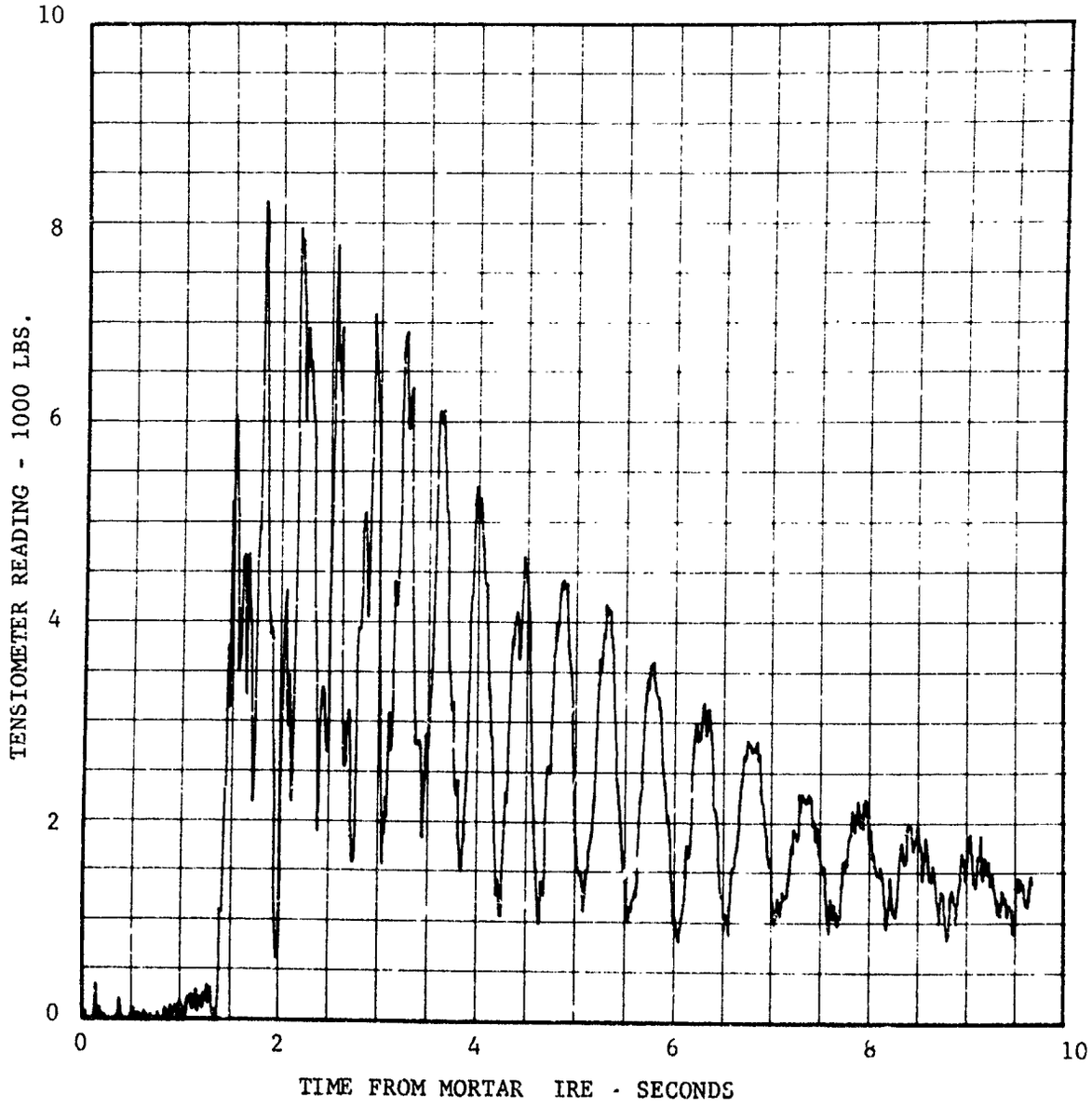

FIGURE V-10 TENSIOMETER READING, BRIDLE LEG NO. 1

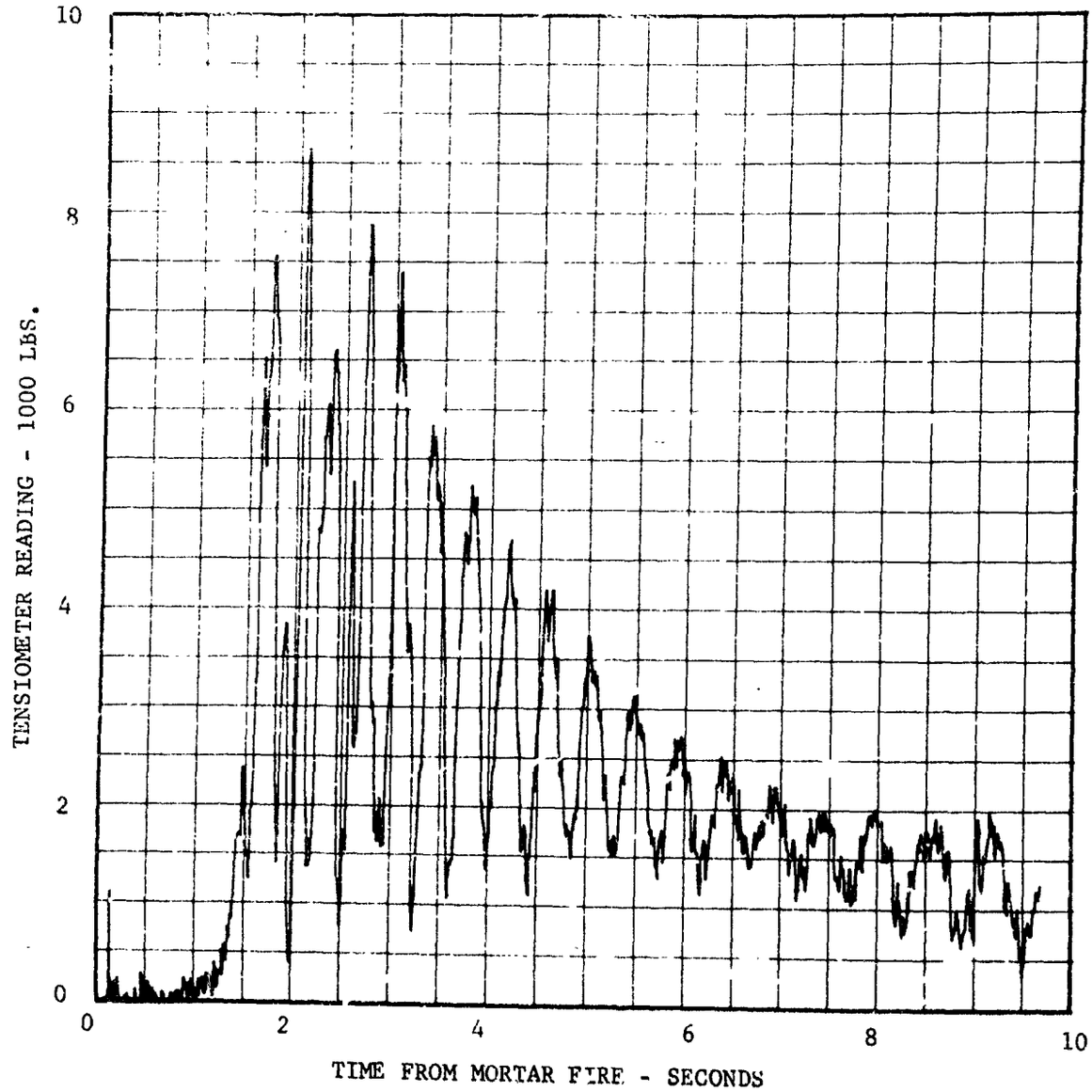

FIGURE V-11 TENSIOMETER READING, BRIDLE LEG NO. 2

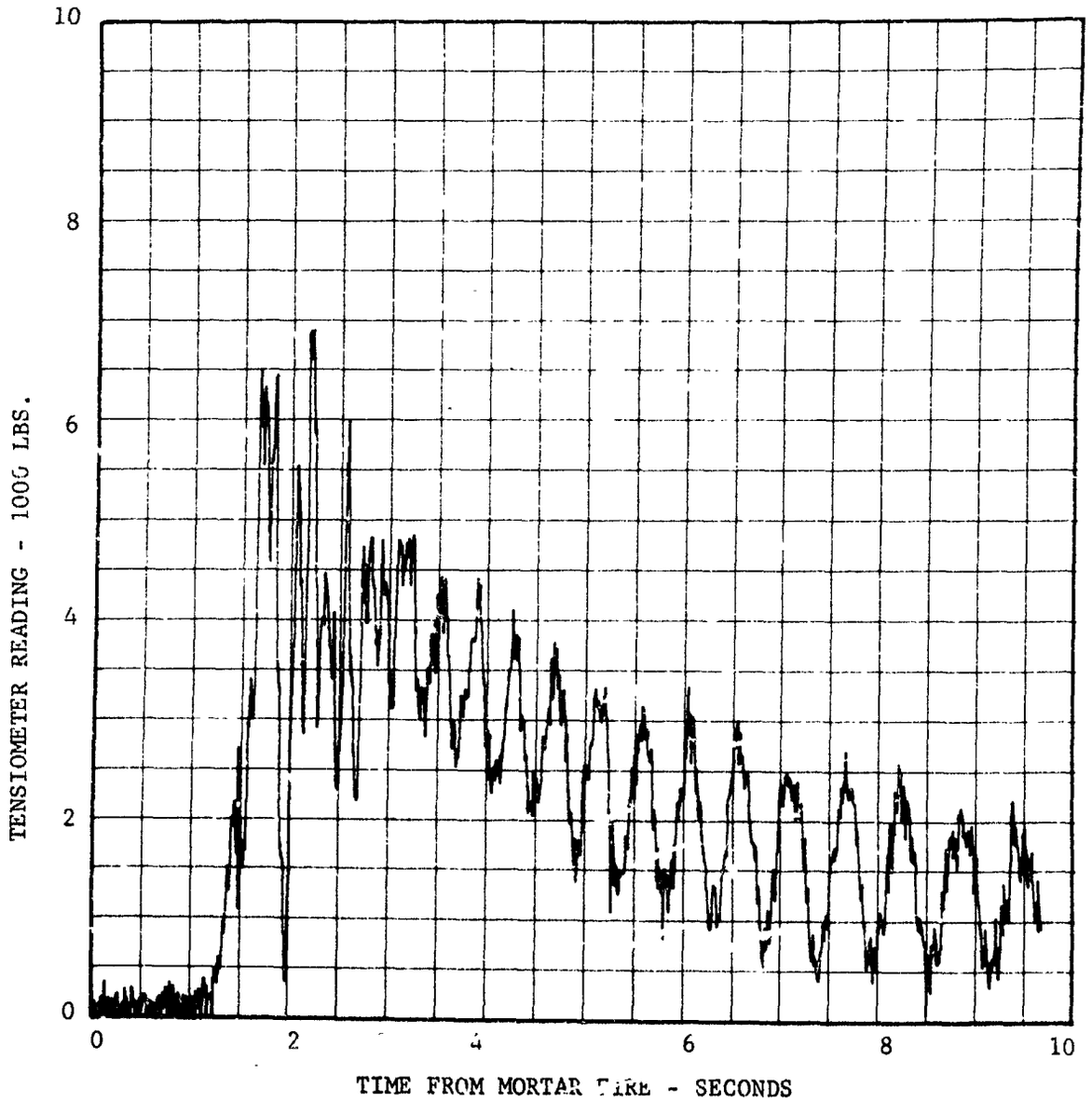

FIGURE V-12 TENSIOMETER READING, BRIDLE LEG NO. 3

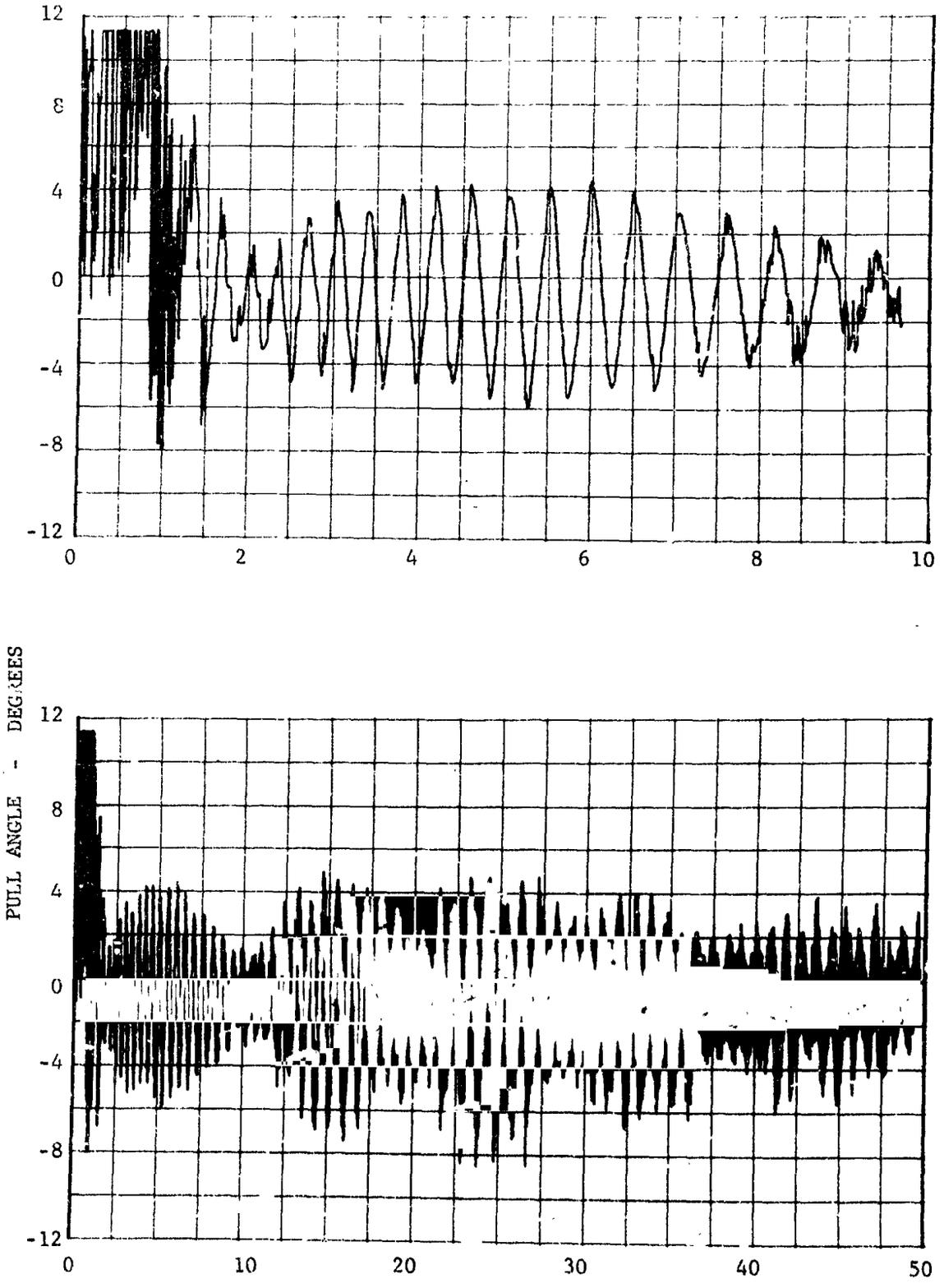

FIGURE V-13 PARACHUTE PULL ANGLE, PITCH PLANE

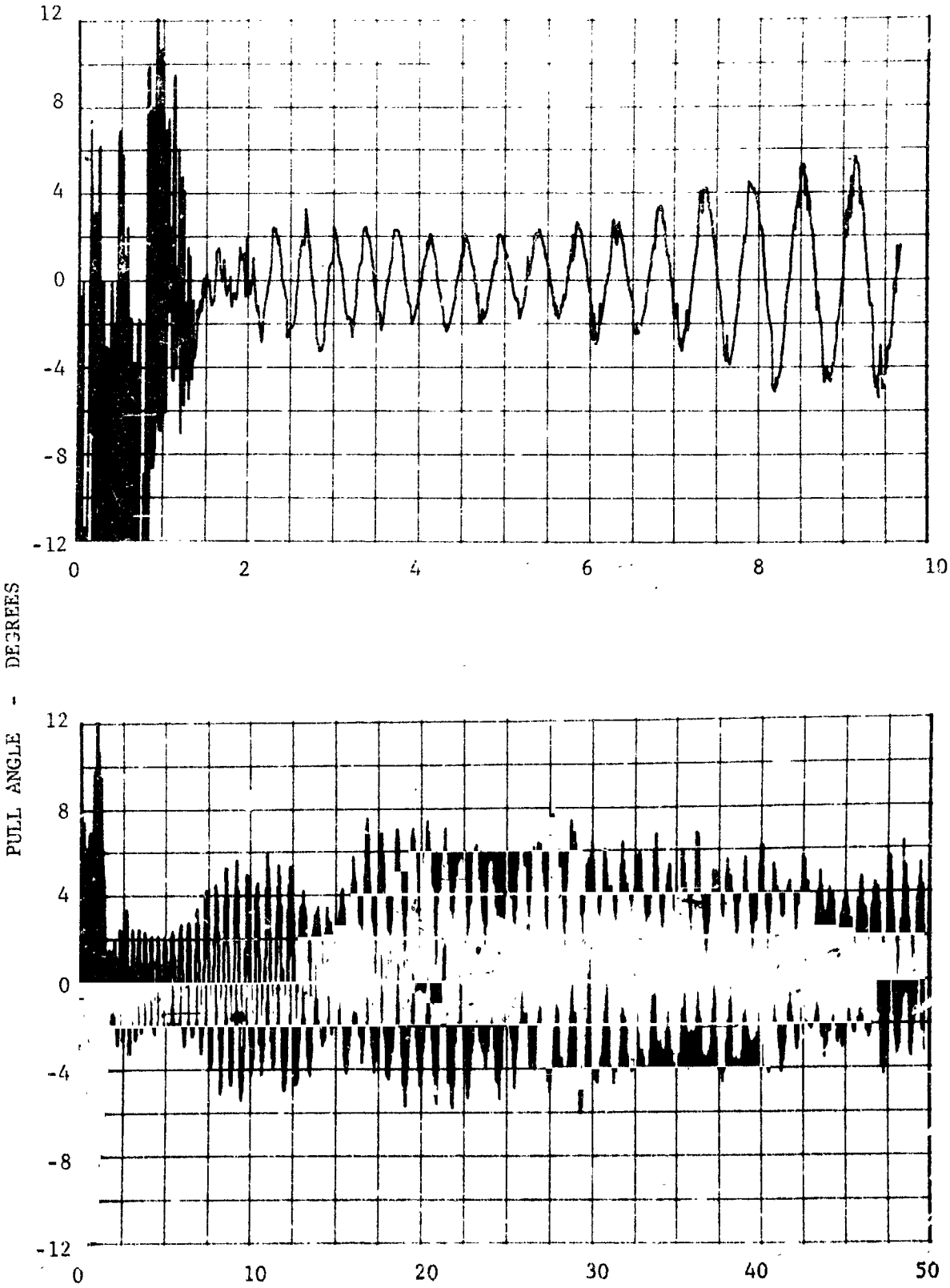

FIGURE V-14 PARACHUTE PULL ANGLE, YAW PLANE

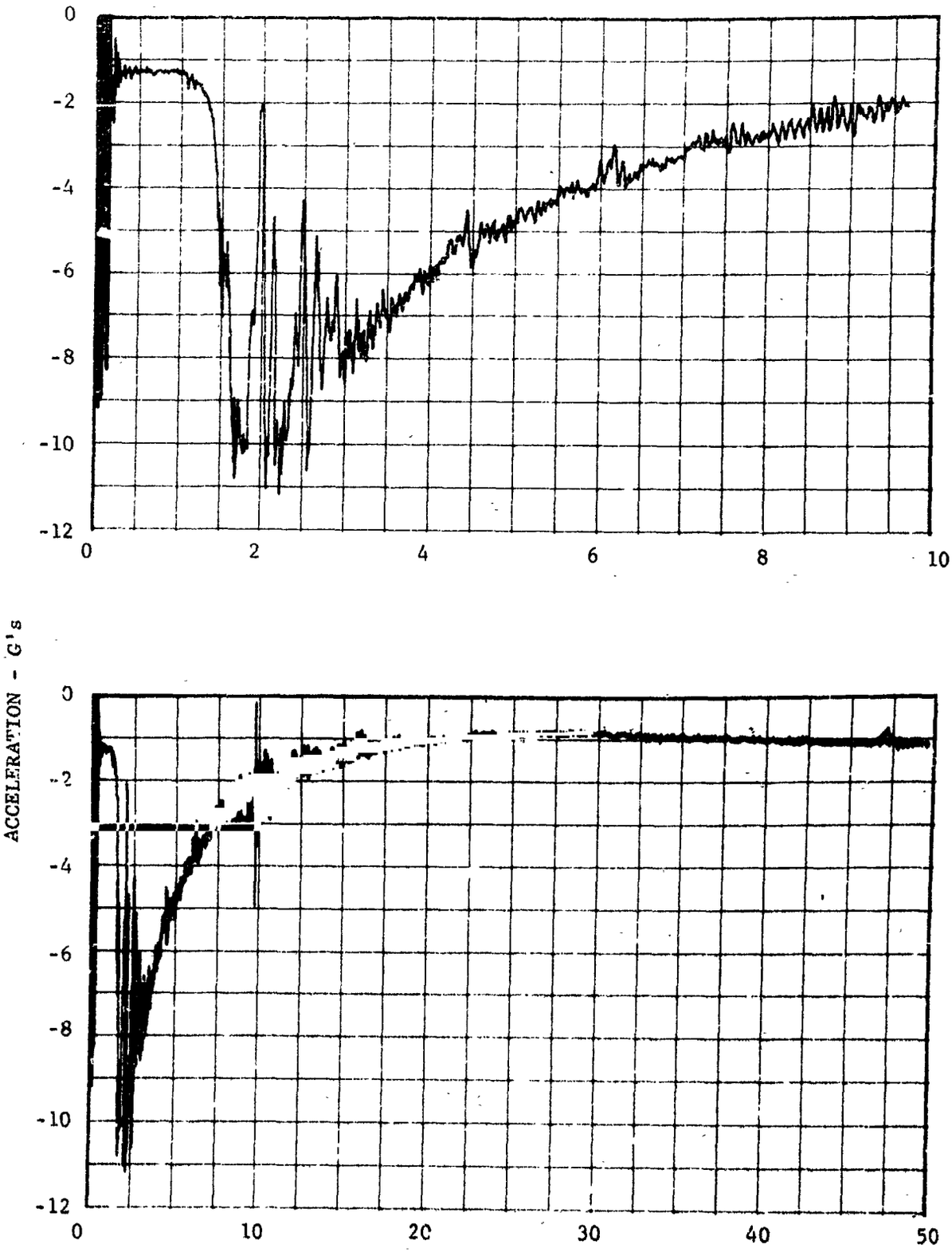

FIGURE V-15 LONGITUDINAL ACCELERATION

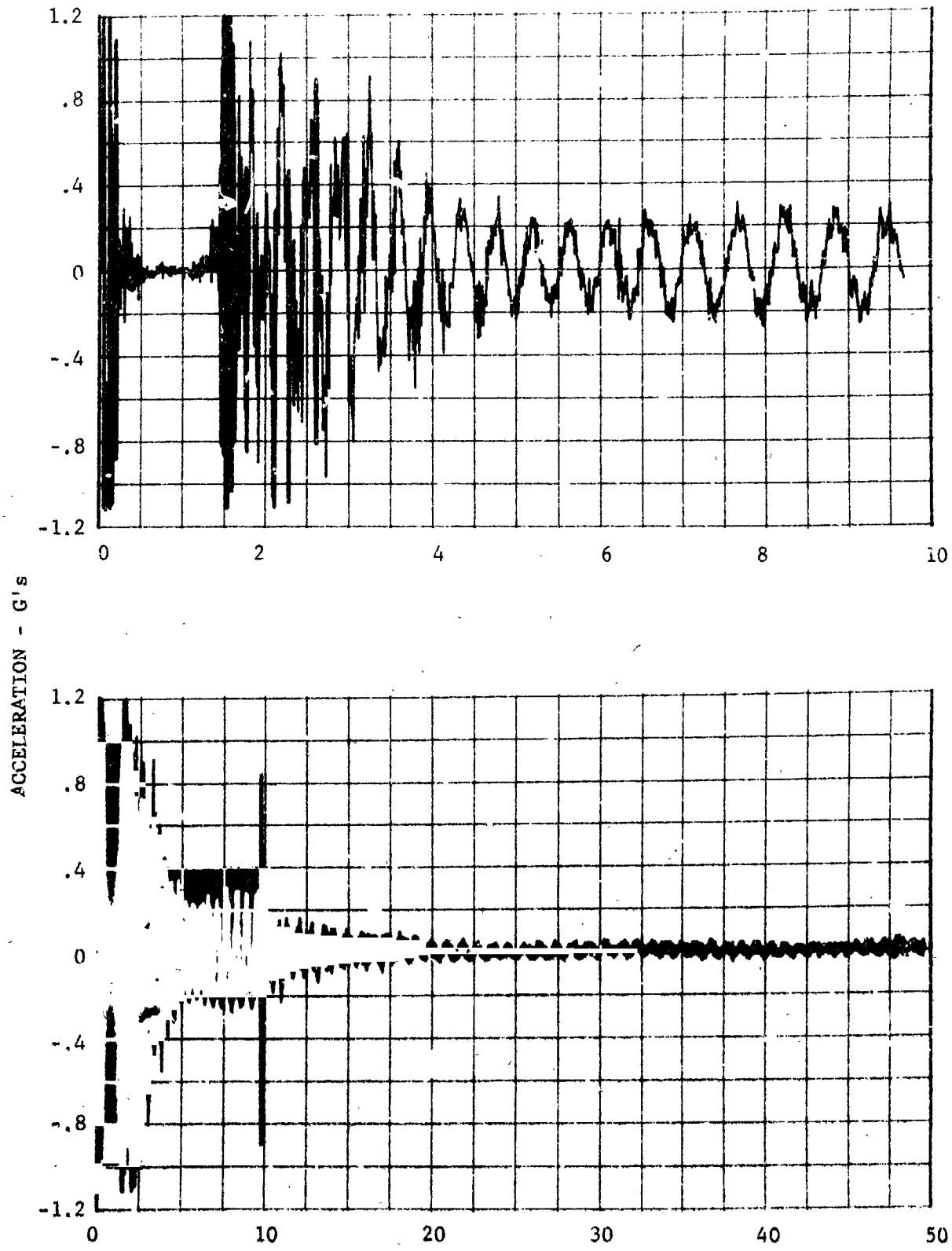

FIGURE V-16 TRANSVERSE ACCELERATION

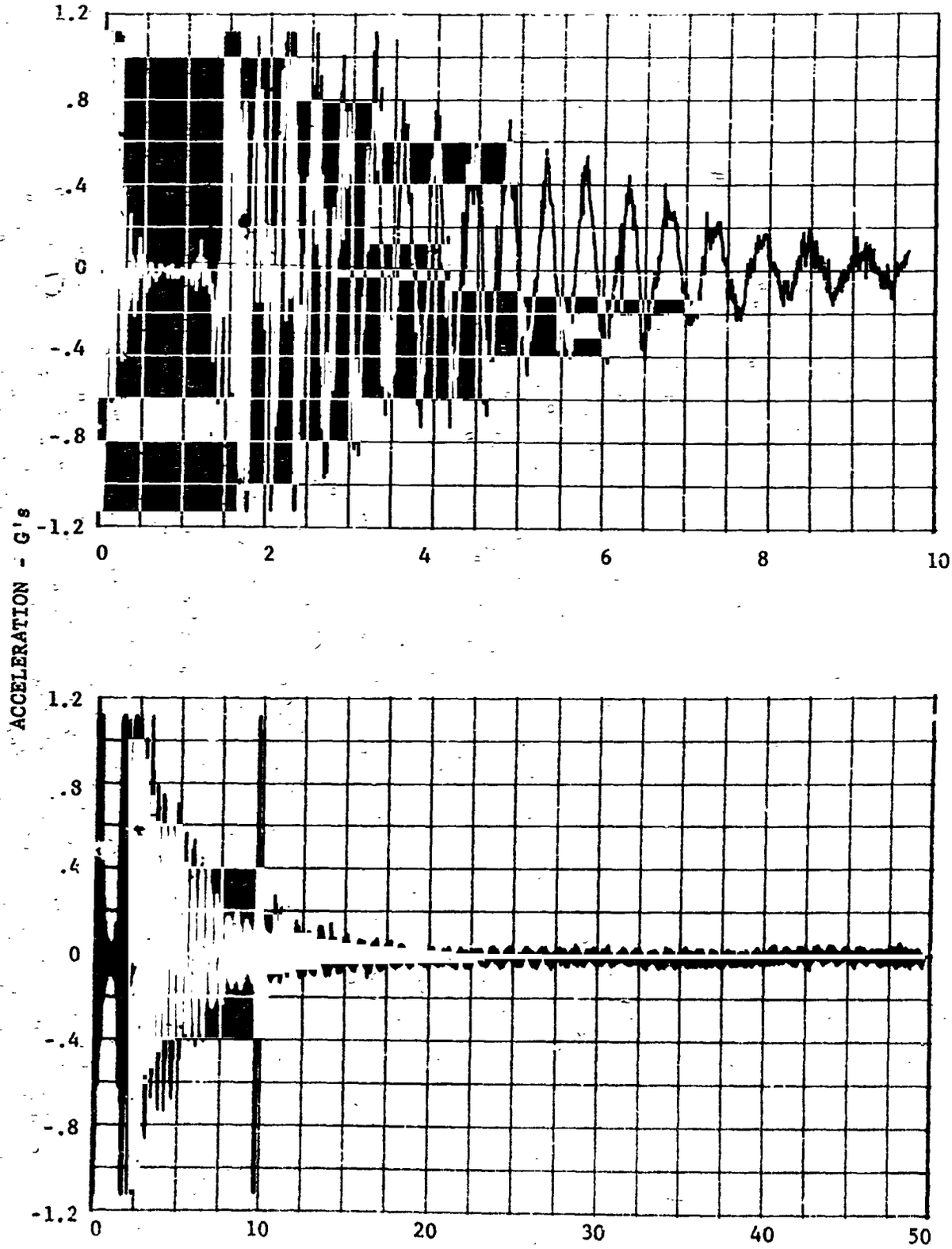

FIGURE V-17 NORMAL ACCELERATION

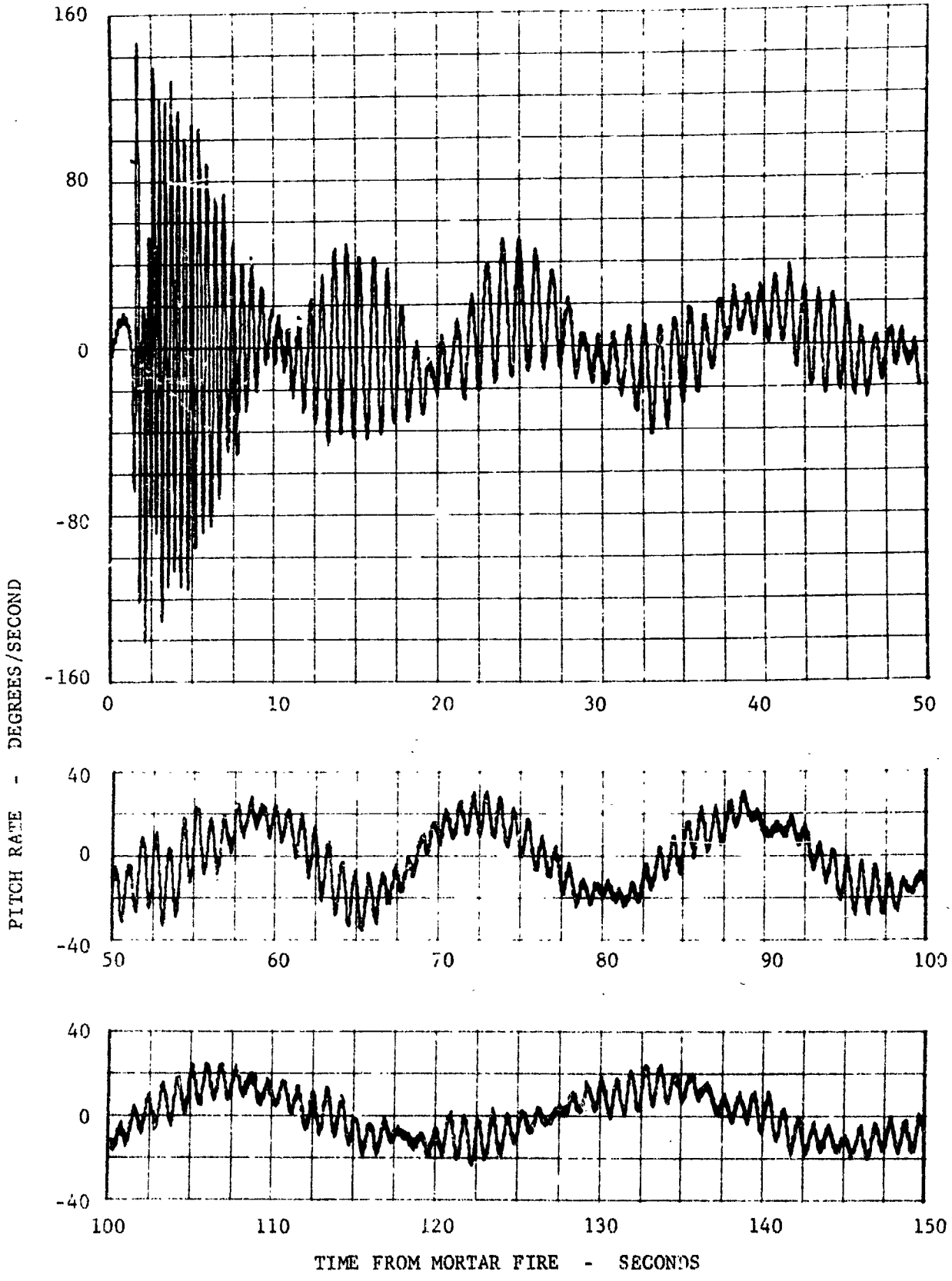

FIGURE V-1[illegible] VEHICLE PITCH RATE

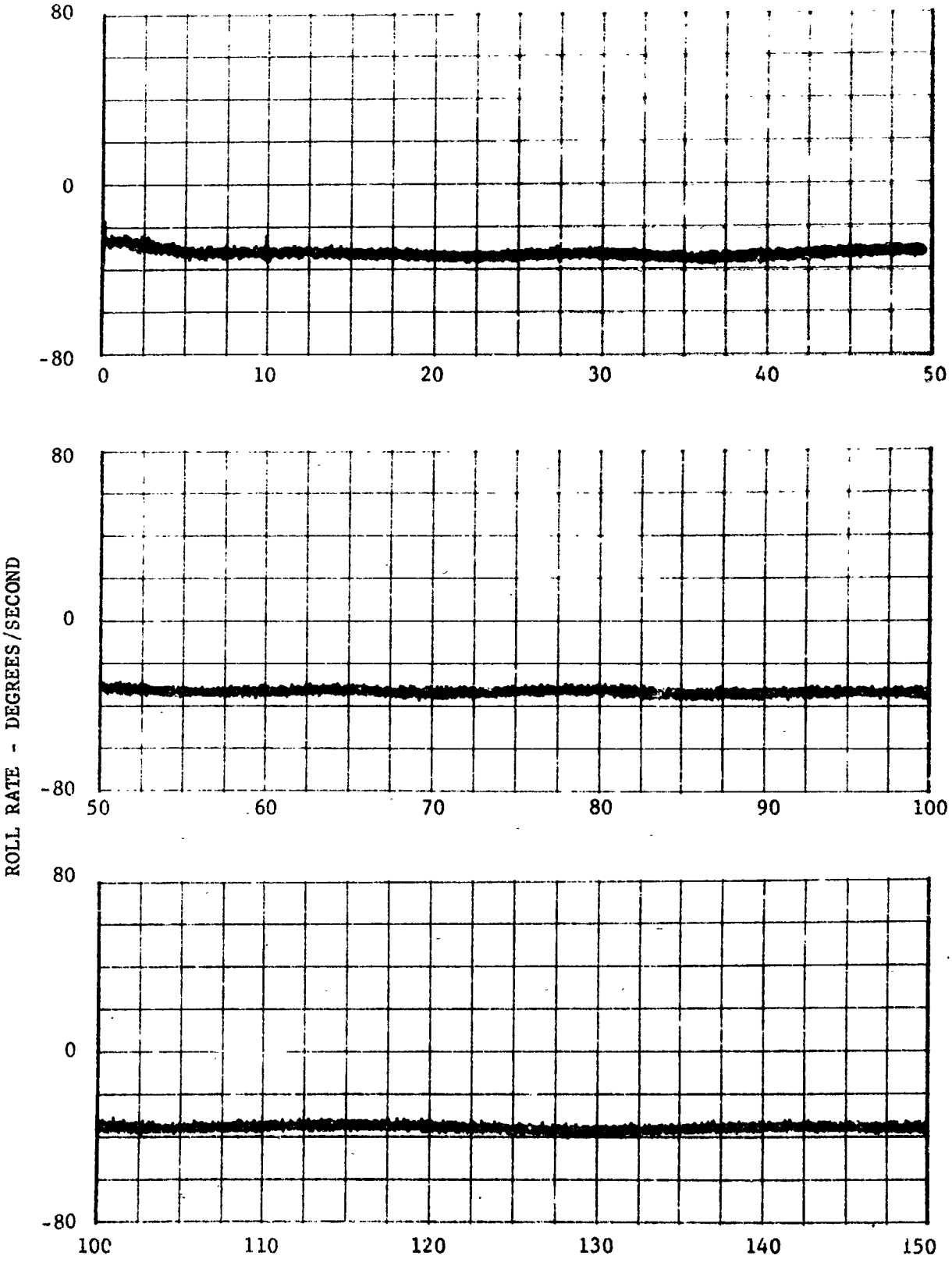

FIGURE V-19 VEHICLE ROLL RATE

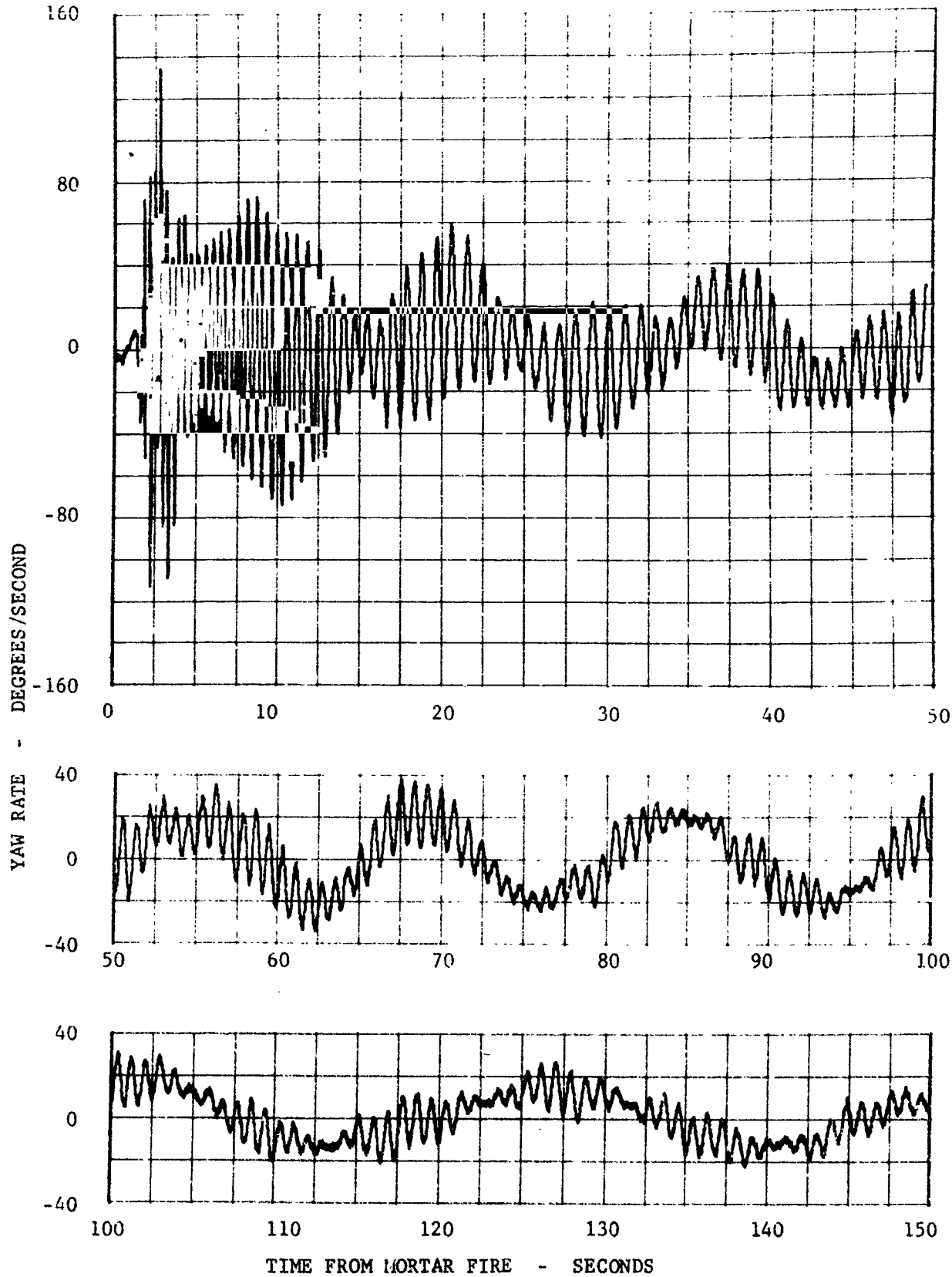

FIGURE V-20 VEHICLE YAW RATE

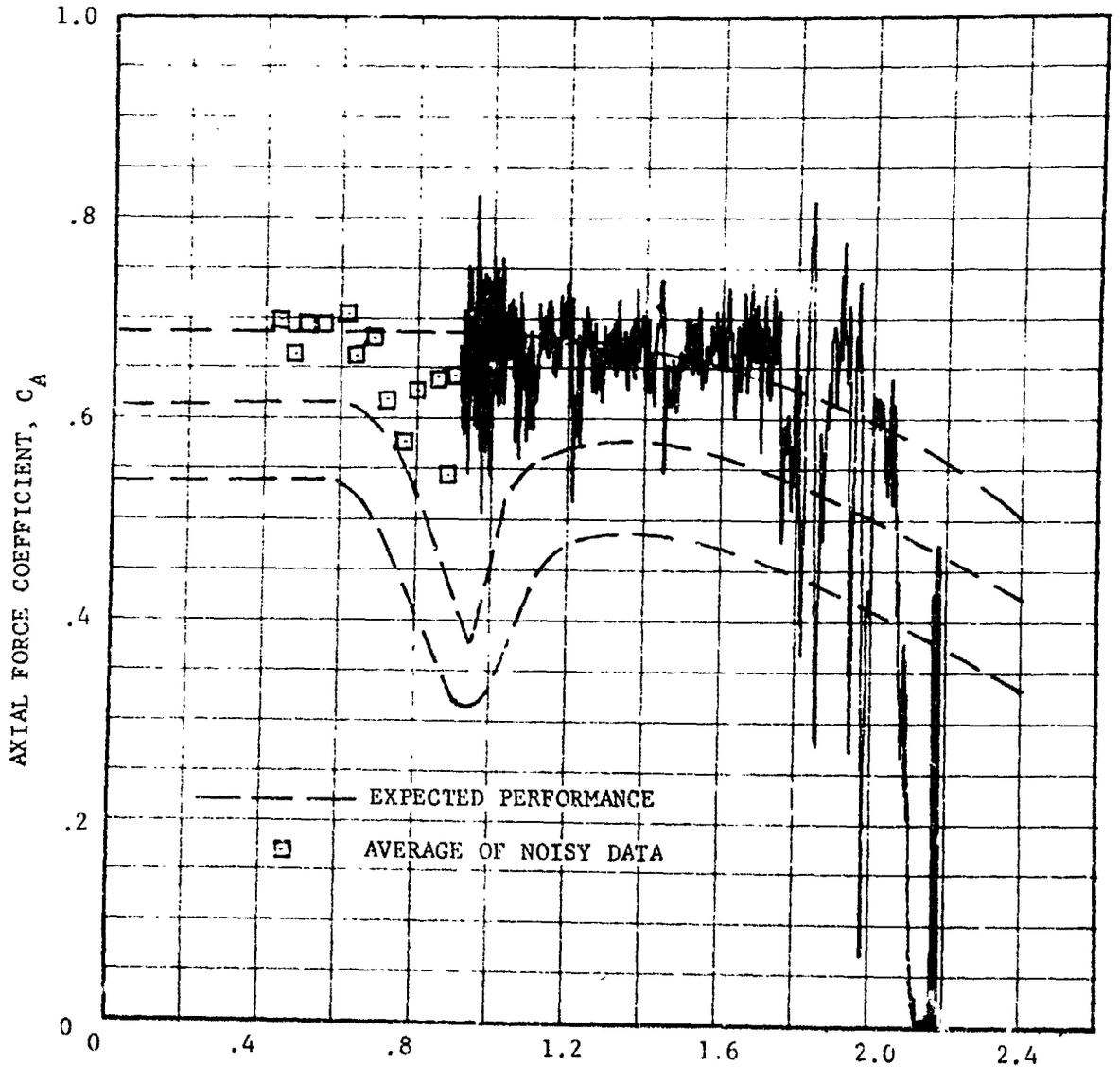

FIGURE V-21 PARACHUTE AXIAL FORCE COEFFICIENT
(ACCELEROMETER DATA)

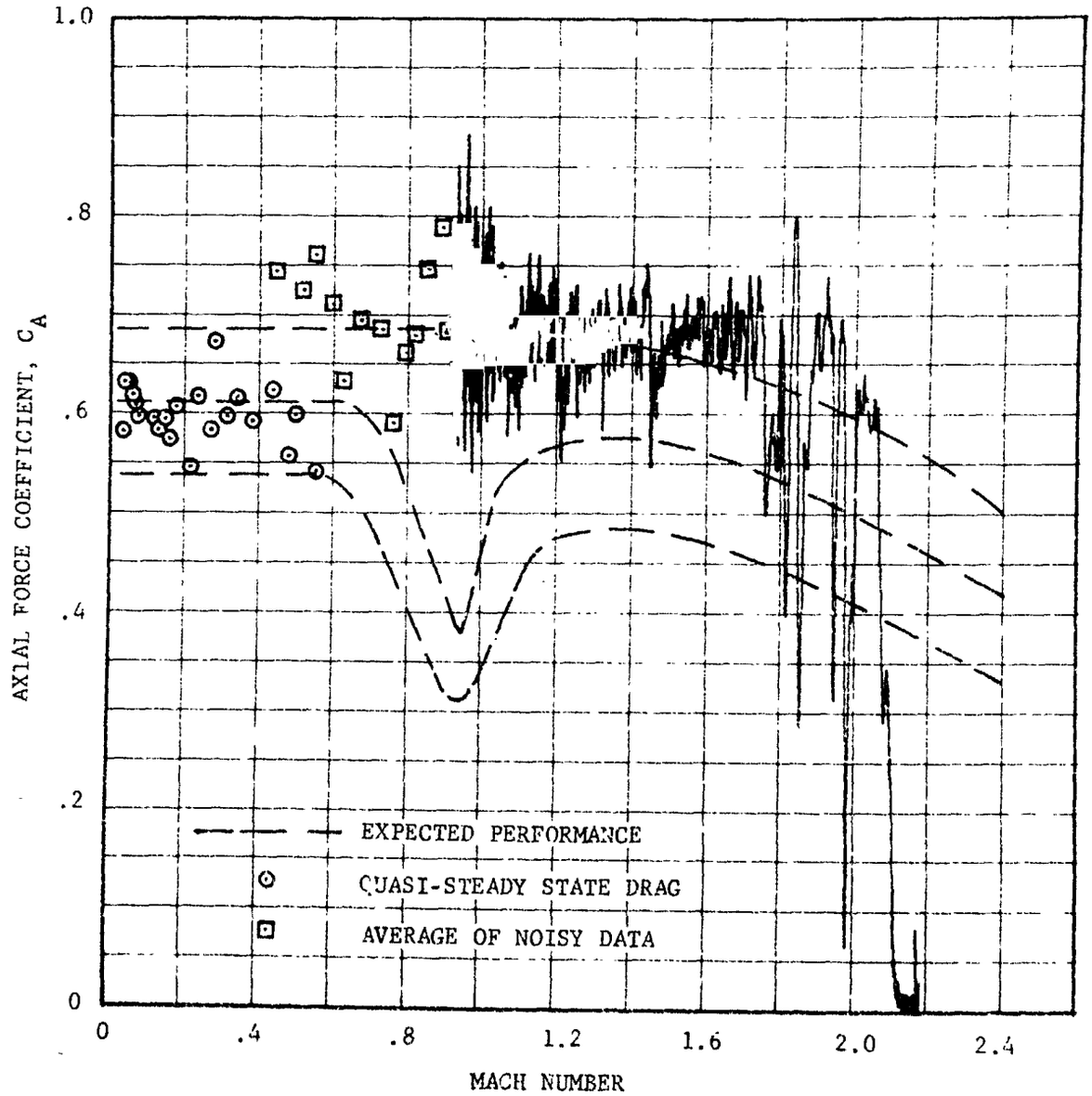

FIGURE V-22 PARACHUTE AXIAL FORCE COEFFICIENT (TENSIOMETER DATA)

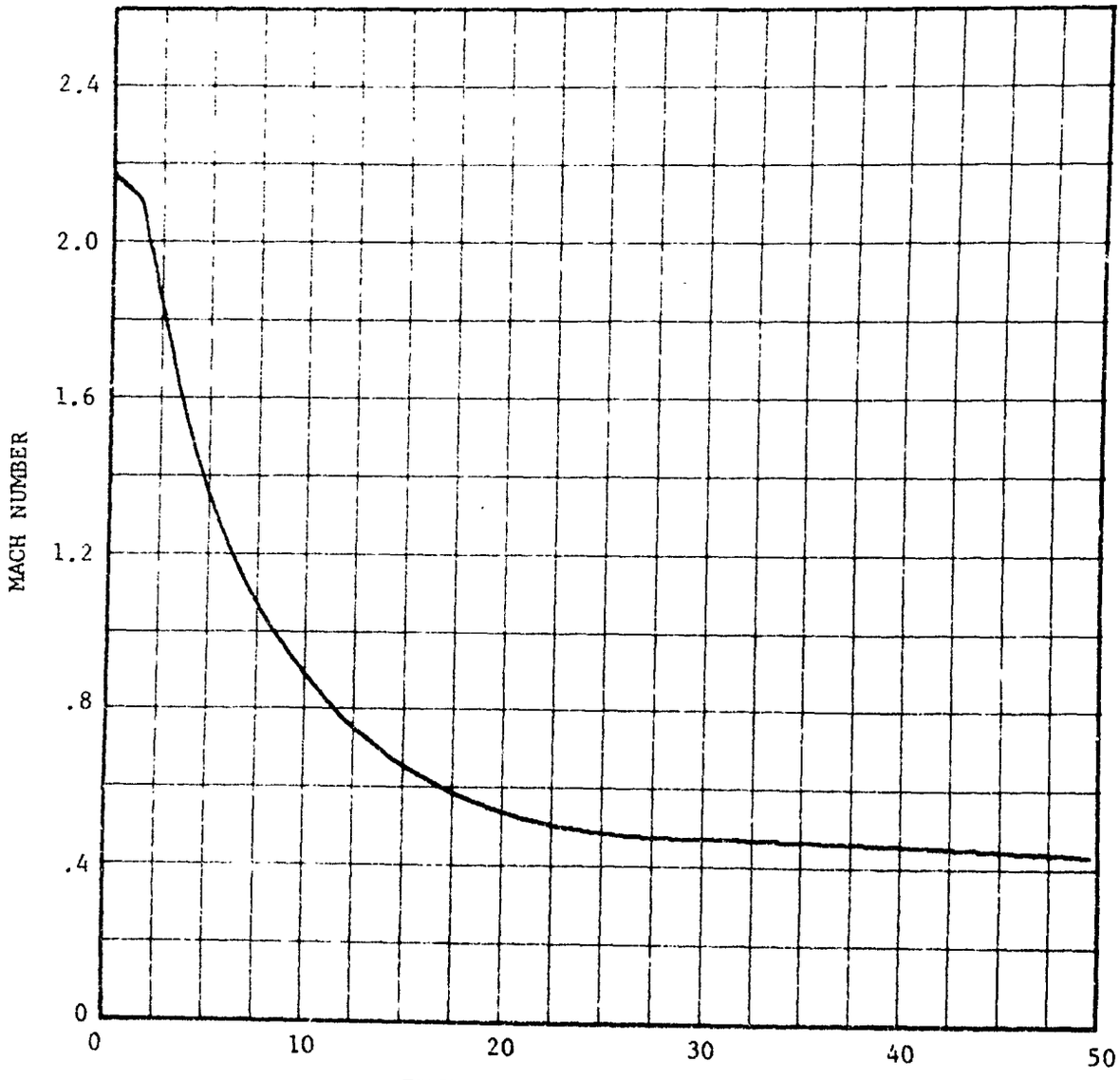

FIGURE V-23 MACH NUMBER TIME-HISTORY

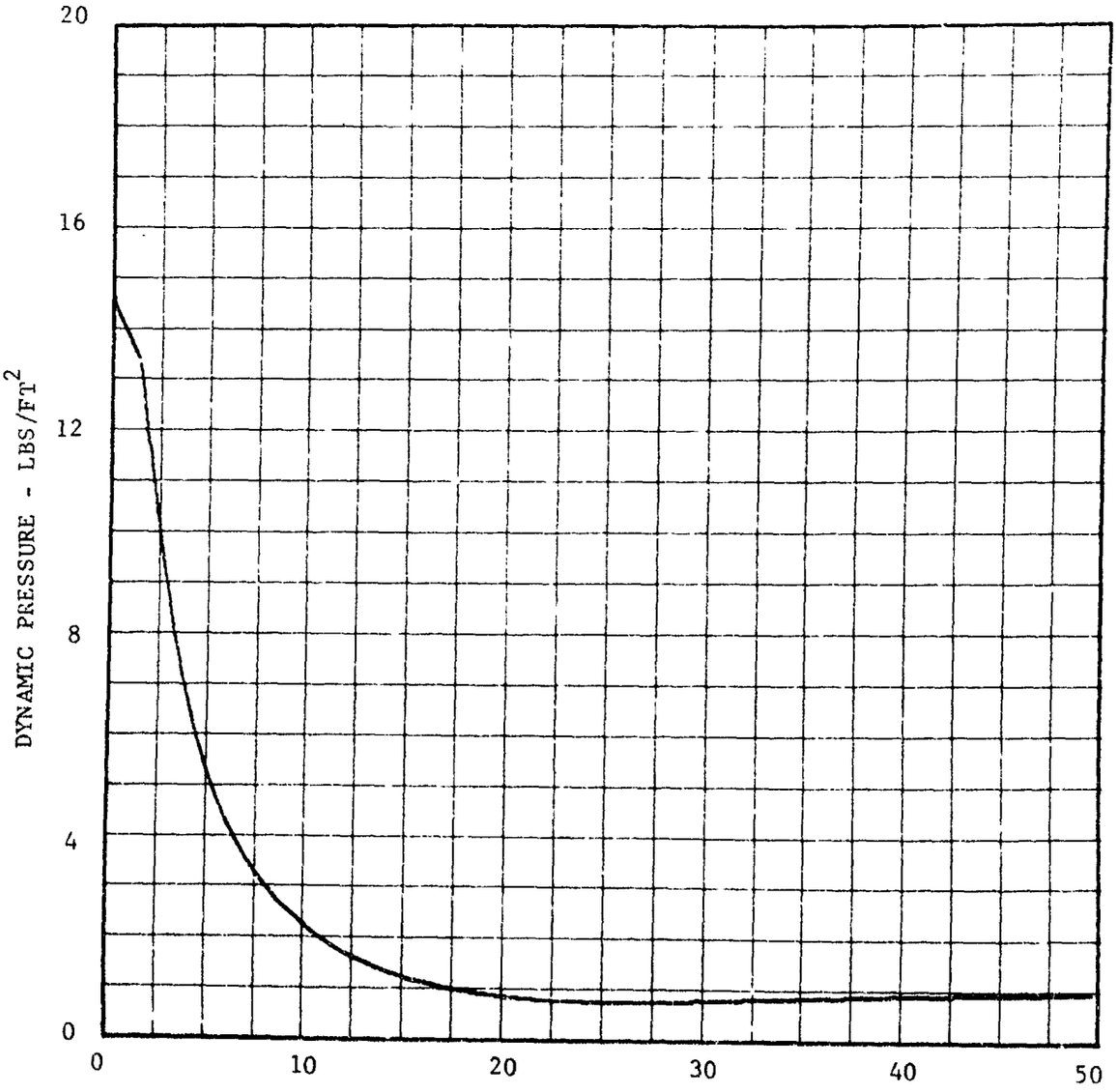

FIGURE V-24 DYNAMIC PRESSURE TIME-HISTORY

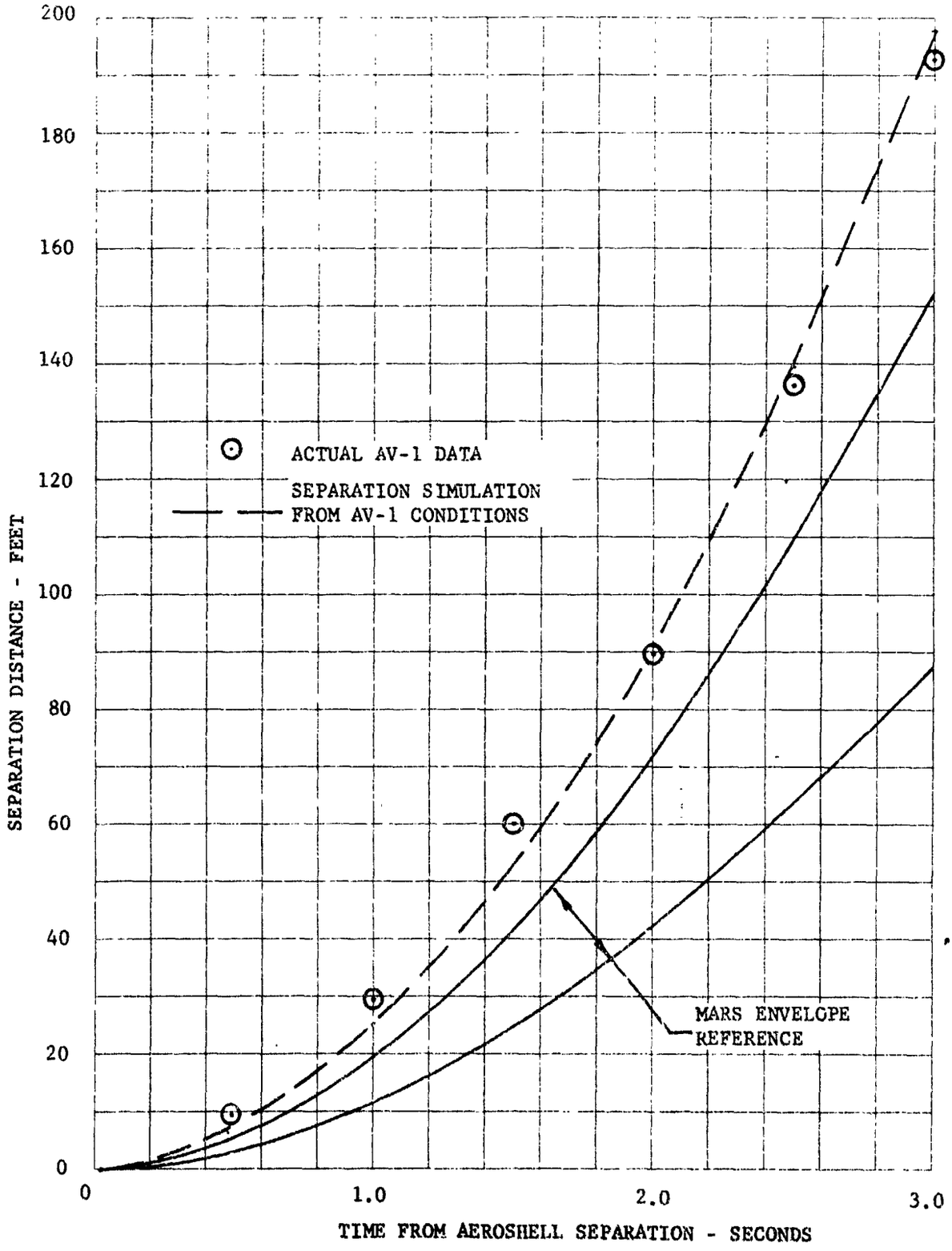

FIGURE V-25 AEROSHELL SEPARATION DISTANCE, 0-3 SECONDS

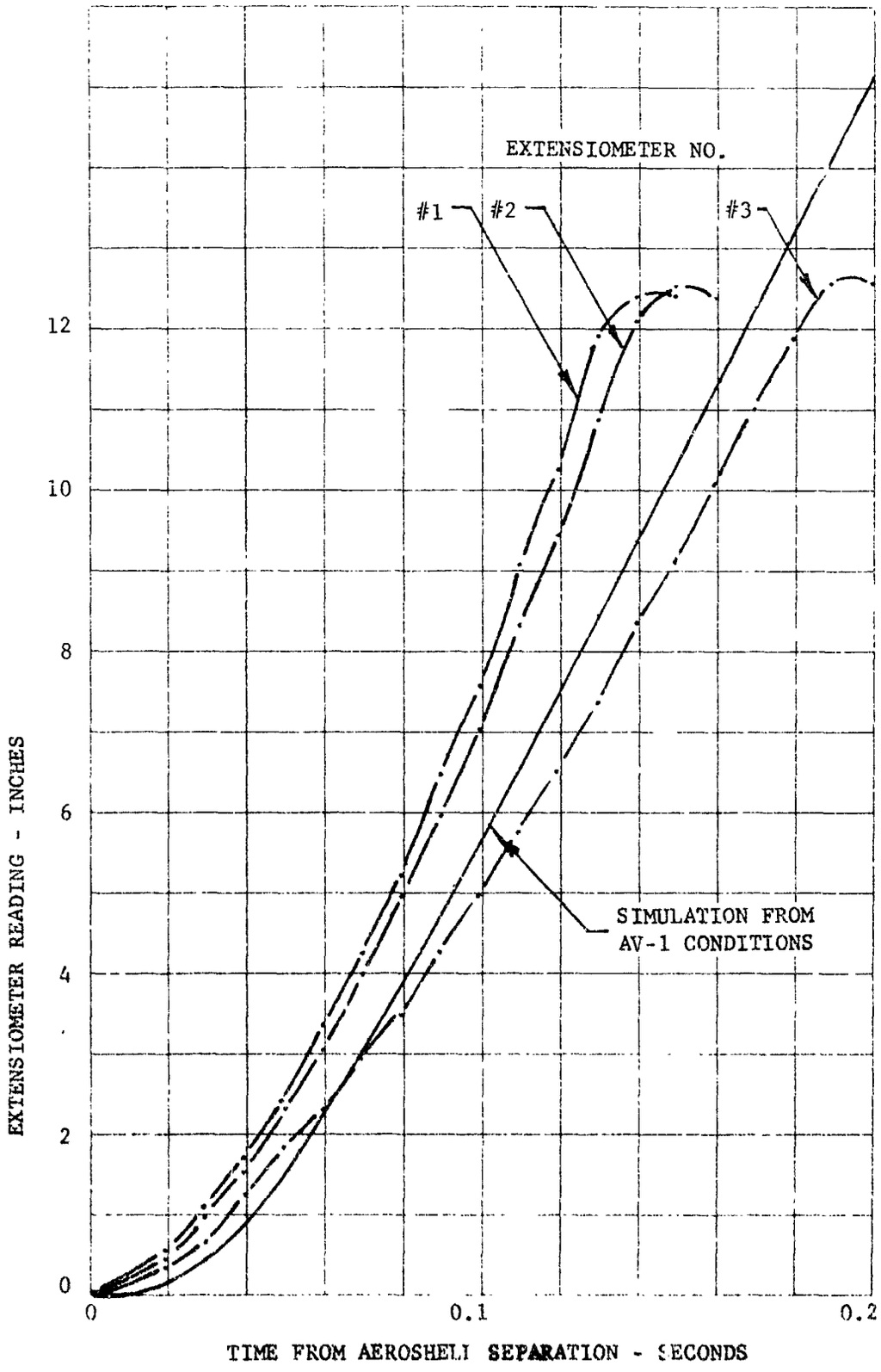

FIGURE V-26 EXTENSIOMETER SEPARATION DISTANCE

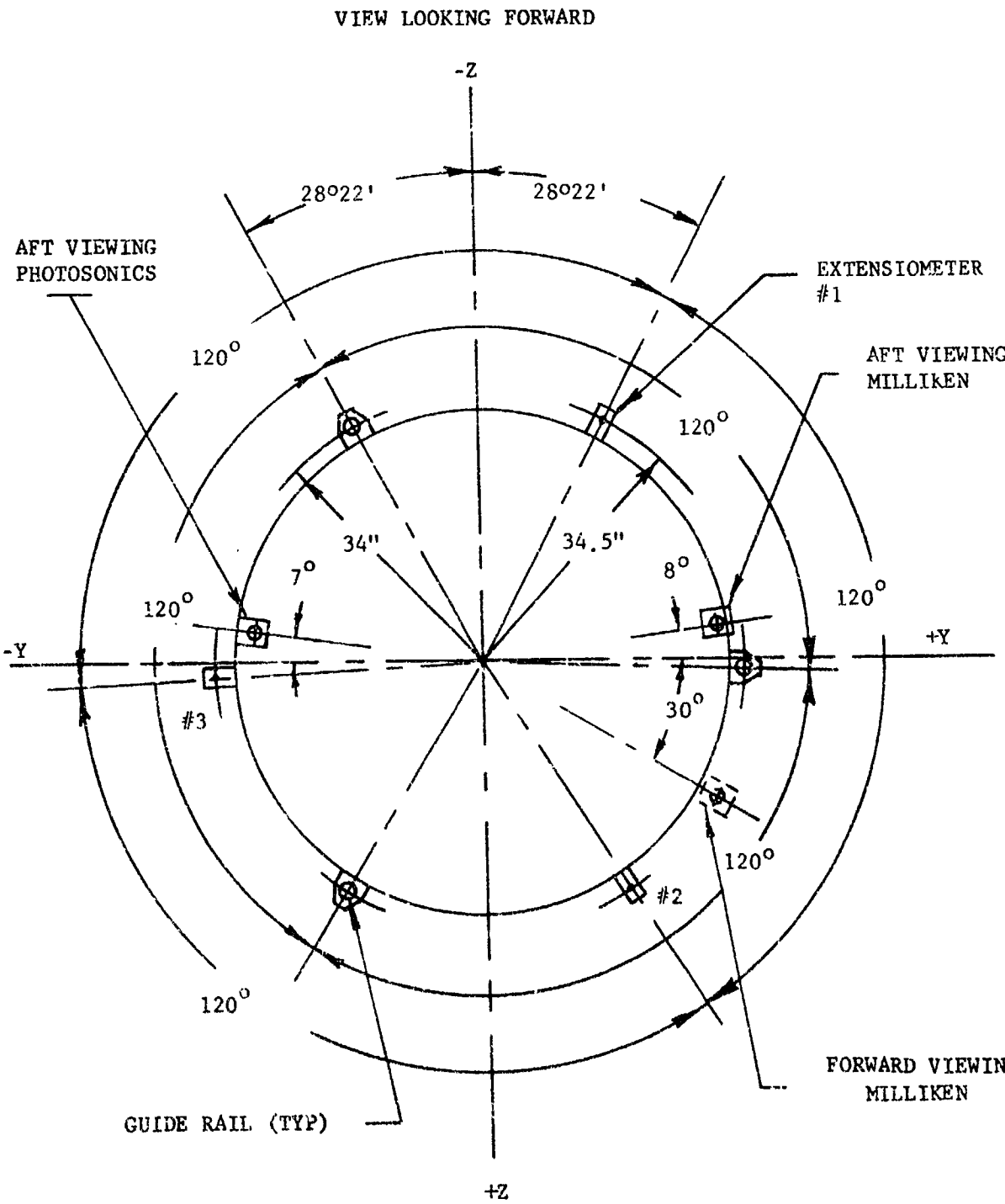

FIGURE V-27 EXTENSIOMETER AND GUIDE RAIL LOCATION

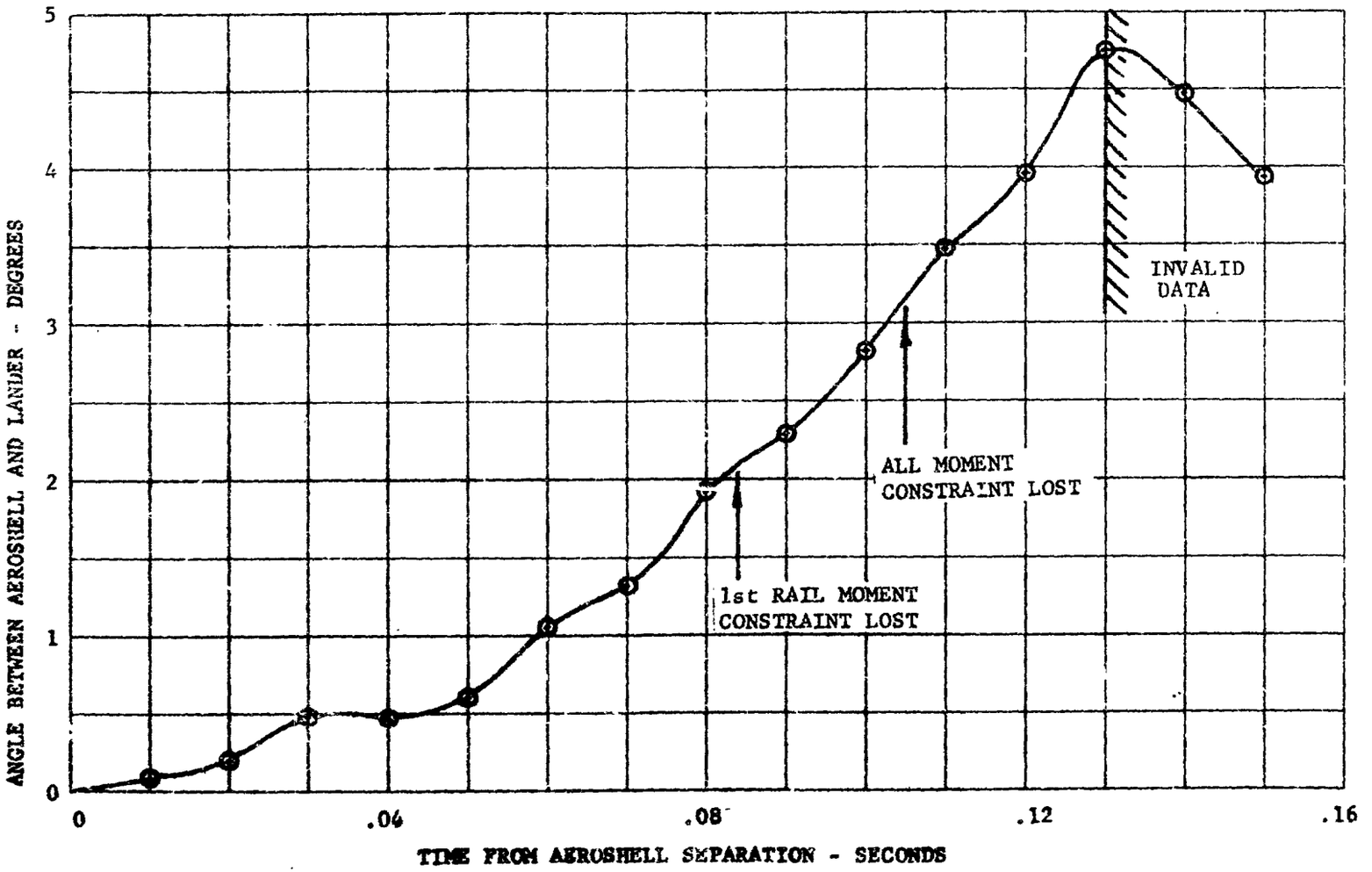

FIGURE V-28 RELATIVE ANGULAR MOTION BETWEEN AEROSHELL AND LANDER

VI. VEHICLE PERFORMANCE ANALYSIS

The following is a summary assessment of the BLDT vehicle performance. The summary is presented by subsystem/discipline:

A. Flight Dynamics

The objective of the flight dynamics portion of the report is to establish the actual flight performance of the AV-1 vehicle from the command for vehicle release from the load bar through the command for decelerator mortar fire. As part of this analysis, the intent is to further establish the rationale for the overtest dynamic pressure condition which existed at parachute deployment.

The vehicle performance requirements for the supersonic vehicle are established based on Mars anticipated environments and characteristics of the BLDT vehicle which might differ from the actual VLC. These performance requirements are:

1. Resultant angle of attack at mortar fire $\leq$17 degrees.
2. Residual spin rate at deployment $\leq$100 degrees/second.
3. Mach Number and dynamic pressure at peak load within the test envelope shown in Figure VI-1.

Figure VI-1 provides the target mortar fire and anticipated peak load conditions of:

	MACH NUMBER	DYNAMIC PRESSURE (psf)
Mortar Fire	2.27	11.8
Peak Load	2.17	10.66

The peak load requirements box is established such that a 2σ dispersion ellipse of dynamic pressure, based on BLDT performance parameters tolerances, is adjacent to the 30% overload limit of the decelerator and at a Mach number greater than 2.0.

The actual flight condition, also shown on Figure VI-1, is at a dynamic pressure in excess of the established envelope which resulted in an overtest condition necessitating the reflight of the supersonic mission.

1. Data Sources

The intent of this section is to evaluate the flight performance of BLDT AV-1 by reconstructing its trajectory using flight test data. The reconstruction is primarily based on three sources of data:

- Meteorological data (density, velocity of sound, and winds);
- Telemetry data (accelerometers and gyros); and
- Radar data (slant range, azimuth and elevation).

a. Meteorological Data - Meteorological data were obtained by standard WSMR radiosonde observations (RAOB) and LOKI rocket probes. The RAOB probe produced pressure, wind direction and velocity and temperature at 5000 feet intervals from surface to approximately 110,000 feet. The LOKI rocket probe produced temperature and wind data at 5000 feet intervals from 80,000 feet to approximately 150,000 feet. The combination of the RAOB and LOKI data defined the atmospheric parameters from surface to altitude. Three atmospheric profiles were obtained for the AV-1 flight as follows:

f-24 hr. data:

LOKI #0130	launched 10 July 1972
RAOB #123	launched 10 July 1972

T-1 hr. data:

RAOB #125	launched 11 July 1972
LOKI #0133	launched 11 July 1972

T+1 hr. data:

RAOB #207	launched 11 July 1972
LOKI #0133	launched 11 July 1972

The T-24 hr. data were used by the real time computer during the actual flight to predict impact and command mortar fire. A comparison of the density of the above 3 sets of data shows that the T-1 hr. data were the average. Therefore, the T-1 hr. data as shown in Table VI-1 were used for all flight performance analysis.

b. Telemetry Data - The flight vehicle telemetry (TM) data was transmitted via an S-band link to the WSMR receiving stations J-10 and J-67 where it was recorded and retransmitted via microwave links to the flight operations control station at building 300. These receiving stations are geographically located to provide continuous coverage of the real time mission. Their locations are shown in Figure VI-2. At Building 300, the TM data were recorded for post-flight usage and also terminated at various displays for observation and control of the mission.

Due to the excessive noise level which was encountered on the Building 300 recorded data, all analysis is performed using the data which was recorded at the J-10 receiving station.

The conditioned and smoothed TM accelerometer and rate gyro data, which were used for flight performance analysis, are shown in Figures VI-3 through VI-6. Figures VI-3 and VI-4 are gyro and accelerometer data respectively for the time period prior to the vehicle release from the load bar. The effect of pointing commands are reflected in the spin and yaw gyro data.

Figures VI-5 and VI-6 are the same data during vehicle powered flight. It is noted that all of the accelerometer and gyro data were smoothed and conditioned except the accelerometer data prior to drop which was only conditioned. These data were filtered with a seventy (70) point standard least squares quadratic leading edge filter. The conditioning was based on a two sigma (2σ) dispersion limit of the filtered data with wild points replaced by the quadratic prediction.

The initial estimates of instrumentation bias, were obtained from these plots by integrating the gyro data during the float period (Figure VI-3 and adjusting the accelerometer data for zero setting during the free fall portion of flight immediately after release from the load bar (Figure VI-4). The TM instrumentation system is designed to provide a 5% end to end error tolerance limit but with the above biases it is judged that the instrumentation accuracies can be assumed to be 2%. This provides the following accuracies:

FUNCTION	TOLERANCE
Gyros	6 deg/sec
Lateral Accelerometers	0.02 g's
Longitudinal Accelerometer	0.10 g's

c. Radar Data - The BLDT vehicle was tracked by (7) seven WSMR FPS-16 radar sets, four (4) were beacon track and three (3) were skin track. The beacon track radars (R114, R123, R125 and R127) were used for continuous track of the vehicle until loss of beacon (T + 40) sec) at which time they switched to skin track. The skin track radars were utilized to track other system components such as balloons, load bar and aeroshell. The stated accuracy of the FPS-16 radars is 0.1 to 0.3 mils in angles and 15 to 45 feet in range, which is approximately 50 feet of space position.

The radars provided slant range, azimuth and elevation data with respect to the radar site. Due to inherent accuracy, only the beacon track radar data were used in performance analysis. These radar locations are shown in Figure VI-2.

The radar data were post flight corrected by WSMR for systematic errors which were determined by pre-flight calibrations. Raw data of range azimuth and elevation were smoothed by standard WSMR filter techniques to produce velocity, altitude, flight path angle and azimuth. The corrected and smoothed data from all four beacon sites were in close agreement providing a high degree of confidence in the data. An example of the close agreement is evidenced in the drop altitude which varied only 34 feet between the four radars.

Velocity, flight path angle and altitude data are presented in Figures VI-7 through VI-9 for radar site R123. These data are earth reference measurements and are not ambient aerodynamic conditions.

2. STEP Trajectory Reconstruction

The Statistical Trajectory Estimation Program (STEP) (Reference 9) was used to determine the reconstructed trajectory. This program solves for the initial conditions (position, velocity, and attitude of the vehicle) so that by integration of the gyros and accelerometers the trajectory matches the radar data (range, azimuth and elevation). Besides solving for initial condition it has the capability of determining the systematic errors (biases and scale factors) on the gyros and accelerometers. The program gives a minimum variance solution on the radar measurements (range, azimuth and elevation). The trajectory is considered to be the optimum when the radar data is randomly dispersed about the

reconstructed trajectory and the variance of the range, azimuth and elevation is within the expected tracking accuracies of the radar.

STEP requires an estimate of the biases and scale factors on the gyros and the accelerometers. In order to obtain these biases on the gyros, the telemetry data were examined from T-45 seconds to T+0 (vehicle drop). These data are shown in Figure VI-3. At this time the vehicle had very small motions and the centers of the oscillatory motions were determined to be the biases on the gyros. These biases are:

Roll gyro (P)	-2.09 degrees/second
Pitch gyro (Q)	-2.05 degrees/second
Yaw gyro (R)	-5.61 degrees/second

To determine the biases on the accelerometers, the data between T+0 and T+1 second was analyzed. These are shown in Figure VI-4. At this time the vehicle is in a near zero force field which permits establishing a new zero setting. The average values of the accelerometers at this time were:

X-accelerometer	-0.603 ft/sec^2
Y-accelerometer	-0.48 ft/sec^2
Z-accelerometer	-1.12 ft/sec^2

The scale factors on the gyros and accelerometers were initialized at unity.

The initial estimation of position and velocity at drop was obtained from smoothed radar data as:

Latitude	33.2334 deg.
Longitude	-106.2351 deg.
Altitude	120,536 ft.
Velocity	100 ft/sec
Flight Path Angle (gamma)	-1.7 deg.
Azimuth	279. deg.

The initial estimates of the body Euler angles are required for body heading (PSI), pitch (THETA) and roll angle (PHI). The initial Euler angle estimates are:

PSI	-13^{o}
THETA	52^{o}
PHI	0^{o}

The initial estimate for PSI was taken from the magnetometer reading at drop while THETA was estimated at 52^{o} based on the results of previously preformed 6 degree of freedom computer analysis.

Given these initial conditions and previously established biases and scale factors STEP was not able to provide a comparative fit to the radar data between T+0 and T+38 seconds. STEP continued to give very poor agreement with the radar data when attempts were made to revise the scale factors on the gyros. The most sensitive parameter was the scale factor on the roll gyro (P). By varying the scale factor on P between 0.98 and 1.01, STEP returned an initial theta (drop pitch attitude angle) between 47 and 57 degrees.

The reason STEP has difficulty in converging on an optimum trajectory was because of the type of trajectory the BLDT vehicle was designed to fly. Between T+2 and T+9 seconds the vehicle has a gyroscopic turn of about 13^{o}. During this turn STEP must have the proper roll angle history to be able to integrate the measured forces in the proper direction. An error in PHI of only a few degrees causes the reconstructed trajectory to diverge from the radar track. During the time of drop, spin up, and main engine ignition the instrumentation package is subject to high shock loads which amplify the data noise level. It is very difficult to remove only the noise due to the shock without also adding biases to the data.

In order to avoid this data noise problem, STEP was initialized at T+12 seconds with the initial position and velocity being obtained from radar data. Using Euler angles, obtained from the previous best STEP trajectories, and radar data from Radar Site R123 for every 0.1 seconds between T+12 and T+38 seconds, STEP was able to obtain a very good reconstructed trajectory. The radar track data deviated from the reconstructed trajectory by the following standard deviations.

$\sigma_{\text{slant range}} = 3.65$ ft.

$\sigma_{\text{azimuth}} = 7.23 \times 10^{-3}$ deg $\approx$ 25 ft. (position error)

$\sigma_{\text{elevation}} = 5.52 \times 10^{-3}$ $\approx$ 18 ft. (position error)

STEP was also programmed to compute the best estimate of the biases and scale factors on the gyros and accelerometers. The following are the biases and scale factor which STEP estimated compared with initial estimates:

	STEP ESTIMATE	INITIAL ESTIMATE
Roll gyro scale factor	.99251	1.000
Pitch gyro scale factor	1.00025	1.000
Yaw gyro scale factor	1.00000	1.000
Roll gyro bias	-2.12 deg	-2.09 deg
Pitch gyro bias	-1.92 deg	-2.05 deg
Yaw gyro bias	-5.60 deg	-5.61 deg
X-accelerometer scale factor	1.001176	1.000
Y-accelerometer scale factor	1.00015	1.000
Z-accelerometer scale factor	.999874	1.000
X-accelerometer bias	-0.60233 ft/sec^2	-0.603 ft/sec^2
Y-accelerometer bias	-0.47968 ft/sec^2	-0.48 ft/sec^2
Z-accelerometer bias	-1.1204 ft/sec^2	-1.12 ft/sec^2

The fact that the STEP systematic errors on the system data very closely approximates the initial data scale factors and biases verifies that both the radar data and the flight TM data accurately depict the vehicle flight from T+12 seconds through mortar fire.

STEP reconstructed trajectory provides a very accurate measurement of altitude and velocity. Combining this value with the met data, velocity relative to the wind, Mach number and dynamic pressure was compiled. Time history of altitude, velocity, Mach Number and dynamic pressure are shown in Figure VI-10 and VI-11. Figures VI-12 and VI-13 show the body and velocity vector orientation versus time. The conditions established by STEP at mortar fire and peak load, provided in Table VI-2, show that the flight performance did not meet the requirements for dynamic pressure as required in Figure VI-1.

The angle of attack, sideslip and total angle of attack are shown in Figures VI-14 and VI-15. The total angle of attack shown on Figure VI-15 never exceeds the value of 15° which is less than the required value of $\leq 17^{\circ}$. The value provided by STEP of 7° at mortar fire differs from the value of 13° derived from analysis of the aft facing camera films. Small roll errors integrated across the time period of T+12 seconds to T+38 seconds will cause small errors in the orientation of the body axis which look like a time shift to the STEP program. This small shift at a time when the angle of attack is changing rapidly provides a large difference in the value of angle of attack.

3. Flight Anomaly Analysis

The major flight anomaly was the low flight trajectory which was experienced in that the vehicle did not achieve the specified flight

altitude for decelerator deployment which in turn resulted in a high dynamic pressure overtest during parachute inflation.

Other flight anomalies to be discussed in this and subsequent sections include:

- o Spin rate, despin rate and spin rate decay
- o Aerodynamic moments
- o Thrust inconsistencies
- o Cg Offset

a. Dynamic Pressure Overtest - Sensitivity analysis reveals that test altitude is most effected by variation in drop attitude. Analysis of the launch films and inspections of recovered spent vehicle show that the support structure was damaged during the launch process. Analysis of the load bar camera film reveals that the vehicle has shifted between calibration and actual drop (See below), causing the support structure configuration to have changed and drop attitude to be uncertain. Comparison six-degrees-of-freedom (6 DOF) (Reference 10) computer runs were made, to determine if balloon launch operations damage to the support structure could cause the overtest conditions, before retesting the supersonic condition with BLDT AV-4. These comparison data showed that the most likely drop attitude was 52°. The actual flight data were input to the 6 DOF for the study. These data were:

- o Atmospheric properties
- o Thrust properties (longitudinal accelerometer)
- o Initial drop heading (magnetometers)
- o Event Times
- o Actual Motor Alignment

The results of this analysis are compared with actual radar data in Figures VI-16 through VI-19.

Figure VI-16 presents the predicted profile of flight altitude rate versus time for a drop pitch altitude of 52^{o} and 55^{o}. Also shown in dashed line is the actual flight altitude rate which was derived from radar data which was verified by the STEP 2 analysis. This shows that the actual altitude rate very closely approximates the predicted 52^{o} drop altitude trajectory.

The 52^{o} drop altitude is further substantiated by the close correlation of actual to predicted values for the following parameters:

- Figure VI-17 - Altitude versus Time
- Figure VI-18 - Dynamic Pressure versus Time
- Figure VI-19 - Flight Path Angle versus Time

The above correlation of data strongly establishes that the drop attitude was the major contributor to the low altitude anomaly. Furthermore, vehicle AV-2 and AV-4 establishes that system biases were within the dispersion analysis ellipse while vehicle AV-1 was considerable outside the dispersion predicted by the 6 DOF program.

A review of physical evidence was conducted to determine anomalies in the initial drop attitude. The scratches on the aeroshell caused by the disengaged stabilizing bars were found to principally indicate clockwise and counter clockwise vehicle rotation about the suspension axis. It was impossible to determine the position of the stabilizing bars at the time of drop.

Overlays of the down looking load bar calibration and drop films were made to determine possible vehicle position changes with respect to the load bar. Similar films from AV-2 and AV-4 were used to establish a baseline. The overlays are shown in Figures VI-20, VI-21 and VI-22. Only significant details have been included. The plumb bob was not useful

because it was moving prior to drop. Note that for AV-2 and AV-4 the shifts are small and are attributable to differences in load bar deflection resulting from different ways the load bar is suspended during drop. For AV-1, however, the position changes appear to be different in nature and of much larger magnitude.

Detailed analysis of the calibration and drop load bar films for AV-1 revealed that the vehicle had rotated in the order of approximately 3 degrees about the suspension axis which changes azimuth but does not change vehicle drop attitude, and also that it had rotated in the order of approximately 1.8 degrees about an axis perpendicular to both the suspension axis and the vehicle Y-axis. This rotation results in a decrease in the vehicle attitude in the order of 1.5 degrees, reducing the drop attitude to 53.5 degrees.

The above conclusion is qualitative in nature because of limitations in the data. However, the evidence strongly supports a nose down attitude bias which could have been as low as 52 degrees as indicated above.

b. Spin Rate - The spin rate decay was interrupted at 7 seconds (see Figure VI-5) for about 3 seconds. This phenomenon can occur due to a number of reasons. The most obvious is an external roll torque due to either aerodynamic forces or propulsive thrust misalignment. A further source was noted during 6 DOF simulations of the effect of cross products of inertia. Previous predictions of flight performance, such as presented in Reference 11 showed such tendency. The magnitude of cross products necessary to duplicate the flight data is estimated to be less than 4 slug-ft^2. The asymmetric pitch/yaw oscillations are also indicative of a principle axes asymmetry of which the cross products of inertia are a measure. These gyro data can also arise from misalignment of the gyros relative to the principle axes of the vehicle.

c. Lateral Accelerations - The Y and Z axes show a bias during powered flight which is probably due to their offset from the center of gravity. This causes centrifugal accelerations due to body motions to be superimposed on their output. This effect, as well as the dynamic noise level of the rocket motors masks any lateral thrust magnitude determination.

B. Capsule Aerodynamic Characteristics

The aerodynamic characteristics of the vehicle agreed with prediction after thrusting and despin and before mortar fire. The aerodynamic forces prior to this time cannot be seperated from thrust vector effects and inertial cross coupling due to roll. Using a simplified inertial model with no cross products of inertia, the total applied moment on the vehicle was evaluated. This flight data was quite noisy due to the required differentiation of the flight data, and is not presented. However, when these

flight moments were compared to the moments generated by a 6 DOF trajectory simulation of the flight, the amplitude of predicted moments compared well with maximum total moments in pitch between +100 and -250 ft-lb (due to the offset cg) and yaw moments within $\pm$ 200 ft-lb.

C. Thermal Control Subsystem

The design requirements for the BLDT Thermal Control subsystem were based on maintaining previously qualified hardware within the maximum and minimum specified qualification temperatures. Except for several insolated electrical heaters, a passive thermal control system was utilized on the BLDT vehicle for ascent and float control. The passive system was based on vehicle attitude and vehicle ascent rate to float altitude with convection, solar radiation, reflected solar radiation and infrared radiation being the major heat transfer parameters being considered.

The design ascent profiles are shown in Figure VI-23 with the fast ascent rate, when integrated with the above mentioned parameters, producing the hot case and the slow ascent rate producing the cold case. Figures VI-24, VI-25, VI-26 and VI-27 show select hot and cold case predicted temperature profiles for the base cover, rocket motor support structure, aeroshell and S-band transmitter respectively. Also shown in these figures are discrete point actual temperatures, extracted from the TM data which were recorded at approximately half hour intervals. It is noted that the actual temperatures generally remain within the hot and cold case predictions and are generally closer to the hot case as would be expected due to the actual ascent rate.

Presented below is a table showing the temperatures measured by the "on-board" thermistors at the time of vehicle release from the load bar and at aeroshell separation compared with the specified requirement at vehicle drop.

	SPECIFICATION REQUIREMENT (°F)		ACTUAL TEMPERATURE (°F)	
	MAX	MIN	DROP	A/S SEPARATION
Rate Gyro	125	0	77	76
Boost Motor #1	165	-65	60	160
Equipment Ballast	165	0	82	81
S-Band Transmitter #1	165	0	103	105
Instrument Beams #1	125	0	62	63
Bridle #1	210	-90	35	36
Aeroshell #1	175	-115	24	32
Boost Motor #2	165	-65	58	169
Mortar Canniscer #1	80	No Min	51	85
Mortar Breech	75	25	55	58
Instrument Beam #2	125	0	61	60
Bridle #2	210	-90	43	41
Aeroshell #2	173	-115	8	16
Rocket Motor Support Structure	(No Prediction)		46	48
Mortar Cannister #2	80	No Min	49	81
Mortar Breech Flange	75	25	51	68
Bridle #3	210	690	41	45
*Main Battery	80	50	45	46

*The thermistor titled "main battery temperature" is misnamed, it really measures rocket motor support structure temperature.

D. Structural Subsystems

The structural system provided adequate vehicle support and dynamic operation through all phases of the mission with the exception that the -Z axis compression fitting, which forms part of the flight vehicle to load bar support structure interface, was driven through the aeroshell supporting structure and into the payload portion of the vehicle.

There was no evidence of any structural failure in the load carrying structure other than that previously noted. Also, the dynamic portions of the structural system, including the aeroshell guide rail separation system and the flipaway lens covers, functioned as required.

As previously noted, the -Z compression fitting supporting structure failed in compression permitting the ball fitting to be forced through the structure and penetrating the payload where it lodged for the duration of the mission. The ball fitting was recovered with the parachute/payload during the recovery operations. Review of the launch films and visual observations during launch indicate that the vehicle was subjected to excessive loads as a result of launch crane travel across a grated concrete depression just prior to launch release. The films also show a pitch motion between the vehicle and the load bar support structure of approximately one foot as the crane crossed the depression which indicates that the supporting ball failure occurred at this point otherwise the vehicle pitch motion would be impossible.

Post recovery inspection and matching of the aeroshell and load bar support structure indicated that the loss of the upper compression fitting allowed the load bar support structure to separate from the two lower compression fitting. Scratches and gouges on the aeroshell in the vicinity of the lower fittings matched up with the load bar support structure legs indicating

that the load bar support structure legs traveled approximately 7.5 inches from their original position.

The socket on the -Z axis of the load bar support structure penetrated the aeroshell a minimum of three times as follows:

1. When the structure supporting the compression ball failed.
2. When a piece of the structure adjacent to the ball was broken off.
3. When an inspection port cover was punched out.

Inspection of the recovered hardware indicated the following condition:

1. Aeroshell - damage from compression pad failure, buckling of the inboard skins, nose cap poked out, 31.5 inch ring frame buckled slightly.

   All damage was ground impact damage except:

   a. Compression pad failure was launch damage.

   b. Buckled ring frame could have been ground damage or flight separation load damage (See page V-11)

2. Rocket Motor Support Structure - no visual damage.
3. Base Cover - Extensive damage resulting from impact.
4. Parachute Truss - no visual damage.
5. Equipment Beam - Damage resulting from impact.
6. Load Bar Support Structure - no visual damage.

E. Propulsion, Azimuth Pointing and Ordnance Subsystems

The Propulsive system on the vehicle include 4 Rocketdyne solid rocket motors and 10 spin/despin solid rocket motors made by Talley Industries. The main motors have classified performance characteristics, and therefore their specific performance parameters will not be given. In addition

to the solid rockets, pyrotechnic ordnance was used to effect load bar separation, aeroshell separation and camera lense cover opening. In addition, cold gas thrusters located on the AFCRL load bar were commanded thru the command system onboard the vehicle. These systems will be discussed in this section.

1. Spin/Despin Motor Performance

The spinup signal which occurred at 1.01 seconds after release from the load bar resulted in nearly simultaneous ignition of the six spin motors. The resulting spin rate was 204 degrees per second indicating approximately 4% high impulse. This rotation rate decayed during main rocket motors burning to a residual rate of 110 degrees/second, whereas the 4 despin motors then produced an incremental rate of 136 degree/second which is 6% higher than predicted. This higher effective performance of the spin/despin motors is probably in part due to plume over-expanding and recirculating to produce a pressure force on the spin/despin bracket. The base cover near the spin motors showed some evidence of plume impingement.

2. Main Propulsion System

The four solid rocket motors were ignited at 2.03 seconds after release from the balloon load bar and produced no noticeable thrust differential. They produced a slightly higher thrust level with an attendant shorter burn time which was well within their specification. There was no noticeable difference in their burn time and the thrust tail off was as expected. During motor support structure alignment verification, a slight distortion in the structure was measured which would have caused the rocket motors to have produced a roll torque. This led to a modification of the

rocket motor installation shimming procedures which should have eliminated this source of roll torque. The resulting change in roll rate during main rocket motor burning is attributable to the thrust damping and is close to the predicted change. The thrust vector alignment relative to the center of gravity was estimated based on the pitch/yaw rates at ignition prior to developing relevant aerodynamics forces and indicate the thrust vector was parallel to the X axis but displaced 0.050" from the center of gravity in the -Z direction and 0.055" in the +Y direction. A portion of this displacement was possibly due to the compression fitting ball which was broken off during launch. This ball was lodged some place in the vehicle and its mass could have shifted the center of gravity by as much as 0.010 inches. A thrust misalignment of this magnitude would cause an increase in dynamic pressure at mortar fire of 0.5 psf.

The anticipated plume recontact and recirculation in the base region did not produce relevant base heating. The ablative heat shield on the base and over the parachute bridle showed no evidence of heat either due to mortar plume radiation nor due to convective impingement. The aft camera lens covers also were not degraded by the rocket motor exhaust although some evidence of a dust-like deposit was noticed.

Post-flight inspection of the blast tube on Rocket Motor 3 (+Y,+Z) showed significant paint blistering. This condition could imply a thrust vector change due to blast tube deformation or nozzle erosion. The shock loading during launch could have dislodged propellant or caused separation of the propellant which, in turn, could give a thrust vector shift or thrust magnitude variation.

3. Azimuth Pointing Subsystem

The azimuth pointing system performed as predicted during flight. During ascent, the wind shears and main balloon inflation produced erratic

torques to the load bar which caused a maximum oscillation amplitude of approximately 2.5 revolutions, peak to peak, at 90,000 ft. altitude. The zero torque azimuth also varied during this period of time continuing until drop with an apparently sinusoidal variation. (See Figure VI-28). The pointing system cold gas thrusters were checked our during ascent by pulsing at times which would reduce the oscillation amplitude. This aided the natural damping of the system in reducing the oscillation amplitude such that when float altitude was attined, residual oscillation was the desired $\pm$180 degrees. Ballasting during ascent caused some change in the oscillations, however the torsional stiffness of the parachute suspension, based on the period of oscillation, agreed well with the cargo parachute torsional test measurements used for design, both before and after ballast dump (Figure VI-29).

There was not sufficient float time to determine the system damping, however, the oscillation amplitudes were not large enough fur the pointing system to require damping assistance to reduce the oscillation energy. When the required drop azimuth had been selected, pointing commands were given to stop the oscillation at the heading, however drift in the zero torque azimuth caused some difficulty in holding the desired azimuth so the vehicle heading was swung 360° and held against the more predictable resisting torque. This azimuth was approximately 180 degrees from null and the torsion was approximately 3.75 ft-lb at drop. This torsion was resisted by the pointing thrusters which produced approximately 0.63 lb. thrust over a 20 foot moment arm. The pointing pressure supply was consumed at 5.5 PSI per second of jet on time with a residual pressure at drop of 1115 PSI. A constant azimuth was maintained for 7 minutes prior to drop with the last pointing commands terminating 8 seconds before drop. The proper azimuth

was maintained to within 2 degrees during the time period and the rates were within 0.5 degrees/second.

During the flight, the magnetometer TM data were smooth and continuous. The control center displays of magnetometer data, both digital and analog, were adequate for steering the vehicle to the required heading.

4. Ordnance Subsystem

All pyrotechnic and pyromechanical devices performed such that all vehicle functions occurred as programmed. Post-flight inspection of the vehicle revealed that all ordnance functions occurred with no damage to the flight vehicle.

F. Electrical Subsystem

The electrical power and sequencing systems operated satisfactorily during the complete mission. All battery voltages and timed events remained within predicted/required limits.

Flight batteries were activated on 6-25-72 without problems. Battery voltages were above minimum at launch and as shown in Table VI-3 during this flight.

Camera batteries operated satisfactorily as evidenced by "on-board" camera operation during flight sequence.

Observation of batteries recovered from the vehicle following recovery showed a very small amount of electrolyte leakage. All battery voltages were still within the normal tolerance range. It is noted that the transient battery had been partially caved in at the electrical connector area.

The actual programmer sequence times are provided in Table VI-1.

The vehicle command system operated as required and received the following commands subsequent to the 08:35:07 launch,

Time	Command
15:47 hrs Z	Safe (Command System Ck.)
17:20 hrs Z	Start Azimuth Pointing (Pointing Continued intermittently till just prior to drop)
17:31:15.5 hrs Z	Arm Vehicle (Power Programmer on Next Pointing Command)
17:37:13:79 hrs Z	Vehicle drop
17:37:52:33 hrs Z	Mortar Fire

G. Instrumentation Subsystem

The 53 commutated data channels and the 16 continuous data channels performed without malfunction and provided useable data for each phase of the mission. The magnetometers supplied azimuth pointing data during the

float phase; the rate gyros, accelerometers, and tensiometers indicated vehicle motion and decelerator loads for the flight phase after drop from the balloon load bar. The displacement transducers provided data during the aeroshell separation phase. A temperature profile was acquired by 18 temperature probes and other commutated channels provided information for vehicle performance such as reception of range commands, programmer events, battery monitors, and other vehicle system monitors.

Although the instrumentation system performed without malfunction there were two anomalies which required investigation prior to the flight of the second vehicle.

The first anomaly involves the AGC measurement for the command receivers. During flight, the ground transmitter acquired the airborne receivers with a strong signal which should have caused the control room meters and the telemetry data to read full scale, however, the meters and TM data indicated a loss of AGC voltage. Investigation of this anomaly indicated that the ground decommutator sensed the airborne signal and reached a saturated condition. The ground system is designed such that it provides a zero output when a saturated condition is sensed. It was also determined that when this condition existed the Command Reception Indicator Panel indicated a slightly negative AGC voltage. Since this indication had no effect on the mission and vehicle status could be determined, no revisions were required for subsequent flights.

The second anomaly involved noise on various telemetry channels. There was excessive noise on four continuous data channels (IRIG 15 through 18) and intermittent noise spikes on all channels. In order to determine the cause of this noise, the following areas were investigated:

1. Receiver Signal Strength
2. TM Transmitter Deviation
3. SCO Pre-emphasis Schedule
4. WSMR Microwave Link

The results of the above investigation revealed the following:

1. Receiver Signal Strength

The recordings of receiver AGC levels for each WSMR receiving station throughout the flight were examined and the noise spikes were correlated with signal drop outs. There were considerably more drop outs experienced early in the flight and were attributed to normal vehicle rotation and the associated change in antenna look angle. Also, the noise level on the four continuous channels (15-18) was correlated with low AGC levels. The increased noise in these channels at low AGC levels was attributed to a dip in the SCO pre-emphasis taper and an over deviation of the TM transmitter. The SCO pre-emphasis taper and the transmitter deviation will be adjusted to reduce this noise susceptability for subsequent flights. Also, the procedure for selecting the telemetry receiving station having the best AGC is being reviewed.

2. TM Transmitter Deviation

It was reported in-flight that the AV-1 TM transmitter was deviating above its $\pm$ 600 KHz limit at approximately 750 KHz and that this could account for some of the noise problems. Post flight investigation at NASA-Langley with the recovered AV-1 transmitter and SCO package and at Roswell on AV-2 and AV-3 vehicles indicated that the transmitter could have been over deviating. Additional tests conducted at Langley with special test equipment determined that optimum performance would be obtained at lower

deviations (± 300 KHz) and adjustment of the SCO pre-emphasis schedule. The special test equipment(Telemetry Indicator and De-emphasis Amplifier) was shipped to Roswell for adjustment of the other vehicles.

3. SCO Pre-emphasis Schedule

It was reported during the AV-1 flight that there was a dip in the pre-emphasis taper which could account for the increased noise susceptibility of channels 15 through 18. The Langley tests confirmed that these channels were not properly adjusted and were dropping out before the lower channels. Additional tests, with the special test equipment, established a new pre-emphasis schedule to improve the signal to noise ratio in the upper SCO channels and to optimize the spectrum utilization. Also, the amplification factor of the SCO mixer amplifier was reduced to provide for less transmitter deviation and a more stable operating point. These changes were verified on AV-3 at Roswell with the test equipment sent from Langley. After verification on AV-3, the adjustments were incorporated into AV-2 and a special CST was run at reduced signal strength to verify system improvement.

4. WSMR Microwave Link

The video portion of the telemetry signal is transmitted from the receiving stations to the WSMR Telemetry Data Center (TDC) via a series of microwave data links. The one inch magnetic tapes that were recorded at stations JIG 10 and JIG 67 were processed at Langley and compared with the data recorded at TDC. The data quality at TDC was apparently degraded by the microwave link. Tests are now being conducted at WSMR to determine what can be done to improve the transmission links to TDC.

H. R. F. Subsystem

The S-Band Telemetry, C-Band Tracking and the Command Control RF subsystem performed within specification requirements throughout the mission. Signal acquisition for all frequencies occurred within 30 minutes of balloon launch.

Evaluation of the flight data indicates that the signal levels for the tracking and command systems were at or near saturation throughout the flight. The S-Band TM strength was considerably lower, however, useable telemetry data was obtained for each phase of the mission. The telemetry AGC records show signal strength variation as the vehicle rotated and swept the antenna pattern nulls past the various ground receiving stations. This modulation caused some dropouts in the telemetered data, but not to the extent of invalidating the data. The only RF anomaly occured during the pre-flight checkout of the command stations, when the C-station transmitter "A" sent dual tones 1 and 11 when only tone 1 should have been triggered and tones 2 and 12 when keying tone 2. No explanation for this was available, so the test conducted specified that C-Station utilize transmitter "B" for the mission.

I. TSE/OSE

The Test Support Equipment and Operational Support Equipment performed within the design requirements for this equipment.

The OSE Command Reception Indicator Panel located at the WSMR Control center indicated many false command tones and commands during the early portion of the float phase. These were not faults in the CRIP but rather TM dropouts at the WSMR receivers which drove the CRIP to false indications.

J. Mass Properties

The BLDT vehicle mass property requirements, at decelerator mortar fire, were established based on the Viking Lander Capsule, to be as follows:

Vehicle Weight	-	1888 ± 12#
Y Axis cg Location	-	0 Offset
Z Axis cg Location	-	-1.41 ± 0.030"
X Axis cg Location	-	31.7" to 33.7"

In order to fulfill the Y and Z axis cg location requirement, the AV-1 vehicle was subject to a spin balance operation at Sandia Corporation Laboratories, Albuquerque, New Mexico. During this operation, lead balance weights were fastened to the vehicle to precisely locate the vehicle cg with respect to the Y and Z axis.

The AV-1 vehicle mass properties are summarized in Table VI-4.

TABLE VI-1

BLDT AV-1 ATMOSPHERIC PROPERTIES

ALTITUDE (5000 FT)	EAST-WEST WIND (FT/SEC)	NORTH-SOUTH WIND (FT/SEC)	SPEED OF SOUND (FT/SEC)	DENSITY (SLUGS/FT^2)
1.	-3.	0.	1144.	.19569-02
2.	-3.	1.	1115.	.16742-02
3.	-8.	-5.	1091.	.14530-02
4.	-1.	9.	1072.	.12446-02
5.	6.	-4.	1052.	.10610-02
6.	11.	-2.	1030.	.90189-03
7.	33.	-13.	1005.	.76199-03
8.	35.	-26.	980.	.63819-03
9.	2.	-48.	962.	.52099-03
10.	-59.	-7.	940.	.42708-03
11.	-33.	-16.	935.	.33355-03
12.	-19.	-4.	938.	.25710-03
13.	-36.	-8.	954.	.19326-03
14.	-51.	-1.	973.	.14611-03
15.	-49.	4.	975.	.11506-03
16.	-51.	18.	977.	.90422-04
17.	-59.	-12.	983.	.70898-04
18.	-77.	2.	993.	.55222-04
19.	-68.	4.	997.	.43712-04
20.	-81.	0.	1001.	.34677-04
21.	-97.	21.	1011.	.27280-04
22.	-96.	8.	1022.	.21543-04
23.	-85.	-3.	1030.	.17157-04
24.	-110.	-3.	1037.	.13736-04
25.	-127.	11.	1047.	.10984-04
26.	-105.	12.	1055.	.88388-05
27.	-116.	2.	1058.	.71950-05
28.	-134.	-8.	1058.	.59006-05
29.	-171.	-.	1064.	.47884-05
30.	-185.	31.	1071.	.38946-05
31.	-208.	49.	1077.	.31743-05
32.	-196.	64.	1076.	.26267-05

TABLE VI-2 STATE VECTOR DATA

BLDT AV-1

	DROP	MORTAR FIRE	FULL OPEN
Time (t) - sec	00.	38.3	40.0
Altitude (h) - ft	120530.	142025.	142729.
Velocity (V) - ft/sec	--	2314.	2197.
Gamma (r) - deg.	--	10.9	9.7
PSI (ψ) - deg	13.	23.9	23.9
Theta (θ) - deg.	52.	-17.3	.5
Mach No. (MN)	--	2.182	2.070
Dynamic Pressure (q) - lb/ft^2	--	14.6	12.8
Angle of Attack (α) - deg.	--	-7.0	8.8
Sideslip (β) - deg.	--	-1.3	5.0
Total Angle of Attack (η) - deg.	--	7.1	10.11
Spin (p) - deg/sec.	--	2.6	26.

TABLE VI-3

BATTERY PERFORMANCE DATA

	MAIN BATTERY	TRANS. BATTERY	PYRO A BATTERY	PYRO B BATTERY	CAMERA BATTERY POSITIVE	CAMERA BATTERY NEGATIVE
1. Activation Voltage						
a. Open Circuit	30.49	33.16	36.85	36.87	16.59	-16.59
b. 5 Second Load*	29.0	26.8	29.1	29.1	13.1	-13.1
2. Prelaunch Voltage						
No Load	30.57	33.11	33.14	32.54	16.14	-16.18
3. Float Voltage						
Drop - 2 hours	29.4	27.6	33.9	33.3	NO TM	NO TM
Drop - 1 hour	29.5	27.8	33.8	32.9	DATA	DATA
Drop - 1 minute	29.4	27.7	31.1	30.9		
4. Flight Voltages						
T + 1 minute	29.4	27.8	30.7	30.8		
T + 6 minute	29.4	27.9	30.8	30.5		
5. Main Battery Amps.	3-6 amps					

* 5 Second Load Levels - 30 amps for main battery
10 amps for all others.

TABLE VI-4

FINAL BLDT MASS PROPERTIES, AV-1

Condition	Weight (lb)	Center of Gravity (Vehicle Sta.)			Moment & Product of Inertia (Slug Ft^2)					
		X	Y	Z	I_{xx}	I_{yy}	I_{zz}	P_{xy}	P_{xz}	P_{yz}
On Load Bar	3592	38.08	0							
At Drop	3367	38.10	0	-1.41	577	493	407	.43	1.73	.25
At Mortar Fire	1896	37.16	0	-1.41	439	349	336	.43	1.73	.16
With Decelerator Deployed	1801	36.02	0	-1.41	43[illegible]	335	322	.46	1.73	.16
With Decelerator Deployed and Aeroshell Dropped	1446	39.64	0	-1.76	252	227	214	.43	3.86	-.17
Aeroshell	355	21.26	0	.17	178	91	91			

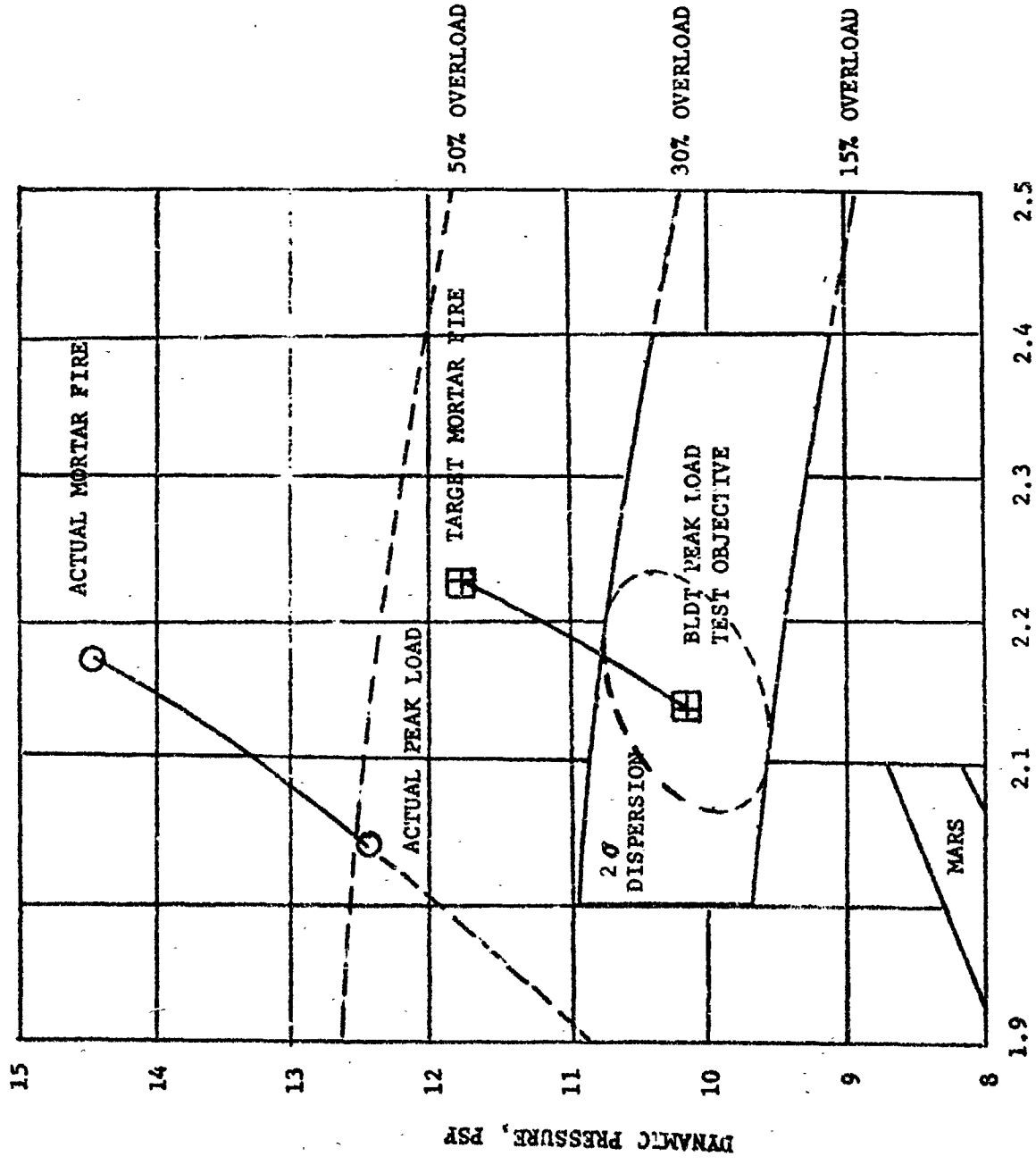

BLDT AV-1 TEST CONDITIONS

FIGURE VI-1

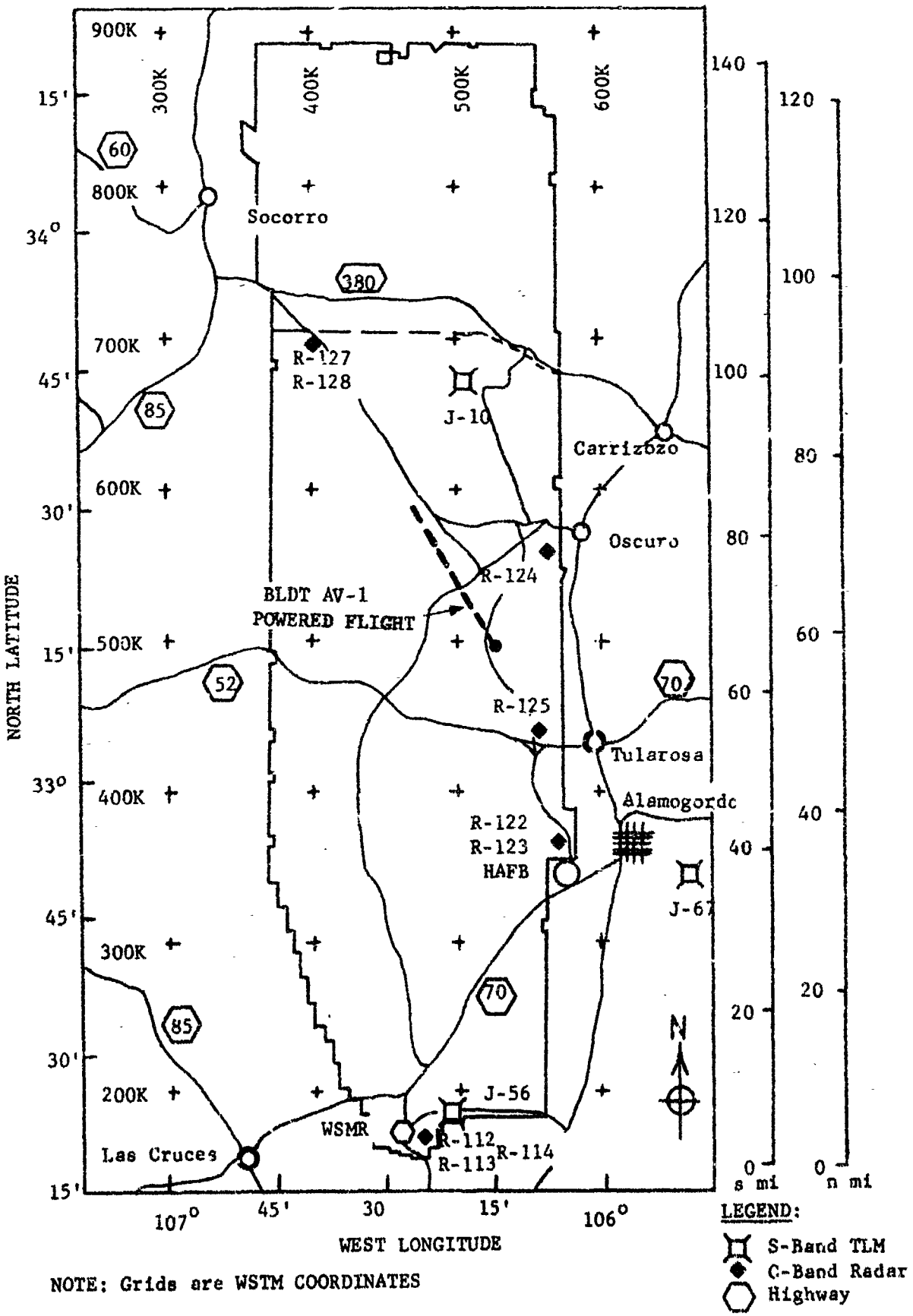

NOTE: Grids are WSTM COORDINATES

FIGURE VI-2 WSMR MAP SHOWING TELEMETRY AND

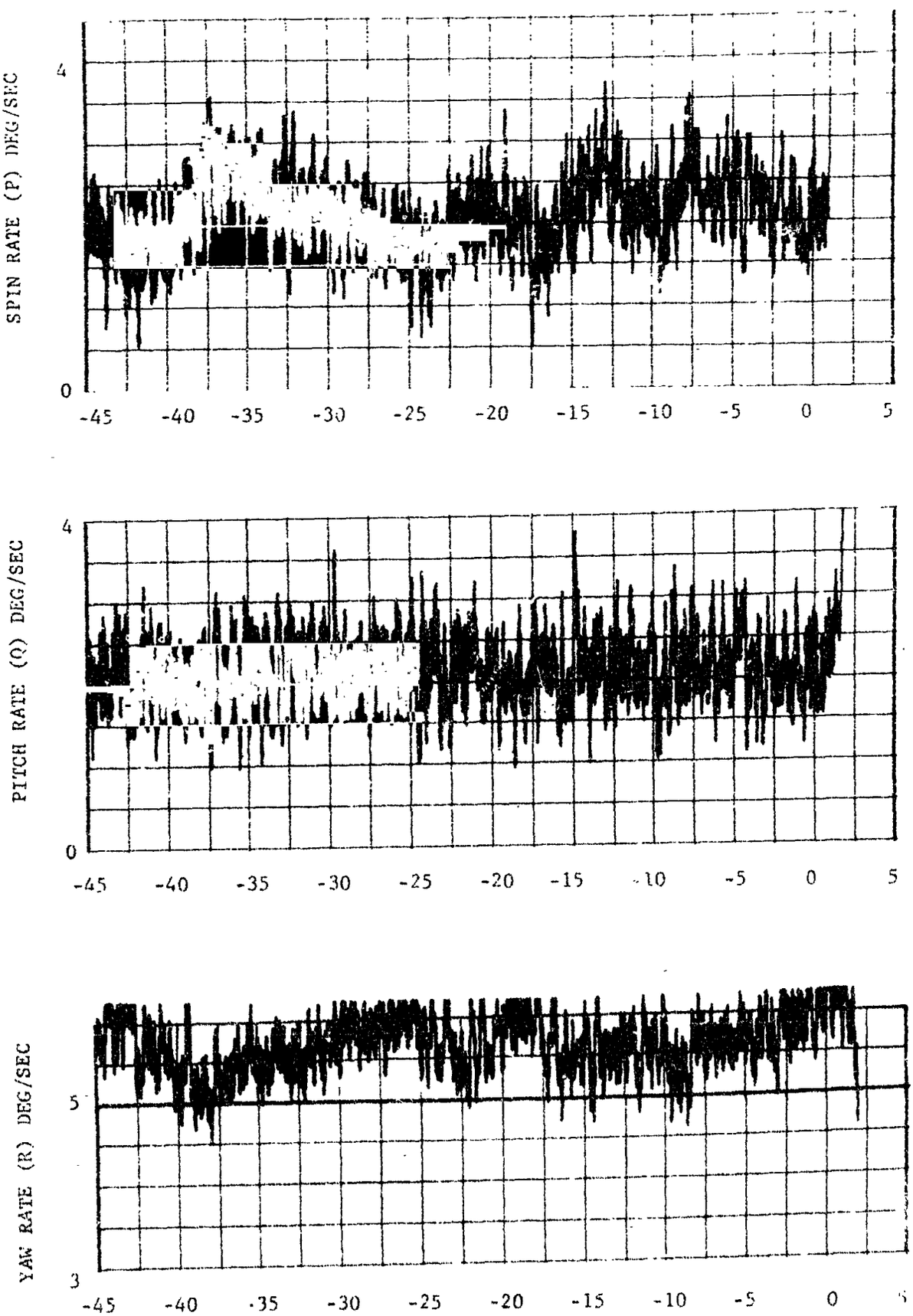

FIGURE VI-3 GYRO DATA PRIOR TO DROP

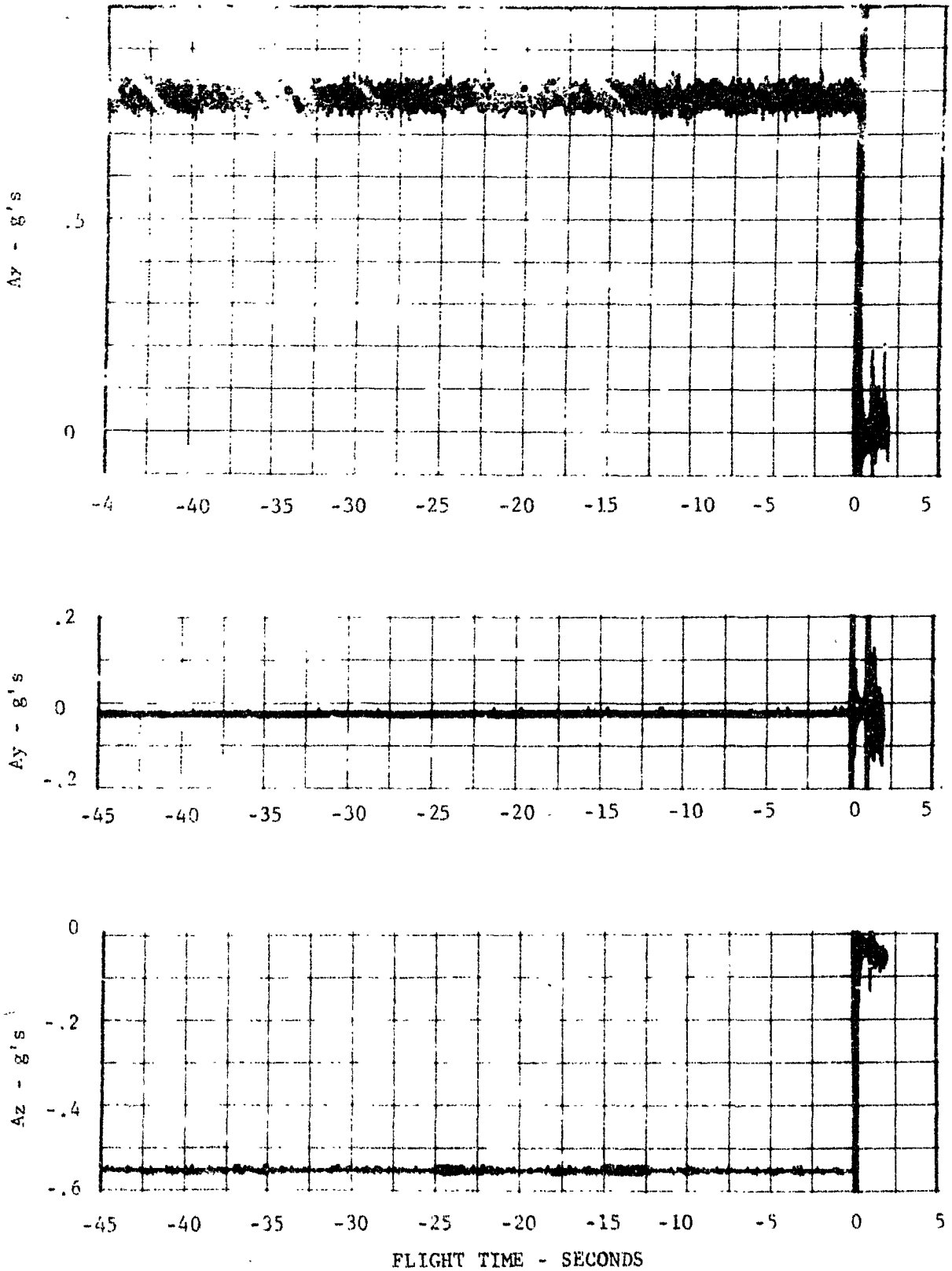

FIGURE VI-4 ACCELEROMETER DATA PRIOR TO DROP

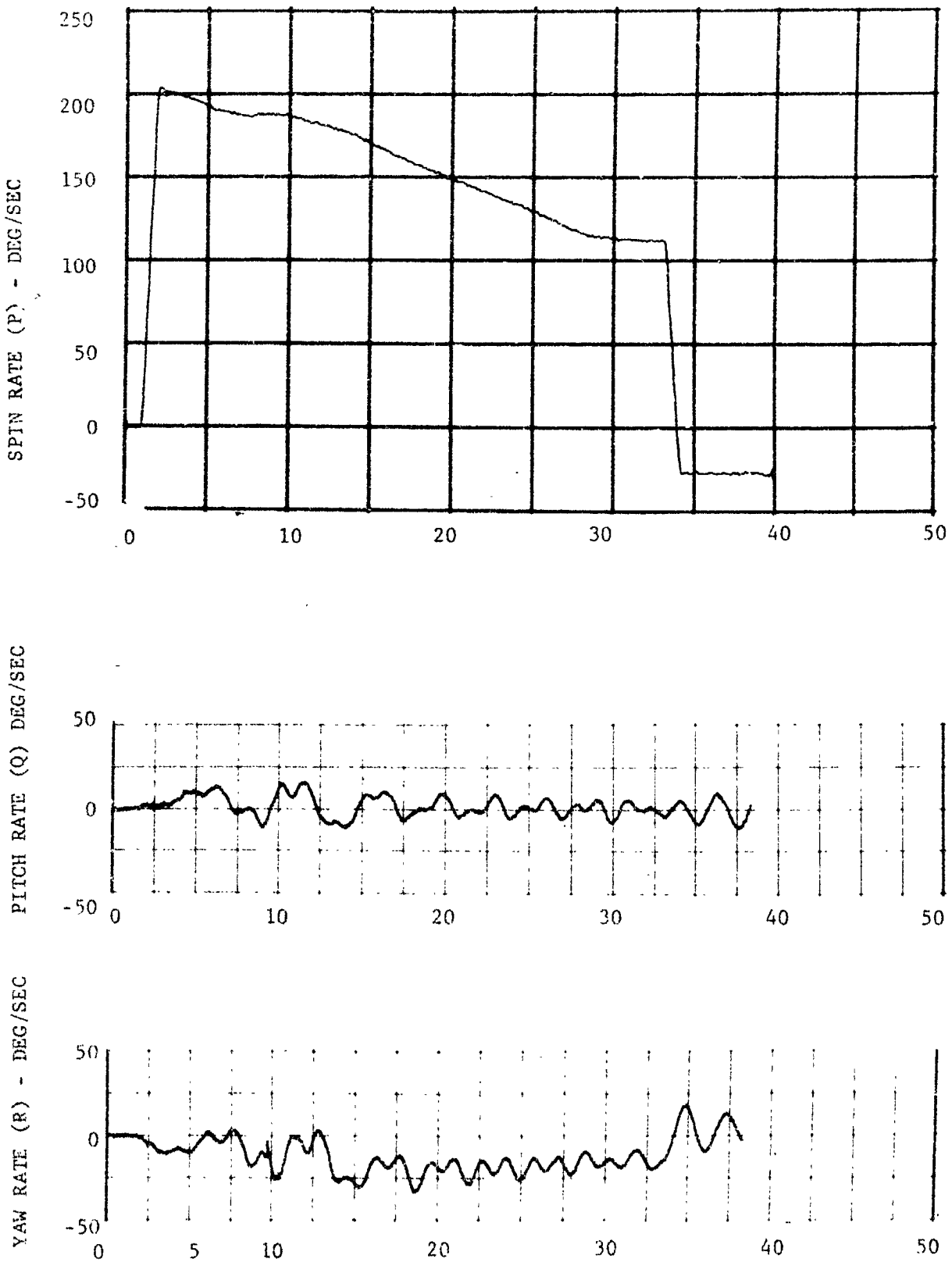

FIGURE VI-5 GYRO DATA DURING POWERED FLIGHT

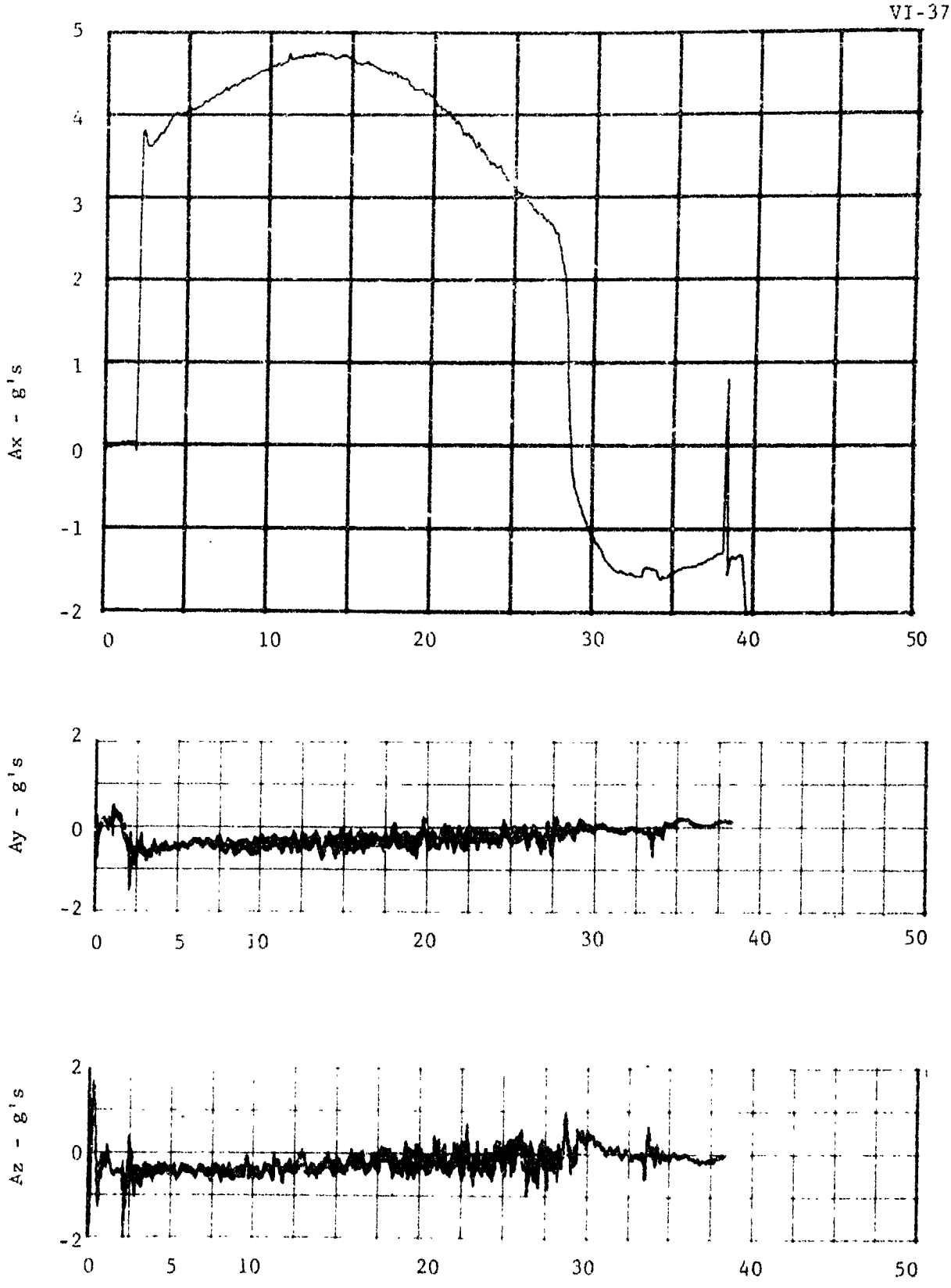

FIGURE VI-6 ACCELEROMETER DATA DURING POWERED FLIGHT

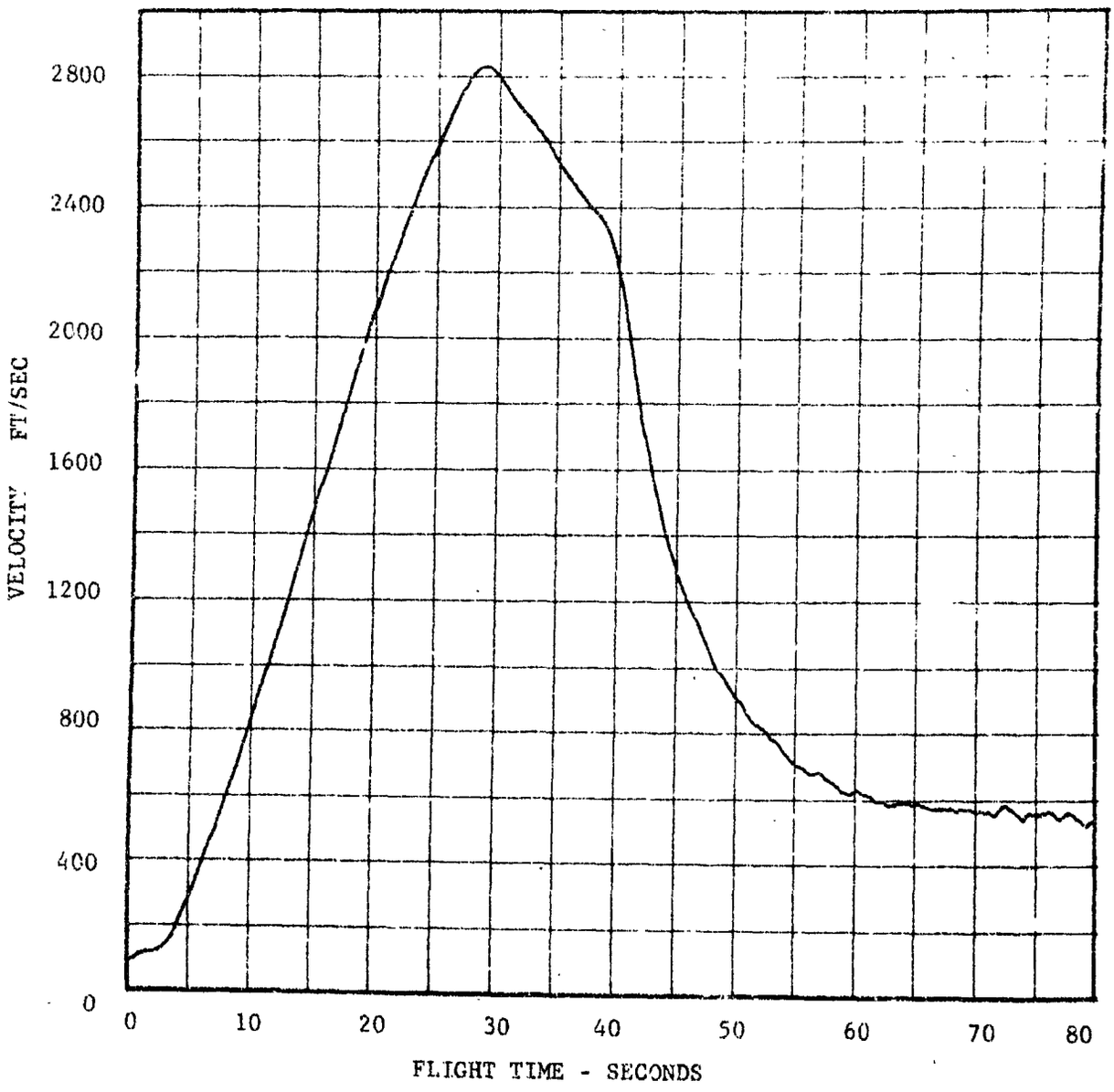

FIGURE VI-7 RADAR (R123) VELOCITY VS FLIGHT TIME

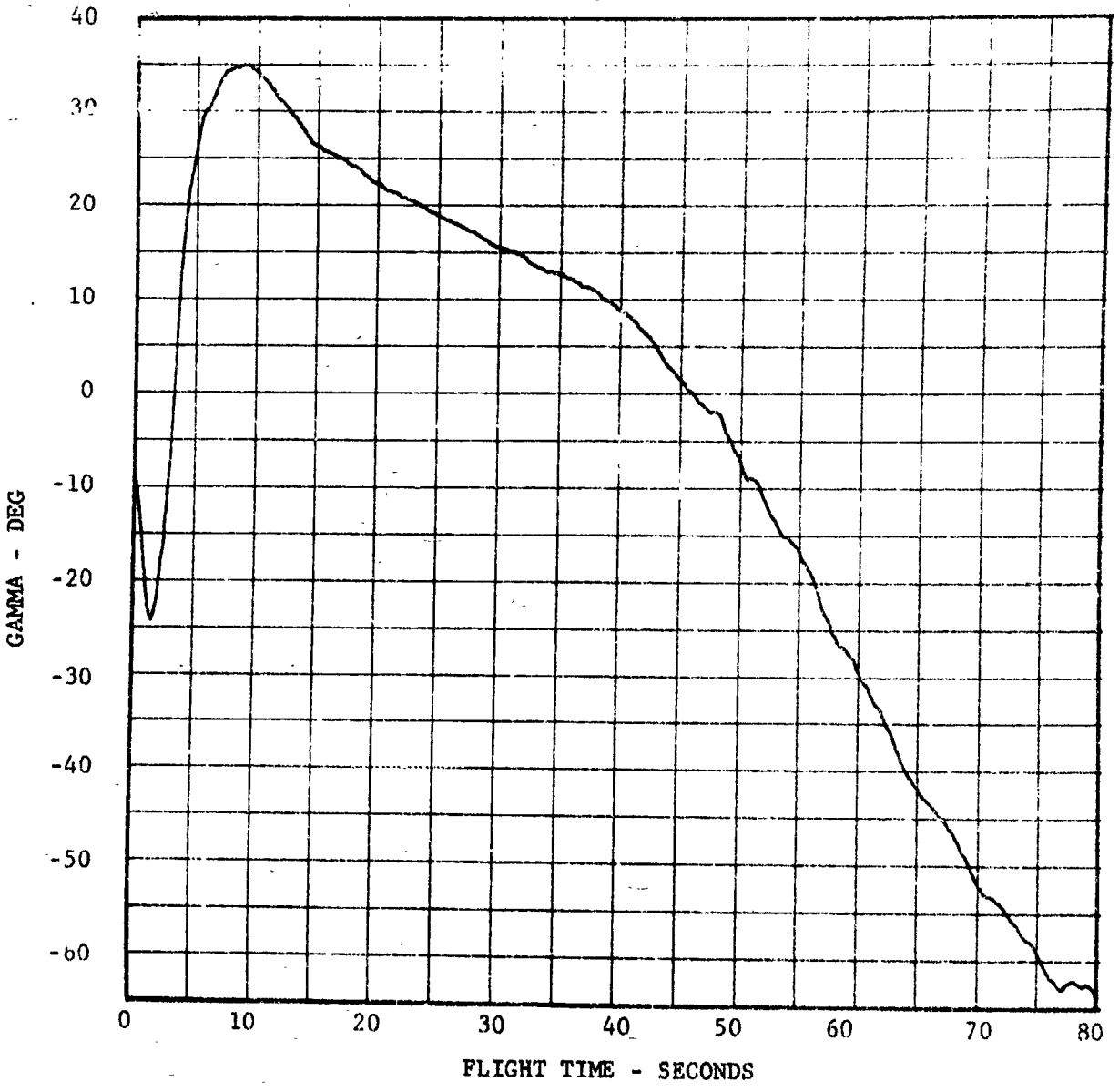

FIGURE VI-8 RADAR (R123) FLIGHT PATH ANGLE VS FLIGHT TIME

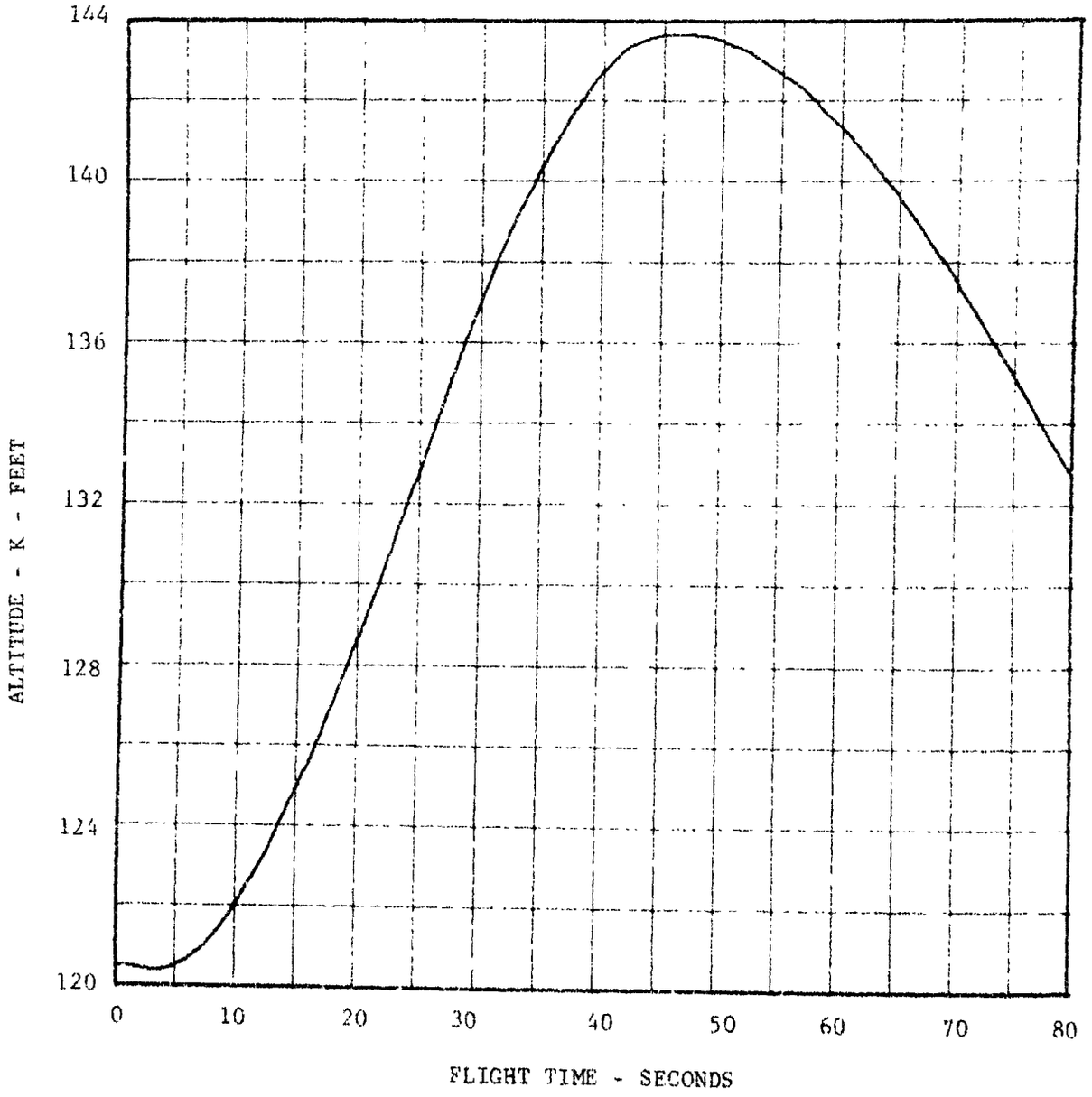

FIGURE VI-9 RADAR (R123) ALTITUDE (MSL) VS FLIGHT TIME

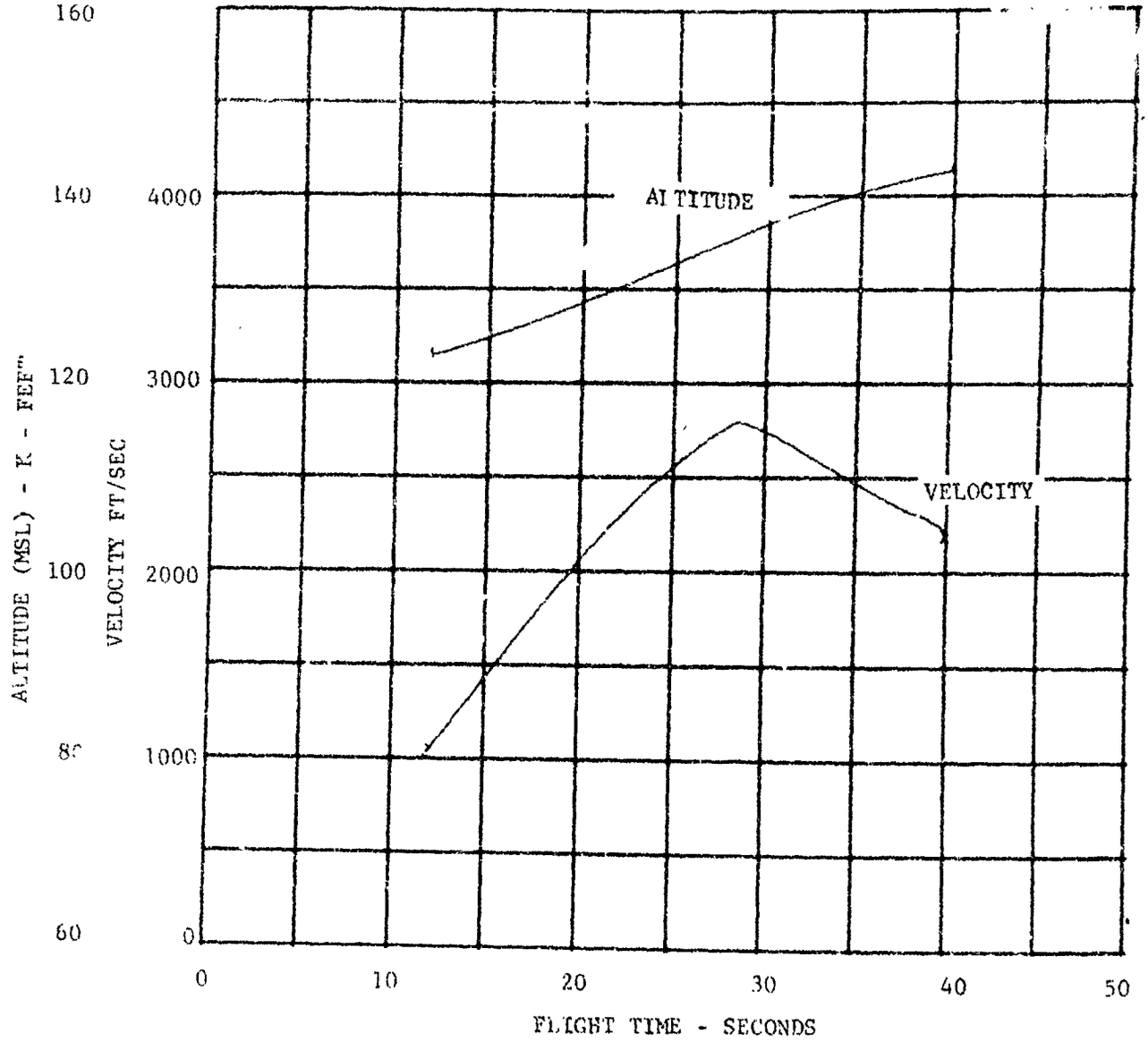

FIGURE VI-10 STEP TRAJECTORY RECONSTRUCTION OF ALTITUDE AND VELOCITY

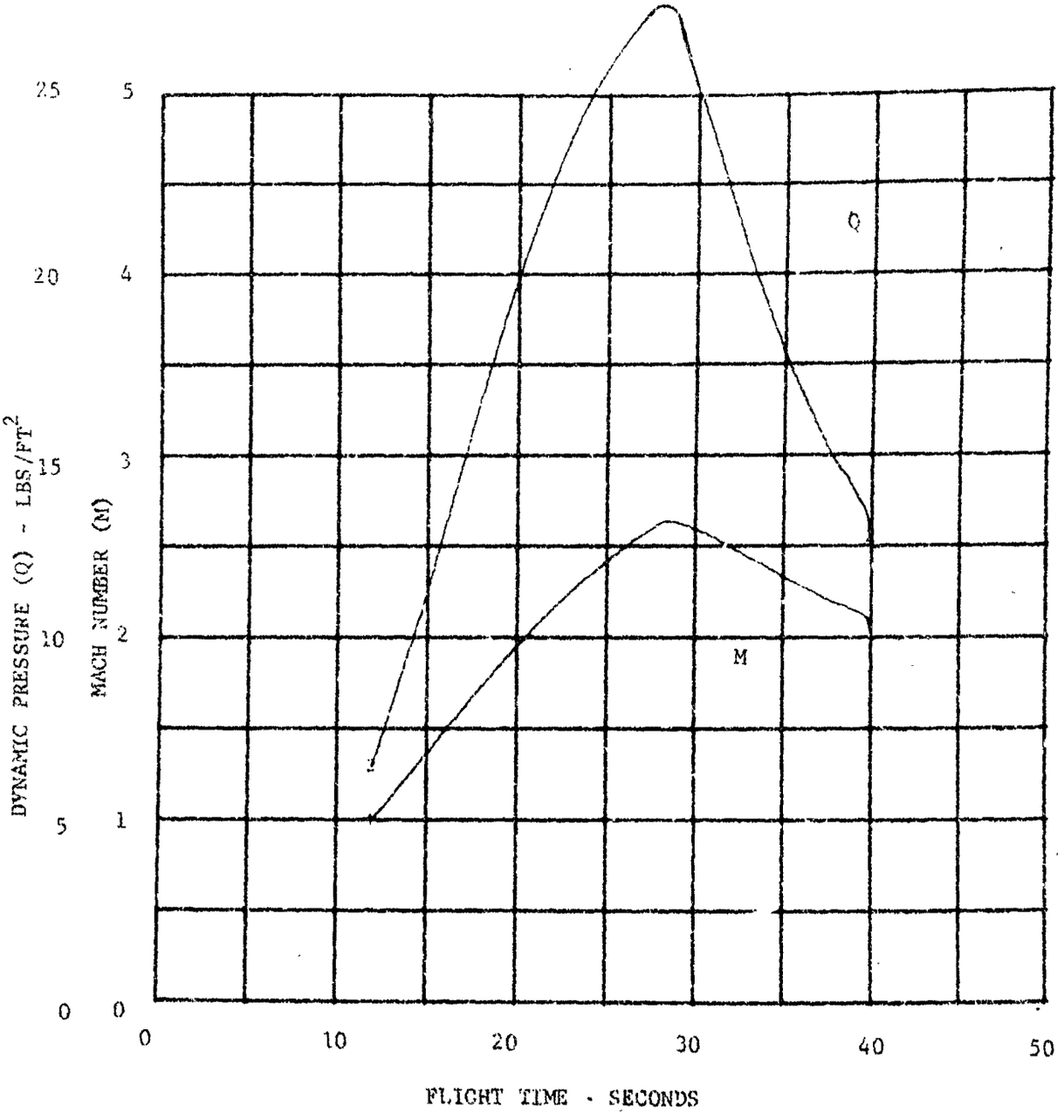

FIGURE VI-11 STEP TRAJECTORY RECONSTRUCTION OF MACH NUMBER AND DYNAMIC PRESSURE

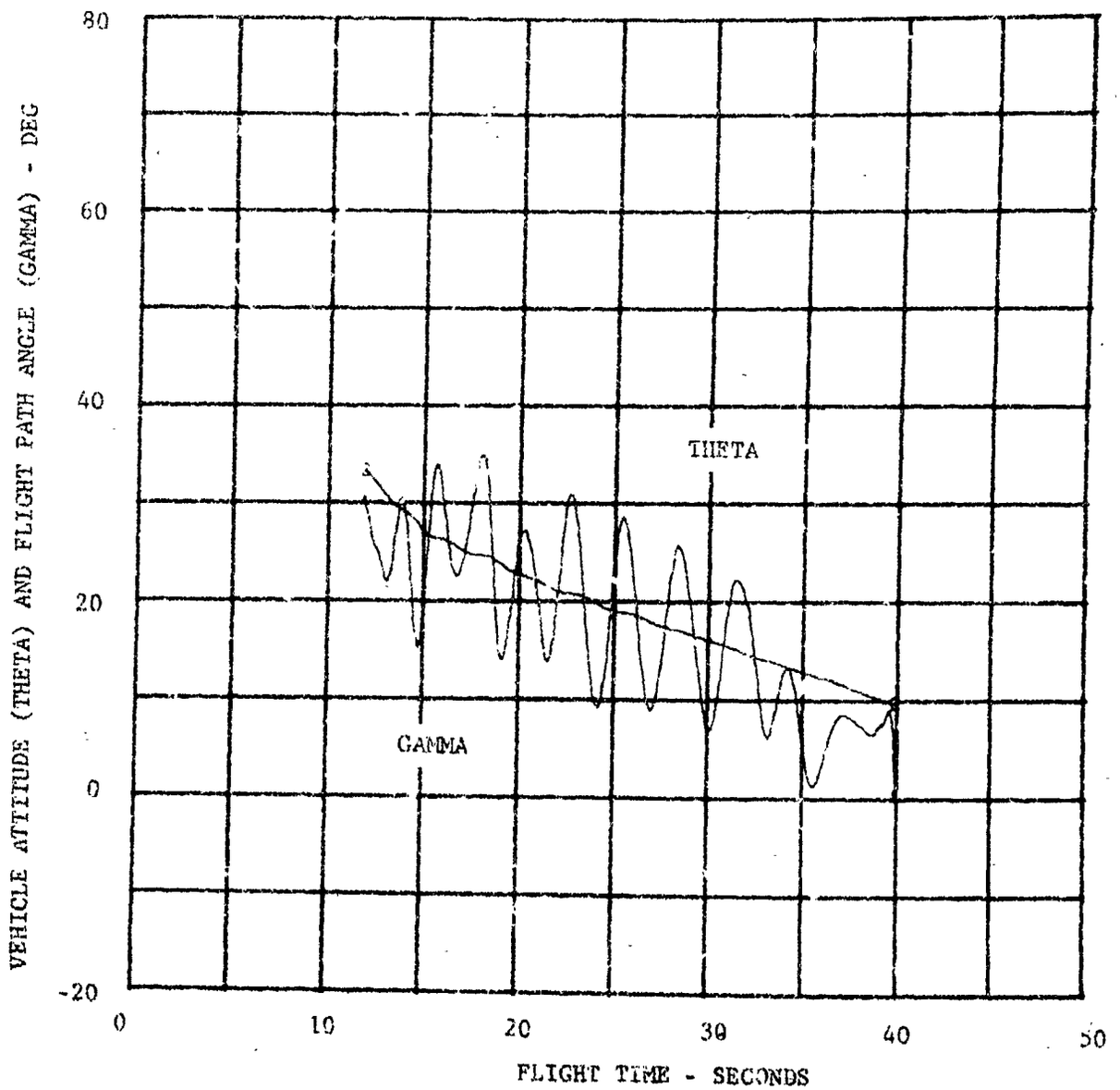

FIGURE VI-12 STEP TRAJECTORY RECONSTRUCTION OF VEHICLE ATTITUDE AND FLIGHT PATH ANGLE

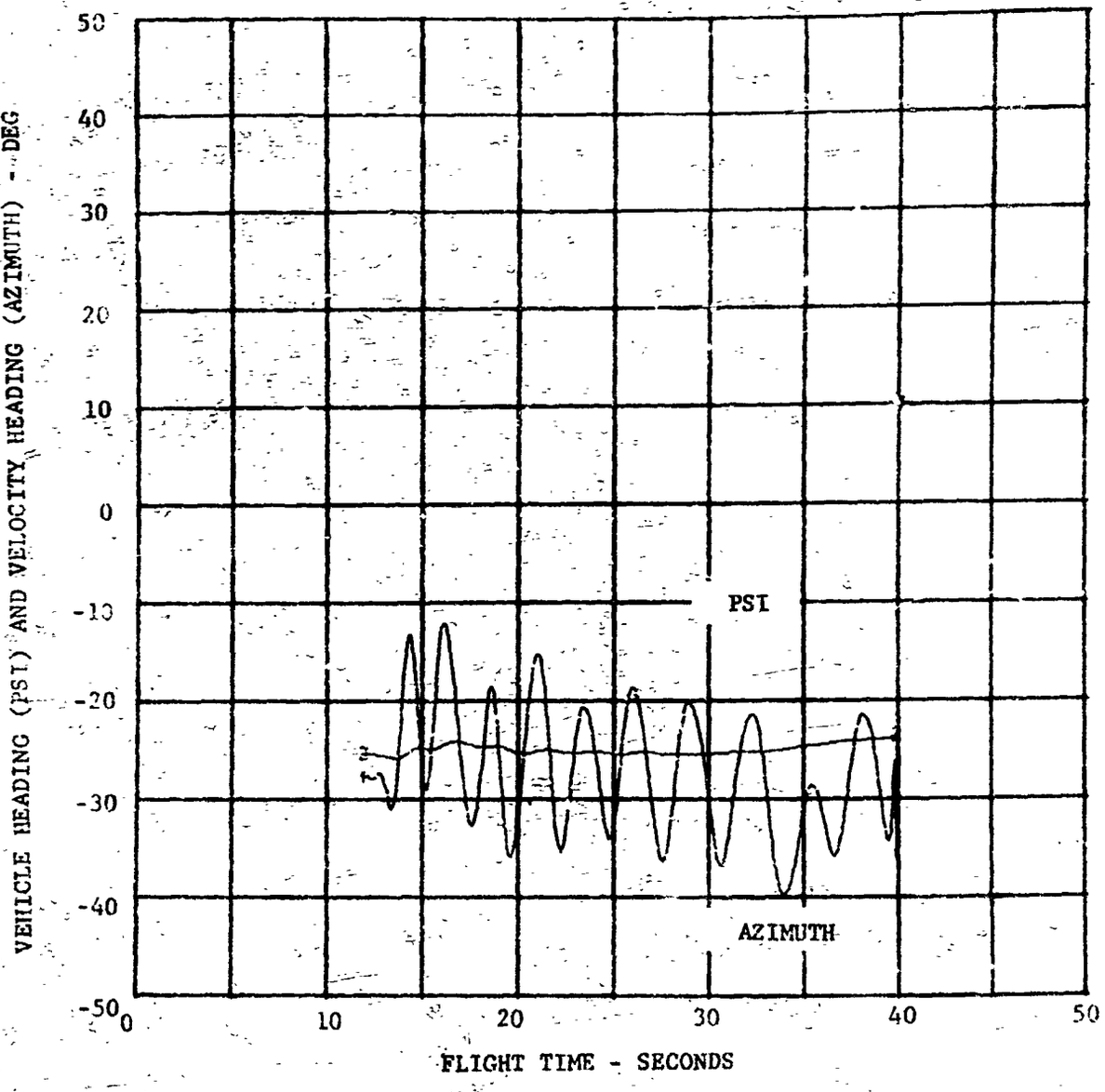

FIGURE VI-13 STEP TRAJECTORY RECONSTRUCTION OF THE BODY HEADING AND THE VELOCITY HEADING

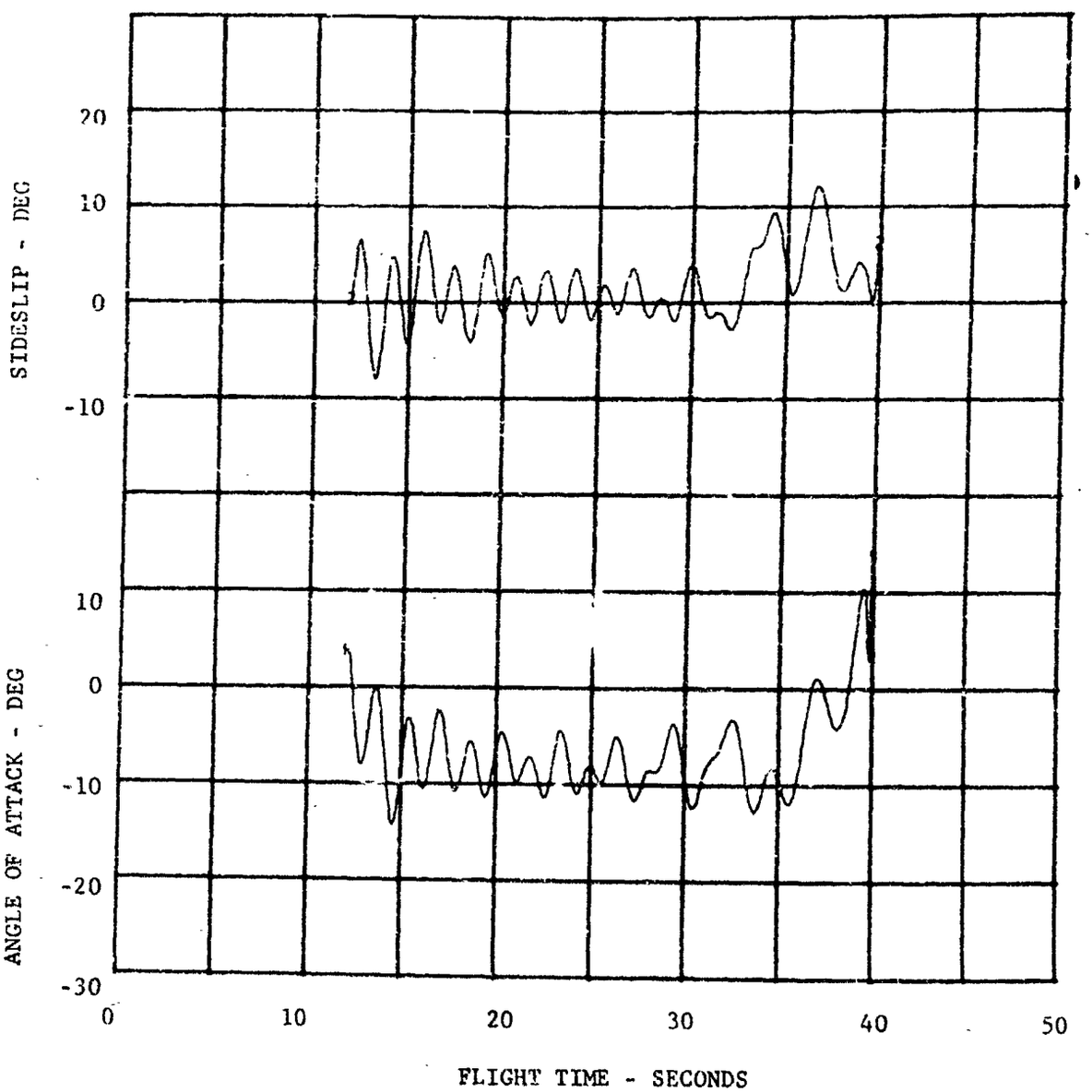

FIGURE VI-14 STEP TRAJECTORY RECONSTRUCTION OF ANGLE OF ATTACK AND SIDESLIP

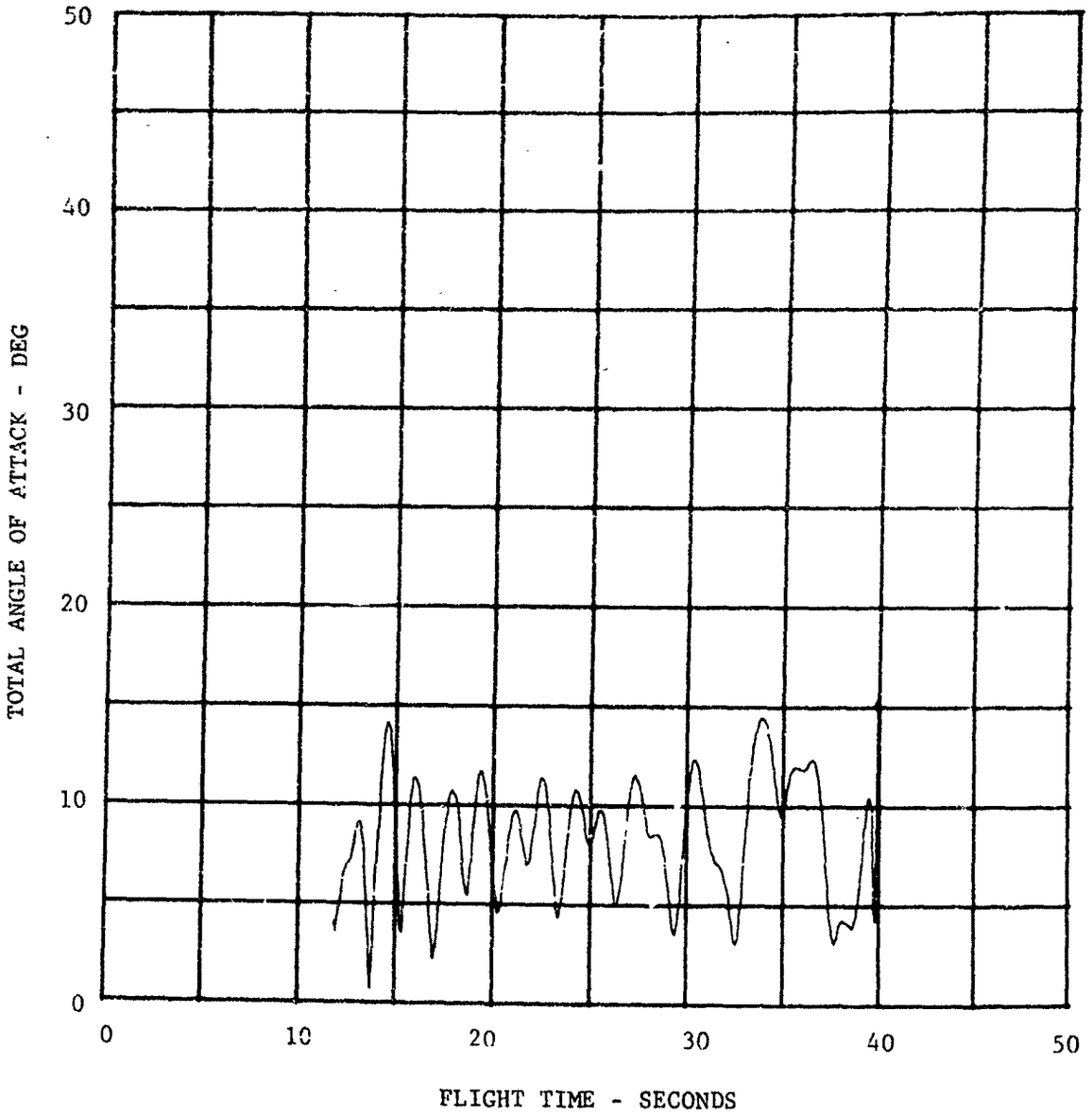

FIGURE VI-15 STEP TRAJECTORY RECONSTRUCTION OF TOTAL ANGLE OF ATTACK

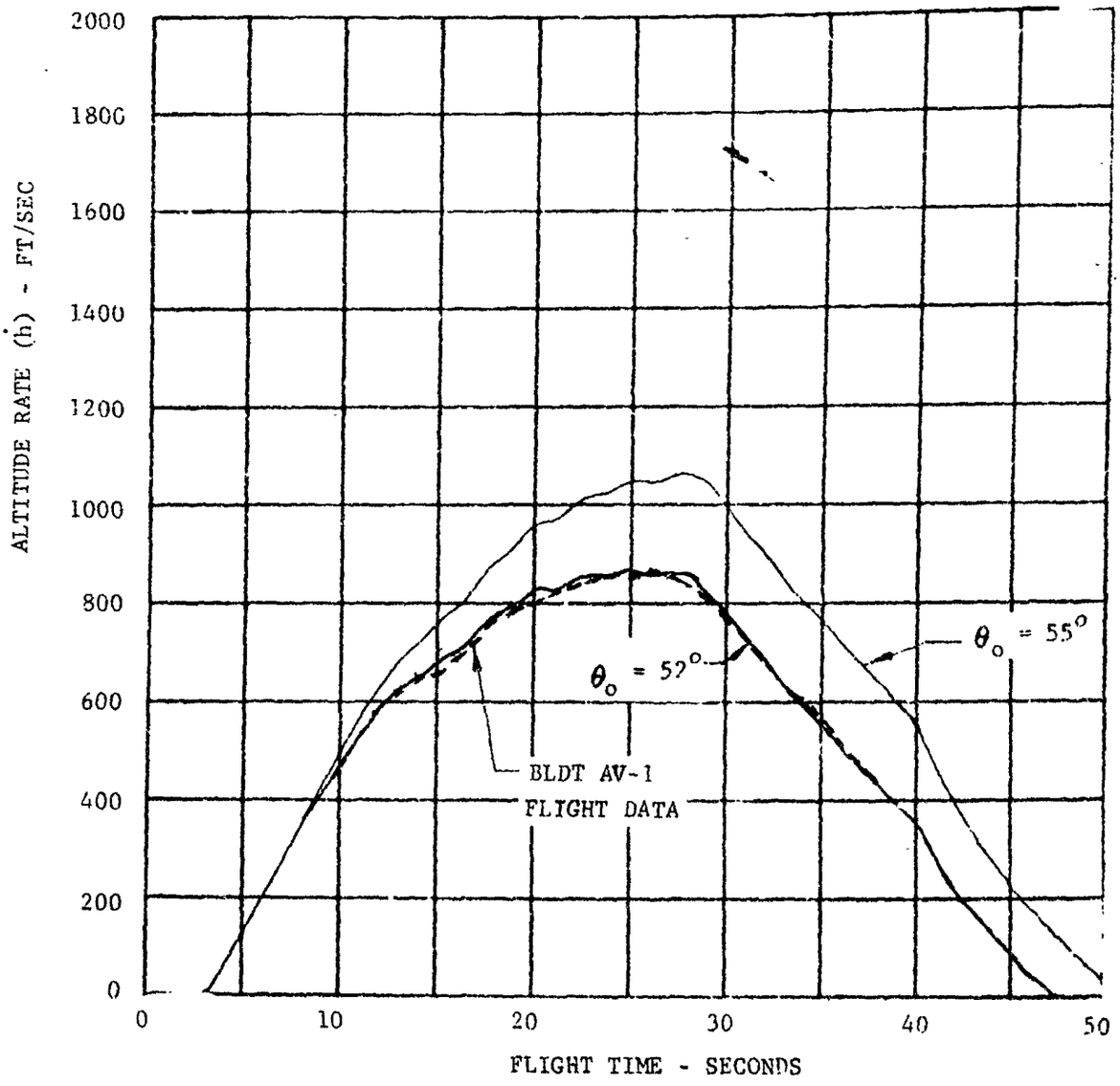

FIGURE VI-16 6 DOF ALTITUDE RATE VARIATIONS WITH DROP ATTITUDE

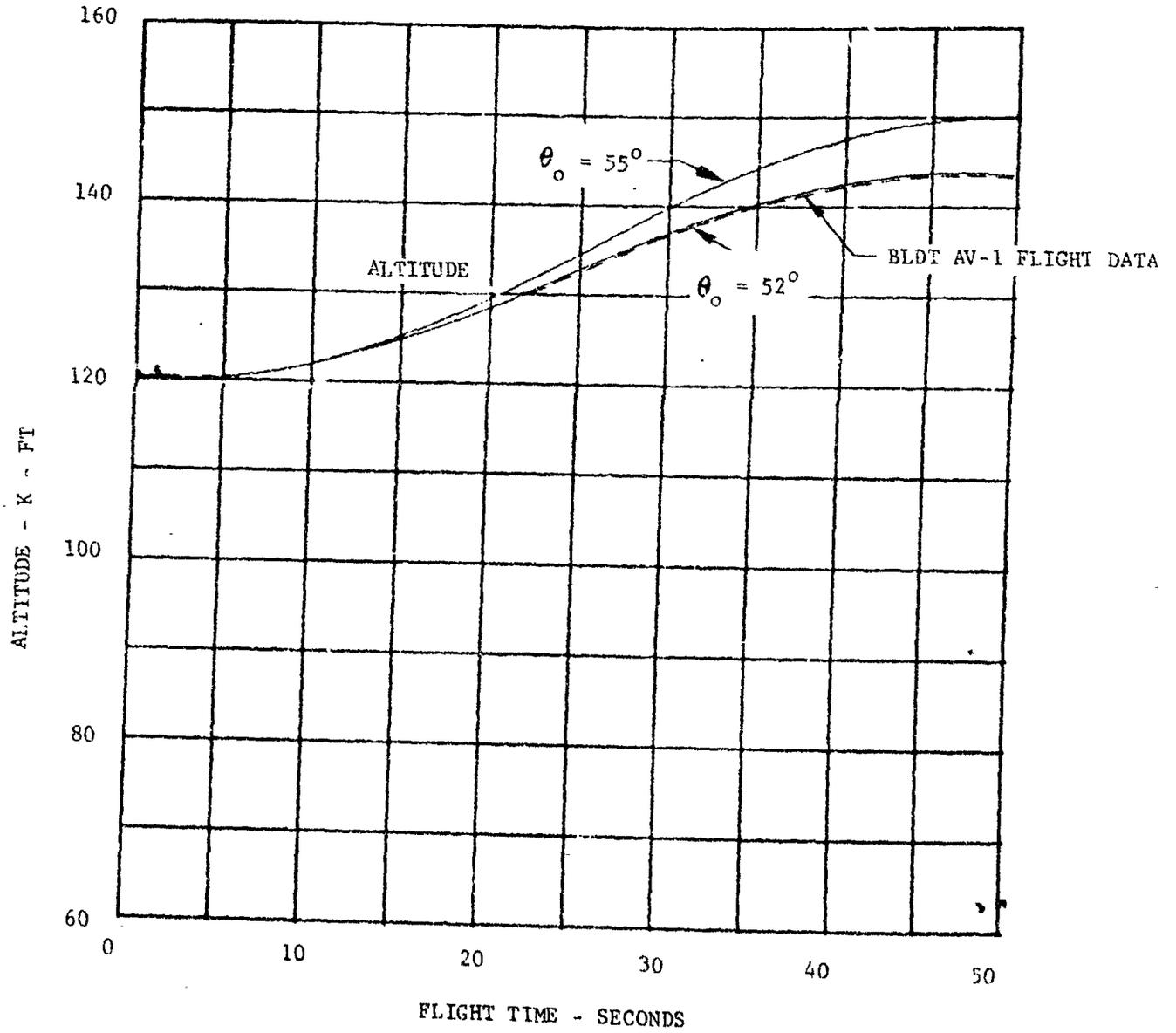

FIGURE VI-17 6 DOF ALTITUDE VARIATION WITH DROP ATTITUDE

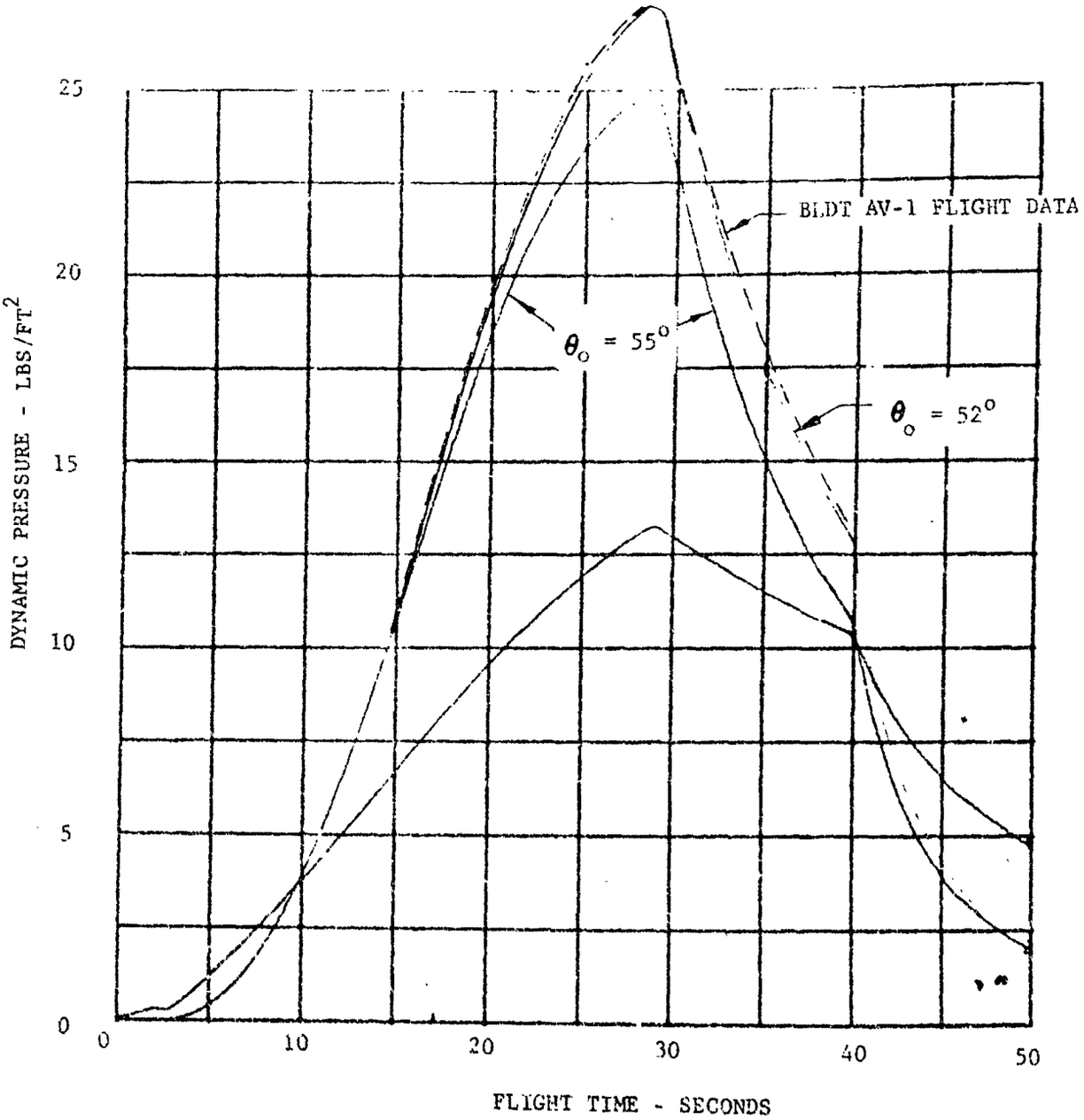

FIGURE VI-18 6 DOF DYNAMIC PRESSURE VARIATION WITH DROP ATTITUDE

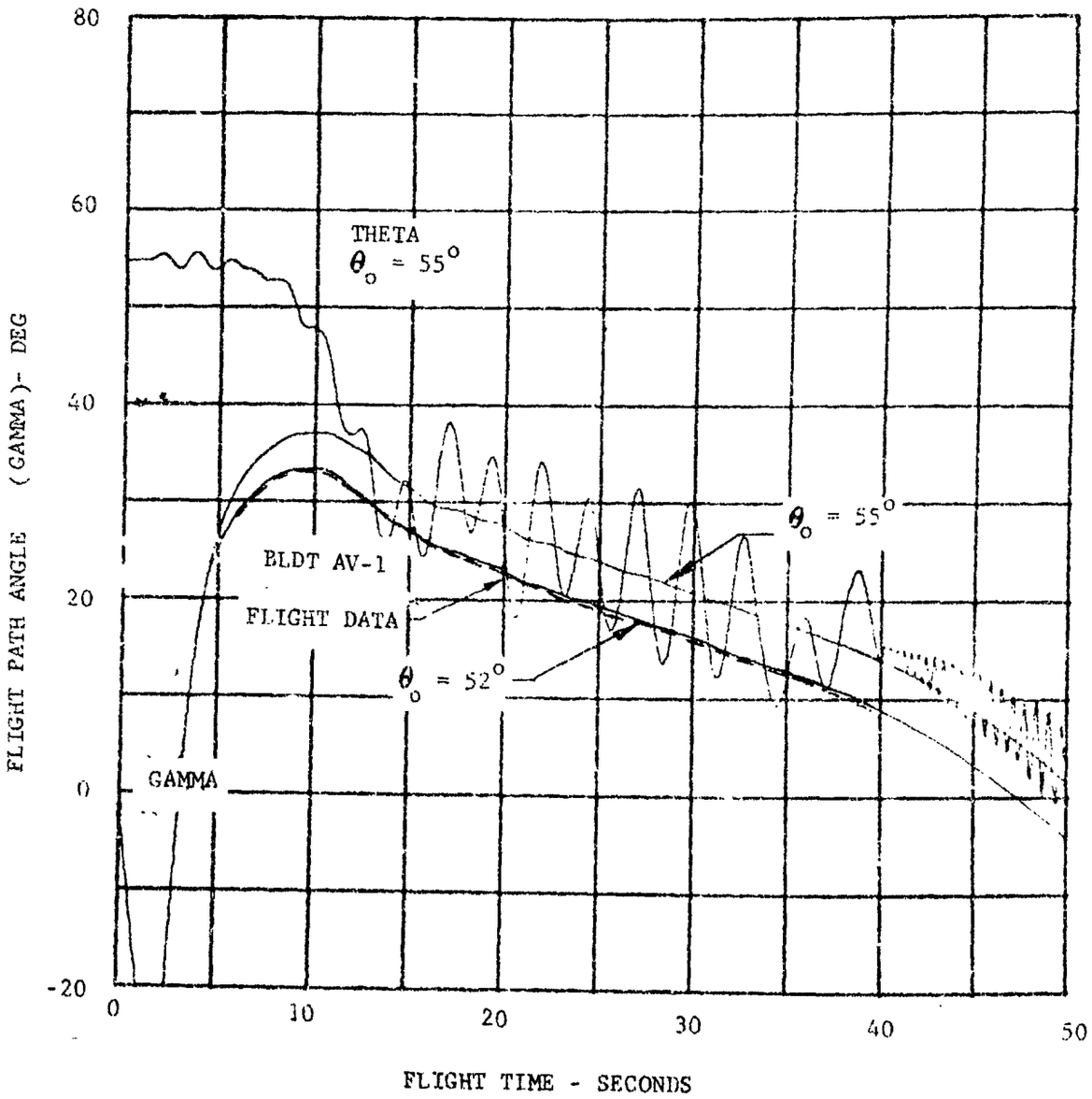

FIGURE VI-19 6 OOF FLIGHT PATH ANGLE VARIATION WITH DROP ATTITUDE

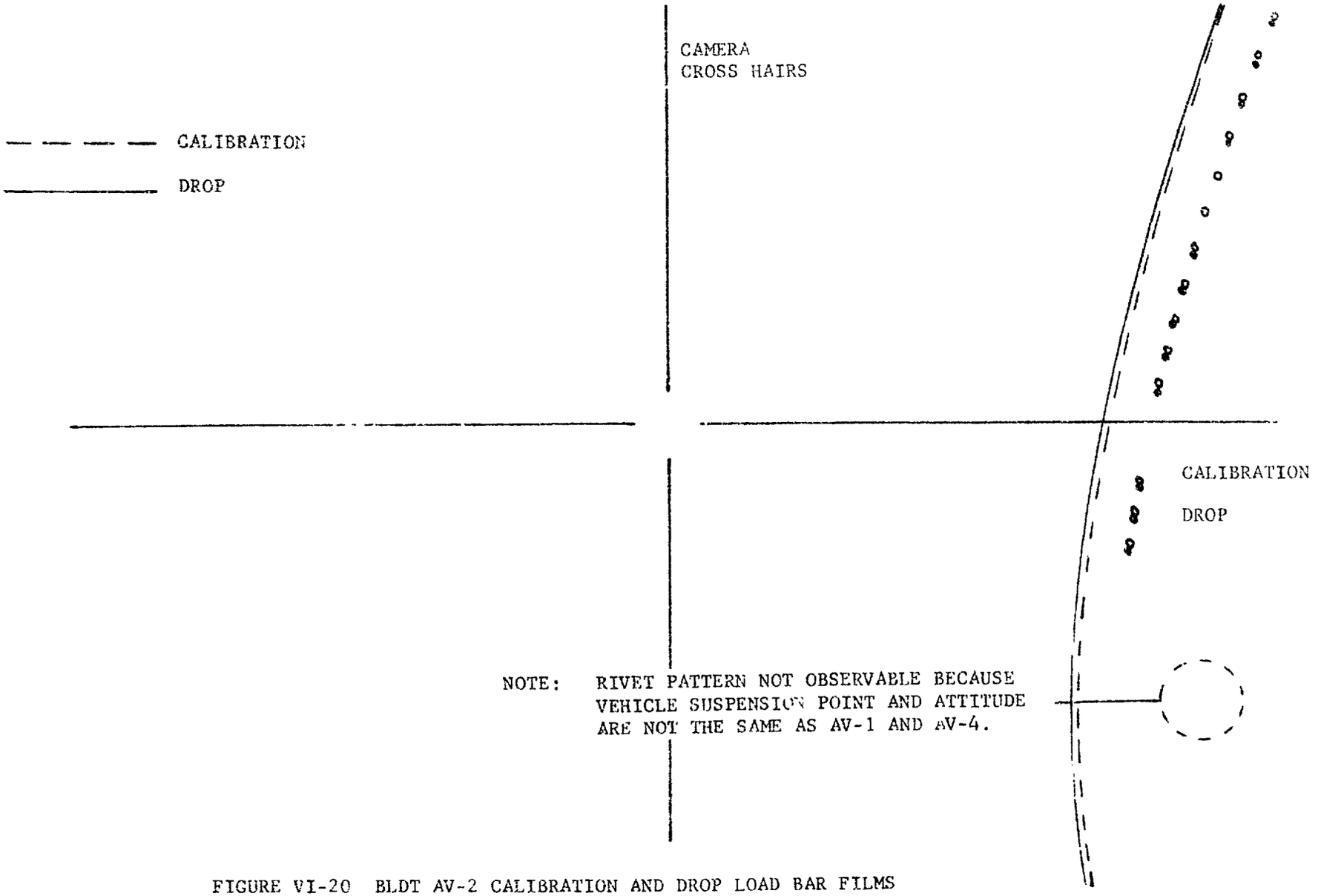

FIGURE VI-20 BLDT AV-2 CALIBRATION AND DROP LOAD BAR FILMS

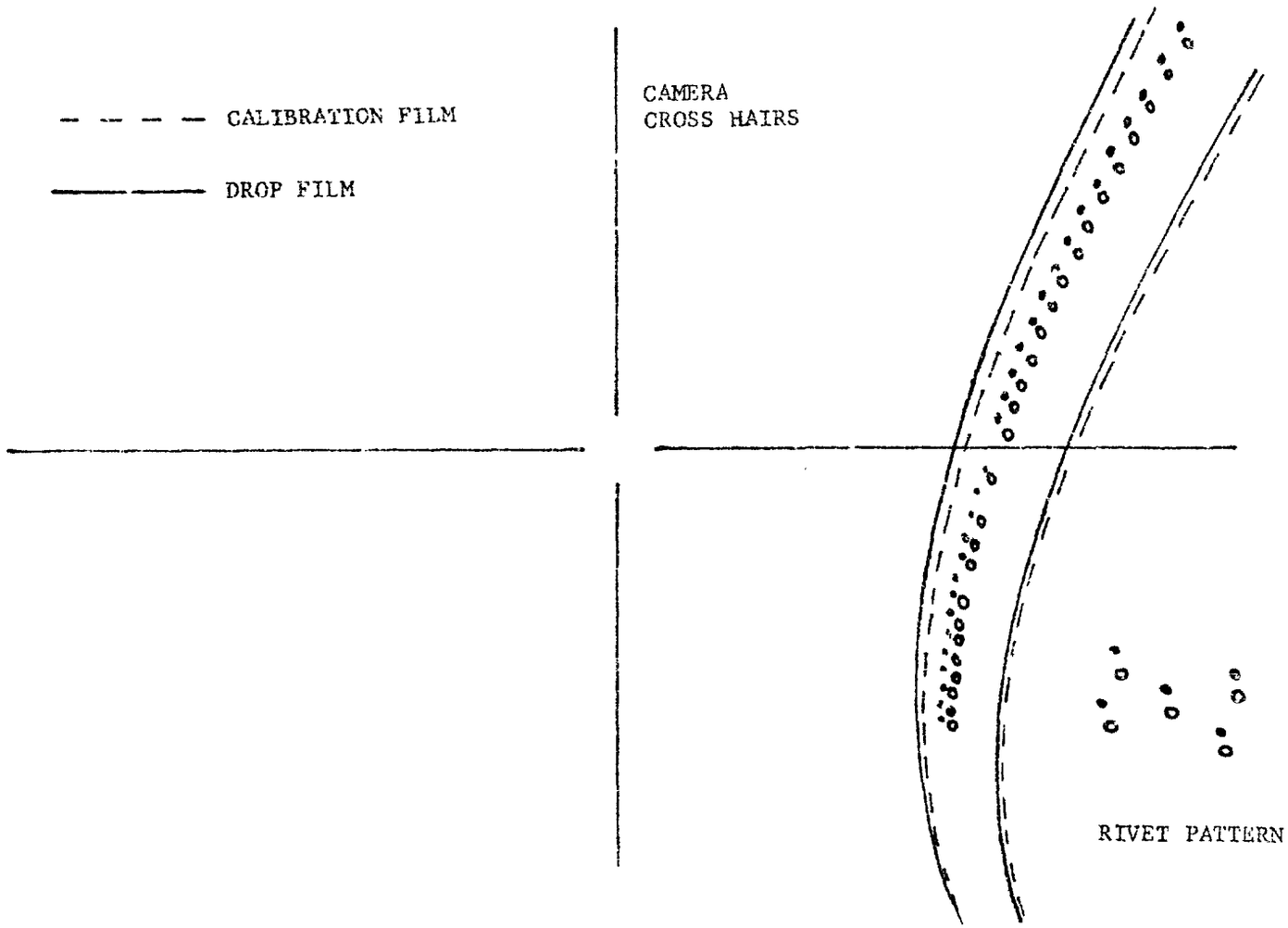

FIGURE VI-21 BLDT AV-4 CALIBRATION AND DROP LOAD BAR FILMS

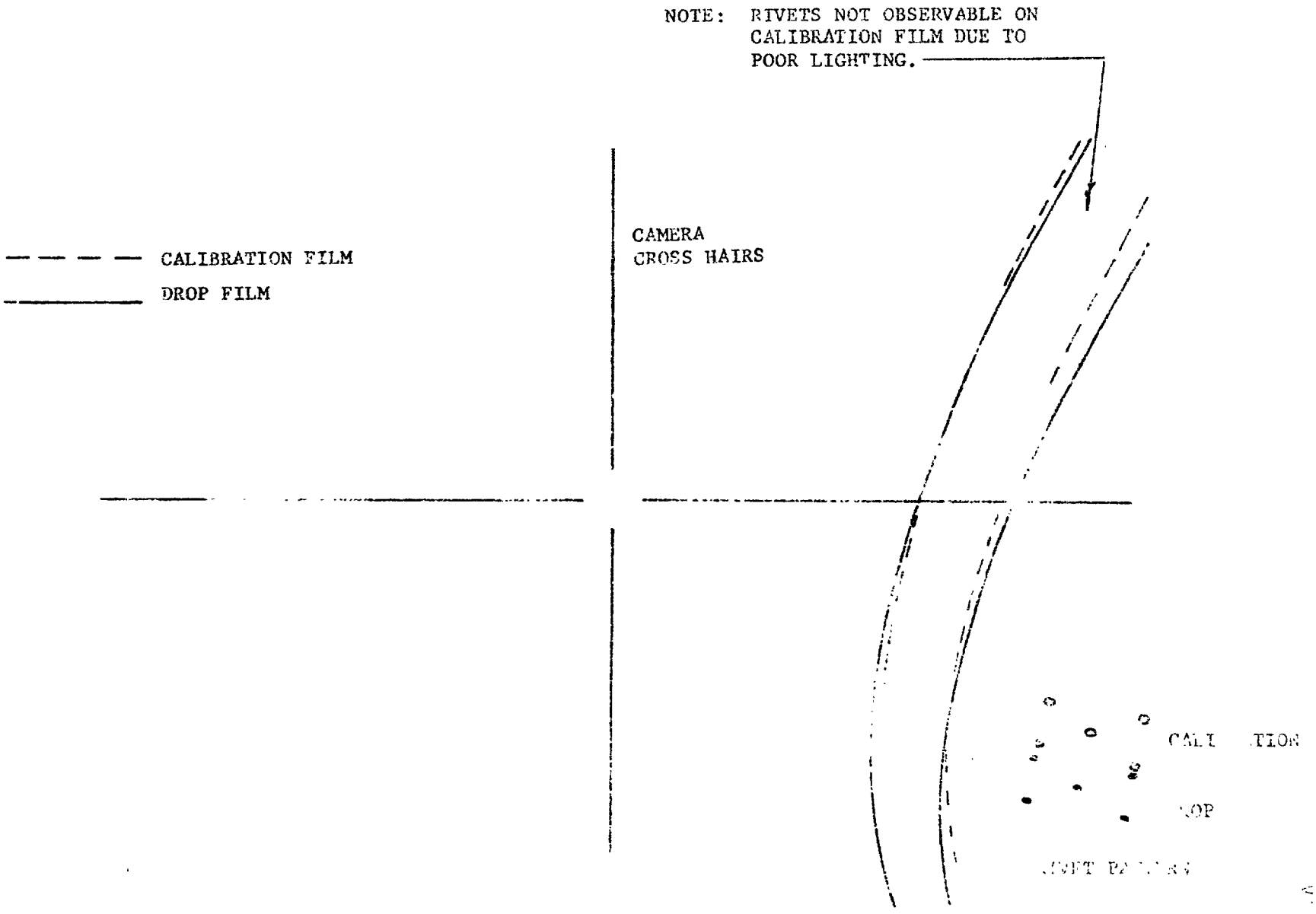

FIGURE VI 22 BIDT AV-1 CALIBRATION AND DROP LOAD BAR FILMS

FIGURE VI-23 MISSION ASCENT PROFILES

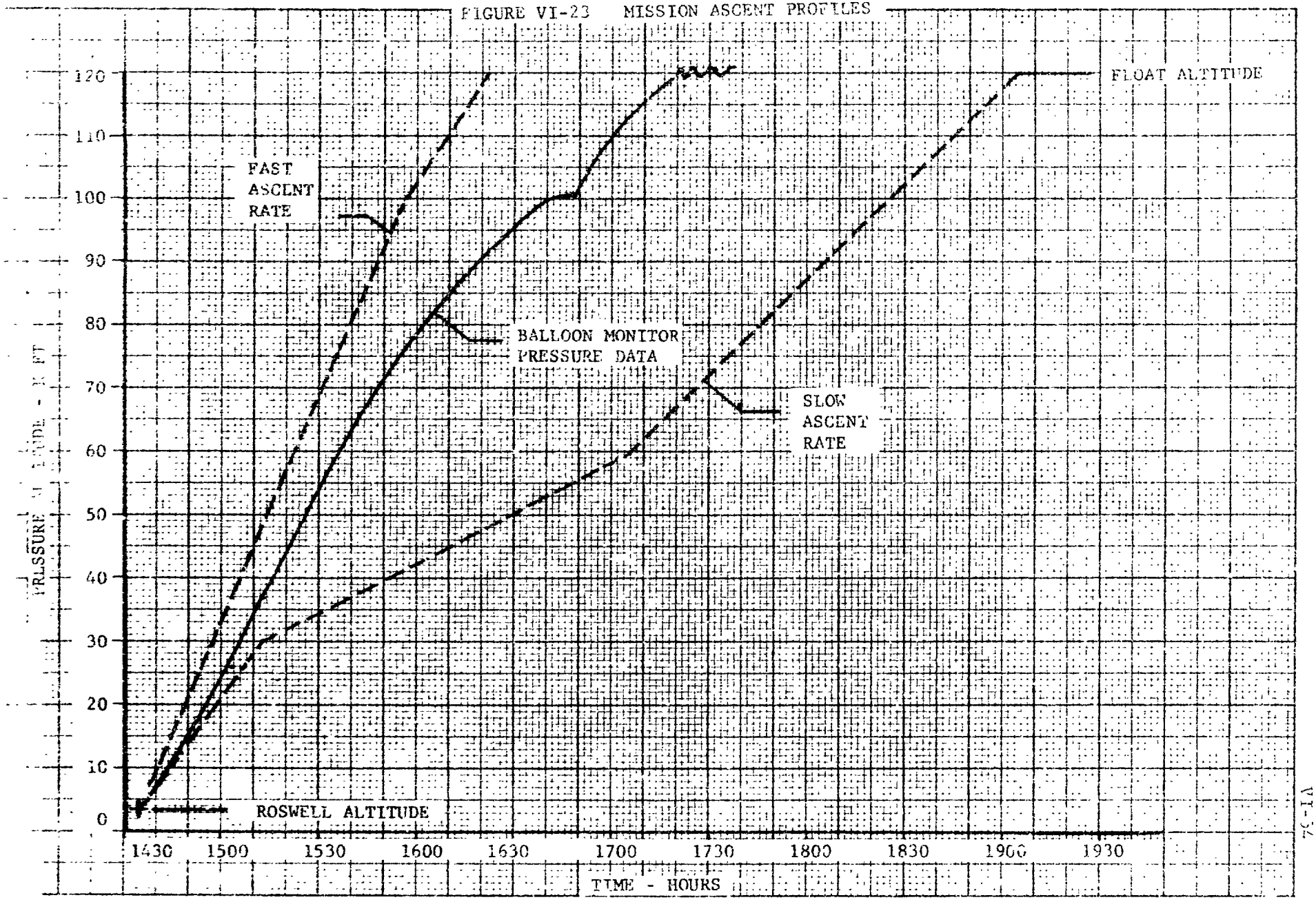

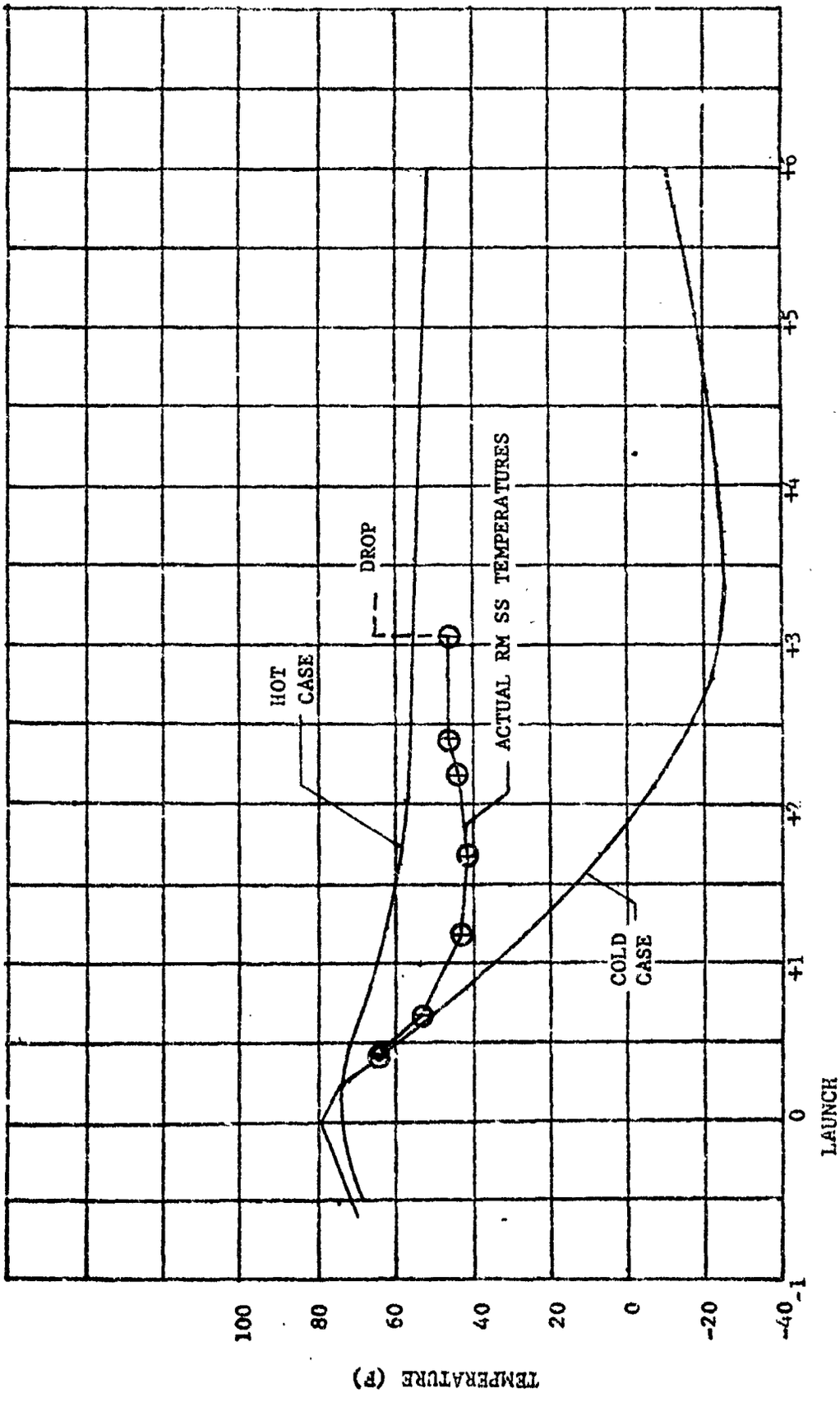

FIGURE VI-24 ROCKET MOTOR SUPPORT STRUCTURE TEMPERATURE HISTORY

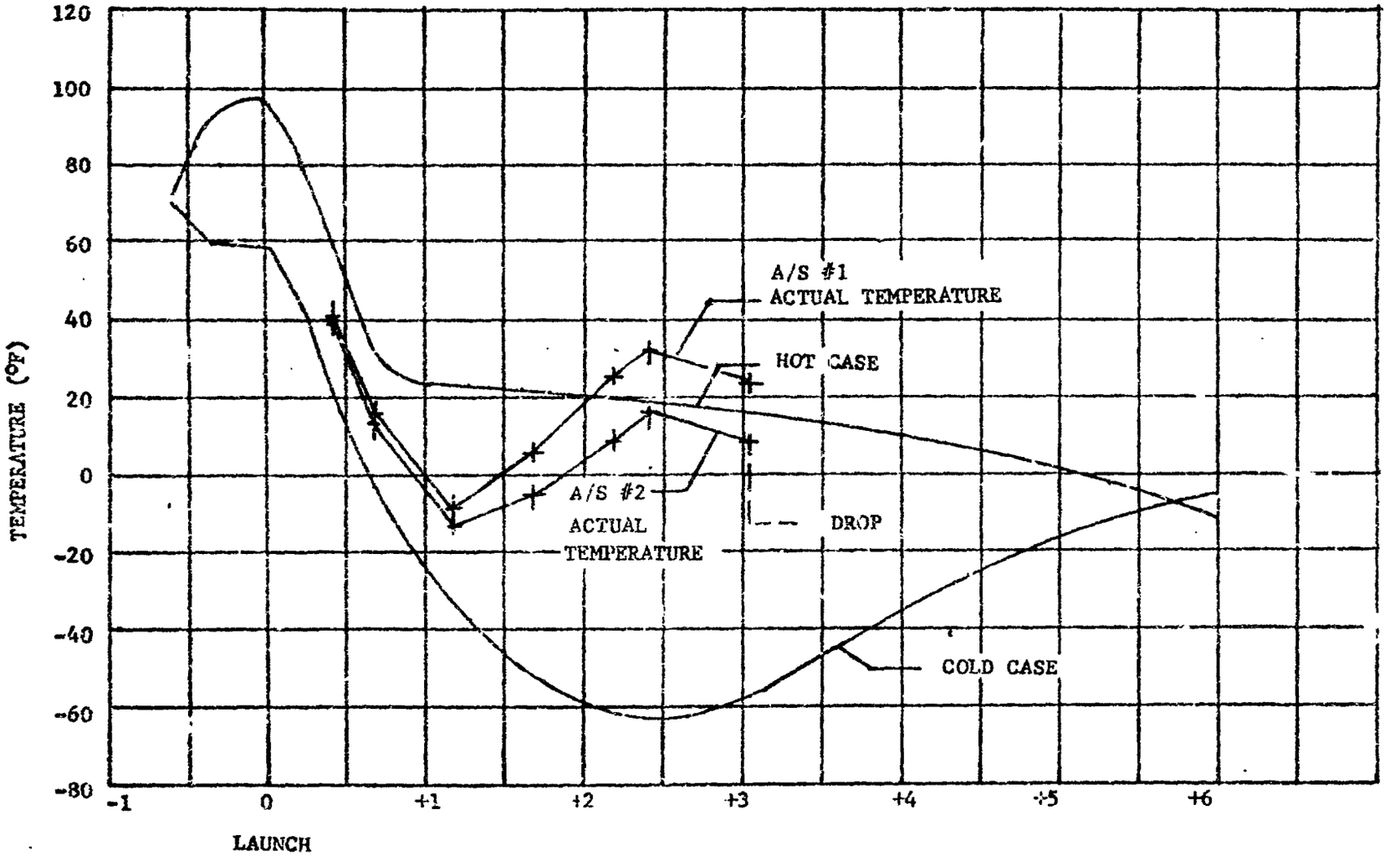

TIME FROM LAUNCH (HRS)

FIGURE VI-25 AEROSHELL TEMPERATURE HISTORY

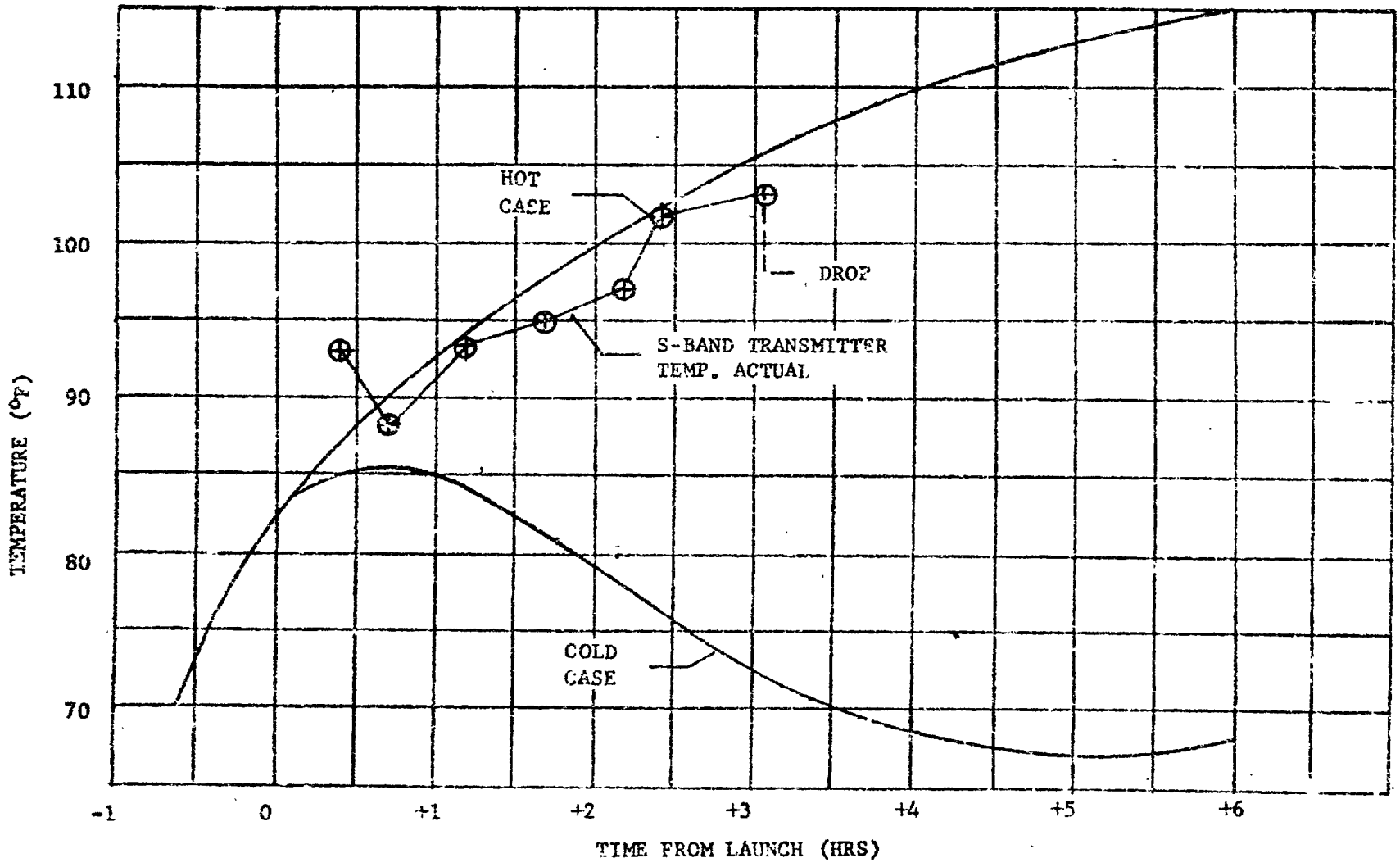

FIGURE VI-26 S-BANL TRANSMITTER TEMPERATURE HISTORY

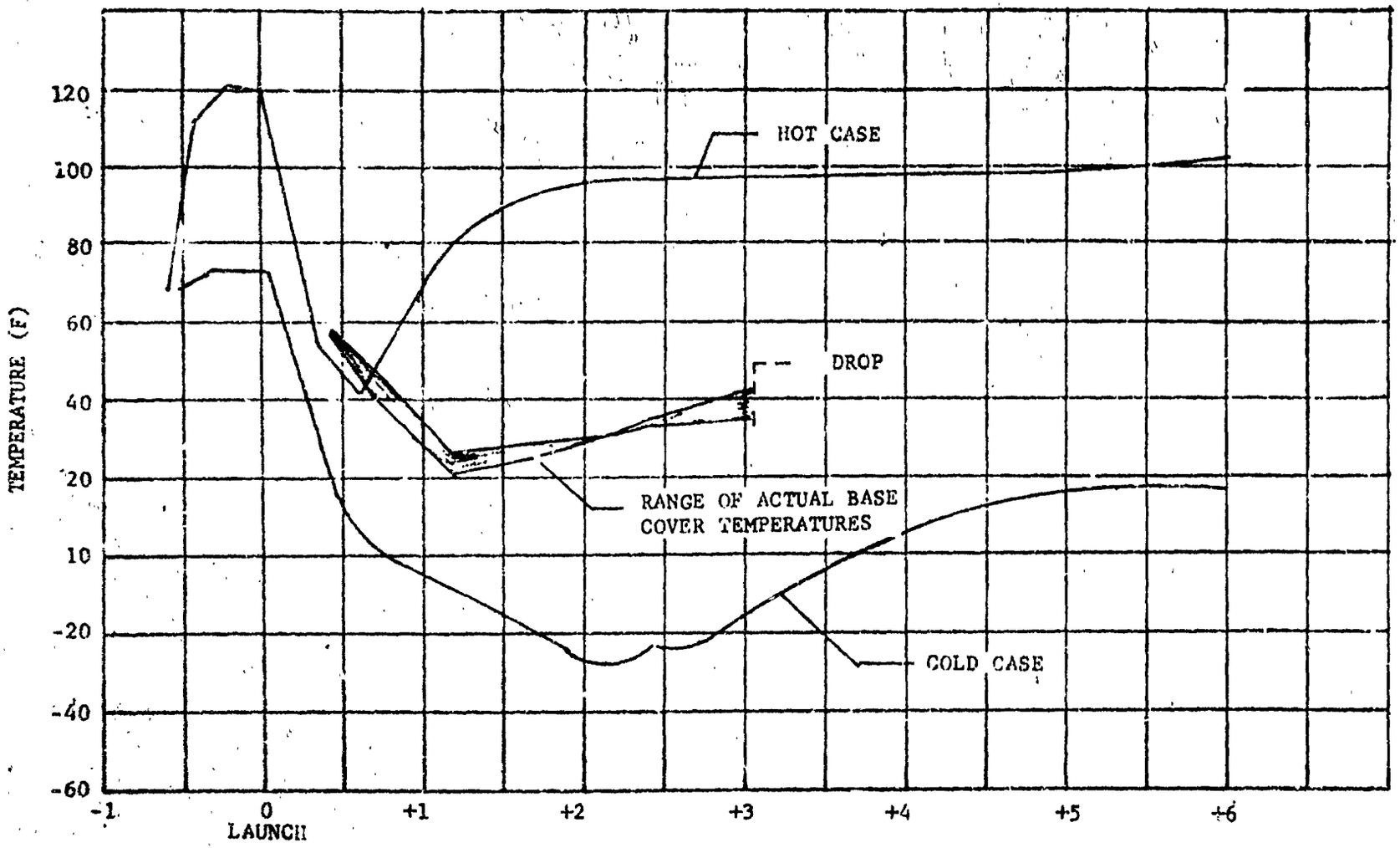

FIGURE VI-27 BASE COVER TEMPERATURE HISTORY

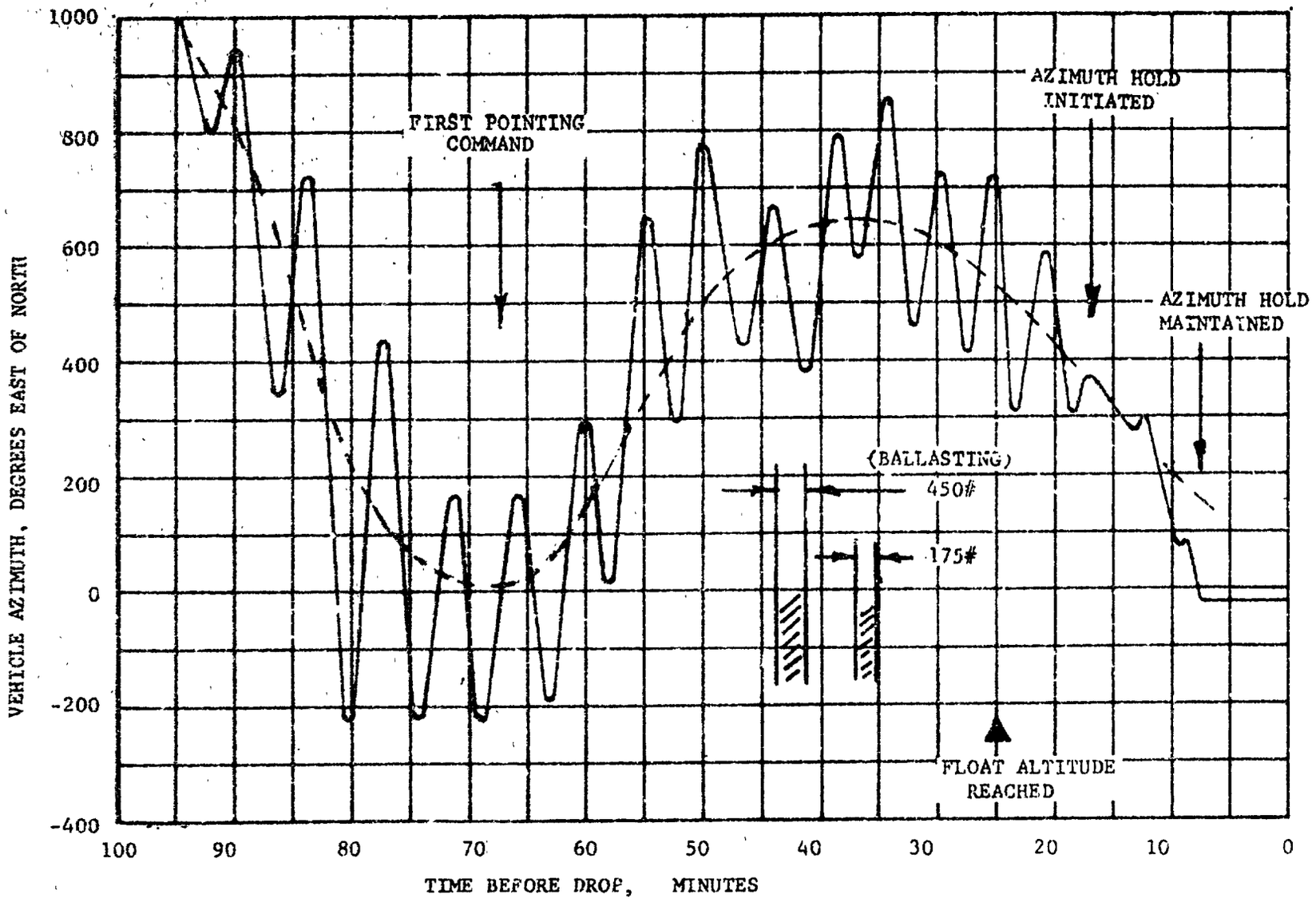

FIGURE VI-28 BLDT AV-1 VEHICLE AZIMUTH HEADING

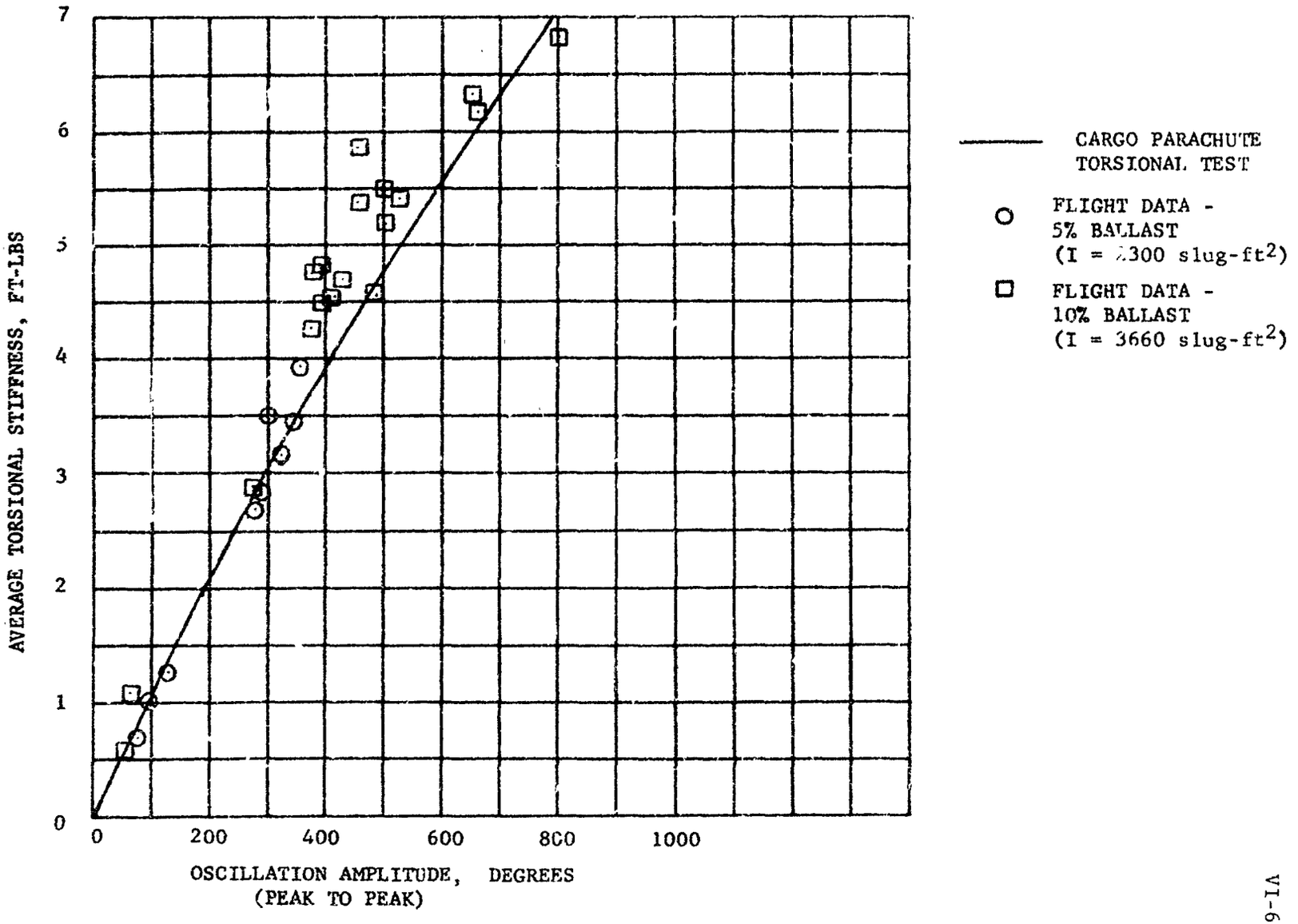

FIGURE VI-29 BLDT AV-1 TORSIONAL STIFFNESS

VII. CONCLUSIONS

The conclusions reached from the in-depth analysis of the AV-1 mission data and films and post-flight inspection of the flight hardware are as follows:

A. The flight vehicle suffered structural damage due to forces imposed during the balloon/vehicle launch process which resulted in the loss of the structural integrity of the interface between the load bar support structure and the flight vehicle and change to the flight vehicle drop attitude.

B. The revised vehicle drop attitude coupled with a low balloon float altitude was responsible for the vehicle altitude at mortar fire being lower than was required for the mortar fire ground command to be issued within the specified Mach number/dynamic pressure performance box.

C. The decelerator mortar fire command was issued by the airborne programmer which timed out while the dynamic pressure was 24% in excess of the nominal test requirement.

D. The excessive dynamic pressure test condition was cause for declaring the flight of vehicle AV-1 a "no test" for the qualification of the Viking Decelerator System since two gores of the parachute failed during the parachute inflation process.

E. Despite the parachute canopy damage, the decelerator system performed within the requirements for a successful Mars landing and the mission produced much useful data concerning the decelerator and flight vehicle performance. Except for dynamic pressure, the flight vehicle performance provided the proper qualification test conditions as follows:

Angle of Attack at mortar fire	$\leq 17^{\circ}$
Residual Spin Rate	$\leq 100^{\circ}$/sec
Parachute Temperature at M.F.	$\leq 80^{\circ}$F

F. The aeroshell separation time-distance history was more than adequate to meet the requirement of 50 feet of separation in 3 seconds.

VIII. REFERENCES AND OTHER DATA SOURCES

A. References

1. MMC RD-3720247, Parachute Test Objectives and Requirements for BLDT Program, Dated March 29, 1972.

2. MMC TR-3720052, Viking Vehicle Dynamics Data Book, Rev. F, July 6,1972.

3. MMC TR-3720074, Volume I, Transonic Aerodynamic Characteristics and Pressure Distributions on 8 Percent Scale Models of the Viking Lander Capsule, Aeroshell and Lander plus Base Cover, February 1971.

4. MMC TR-37209014, Viking Aerodynamics Data Book, Rev. C, June 1972.

5. GAC GER 15215, Rev. A, Viking Decelerator Design Analysis Report, March 20, 1972.

6. NASA TND-5296, Inflation and Performance of Three Parachute Configurations from Supersonic Flight Tests in a Low Density Environment, July 1969.

7. MMC TR-3720181, Scale Model Test Results of the Viking Parachute System at Mach Numbers from 1 through 2.6, November 1971.

8. MMC Memorandum 8943-72-116, Viking Parachute Swivel Loads and Pull-Off Angles from Dynamic Simulation, R. D. Moog, 10 May 1972.

9. NASA CR-1482, Statistical Trajectory Estimation Programs (STEP), Volumes I and II.

10. Users Guide No. 837L7041032, BLDT Six Degrees of Freedom Trajectory Program, dated February 1972.

11. TN-3770115, Aerothermodynamics Analysis of the BLDT Vehicle (CDR Configuration) dated July 1971.

B. Abbreviations

A/B	Airborne
AGC	Automatic Gain Control
A/S	Aeroshell
AV	BLDT Flight Vehicle Designator
BLDT	Balloon Launched Decelerator Test
Cg	Center of Gravity
CST	Combined System Test
DGB	Disk-Gap-Band
GAC	Goodyear Aerospace Corporation
g's	Gravitational acceleration - 32.2 FPS^2
IRIG	Inter Range Instrumentation Group
K	1000
KHz	Kilohertz
LADT	Low Altitude Drop Test
MMC	Martin Marietta Corporation
NASA	National Aeronautics and Space Administration
P	Roll Rate
PSF	Pounds per Square Foot
PSI	Pounds per Square Inch
PEPP	Planetary Entry Parachute Program
q	Dynamic Pressure
Q	Pitch Rate
R	Yaw Rate
RAOB	Radiosonde Observations
RF	Radio Frequency
RMSS	Rocket Motor Support Structure

s	Aerodynamic Reference Area
SCO	Subcarrier Oscillation
S/N	Serial Number
T	Time
TDC	Telemetry Data Center
TM	Telemetry
VLC	Viking Lander Capsule
V	Time Rate of Change of Velocity
WSMR	White Sands Missile Range
X,Y,Z	BLDT Vehicle Axis Designators
Z,Zuler	Greenwich Mean Time

APPENDIX A

DESCRIPTION OF

BALLOON LAUNCHED DECELERATOR

TEST VEHICLE

APPENDIX A

DESCRIPTION OF BALLOON LAUNCHED DECELERATOR TEST VEHICLE

The BLDT Vehicle utilized for the high altitude qualification tests of the Viking Mars Lander Decelerator consisted of six (6) major subsystems which were:

- o Structural Subsystem
- o Electrical Subsystem
- o Instrumentation Subsystem
- o R. F. Subsystem
- o Propulsion/Pyrotechnic Subsystem
- o Thermal Control Subsystem

The BLDT vehicles are designed to be flown as supersonic, transonic and free fall vehicles in order to simulate the various anticipated Mars entry conditions for decelerator deployment.

A. Structural Subsystem

The vehicle structural configuration provides an external envelope which simulates the Viking Lander Capsule in order to qualify the Decelerator in the wake of a blunt body similar to the actual Mars VLC. The general configuration of the BLDT vehicle is shown in Figures A-1 through A-7.

At the initiation of the BLDT vehicle design, the test bed was to match the Mars VLC Cg and mass properties at decelerator deploy command, insofar as practical. The requirement was for the BLDT vehicle to have a weight of 1888 pounds with a Cg offset of 1.41 inches in the -Z direction at the time of decelerator mortar fire command. The final mass properties

(1) -Z AXIS Cg OFFSET = 1.41" ± 0.030"

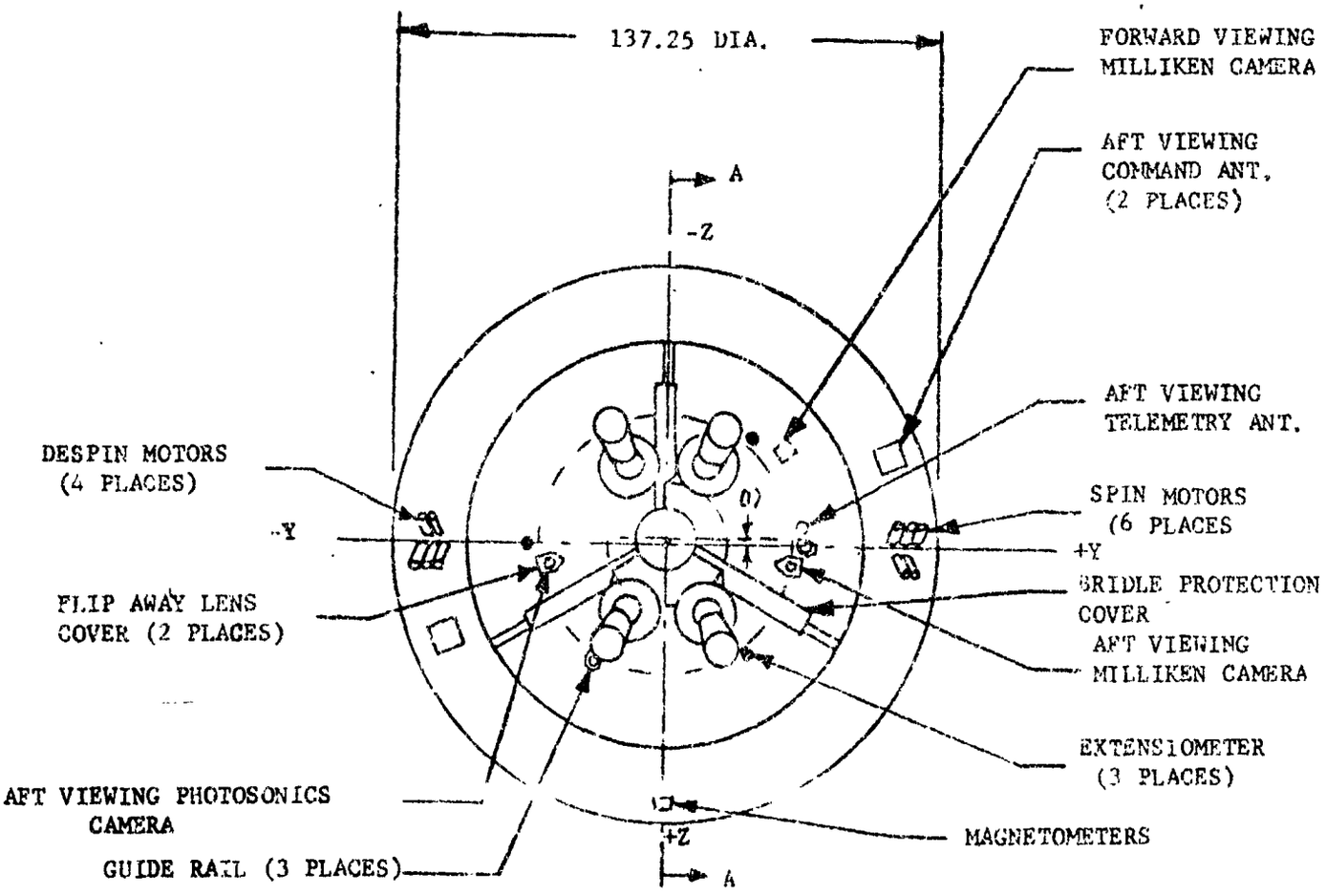

VIEW LOOKING AT AFT END OF VEHICLE

BLDT SUPERSONIC VEHICLE CONFIGURATION

FIGURE A-1

(1) X AXIS Cg AT MORTAR FIRE = 31.7" to 33.7"

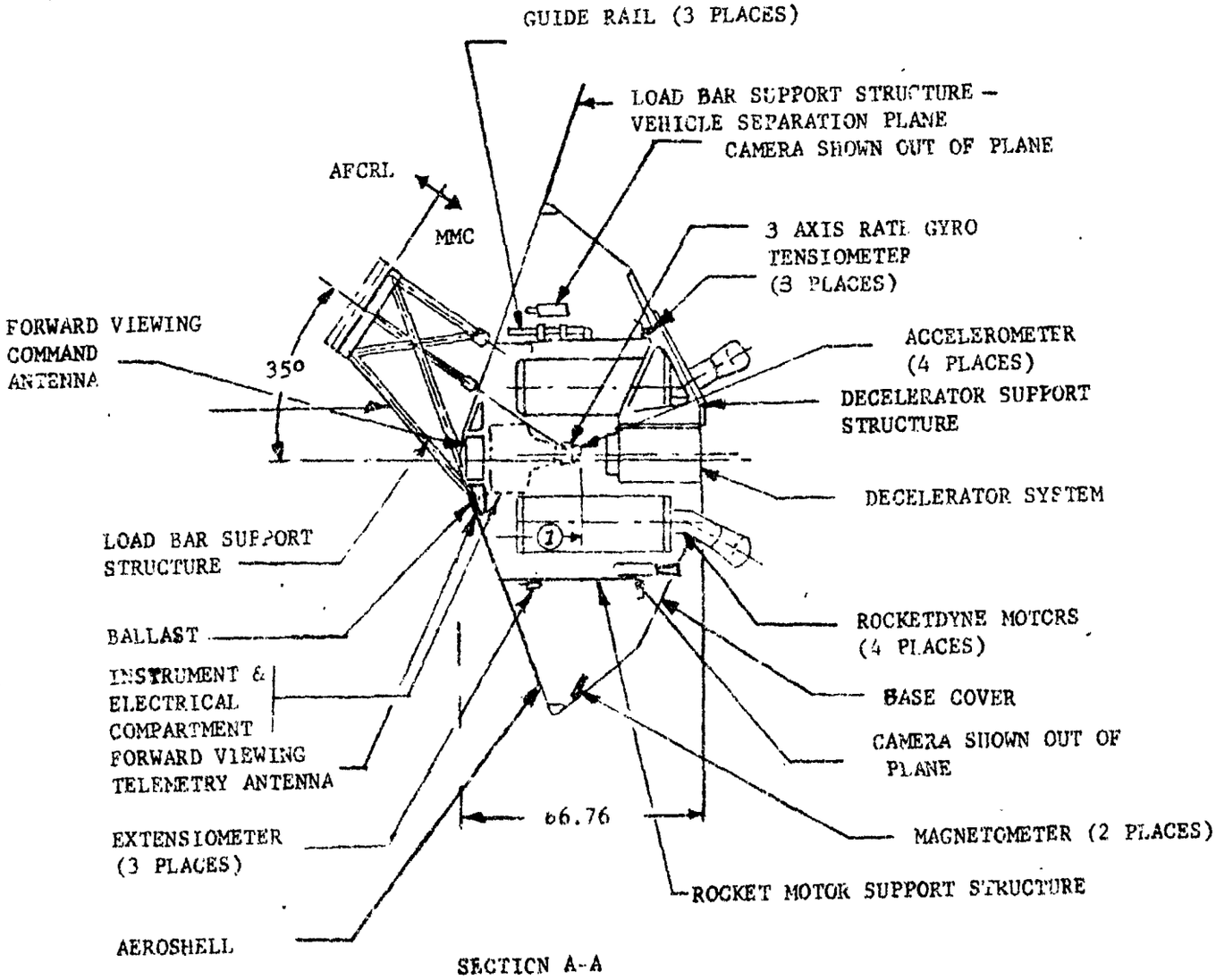

SECTION A-A

BLDT SUPERSONIC VEHICLE CONFIGURATION

FIGURE A-2

(1) -Z AXIS Cg OFFSET = 1.41" ± 0.030"

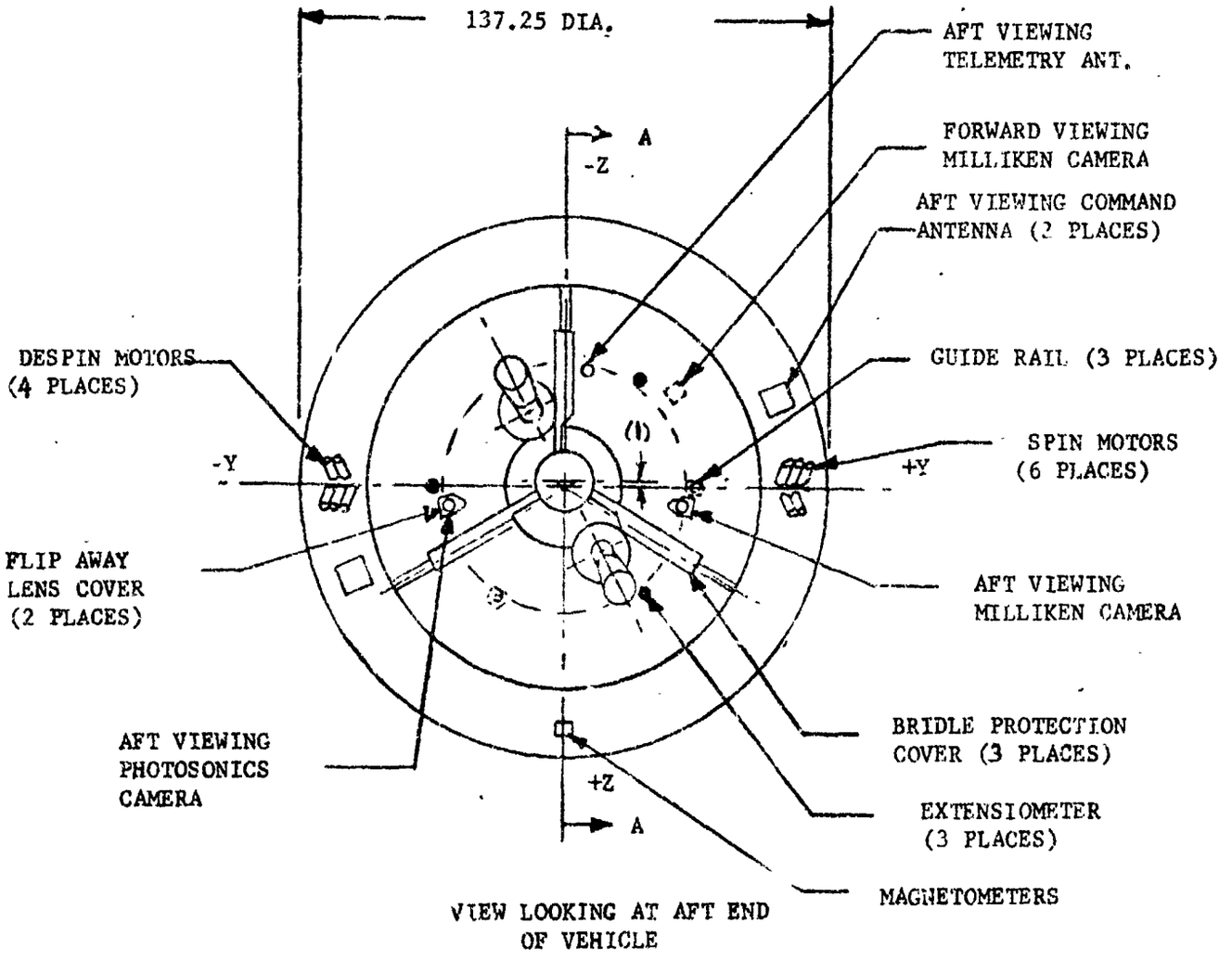

BLDT TRANSONIC VEHICLE CONFIGURATION

FIGURE A-3

(1) X AXIS Cg AT MORTAR FIRE = 31.7" to 33.7"

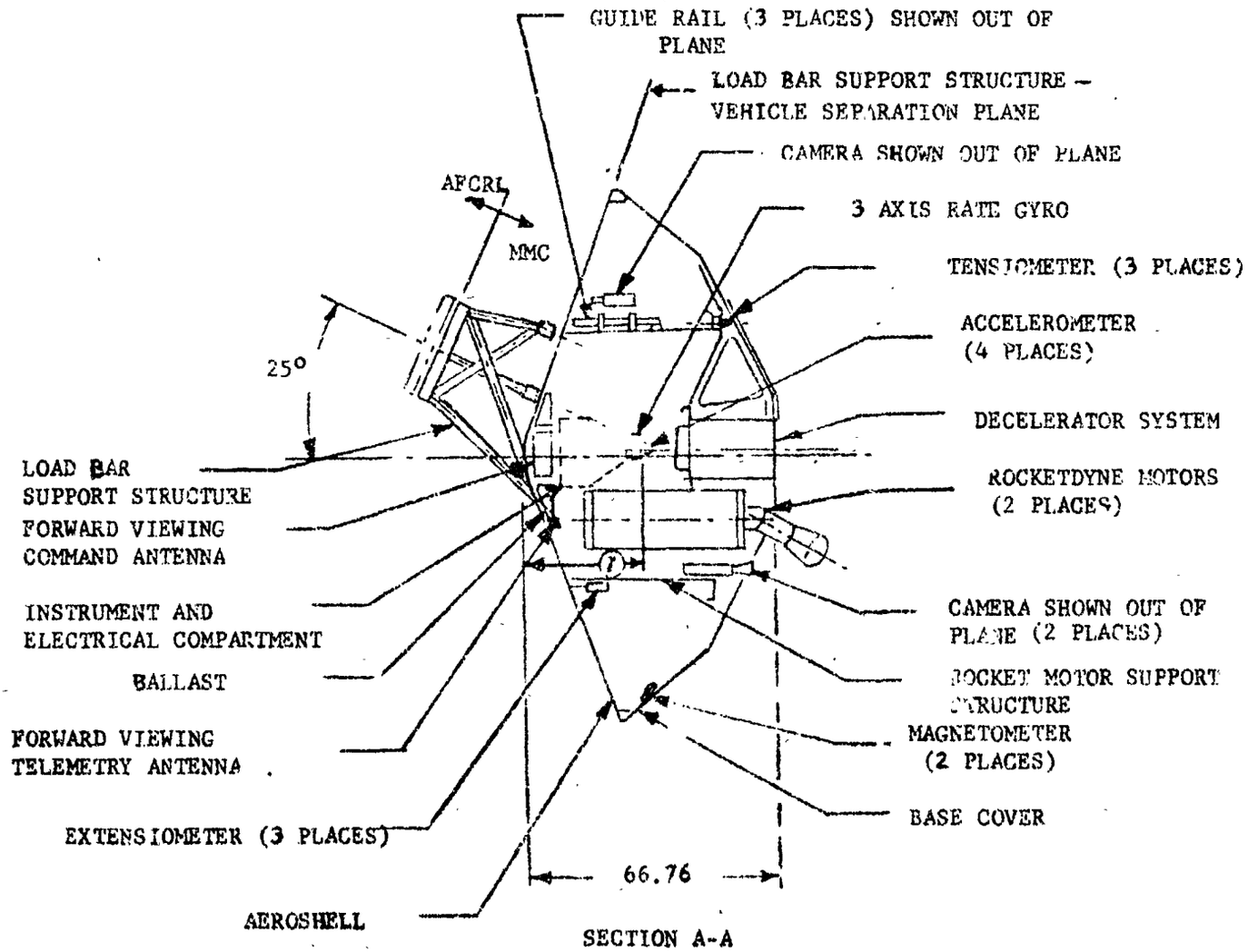

SECTION A-A

RLDT TRANSONIC VEHICLE CONFIGURATION

FIGURE A-4

(1) -Z AXIS Cg OFFSET = 1.41" ± 0.030"

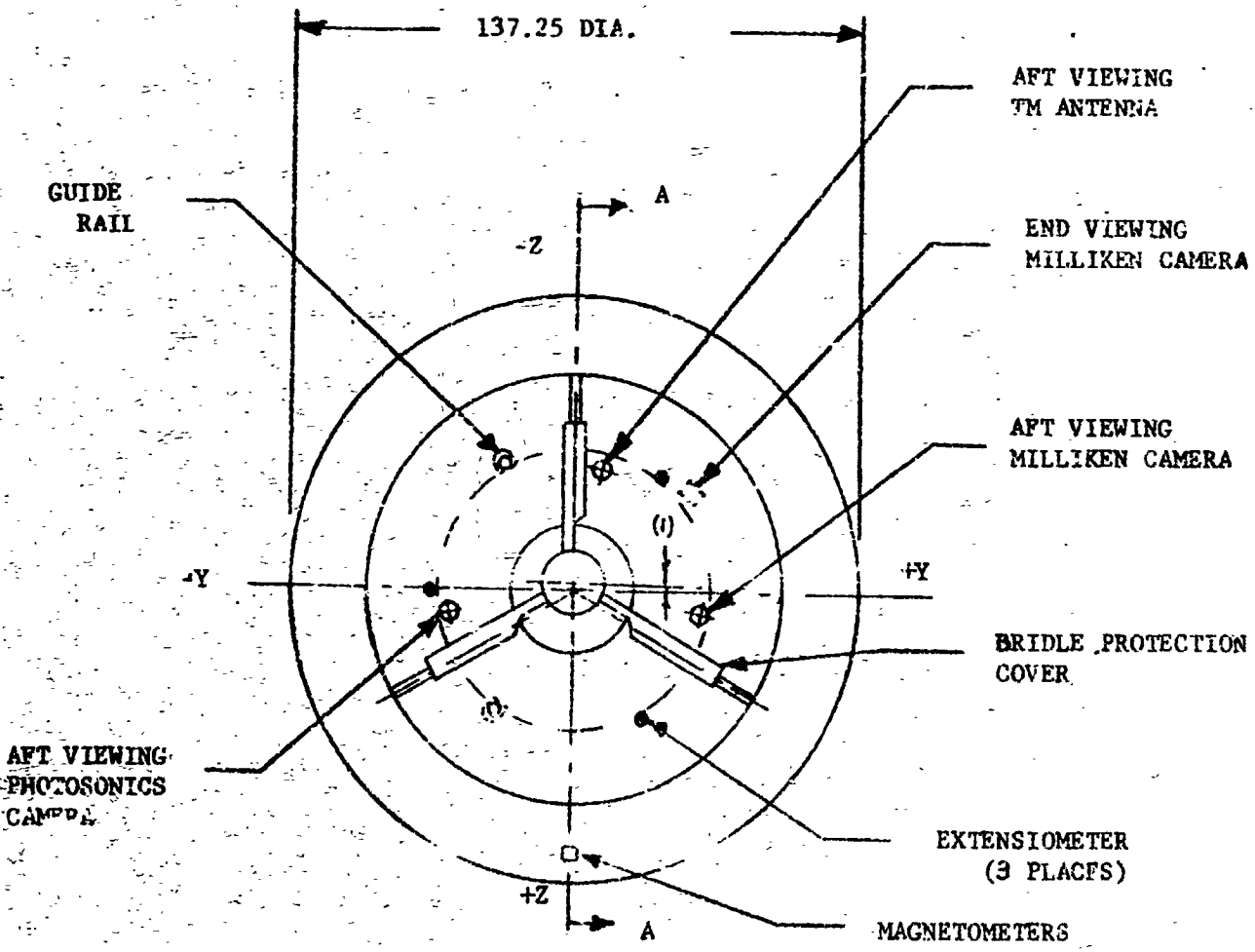

VIEW LOOKING FORWARD

BLDT SUBSONIC VEHICLE CONFIGURATION

FIGURE A-5

(1) X AXIS Cg AT MORTAR FIRE = 31.7" to 33.7"

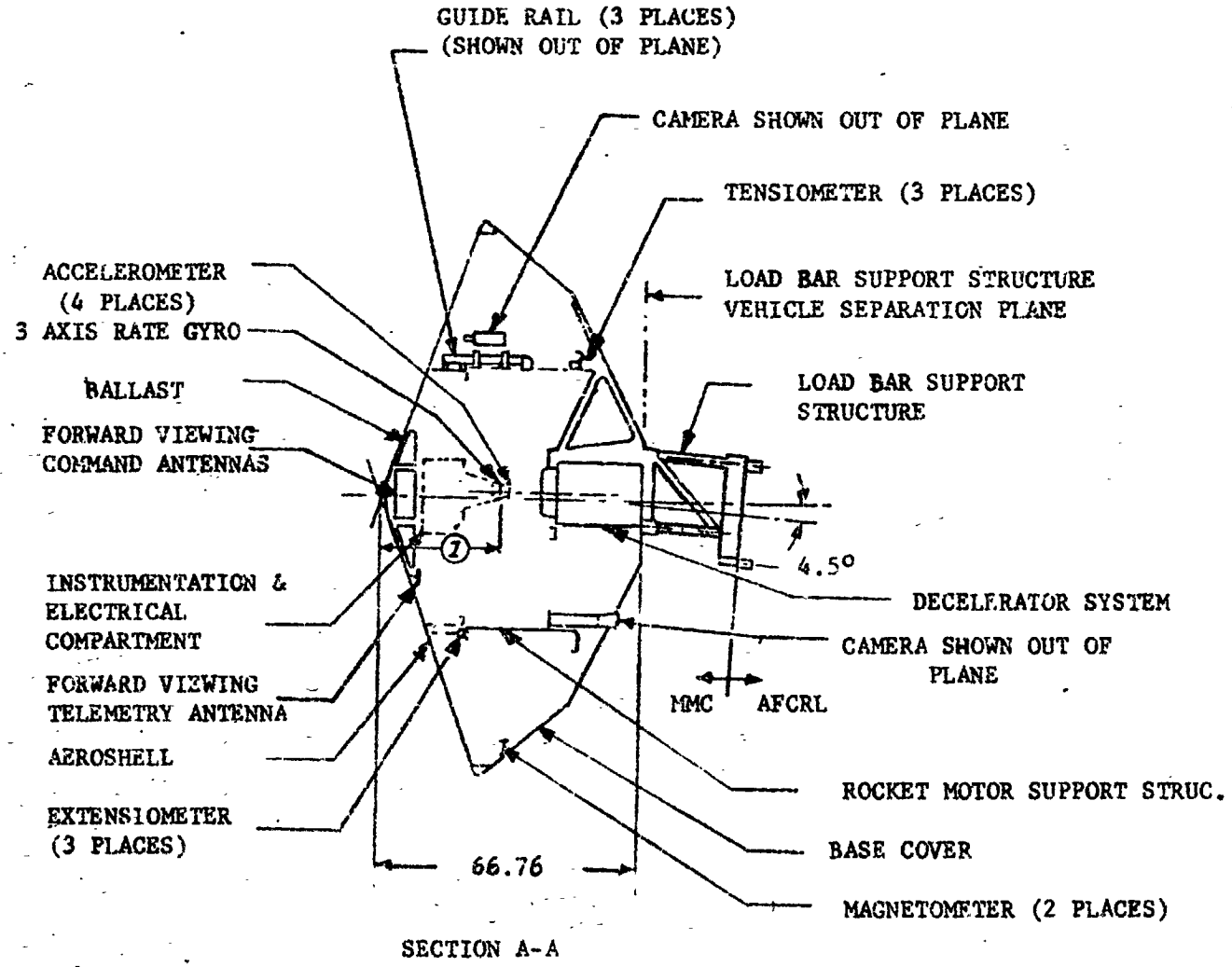

SECTION A-A

RLDT SUBSONIC VEHICLE CONFIGURATION

FIGURE A-6

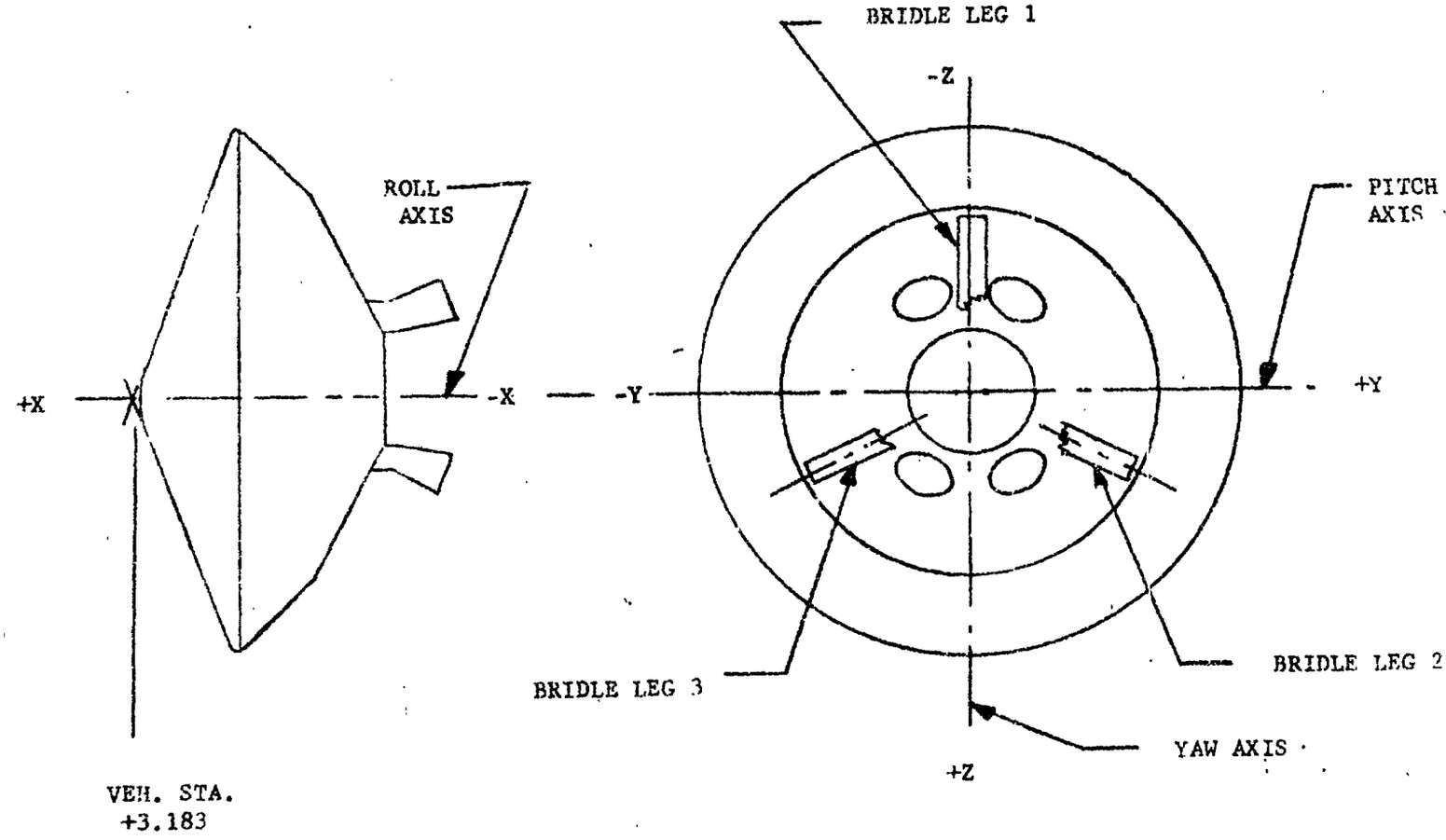

BLDT COORDINATE SYSTEM
FIGURE A-7

for each vehicle, included in the individual reports, indicates the revisions which were made to the mass properties subsequent to the BLDT vehicle design.

The structural subsystem consisted of six (6) major components as follows:

1. Rocket Motor Support Structure

The rocket motor support structure is a cylindrical component, approximately 64 inches in diameter, which provides the major vehicle internal longitudinal support structure as well as providing the motor mounts for the supersonic and transonic vehicles.

2. Instrument Beam

The instrument beam is a structural beam which was tied to the forward surface of the RMSS and ran symmetrically along the Y, -Y axis. It also contained an aft facing pylon to mount the accelerometers and rate gyros at or near the vehicle longitudinal Cg.

3. Base Cover

The base cover is a lightweight external shell providing an aft configuration similar to the Mars VLC.

4. Decelerator Support Structure

The decelerator support structure is a three leg structure, similar to the Mars VLC decelerator support structure, with a cylindrical center section for mounting of the decelerator cannister parallel to the BLDT longitudinal centerline. The decelerator support structure assembled into the base cover to provide an intermediate assembly.

5. Aeroshell

The Aeroshell which is the forward surface of the vehicle provides a conical blunt aerodynamic surface approximately 11.5 feet in diameter with a 140° included angle. The aeroshell provides a forward configuration similar to the Mars VLC.

6. Load Bar Support Structure

The load bar support structure is a tubular structural member which provides the interface with the Air Force Cambridge Research Laboratory (balloon) load bar as well as providing the correct hanging pitch attitude.

B. Electrical Subsystem

The electrical subsystem provides the flight power, cabling and switching/sequencing devices required to properly sequence and activate the various functions. The electrical subsystem is shown schematically in Figure A-8.

The vehicle is powered by five (5) silver zinc batteries as follows:

1. Main Battery - 60 AH - MMC P/W PD9450026

Provides power for telemetry, command system A and A/B heaters.

2. Transient Battery - 16 AH Engle Pitcher Model 4332

Provides power for timing correlator, C-band transponder and command system B.

3. Pyro Battery A - 1.0 AH - ESB Model 392

Provides power to all pyro A circuit ordnance devices and airborne programmer A.

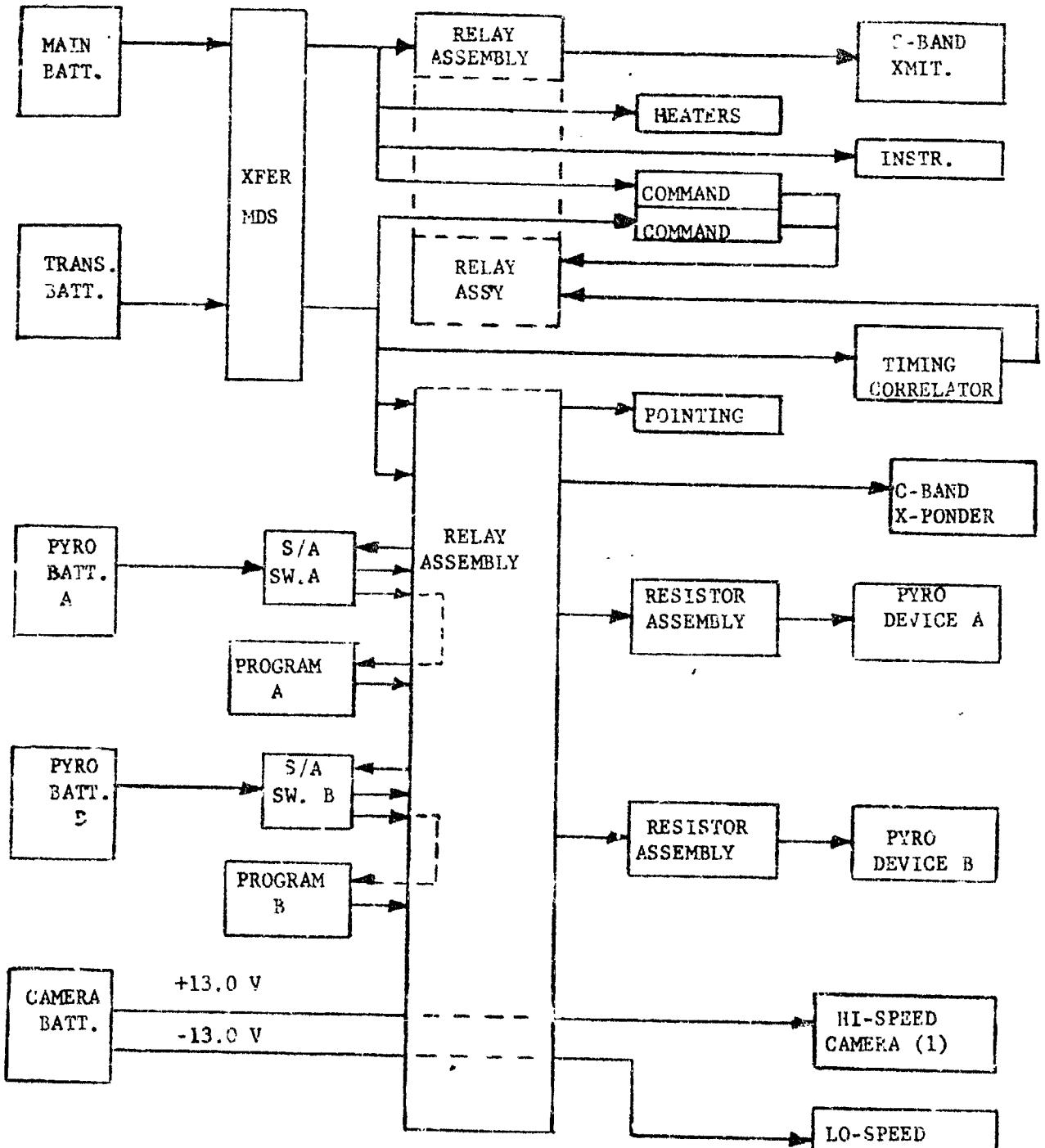

BLDT POWER SUBSYSTEM
BLOCK DIAGRAM

FIGURE A-8

4. Pyro Battery B - 1.0 AH - ESB Model 392

Provides power to all Pyro B circuit ordnance devices and airborne programmer B.

5. Camera Battery - 1.0 AH - ESB Model 393 (Similar to model 392 except tapped at 9 cells and 18 cells).

Provide ±13 volts power to onboard high speed cameras.

The electrical subsystem provides completely redundant airborne sequencing programmers and completely redundant pyrotechnic circuits.

In addition, the electrical subsystem provides all power switching relays, motor driven switches, power limiting resistors and airborne heaters.

C. Instrumentation Subsystem

The BLDT Instrumentation subsystem provides for the real time measurement and conditioning of the parameters listed in Table A-1 and provides timing correlation for the real time measurements and airborne camera. The instrumentation subsystem utilizes a PAM/FM/FM configuration as shown schematically in Figure A-9.

Additionally, the instrumentation subsystem provides the following photographic coverage:

1. Aft Looking Photosonics

Approximately 450 frames/second to record the decelerator deployment sequence.

2. Aft Looking Milliken

Sixty-four frames/second to record the decelerator deployment sequence.

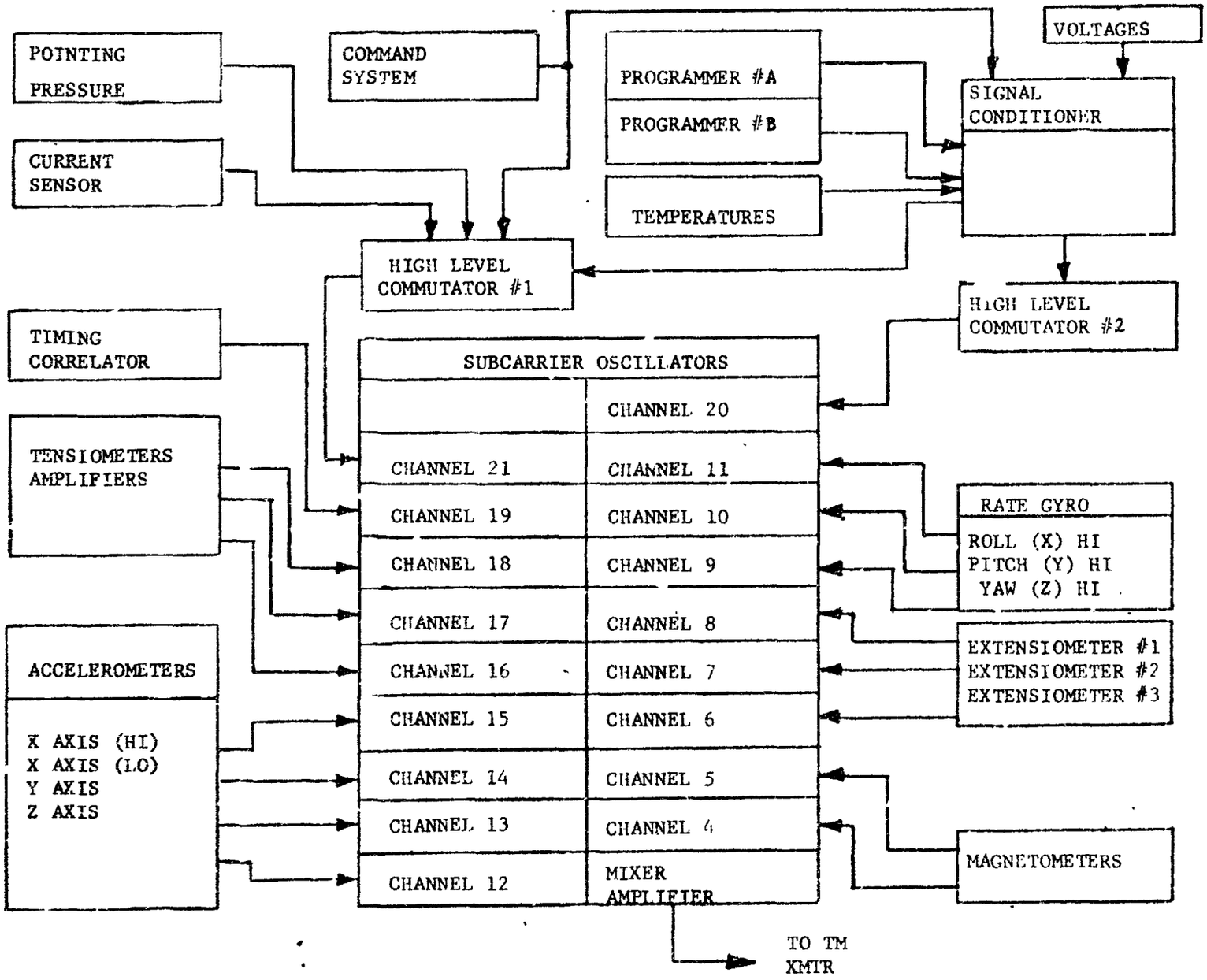

FIGURE A-9 BLDT INSTRUMENTATION SYSTEM

3. Forward Looking Milliken

Thirty-two frames/second to record the Aeroshell separation sequence and obtain a time/distance history.

D. R. F. Subsystem

The R. F. Subsystem consists of the TM transmitter, the C-Band transponder and the redundant command receiver/decoders with all of the required antenna systems.

1. TM Transmitter

The telemetry transmitter provides for the FM transmission of the composite FM data from the Instrumentation Subsystem mixer amplifier. The transmitter provides 5 watts power output in the S-Band (2285.5 MH_z) range. The TM transmitter and antenna system is shown schematically in Figure A-10.

2. C-Band Tracking Transponder

The GFE tracking transponder was provided by White Sands Missile Range and is compatible with tracking radar AN/FPS-16 utilized at WSMR. The transponder and antenna system is shown schematically in Figure A-10.

3. Command Receiver/Decoder

The vehicle command system, including antenna, multicoupler, receivers and decoders, is shown schematically in Figure A-11

The redundant receiver/decoders operate on an assigned frequency of 541 MH_z and provide a 28 volt nominal decoder output for command inputs with seven command tones selected from IRIG-103-61 channels 1 through 20.

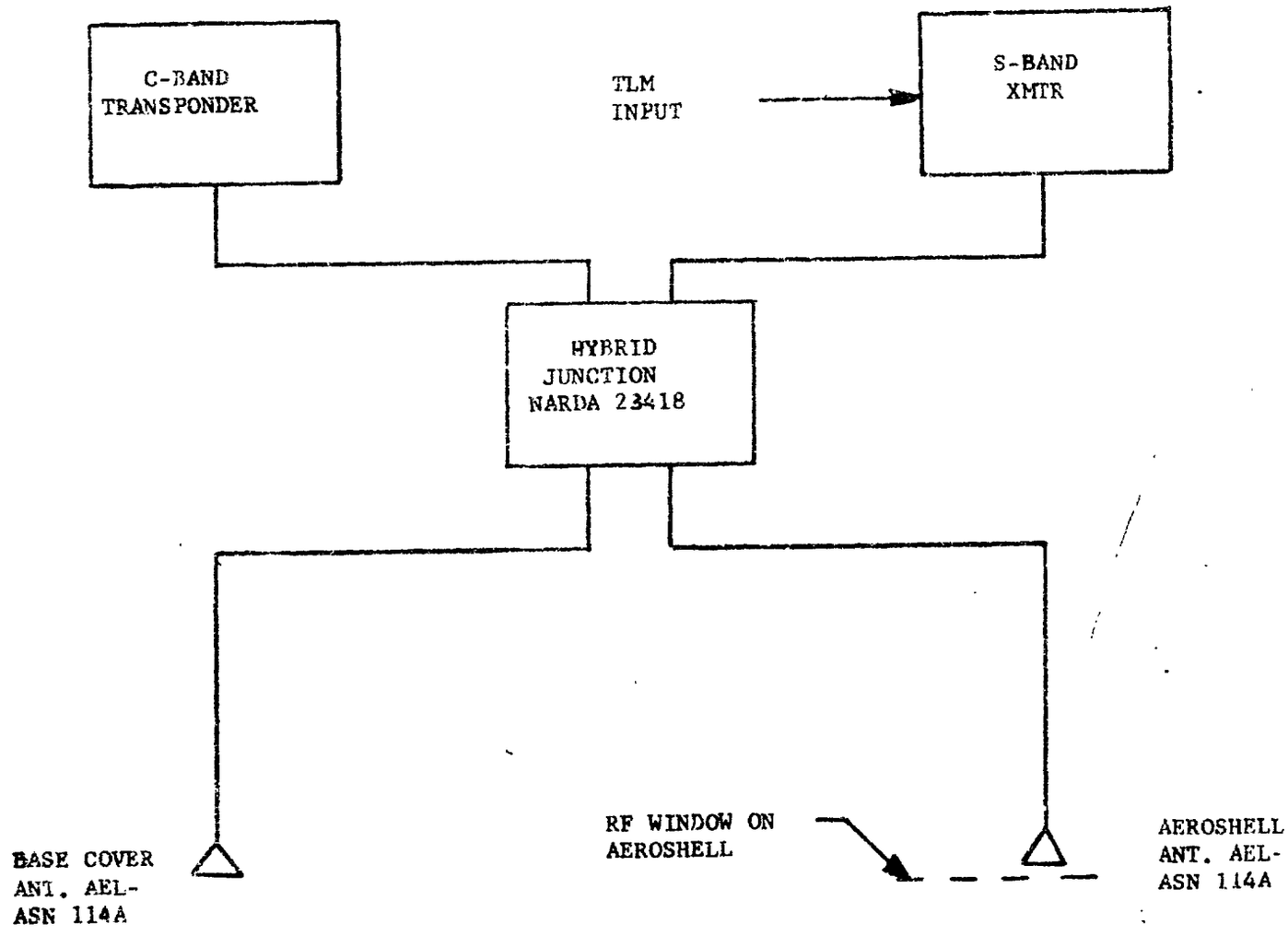

FIGURE A-10 TRACKING & TELEMETRY ANTENNA SYSTEM

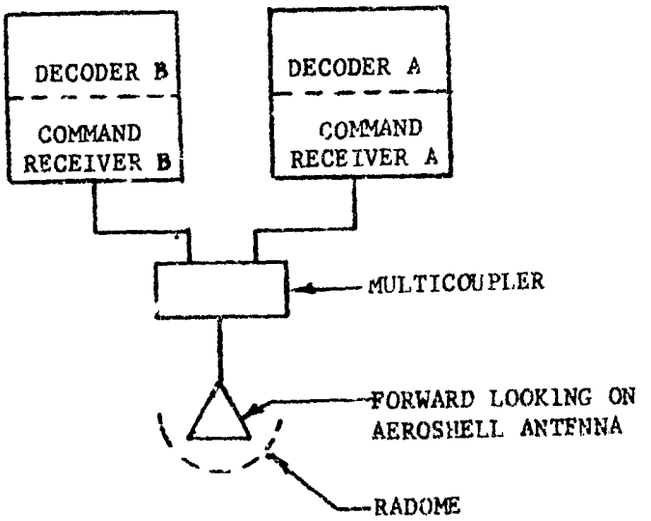

SUBSONIC CONFIGURATION

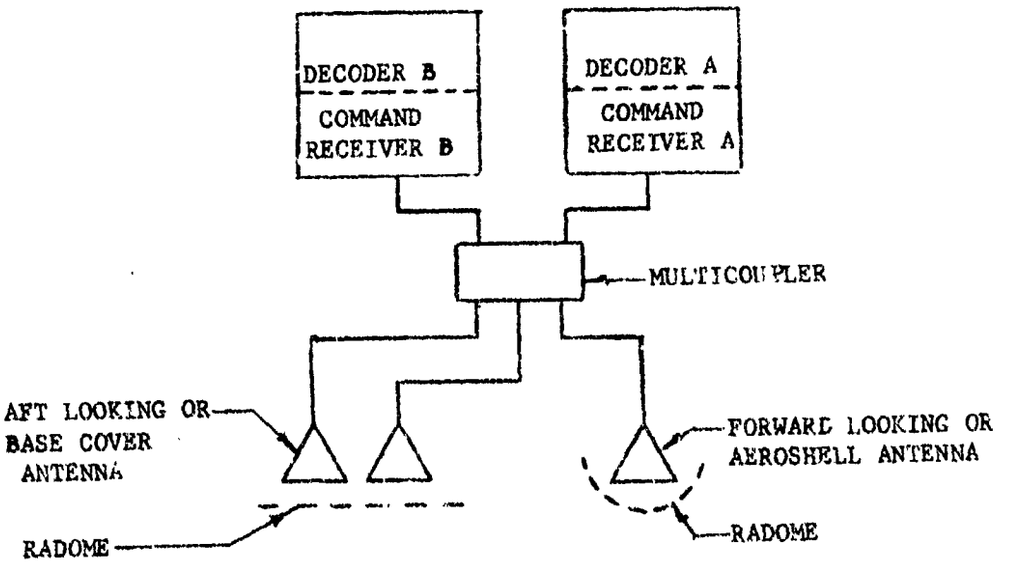

SUPERSONIC AND TRANSONIC CONFIGURATION

FIGURE A-11

The system coding is such that triple tone ground commands result in the following airborne functions:

Function	Commands		
	Primary	Backup	Redundant
Release from load bar	X		X
Mortar Fire	X		X
Arm Ordnance Bus	X		X
Safe Ordnance Bus	X	X	
Turn RF on	X		
Turn RF off	X		
Pointing, Clockwise	X	X	
Pointing, Counterclockwise	X	X	

E. Propulsion/Pyrotechnic Subsystem

The propulsion/pyrotechnic subsystem consists of the solid rocket motors required on the supersonic and transonic vehicles, the azimuth pointing system required on the supersonic and transonic vehicles and the pyrotechnic devices required on all three configurations.

The main propulsion assembly consists of a set of Rocketdyne RS-B-535 solid propellant rocket motors each having the following characteristics:

	Nominal	3 σ Variation
Total Impulse, lbf-sec	Classified	0.6%
Burn Time Avg. Thrust, lbf	Classified	1.9%
Nozzle Cant Angle, deg	35	0.1
Thrust Vector Alignment, deg**		0.2
Ignition Interval, msec	49	+27, -17
Burn Time, sec	Classified	1.8%
Loaded Weight, lbm	461.2	0.25***
Burnout Weight, lbm	91.7	3.7****

The supersonic configuration vehicles are provided with 4 of the above motors with the transonic vehicle containing 2.

The spin/despin system is required to reduce trajectory dispersions during booster burn and despin after burnout. Spin Motors having the following characteristics are used:

	Nominal*	3 σ Variation
Total Impulse, lbf-sec	76.5	3.0%
Burn Time Avg. Thrust, lbf	86.2	8.0%
Ignition Interval, msec	10.0	+10.0, -5.0
Burn Time, sec	0.87	+11.0%
Loaded Weight, lbm	1.2	0.1
Burnout Weight, lbm	0.9	0.1

* Vacuum Conditions, 70°F
** Alignment with respect to nozzle geometric centerline.
*** Actual weighing tolerance.
**** Variation from predicted value.

The supersonic and transonic vehicles utilized 6 each of the above motors for spin-up and 4 each of the above for despin.

Other pyromechanical and pyrotechnic functions included in the vehicle are:

Function	Supersonic	Transonic	Subsonic
Aeroshell Sep. Nuts	3	3	3
Load Bar Release Nuts	0	0	3
Tension Rod Separator	1	1	0
Cable Cutters	2	2	0
Decelerator Mortar*	1	1	1

* Part of Decelerator System

Also included in the propulsion subsystem is an azimuth pointing system which is used to orient the supersonic and transonic vehicle azimuth at drop in order to assure impact within the White Sands Missile Range in the event of a complete decelerator failure.

The pointing system is comprised of a gaseous nitrogen thruster system located on the balloon load bar. The system provides paired clockwise or counterclockwise rotational moments in response to ground commands. The azimuth pointing system is shown schematically in Figure A-12.

F. Thermal Control Subsystem

The thermal control subsystem consists of those passive and active components required to maintain vehicle components within the required temperature levels. These components were generally:

1. Internal and external blankets,
2. Active heaters,
3. Base cover ablative material.

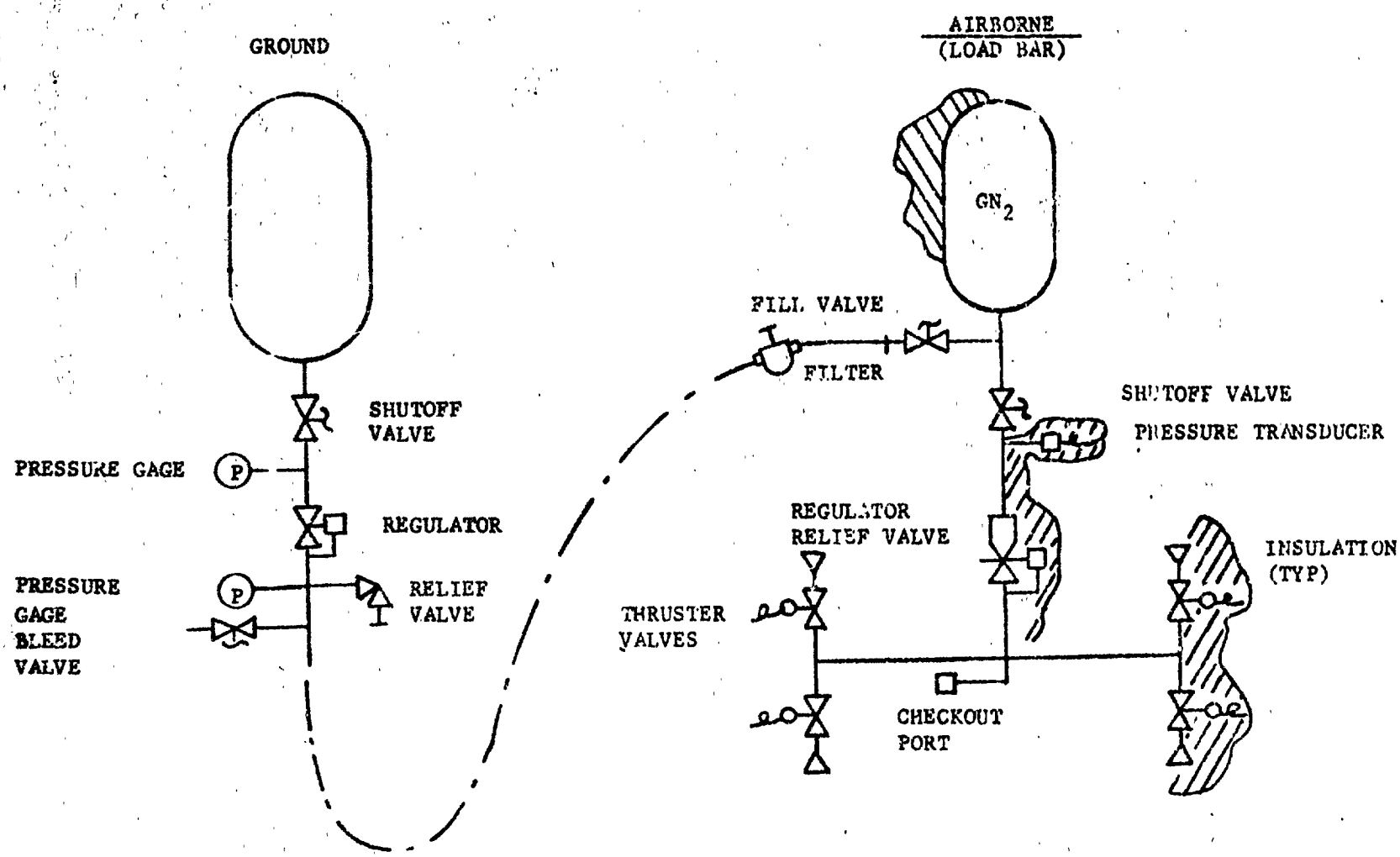

FIGURE A-12 BLDT POINTING SYSTEM

TABLE A-1

BLDT Telemetry Measurement List

No.	Measurement	Range	Accuracy End-to-End	Resolution	Response	Remarks
1	Accel. X Axis	-2,+5g * -2,+3g **	5%	0.07g 0.05g	100 Hz	Low Range
2	Accel. X Axis	-15, 1g * -7, +1g **	5%	0.16g 0.08g	100 H_z	High Range
3	Accel. Y Axis	+1.0g	5%	0.01g	100 H_z	
4	Accel. Z Axis	+1.0g	5%	0.01g	100 H_z	
5	Heading	360 deg.	±5 deg.	1 deg.	5 H_z	Magnetometer No. 1
6	Heading	360 deg.	±5 deg.	1 deg.	5 H_z	Magnetometer No. 2
7	Rate Gyro, X Axis	±300°/sec.	5%	3.0°/sec	20 H_z	
8	Rate Gyro, Y Axis	±300°/sec.	5%	3.0°/sec	20 H_z	
9	Rate Gyro, Z Axis	±300°/sec.	5%	3.0°/sec	20 H_z	
10	Strain Link	0 to 12,000 lbs. ***	5%	120 lbs.	100 H_z	Parachute Linkage No. 1

* Supersonic Flight

** Transonic and Subsonic Flight

*** Amplifier will be adjusted to read 18,000 pounds full scale for supersonic flight only.

TABLE A-1 (CONTINUED)

BLDT Telemetry Measurement List

No.	Measurement	Range	Accuracy End-to-End	Resolution	Response	Remarks
11	Strain Link	0 to 12,000 lbs. *	5%	120 lbs.	100 H_z	Parachute Linkage No. 2
12	Strain Link	0 to 12,000 lbs. *	5%	120 lbs.	100 H_z	Parachute Linkage No. 3
13	Timing Pulse	25 PPS, 0 to 1.25 VDC	1%	ON/OFF	125 H_z	Camera Correlation
14	Temperature	+25 to +150°F	5%	1.5F	10 H_z	Mortar Breech, Temp. Commutated at 30 SPS
15	Voltage	5 VDC	5%	0.05 VDC	10 H_z	Commutator #1 Full Scale Calibration at 30 SPS
16	Voltage	0 VDC	5%	0.05 VDC	10 H_z	Commutator #1 Zero Scale Calibration at 30 SPS
17	Voltage	0 to 36 VDC	5%	0.36 VDC	10 H_z	Main Battery, Commutated at 30 SPS
18	Current	0 to 16A	5%	0.16 A	10 H_z	Main Battery, Commutated at 30 SPS
19	Voltage	0 to 37 VDC	5%	0.37 VDC	10 H_z	Pyro Battery A Commutated at 30 SPS
20	Event, Cont.	0 to 14 VDC Step Change	± 50ms	(HI/LO)	10 H_z	Prog. A Reset Commutated at 30 SPS

* Amplifier will be adjusted to read 18,000 pounds full scale for supersonic flight only.

TABLE A-1 (CONTINUED)

BLDT Telemetry Measurement List

No.	Measurement	Range	Accuracy End-to-End	Resolution	Response	Remarks
21	Event, Pulse	0 to 14 VDC 0.1 sec Duration	± 50 ms	(ON/OFF)	10 H_z	Prog. A TM Chan. Commutated at 30 SPS
22	Event, Pulse	0 to 14 VDC 0.1 sec Duration	± 50 ms	(ON/OFF)	10 H_z	Prog. B TM Chan. Commutated at 30 SPS
23	Event, Cont.	0 to 4 VDC Step Change	± 50 ms	(HI/LO	10 H_z	CW Point. Val e Signal Commutated at 30 SPS
24	Event, Cont.	0 to 4 VDC Step Change	± 50 ms	(HI/LO)	10 H_z	CCW Point. Valve Signal Commutated at 30 SPS
25	Event, Cont.	0 to 4 VDC Step Change	± 50 ms	(HI/LO)	10 H_z	Safe/Arm Sw. A Arm Position Comm. at 30 SPS
26	Event, Cont.	0 to 4 VDC Step Change	± 50 ms	(HI/LO)	10 H_z	Safe/Arm Sw. A Safe Position Comm. at 30 SPS
27	Pressure	0-2500 psia	5%	25 psi	10 H_z	Pointing system, Pressure Commutated at 30 SPS
28	Extensiometer	0 to 12"	5%	0.12"	5 H_z	#1 Aeroshell Sep. Dist.
29	Extensiometer	0 to 12"	5%	0.12"	5 H_z	#2 Aeroshell Sep. Dist.
30	Extensiometer	0 to 12"	5%	0.12"	5 H_z	#3 Aeroshell Sep. Dist.
31	Voltage	0 to 37 VDC	5%	0.37 VDC	10 H_z	Pyro Battery B Commutated at 30 SPS
32	Voltage	0 to 33.5 VDC	5%	0.33	10 H_z	Transient Battery Commutated at 30 SPS

TABLE A-1 (CONTINUED)

BLDT Telemetry Measurement List

No.	Measurement	Range	Accuracy End-to-End	Resolution	Responce	Remarks
33	Event, Cont.	0 to 4 VDC Step Change	± 50 ms	(HI/LO)	10 H_z	Safe/Arm Sw. B. Arm Position Comm. at 30 SPS
34	Event, Cont.	0 to 4 VDC Step Change	± 50 ms	(HI/LO)	10 H_z	Safe/Arm Sw. B Safe Position Comm. at 30 SPS
35	Event, Cont.	0 to 14 VDC Step Change	± 50 ms	(HI/LO)	10 H_z	Programmer B Reset Commutated at 30 SPS
36	Deleted					
37	Temperature	-90 to +210°F	5%	3.0°F	10 H_z	Bridle Temp. #1 Commutated at 30 SPS
38	Temperature	-90 to +210°F	5%	3.0°F	10 H_z	Bridle Temp. #2 Commutated at 30 SPS
39	Temperature	-90 to +210°F	5%	3.0°F	10 H_z	Bridle Temp. #3 Commutated a 30 SPS
40	Temperature	-90 to +210°F	5%	3.0°F	10 H_z	Cannister Temp. #1 Commutated at 30 SPS
41	Temperature	-90 to +210°F	5%	3.0°F	10 H_z	Cannister Temp. #2 Commutated at 30 SPS
42	Temperature	0 to +125°F	5%	1.5°F	10 H_z	Instr. Beam Temp. #1 Commutated at 30 SPS
43	Temperature	0 to +175°F	5%	2.0°F	10 H_z	Main Battery Temp. Commutated at 30 SPS

TABLE A-1 (CONTINUED)

BLDT Telemetry Measurement List

No.	Measurement	Range	Accuracy End-to-End	Resolution	Response	Remarks
44	Temperature	-100 to +150°F	5%	2.5°F	10 H_z	Rocket Mtr. Supp. Str't. Temp. Commutated at 30 SPS
45	Event	0 or 5 VDC	± 50 ms	HI/LO	10 H_z	Command Tone #1 Commutated at 30 SPS
46	Event	0 or 5 VDC	± 50 ms	HI/LO	10 H_z	Command Tone #2 Commutated at 30 SPS
47	Event	0 or 5 VDC	± 50 ms	HI/LO	10 H_z	Command Tone #3 Commutated at 30 SPS
48	Event	0 or 5 VDC	± 50 ms	HI/LO	10 H_z	Command Tone #4 Commutated at 30 SPS
49	Event	0 or 5 VDC	± 50 ms	HI/LO	10 H_z	Command Tone #5 Commutated at 30 SPS
50	Event	0 or 5 VDC	± 50 ms	HI/LO	10 H_z	Command Tone #6 Commutated at 30 SPS
51	Event	0 or 5 VDC	± 50 ms	HI/LO	10 H_z	Command Tone #7 Commutated at 30 SPS
52	Voltage	0 to 4 VDC	5%	0.04 VDC	10 H_z	Command Receiver A Signal Level Commutated at 30 SPS
53	Event	0 or 28 VDC 0.1 sec duration	± 50 ms	ON/OFF	10 H_z	Mortar Fire Commutated at 30 SPS
54	Temperature	+25 to 150°F	5%	1.5°F	10 H_z	Mortar Breech Flange Temp. Commutated at 30 SPS

TABLE A-1 (CONTINUED)

BLDT Telemetry Measurement List

No.	Measurement	Range	Accuracy End-to-End	Resolution	Response	Remarks
55	Temperature	0 to +175°F	5%	2.0°F	10 H_z	S-Band Transmitter Temp. Commutated at 30 SPS
56	Temperature	-100 to +150°F	5%	2.5°F	10 H_z	Aeroshell Temp. #1 Commutated at 30 SPS
57	Temperature	-100 to +150°F	5%	2.5°F	10 H_z	Aeroshell Temp. #2 Commutated at 30 SPS
58	Temperature	0 to +175°F	5%	2.0°F	10 H_z	Equipment Ballast Temp. Commutated at 30 SPS
59	Temperature	0 to +125°F	5%	1.5°F	10 H_z	Instrument Beam (#2) Temp. Commutated at 30 SPS
60	Temperature	0 to +125°F	5%	1.5°F	10 H_z	Gyro Temp. Commutated at 30 SPS
61	Temperature	-100 to +150°F	5%	2.5°F	10 H_z	Boost Motor #1 Temp. Commutated at 30 SPS
62	Temperature	-100 to +150°F	5%	2.5°F	10 H_z	Boost Motor #2 Temp. Commutated at 30 SPS
63	Voltage	0 to 4 VDC	5%	0.04 VDC	10 H_z	Command RCVR B Signal Level Commutated at 30 SPS
64	Voltage	5 VDC	5%	0.05 VDC	10 H_z	Commutator #2 Full Scale Calibration at 30 SPS
65	Voltage	0 VDC	5%	0.05 VDC	10 Hz	Commutator #2 Zero Scale Calibration at 30 SPS

APPENDIX B

DESCRIPTION OF BLDT

SYSTEM MISSION

APPENDIX B

A. Description of BLDT System Mission

1. Purpose of the System

The BLDT System is designed to subject the Viking Decelerator System to Qualification Test Requirements at simulated Mars Entry atmospheric conditions.

2. System Requirements

The Viking Decelerator System earth atmospheric test conditions which result from consideration of the variation in probable Mars atmospheres are:

	Supersonic Case 1	Supersonic Case 2	Transonic Case	Subsonic Case
Peak Load Mach No.	2.17 ± 0.17	2.06 ± 0.16	1.15 ± 0.10	0.46 ± 0.03
Peak Load Dyn. Press. (PSF)	10.09 ± 0.57	9.39 ± 0.55	4.52 ± 0.30	6.46 ± 0.80
Angle of Attack at M/F (Degrees)	≤ 17	≤ 17	≤ 20	≤ 17

The design of the BLDT test bed is constrained by the Viking Lander Capsule design to the following.

- Vehicle weight at mortar fire - 1888 pounds.
- Cg offset in minus Z direction - 1.41 inches.
- Vehicle external envelope similar to VLC (See Appendix A)
- Decelerator Temperature at mortar fire - $80^{\circ}F$

3. System Description

The BLDT System design which evolved from the above test requirements provides for a large volume, high lift balloon system capable of floating the BLDT Vehicles at altitudes from which the test conditions can be achieved with reduced or no propulsion capability. The predicted test altitudes and balloon lift capability involved in the system design are:

	Supersonic Case 1	Supersonic Case 2	Transonic Case	Subsonic Case
* Balloon Float Altitude (FT)	119,000	119,000	120,500	92,000
* Decelerator Mortar Fire Alt. (FT)	147,800	148,600	137,500	89,300
BLDT Vehicle Launch Weight (LBS)	3,550	3,550	2,800	2,050

The system concept provides for the launch of the balloon/flight vehicle system from the Roswell Industrial Air Center, Roswell, New Mexico with the system ascending to float altitude during the approximately 100 mile westward flight to the White Sands Missile Range. Once over the range, the flight vehicle is released from the balloon load bar to complete its flight sequence.

For the powered flight tests, the vehicle concept provides for spin rotation of the vehicle prior to solid rocket motor boost to minimize thrust dispersion effects. Following the boost phase, the vehicle is despun and allowed to coast to the correct dynamic pressure condition. For the subsonic case, the vehicle is released from the load bar and allowed to free fall until the correct velocity is attained.

---

*. USS62 Pressure Altitude

At the White Sands Missile Range, a ground computer system is programmed to receive tracking data which when integrated with predicted meteorological parameters provides the intelligence for the computer to issue a mortar fire command at the required test dynamic pressure for the powered flights. For the non-powered flight, the computer issues a timed mortar fire command following a delay for the correct velocity test conditions to be attained. In both powered and non-powered flights the vehicle incorporates an on-board programmer which provides a backup mortar fire command. Figure B-1 and B-2 depicted a typical powered and non-powered flight.

The system design includes all of the handling, checkout and control equipment necessary for prelaunch checkout, flight control and recovery of the system components.

4. Operations Description

A typical sequence flow of the mission operations from assembly and checkout at Roswell, New Mexico through vehicle flight and recovery at WSMR, is shown in Figure B-3. Each of the sequence events is described below:

a. BLDT Vehicle Assembly and Checkout - This phase of the mission operation encompasses the assembly and checkout of the various system components. The BLDT vehicle, while connected to ground electrical power and in partially assembled condition, is subjected to subsystem and combined system testing in a close loop and open loop mode. The vehicle is then assembled including airborne batteries and subjected to a full flight readiness test on airborne power and in an open loop mode.

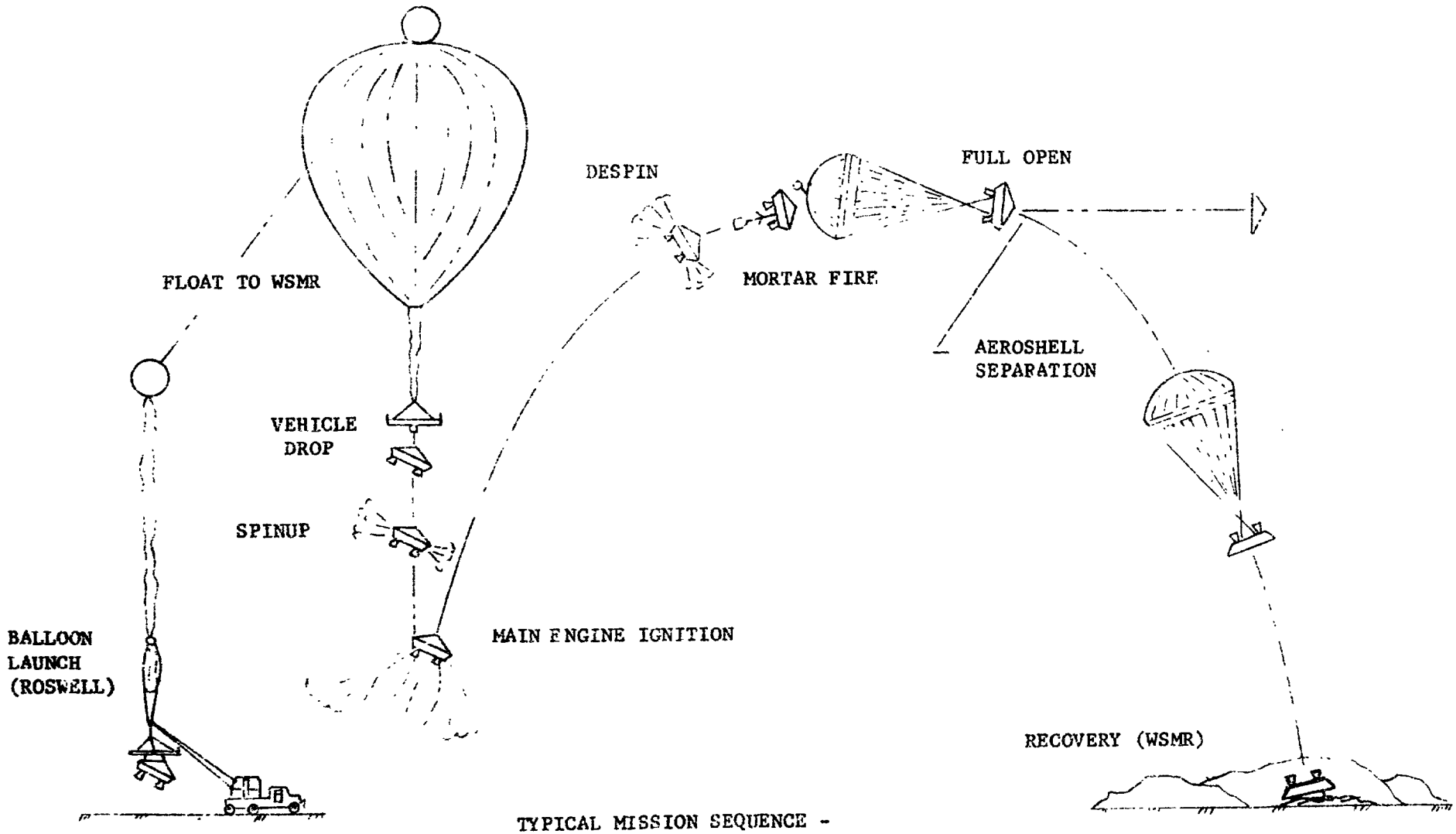

TYPICAL MISSION SEQUENCE -
POWERED FLIGHT

FIGURE B-1

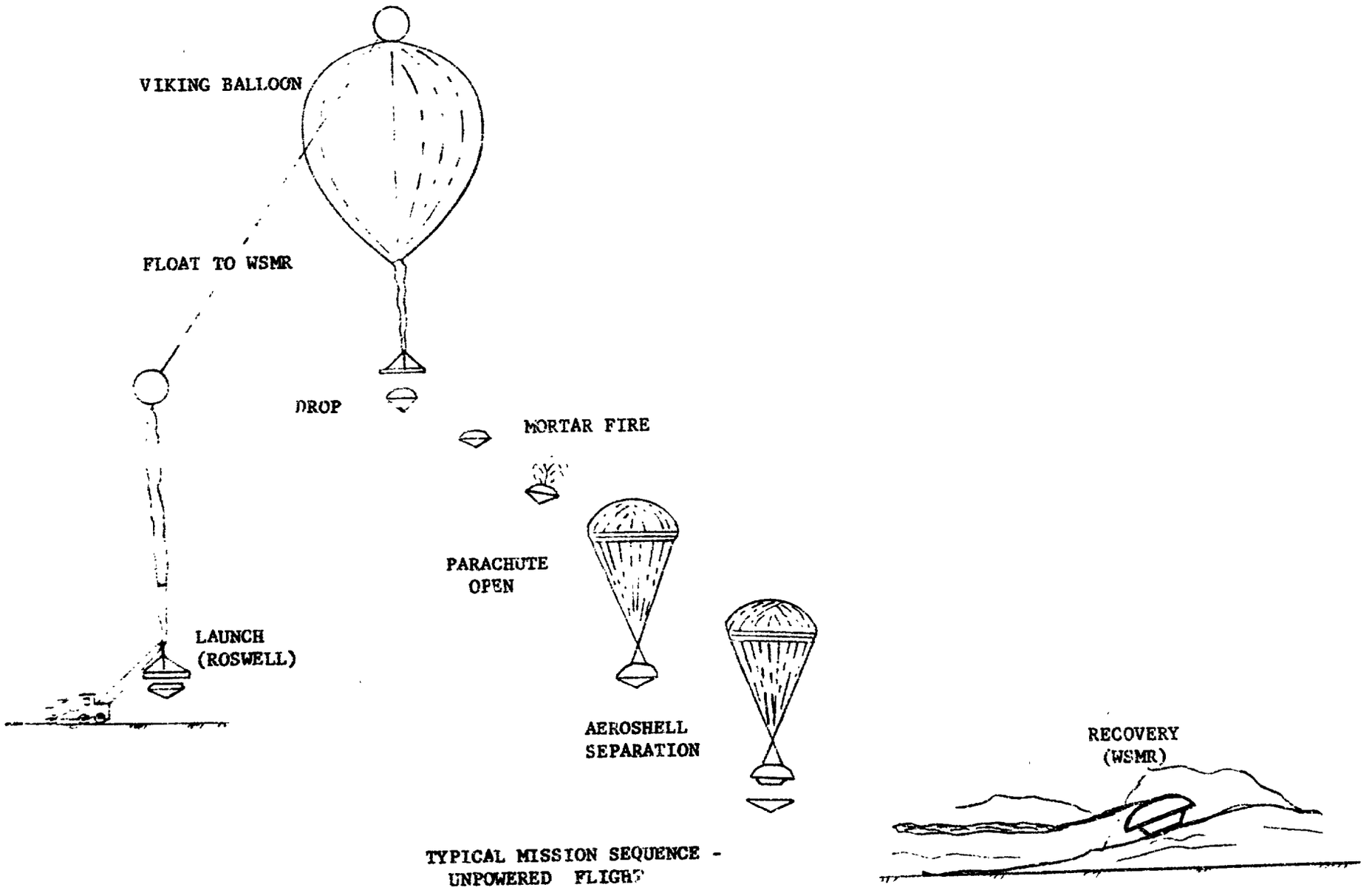

TYPICAL MISSION SEQUENCE - UNPOWERED FLIGHT

FIGURE B-2

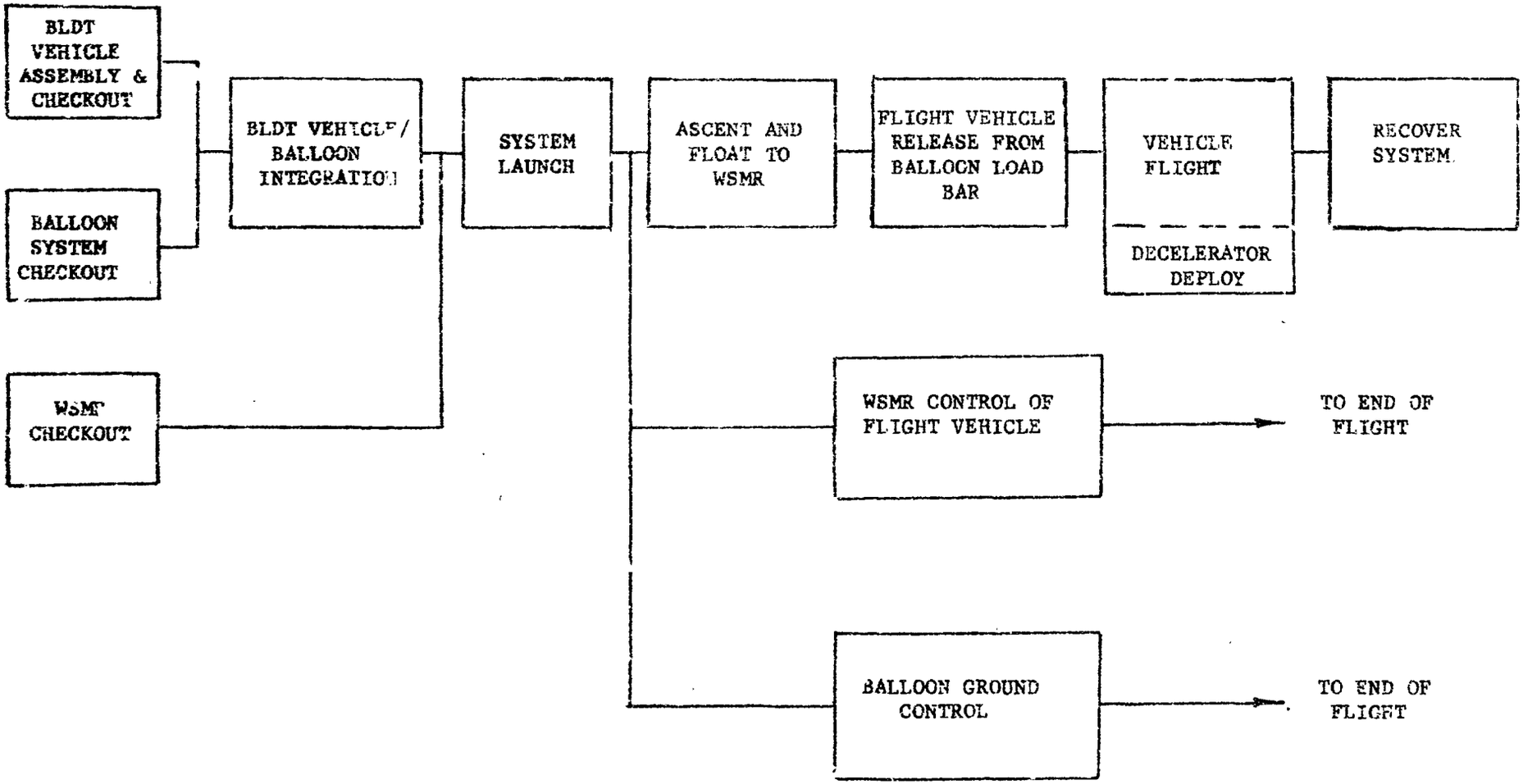

TYPICAL OPERATIONS SEQUENCE

FIGURE B-3

While the flight vehicle is undergoing checkout and assembly, the balloon system is also being partially assembled and subjected to flight readiness testing. These checkout and assembly events were performed at the Roswell Industrial Air Center.

Coincident with the checkout of the flight system, the ground control system at the White Sands Missile Range is readied for the mission by assuring that:

1) The flight TM data is routed to the correct terminal data stations.
2) The ground command system is capable of transmitting acceptable commands.
3) The communications links are correctly activated.
4) The command station personnel are prepared to accept vehicle control.

b. BLDT Vehicle/Balloon Integration - When the prerequisite flight vehicle balloon system and WSMR Control Center checkout are completed and the meteorological constraints at the launch site and WSMR (Launch winds, float winds, local weather, etc.) are satisfactory, the flight vehicle and balloon systems are moved from the checkout hanger to the launch runway where system integration and final checkout is made.

The flight vehicle is connected to ground power and final subsystem testing is completed to assure all subsystems are functioning. The vehicle ordnance is electrically connected and the vehicle access panels are installed. In this time period the launch balloon and float balloon are layed-out and integrated with the flight vehicle, the abort recovery cargo chutes, the balloon winch and the launch crane.

When the system integration is completed, the launch stand is removed from the flight vehicle leaving the flight vehicle suspended from the balloon load bar which in turn is suspended from the launch crane. Also, the launch balloon is filled with a precisely metered quantity of helium.

c. System Launch Following the integration of the flight vehicle and balloon into the BLDT system, the system is ready for launch.

The launch process begins with a ground winching operation in which the launch balloon is permitted to rise and which upon rising takes the float balloon (uninflated) and the cargo abort chutes from a horizontal attitude to a vertical attitude above the launch crane. Once the system is in the vertical attitude, the winch cable is separated from the balloon system through the use of an ordnance device. At this point, the two balloons with the abort cargo chutes are floating above and tethered to the launch crane with the balloon load bar and flight vehicle suspended from the crane beneath the tethered balloon. At this point, the total system for a powered flight extend from ground level to approximately 1000 feet above ground level (800 feet for a non-powered flight).

With all of the preceeding operations complete, it only remains to release the flight system from the launch crane. To do this, the launch crane is driven down wind at a velocity necessary to position the crane approximately under the balloon at which point the crane release device is actuated and the balloon floats free of the ground system taking with it the balloon load bar and flight vehicle.

d. Ascent and Float Phase - During the ascent and float phase, the balloon system, floating freely, responds to the wind directions and velocities encountered as it ascends to the design float altitude. Generally, once clear of low altitude wind influence, the balloons float in a westerly direction intersecting the WSMR at about mid-range.

As the system ascends, the helium which was loaded in the launch balloon is forced down into the float balloon which slowly inflates the float balloon and causes the system to ascend. This process continues until the float balloon becomes fully inflated at which point no further lift can be obtained. The balloon ascent to float altitude is rapid enough to arrive at the float altitude prior to intersecting the WSMR.

The balloon ascent and direction is somewhat controllable through the use of ballast dumping operations to control floating altitude and rise rates in order to take advantage of winds at the upper levels. The control of the balloon during the ascent and float phase is from the Air Force Cambridge Research Laboratory control center at Hollaman Air Force Base. Alamagordo, New Mexico.

When the ascending system passes through approximately 30 K feet, the WSMR tracking radar, command networks and TM receiving stations are able to acquire the flight vehicle and start checkout. Part of the float checkout assures operation of the command nets by sending commands which do not change vehicle configuration (i.e. safe ordnance circuits, turn R.F. on, etc.) and verifying receipt of the commands through flight vehicle TM data being received at the control center.

e. Vehicle Release from Load Bar - Once the BLDT system reaches the proper float altitude and intersects the range, the vehicle ordnance circuits are armed, the vehicle flight azimuth is attained using a cold gas pointing system and the vehicle release from the load bar is commanded. All of these functions occur as a result of ground commands issued by the flight vehicle control crew at WSMR.

f. Vehicle Flight - The vehicle flight events are a function of the type of mission being flown. Table B-1 presents a sequence of

events and event times for the Supersonic, Transonic and Subsonic missions. All of the event times in Table B-1 are times from release of the flight vehicle from the balloon load bar with the exception of the ground mortar fire command for the powered flights. This command is time variable and is issued by the ground computer during the vehicle coast following despin when the vehicle achieves the correct dynamic pressure.

For the powered flights following release of the vehicle from the load bar, the vehicle is under control of the redundant airborne programmers with the exception of the issuance of the decelerator mortar fire. The vehicle functions provide a flight profile as shown in Figures B-1 and B-2.

During the vehicle powered flights, the vehicle is tracked by the WSMR tracking devices to provide the ground computer with the intellegence for issuing the mortar fire command. For all flights, tracking devices provide data for post flight analysis and to support vehicle recovery operations.

For the non-powered, free fall mission, the vehicle functions are commanded by the on-board redundant programmers except for the mortar fire which is issued as a timed output from the ground computer.

g. Recovery Operations - During this phase of the mission, all of the system components are located and moved to WSMR facilities for post flight inspection. Also during this phase the various system cameras are recovered and the film processed for post flight analysis.

TABLE B-1

VEHICLE FLIGHT SEQUENCE OF EVENTS

SUPERSONIC CASE 1	SUPERSONIC CASE 2	TRANSONIC	SUBSONIC	FUNCTION	SOURCE
T_D - 30 min.	T_D - 30 min.	Drop - 30 min.	Drop - 30 min.	Attain Float Altitude	--
T_D - 10 min.	T_D - 10 min.	T_D - 10 min.	--	Start Azimuth Pointing	Ground Command
T_D - 5 min.	T_D - 5 min.	T_D - 5 min.	T_D - 5 min.	Arm Ordnance Bus	Ground Command
T_D - 10 sec.	T_D - 10 sec.	T_D - 10 sec.	--	Confirm Drop Azimuth	A/B T/M
T_D	T_D	T_D	T_D	Drop from Load Bar. Initiate A/B Programmer.	Ground Command
T_D+1 sec.	T_D+1 sec.	T_D+1 sec.	--	Ignite Spin Motors/ Enable Boost Motor	A/B Programmer
T_D+2 sec.	T_D+2 sec.	T_D+2 sec.	--	Ignite Boost Motors	A/B Programmer
--	--	--	T_D+12 sec.	Start AFT Looking Camera, Enable Mortar	A/B Programmer
--	--	--	T_D+16 sec.	Initiate Mortar Fire/ Start AFT Hi-Speed Camera	Ground Command
--	--	--	T_D+18 sec.	Initiate M/F Backup	A/B Programmer
--	--	--	T_D+30 sec.	Separate Aeroshell	A/B Programmer
T_D + 33 sec.	T_D+33 sec.	T_D+33 sec.	--	Ignite Despin Motors/ Release Camera Lens Covers/Start AFT Camera Enable Mortar	A/B Programmer
T_D (q cond. correct)	T_D (q cond. correct)	T_D (q cond. correct)	--	Initiate Decelerator Mortar Fire/Start AFT Hi-Speed Camera	Ground Command
T_D+37 sec.	T_D+38 sec.	T_D+39 sec.	--	Initiate M/F Backup	A/B Programmer
T_D+47.6 sec.	T_D+47.6 sec.	T_D+47 sec.	--	Separate Aeroshell	A/B Programmer

APPENDIX C

GAC Post Test Failure Analysis

Excerpts from Reference: GAC Report RSE-20726-22, July 26, 1972

This report is the primary post test analysis and reports the combined efforts and concurrence of MMC and GAC personnel.

I. INTRODUCTION

The post test analysis of the decelerator system from the AV-1 vehicle was conducted to determine the damage, cause, and effects of same. The analysis consisted of review of telemetry data, on-board films, MMC film and data reduction, a visual examination of the test article, physical testing of the chute material and review of manufacturing specimens made at the time of the parachute assembly.

MMC film and data reduction was reviewed and concurred with by analysis of the films themselves. (Reference MMC IDC 8943-72-158).

The flight profile as reported was approximately on target for Mach number with a lower altitude and associated higher q. The load traces and accelerometer data exhibited nothing unexpected except that peak load occurred approximately 0.2 seconds later than anticipated and the peak load was a little less than anticipated (500-1000 pounds less) based on the actual test point.

Overall parachute performance was acceptable with the structural integrity of the parachute maintained with the descent rate acceptable and even somewhat better than anticipated.

The deceleratol . . was examined and the following anomalies existed on the parachute with none noted on the mortar, bridle, thermal protective components or swivel: See Parachute Defects Plot, attachment 1 of this report.

1. Smudges (see defects plot)
2. Deployment bag missing
3. Retention pins missing
4. Pierced holes (see defects plot)
5. Min-K buffer abraided
6. Gore length damage (see defects plot)
7. Small damage areas (see defects plot)
8. Broken vent tape reinforcement (see defects plot)
9. Local tears at vent band (see defects plot).

A. Incidental Anomalies

The following is an analysis of the first five items.

The smudges all occurred in an area of the band and are presumed to be residue from products of combustion of the mortar. The areas of the smudge exhibited no evidence of having seen excessive heat either by visual or feel. Areas of smudge varied from dime size to half dollar. The Nomex deployment bag is porous and is expected to pass some residue without damage to the parachute. The Nomex paper previously wrapped around the deployment bag in LADT tests was not used because of the absence of the funneling effect typical of the LADT test vehicle, and was shown to be unnecessary in this test by virtue of the very minimal passage of residue. Residue on the bridle legs and noted on the bag in the film verify the source of the smudge.

The missing deployment bag was not totally unexpected since no attempt had been made to structurally protect it from the supersonic buzzing effects of the deployment. The bag was seen to disappear approximately 2.88 seconds after mortar fire which was well after peak load and indicated the attachment of the bag to the chute was adequate to maintain integrity through the initial chute filling stages which is all that is required.

The abraised Min-K buffer is associated with the missing deployment bag. The attachment of this to the chute is as follows:

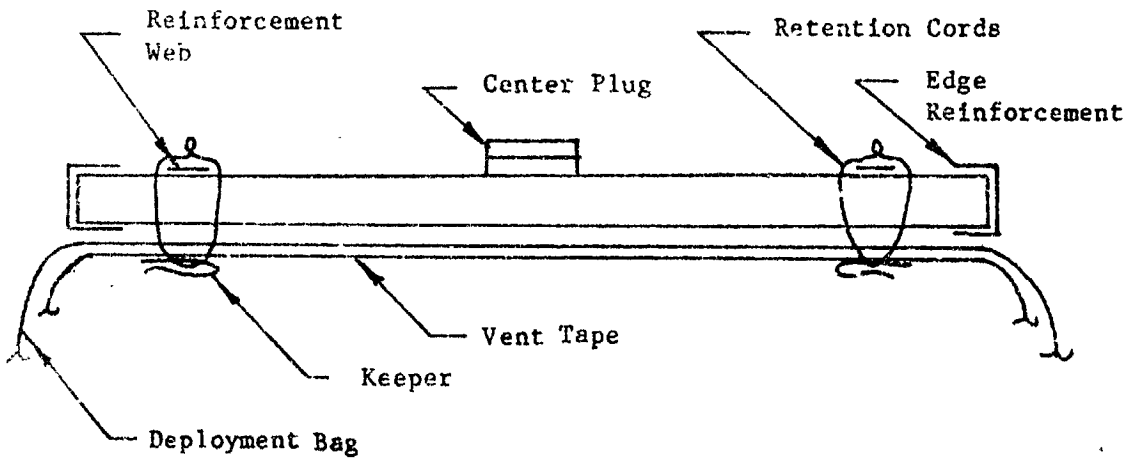

The buffer was severely abraided leaving the edge reinforcement held to the reinforcement web on the buffer with the quartz threads that make the buffer sandwich. The retention cords holding the buffer to the chute were all intact. The abrasion of the buffer is as expected in the supersonic environment and happens well after the purpose of the buffer has been served; that is to act as a buffer between the pack restraint straps and the pack and as additional thermal protection.

Two areas exhibited miniscule punctures of approximately less than pencil point size. These are attributable to ground damage.

The suspension line locking pins (see Section D-D drawing 3064110-100, sheet 2) were missing. The locking pins are located approximately eight feet from the swivel. Both pins were missing and in one case the -7 tie line was attached to the loop on the suspension line and in the other the tie-line was also missing. The tie-line that was left appeared to be untied at the pinrather than broken and the loss of the pins is attributed to high speed shipping of the pin and attachment. The pins were satisfactorily pulled as evidenced by the fact that there was no damage to the band area which would have been in evidence if the pins had not pulled properly and the band been forced to be drawn through the loop formed by the retention cords and unpulled pins. Pins have previously been lost on LADT tests with no damage in evidence.

B. Areas of Damage

There are three distinct areas of damage in the disk (reference the damage chart herein) and Item 6, 7, 8 of page 7.

1. Two major gore length tears in gores number 36 and 38 with loss of cloth in panels C and D in both gores.

2. In each of four gores (numbers 14, 15, 16 and 18) there are local tears from three inches to 18 inches in length that are parallel to each other. They are located at approximately the same areas in the gore, i.e., mid-gore and three tears at the same locals in panel C with the fourth tear in panel D. There are two significant observations concerning these tears.

   a. They are <u>not</u> adjacent to panel or to gore seams.

   b. There is evidence of abrasion adjacent to the tears in gores 14, 16 and 18 as manifested by surface roughness and local areas having the loss of one set of woven threads but not the other.

3. Seven radial tapes to circumferential vent band connections (gore numbers 39 through 45) had failed by tensile failure of the sewing threads connecting the tape and webbing followed by abrasion failure of the doubler tapes at these joints. The radial tapes and vent band remained intact. The cloth failed adjacent to the vent tape as a result of the above joint failures.

Study of the physical damage, the two on-board high speed camera films, the packing procedure of GER-15133, Revision B along with considerations of the tensiometer traces has lead to the following, "most probable" failure hypothesis:

Immediate subsequent to emergence of the disk skirt from the deployment bag, abrasion damage was induced in panels C and/or D of gores 36 and 38 as well as in these same panels of gores 14,

15,16 and 18. The resulting strength reduction in these cloth areas facilitated the origins of subsequent unsymmetrical pressure stress failures as the disk inflated. The inflation of the disk started early, i.e., before all of the disk had emerged from the bag. The disk also filled unsymmetrically so that the gore numbers 36 and 38 regions were subjected to higher pressures than were the gores 14 through 18 regions that were last to inflate. For this reason, it is believed that the energy of tear propogation was much higher in gores 36 and 38 than in gores 14, 15, 16, and 18. In fact, the former two tears propogated both directions, i.e., towards the vent as well as the skirt throughout the entire gore length. The seven radial to vent band juncture failures occurred last as a result of the unsymmetrical pressure loading on gores 39, 40, etc. that transferred circumferential membrane forces to radial tape number 39. This tape was a free edge because of the full gore tear. The tension in this tape subjected its terminal joints located at skirt end vent bands to "kick" loads of sufficient magnitude to fail the vent band joint, e.g., per design, this joint is of lesser strength than is the radial tape to skirt band juncture. Subsequent to failure of the number 39 joint, the 40 through 45 numbered joints failed progressively due to load transfer.

The above failure hypothesis is based upon the following listed observations:

1. <u>On-Board High Speed Films</u>

Event frame numbers and corresponding times from mortar fire were successfully correlated between the two cameras and the load cross

These data are documented in MMC IDC 8943-72-158.

a. On the whole, the suspension system appears rather lightly loaded from mortar fire until full open.

b. All suspension lines appear to have tension when the leading edge of the disk emerges from the bag. Prior to this they have little load. Subsequent to this time, the lines are very slack and flail about considerably as the canopy inflates in a very unsymmetrical mode.

c. The mouth of the disk starts to inflate while a large amount of disk is still packed in the bag. The appearance here is that of an inflating "cone" with its base at the disk edge with a definite amount of uninflated disk out of the bag and a majority still packed, see Figure C-1.

d. During the period from mortar fire until bag strip, the path of the suspension lines and the chute describes a curve due to the angle of attack of the vehicle, i.e., the system is ejected at an angle to the airstream. Due to the slack lines and because of inflation prior to bag strip, the total distance that the bag traveled rearwards along this curved path was less than intended and less than in any other prior Viking flight test. Rearward movement along this curved path yields the appearance in the motion pictures of the bag traversing from right to left. Subsequent to bag strip, the apparent motion of the bag is from left to right that indicates the bag has stopped with relation to the vehicle and that it is being pulled forward, by the vehicle and by the inflating chute, along the approximate curved path of deployment.

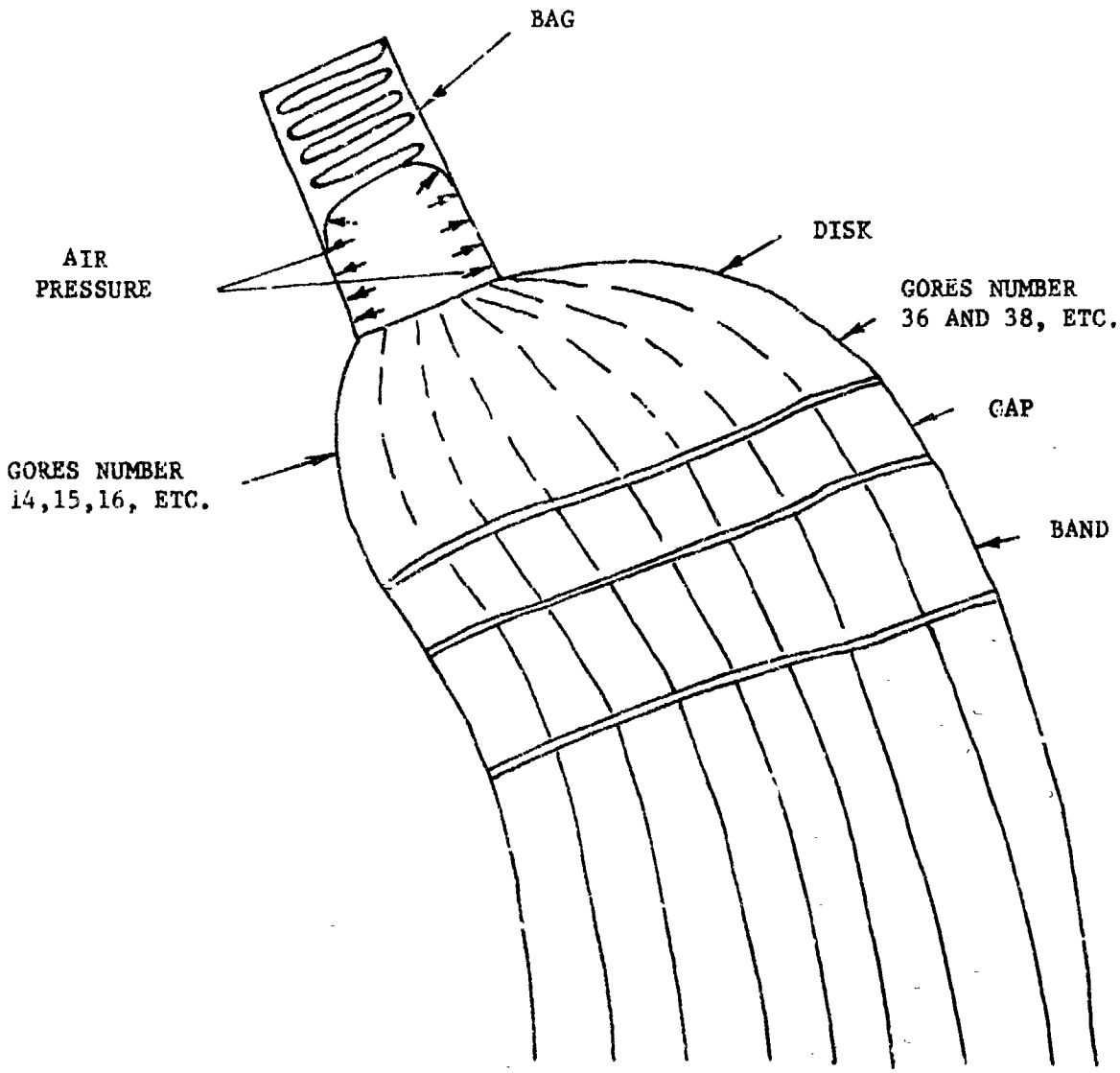

FIGURE C-1 SKETCH OF DISK DEPLOYMENT FROM THE BAG

e. As the bag reverses direction and apparently moves from left to right, the disk is inflating. At approximately 1/30 of a second after the bag disappears behind the inflating disk, the major gore tears begin to come into view. These are located on the canopy side that fills first and is most rearward in the field of view so that the nearer canopy regions must subsequently unfurl and inflate in order to bring the far side into view. First evidence of the above major tear is seen at one o'clock on the film whereas the apparent left to right movement of the bag is horizontal on the film and, the attached bag is never observed on the right of the canopy apex or has the bag had sufficient time to travel to the vicinity of the tear. Hence, impact of the bag upon the canopy disk is considered improbable.

f. The 18 inch tear in gore number 15 can be observed on the film. Although it is first seen after full canopy inflation, it is believed to have initiated earlier.

2. Physical Damage

The following significant observations support 1) the location of failure initiation and, 2) the type of failure. Location:

a. Both tears along radials number 37 and 39 were moving towards the vent as they crossed the A to B panel seams. If they had been traveling in the opposite direction, the tears would have most likely followed the gore and/or the panel seams; this was not the case. The tears followed only the gore seams with no damage parallel to the A and B panel seams.

b. The tears along radial numbers 37 and 39 were very clean in both panels A and B which indicates a progressing (or rapidly traveling) tear parallel to the seam as opposed to a pure tensile failure normal to the seam.

c. The tear along radial 36 was moving towards the skirt in the D panel since,

1) Both parent disk cloth and cloth reinforcement were cleanly torn away.

2) The tear moved along the skirt tape from radial 36 to the cloth reinforcement on radial 37.

3) The tear traveled around the number 37 cloth reinforcement and was certainly directed towards the vent as it moved along radial number 37. Had the direction been opposite, there would be no remaining piece of parent cloth at the top of the number 37 cloth reinforcement.

4) Presence of the 20 inch triangular piece of cloth implies that tears traveled several directions from this area.

5) Tears did occur in panels C and D of gores numbered 14, 15, 16 and 18. Study of the packing procedure (reference Figure 5 of GER-15133, Revision B) shows the mid width of these gores to be directly opposed and adjacent to gores 36 and 38 in the packed condition. A sketch of the panels C and D disk areas leaving the bag mouth is included in Figure C-2 for clarification.

3. Type of Failure

The following observations strongly indicate that the primary tears did not result due to only excessive pressure stresses.

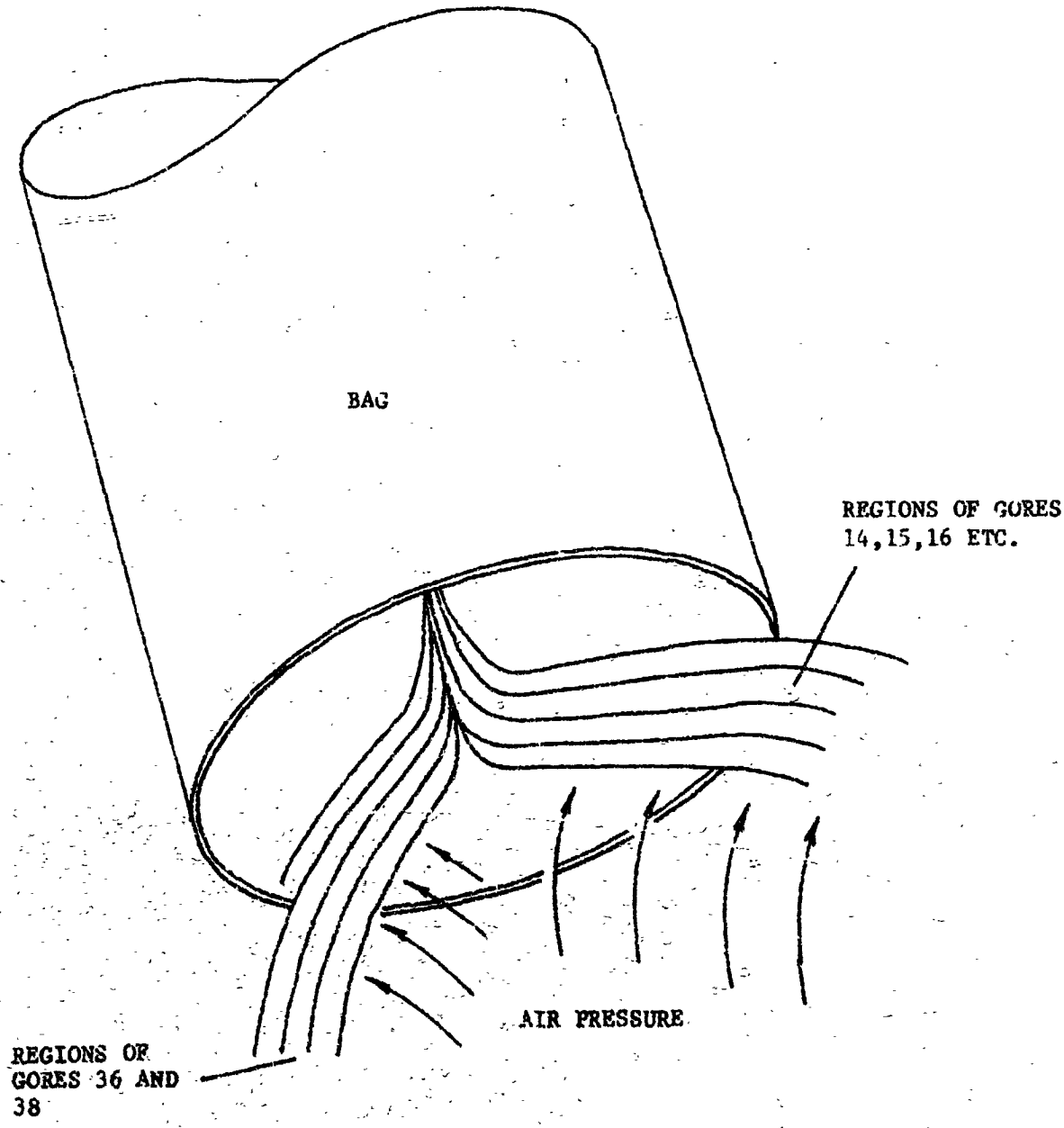

FIGURE C-2 SKETCH OF PANELS C AND D DISK AREAS DEPLOYING FROM BAG

a. Complete absence of any signs of excessively loaded seams. The seams should rake prior to failure; no seam raking could be found.

b. The post test structural integrity of material in vicinity of gores 36 and 38 and in particular, gore 37 was surprisingly intact.

c. The fact that the tears in gores 14, 15, 16 and 18 were remote from either panel or gore seams certainly indicates failure other than pure tension. This is further evidenced by the abrasion damage adjacent to these tears as stated at the outset of this discussion.

C. Materials and Manufacturing

The following summarizes the material and manufacturing investigation relating to BLDT #1 flight.

Along the edge of tape 39, on gore 38, was a clean severance of cloth from tape. Its appearance is not one that would be associated with a pure tensile failure. It could, however, be associated with other factors such as severe needle damage causing a clean perforation upon loading or a rapid tearing action.

In investigating the possibility of needle damage, the sewing at the failure was closely examined for stitch count, needle hole size, and evidence of a damaged needle (burred or dull). This examination showed everything to be normal.

To further investigate the above situation, the daily sewing samples that were fabricated during fabrication of the BLDT #1 parachute was

examined for the same flaws. Again, there was no evidence of abnormality. One of the daily sewing samples was then used to try to duplicate a tear that would produce a clean separation as was observed on the chute. The test consisted of starting a small tear along the seam edge, and with a rapid motion, tearing the cloth. This test resulted in a failure almost identical to that observed in the parachute. Consequently, the clean severance of cloth and tape has been attributed to a high speed, running tear action, rather than excessive sewing machine damage.

In order to determine whether or not the parachute materials had been degraded in strength beyond expectations, physical tests were conducted on various segments of the chute. The four main areas of concern were:

1. Gore seams
2. Panel seams
3. Basic cloth (warp direction)
4. Basic cloth (fill direction)

In the case of the gore seam, however, test specimens from the fabricated chute would involve testing with the seam on the bias. All former testing has been conducted with the seam normal to the yarn direction. Consequently, there would be no meaningful base line data with which to compare the results. NASA personnel volunteered to perform a cylinder burst test of a gore seam. Again, there would be no way of correlating the data with presently known strengths. It was decided that testing of the other three elements would produce trends that could be related to the strength retention of the gore seam.

Consequently, test specimens were cut from the chute as shown in Figure C-3.

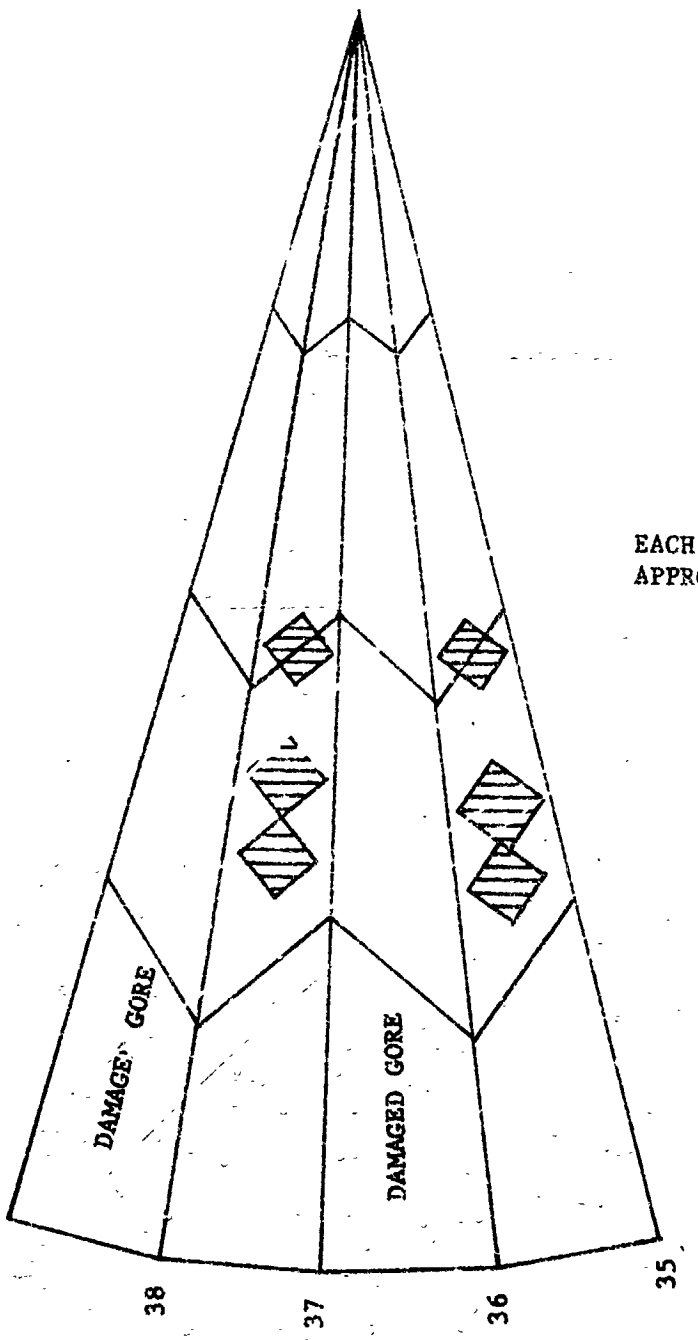

EACH PANEL
APPROX. 12" x 12"

FIGURE C-3 LOCATION OF TEST SPECIMENS

All test specimens were ravelled down to an effective width of one inch. The gage length was six inches and the jaw separation rate was 12 inches per minute.

The test results are summarized in Table I.

TABLE I

STRENGTH OF MATERIAL FROM BLDT #1 CHUTE

	Strength (lb/in)		
	Gore 35	Gore 37	
Disk Cloth (warp)	112	105	
	109	86*	
	110	117	
	112	108	
	114	111	
Average	111.4	105.4	
Disk Cloth (fill)	111	102	
	108	102	
	110	92	
	111	109	
	109	95	
Average	109.8	100.0	
Disk Panel Seam	91	95	
	93	91	
	94	87	
	95	77*	not included
	84	66*	in averages
Average	91.4	91.0	

* Specimen failure was a tearing action. This is due to the difficulty in installing the wrinkled specimens properly in the jaws causing a non-uniform stress distribution across the width of the specimen. In the case of the seamed specimens, the failure was not near the seam.

Based on receiving inspection tests, the average strength of the cloth used in fabrication of the chute was 117 lb/in in the warp direction and 112.9 lb/in in the fill direction. Using these values, a cloth strength reduction in gore 35 (adjacent to damaged gores) of 2 to 4.5 percent is evident. A percentage of this magnitude is predictable as a result of heat compatibility exposure. Gore 37 (between damaged gores) resulted in a strength reduction of 10 to 11 percent. The difference between gores 35 and 37 becomes obvious upon examination of the films. Gore 37 underwent a violent flagging action throughout the flight while gore 35 saw minimal flagging.

From previous development testing, the average strength of the disk panel seam is 94 lb/in. Test results from both gores show a strength reduction of approximately 3 percent which can be attributed to the heat compatibility exposure.

It should be pointed out that all specimens were quite wrinkled which causes difficulty in aligning the specimens in the grips for testing. Consequently, the test values are considered minimum.

Based on the test results, it is concluded that the material strengths had not degraded below expectation.

D. Aerodynamic Heating

Aerodynamic heating effects on AV-1 (BLD1 1) were investigated as follows:

Reference: (1) RSE-10208-16 dated 08 February 1971.

Reference: (Continued)

(2) Bobbitt, P.J.: "Theoretical Analysis of the Aerodynamic Heating at the Flow Stagnation Line of a Disk-Gap-Band Parachute at Supersonic Speeds", NASA/LRC, UWP-748, 01 May 1969.

An estimate of the temperatures at first full open for the first BLDT test was made using the method discussed in Reference (1). Essentially, this method consists of using heating rates generated in accordance with Reference (2) in a one-dimensional heat transfer computer simulation. For the present case the following known or assumed conditions were used:

$h = 140{,}000$ feet

$\gamma = 0$

$M_{M.F.} = 2.17$

$M_{P.L.} = 2.04$ Linear decay

Time to line stretch - 1.03 seconds

Time from line stretch to first full open = 0.55 seconds

Since these conditions closely approximate conditions assumed in Reference (1), the results of that memorandum were extended to the present case. The results are shown in Figure C-4 and indicate the temperature effect to be relatively minor especially considering the fact that damage was apparent from the films prior to the time of first full open. It is noted, however, that very limited heating is assumed to occur during line stretch and that the inflation time is very short. An estimate of Bobbitt assuming an equilibrium surface temperature is achieved produces a temperature of 159°F. If it is assumed that even higher heating rates exist prior to full open than do after full open at a given set of conditions (a possibility suggested by Bobbitt), then even higher

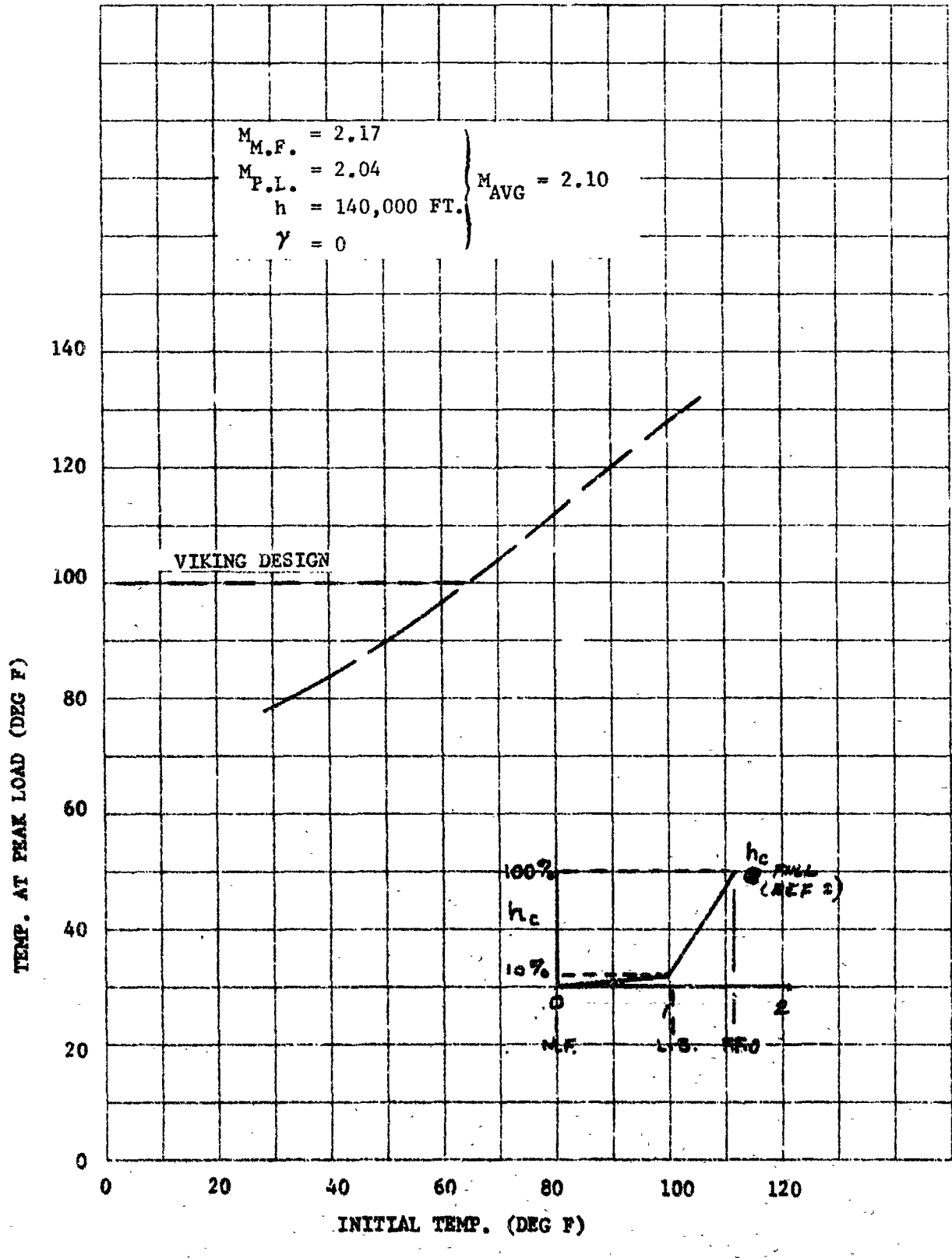

FIGURE C-4 AERODYNAMIC HEATING EFFECT - BLDT TEST NO. 1

temperatures could be expected. The stagnation temperature in a Mach 2 flow at 140,000 feet is 375°F. This, of course, represents an upper limiting value.

E. Conclusions of Analysis

1. Damage encountered on this test did not compromise the structural integrity of the parachute or the required performance of the decelerator system.

2. Primary disk damage originated from small localized damage in the lower panel regions as those regions emerged from the deployment bag.

3. The small areas of damage in gores 36 and 38 saw pressure early enough and high enough to cause significant damage. By the time other damaged areas saw the environment, the energy was insufficient to propagate damage.

4. Angle of attack phenomena combined with excessive dynamic pressures and lower than MARS design relative bag strip velocities created frictional conditions which were responsible for the panel initial damage.

5. Reduction in dynamic pressure and its associated improvement on bag strip characteristics should significantly improve the probability of a normal deployment.

6. Damage to the radial tape reinforcements is considered secondary and would not have occurred without gore damage.

7. Smudges on the canopy, loss of the deployment bag and damage to the buffer are considered incidental to the test and are in no way detrimental to the performance of the decelerator system.

8. The absence of the suspension line retention pins does not appear to relate to any visible parachute damage.

9. There does not appear to be any basis to suspect manufacturing or material associated problems.

ATTACHMENT I

DAMAGE CHART

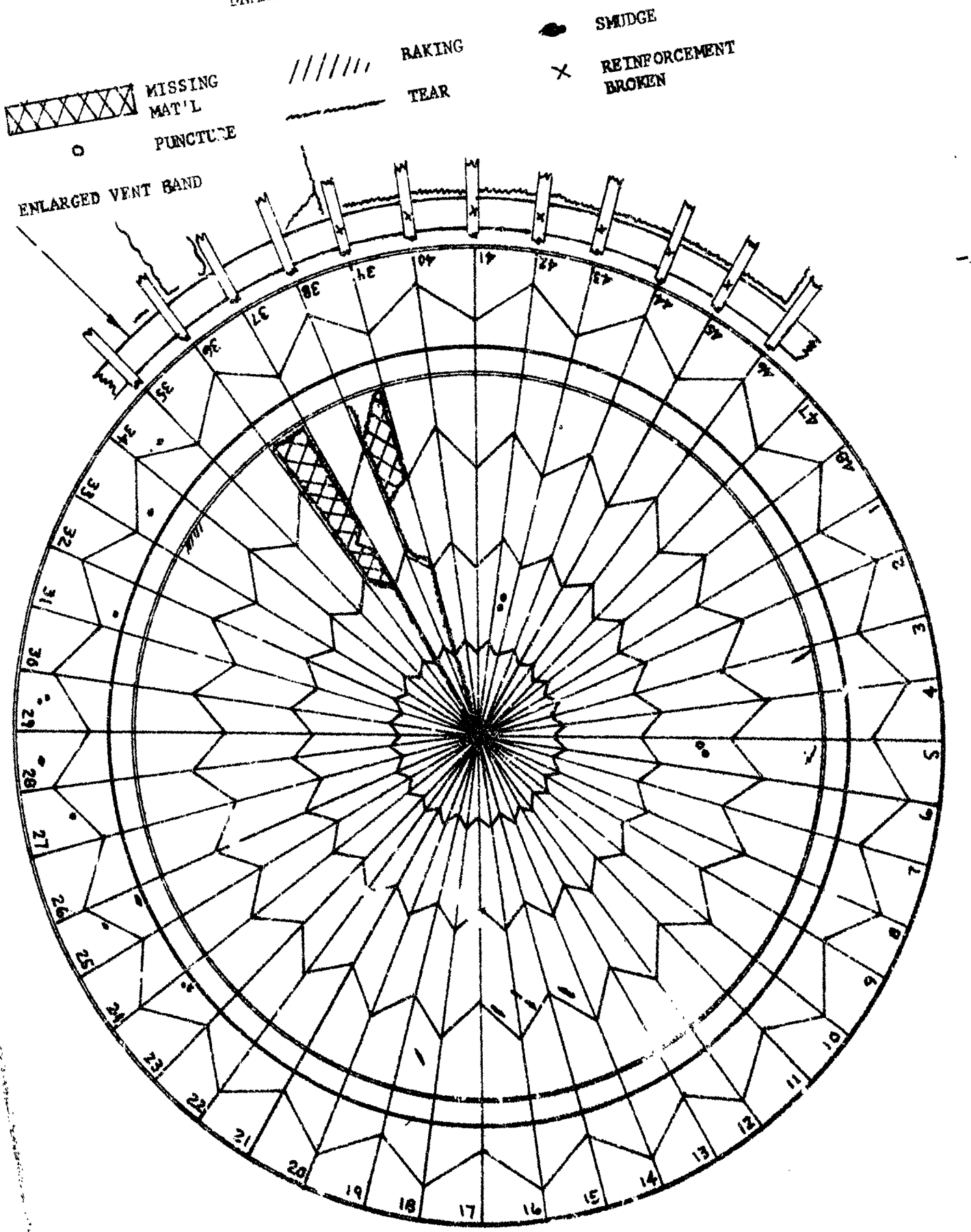

APPENDIX -

PARACHUTE DIMENSIONS

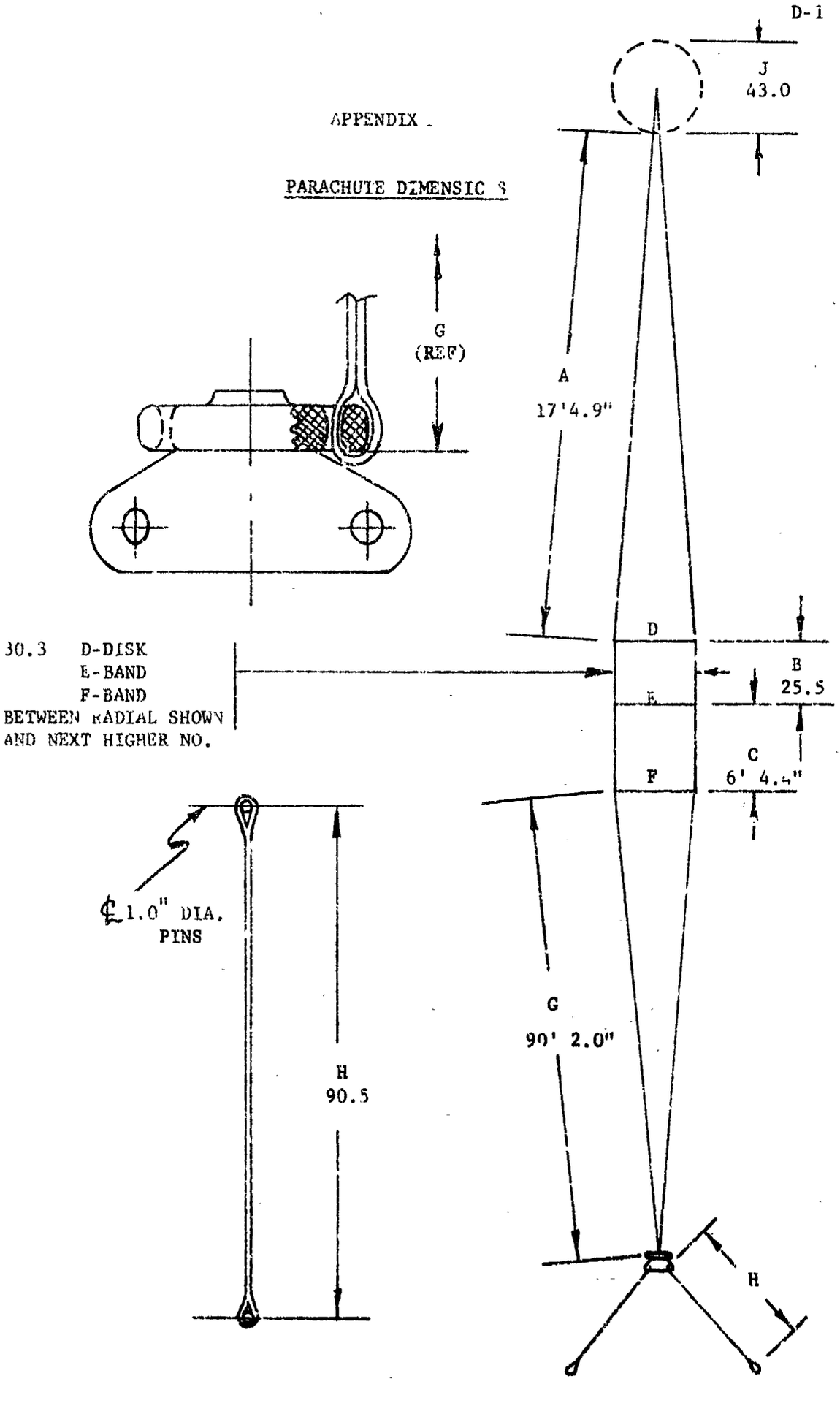

PRE-FLIGHT

RADIAL NO.	A(DISC) FT-INCHES	B(GAP) INCHES	C(BAND) INCHES	D(DISC) INCHES	E(BAND) INCHES	F(BAND) INCHES	G(SUSP) FT-INCHES
1	17-3 1/8	25 1/4	75	30 7/16	30 1/4	30 1/4	90 - 2
2	3 1/4	1/2	75 1/4	1/4	3/8	3/16	1 1/2
3	3 1/4	1/4	1/2	3/16	1/16	1/4	2 1/2
4	3 1/8	1/4	1/4	1/2	1/2	5/16	2
5	3 1/4	1/4	1/4	1/4	1/4	7/16	2 1/4
6	3 1/8	5/16	1/2	1/2	1/2	1/2	1 3/4
7	3 1/4	3/16	5/8	3/8	1/4	3/16	2 1/4
8	3 1/2	3/16	5/16	3/8	1/4	1/4	1 3/4
9	3 1/2	1/4	1/4	1/4	1/4	3/8	1 3/4
10	4	3/8	1/4	1/4	5/16	3/8	1 1/4
11	3 7/8	3/8	5/8	2/16	3/8	3/8	1 1/4
12	3 3/4	1/4	1/2	7/16	5/16	7/16	2
13	3 1/2	1/4	3/8	1/4	1/4	7/16	2 1/2
14	3 5/8	3/8	1/2	3/8	1/4	7/16	2 1/4
15	3	1/4	3/8	1/4	3/8	1/2	2
16	3 1/4	1/4	1/2	7/16	1/4	1/8	2
17	3 1/2	5/16	7/16	7/16	5/16	5/16	1 1/2
18	3	1/4	3/8	1/8	1/8	3/8	1 3/4
19	3 1/8	1/2	3/8	1/4	1/2	1/4	2
20	3 1/4	1/4	3/8	3/16	0	9/16	2
21	3 1/2	3/8	5/8	7/16	3/8	1/8	2
22	3 1/2	1/4	5/8	1/2	7/16	5/16	2
23	3 5/8	1/4	5/8	1/4	1/4	3/8	2 1/4
24	3 1/2	1/4	1/4	3/16	5/16	3/16	2

PRE-FLIGHT (CONTINUED)

RADIAL NO.	A(DISC) FT-INCHES	B(GAP) INCHES	C(BAND) INCHES	D(DISC) INCHES	E(BAND) INCHES	F(BAND) INCHES	G(SUSP) FT-INCHES
25	17 - 3 1/8	25 1/4	75 5/16	30 3/16	30 5/16	30 1/4	90-2 1/4
26	3 3/4	1/4	5/8	3/16	1/4	3/16	1 1/2
27	3 1/2	5/16	3/8	1/4	3/8	3/8	-2
28	3	1/4	1/4	7/16	7/16	1/8	2
29	3	1/4	3/16	5/16	1/8	3/16	2 1/4
30	3 3/4	5/16	5/16	0	1/2	7/16	2
31	3 3/4	5/16	1/4	5/16	3/16	1/4	1 3/4
32	3 7/8	5/16	3/8	3/8	3/16	1/8	2 1/8
33	3 1/2	5/16	1/4	3/16	1/4	5/15	2 1/8
34	4	1/4	5/15	5/16	1/2	3/16	2 1/4
35	3 7/8	5/16	3/8	7/16	3/16	3/16	2 1/4
36	3 3/8	1/4	1/4	3/16	3/16	1/4	1 3/4
37	3 1/2	3/8	1/4	7/16	1/2	3/8	2 1/4
38	3 7/8	5/16	1/4	1/8	1/4	3/16	2 1/4
39	3 1/2	5/16	3/8	3/8	1/8	1/8	2 1/2
40	3 3/4	1/4	1/4	3/8	7/16	1/2	2 1/8
41	3 1/2	5/16	3/16	1/4	0	1/8	1 3/4
42	3 1/2	3/8	1/4	3/8	5/16	1/4	1 3/4
43	3 7/8	3/8	3/8	7/16	5/16	1/4	1 1/2
44	3 3/4	3/8	1/4	1/16	7/16	3/16	1 3/4
45	3 5/8	1/4	3/16	1/8	1/8	5/8	2
46	4	3/8	1/4	3/8	1/4	1/8	2
47	3 1/8	3/8	1/8	3/8	9/16	1/4	1 3/4
48	3 7/8	1/4	1/4	1/4	1/8	1/4	1 1/2

PRE-FLIGHT (CONTINUED)

BRIDLE LEG	H
S/N 40	$90\frac{1}{2}$
S/N 41	$90\frac{5}{8}$
S/N 42	$90\frac{1}{2}$

VENT DIAMETER	
RADIAL	J
1/25	$42\frac{1}{2}$
7/31	$42\frac{1}{2}$
13/37	$42\frac{1}{2}$
19/43	$42\frac{1}{2}$

POST FLIGHT

RADIAL NO.	A(DISC) FT-INCHES	B(GAP) INCHES	C(BAND) INCHES	D(DISC) INCHES	E(BAND) INCHES	F(BAND) INCHES	G(SUSP) FT-INCHES
1	17 - 5 7/8	25 1/2	77 1/4	30 3/8	30-0	30 1/2	95 - 11 1/2
2	17 - 5	25 5/8	77 3/8	1/4	1/4	1/6	10
3	17 - 5 7/8	25 1/2	78 1/4	30-0	3/8	1/8	4 1/2
4	17 - 5	25 5/8	78 1/4	1/2	0	1/4	5 1/2
5	17 - 5 5/8	25 1/2	78 1/2	1/4	3/8	3/8	4 3/4
6	17 - 5 1/4	25 1/2	78 5/8	3/8	1/4	3/8	8
7	17 - 5 3/8	25 3/8	79 1/4	3/8	3/8	3/8	4 1/4
8	17 - 5 7/8	25 1/2	79 1/8	1/4	1/4	5/16	4
9	17 - 5 1/2	25 1/2	78 1/2	1/4	1/4	1/4	5 1/2
10	17 - 5 3/4	25 1/2	78 1/8	1/4	1/4	1/8	6
11	17 - 5 3/4	25 3/8	77 3/8	3/16	5/16	1/4	9 1/4
12	17 - 4 3/4	25 3/8	77 1/8	1/4	3/8	1/4	9 1/2
13	17 - 4 3/4	25 3/8	77 1/8	1/4	5/16	1/4	8
14	17 - 4 1/8	25 5/8	76 1/8	1/4	1/4	3/16	10
15	17 - 4 1/8	25 3/8	77	1/8	1/4	3/8	7
16	17 - 4 1/4	25 3/8	77 1/4	1/8	3/8	1/16	7
17	17 - 5 1/4	25 1/2	77 3/8	3/8	1 1/4	1/4	5 3/4
18	17 - 4 3/8	25 1/2	77 3/16	1/8	1/4	1/4	7 1/4
19	17 - 4 1/2	25 3/8	77 5/8	1/4	1/8	1/8	4
20	17 - 5 5/8	25 1/2	77 1/2	1/4	1/2	1/4	3/4
21	17 - 4 3/8	25 1/4	77 1/4	1/4	0	1/8	2
22	17 - 5 1/4	25 1/8	77 3/8	3/8	5/16	1/4	2 1/2
23	17 - 5 3/4	25 3/8	77 1/2	1/8	1/4	1/4	10
24	17 - 5 1/8	25 1/2	77	3/18	1/4	1/16	10 3/4

POST FLIGHT (CONTINUED)

RADIAL NO.	A(DISC) FT-INCHES	B(GAP) INCHES	C(BAND) INCHES	D(DISC) INCHES	E(BAND) INCHES	F(BAND) INCHES	G(SUSP) FT-INCHES
25	17 - 5 1/8	25 1/2	76 3/4	30 1/4	30 1/4	30 1/2	95 - 1 1/4
26	17 - 4 3/8	25 3/8	76 5/8	1/4	3/8	1/8	3 1/2
27	17 - 5 1/2	25 1/7	76 3/4	1/4	1/4	5/16	3
28	17 - 5	25 1/2	76 1/8	1/2	3/8	1/8	4 1/2
29	17 - 5 1/4	25 1/2	76 3/8	5/16	1/2	1/8	5 3/4
30	17 - 5	25 1/2	76 1/4	0	1/8	1/2	2 3/4
31	17 - 6	25 3/8	76 1/8	1/4	1/2	1/4	5 3/4
32	17 - 6 1/4	25 1/2	76 3/8	5/16	1/8	1/4	4 3/4
33	17 - 6 1/2	25 1/2	76 1/2	3/16	1/4	1/2	11
34	17 - 7 1/4	25 1/2	76 1/4	1/4	5/16	3/8	11
35	17 - 7 3/4	25 5/8	76 3/8	5/16	1/2	3/8	9
36	17 - 9 1/4	26-0	75 7/8	1/2	1/4	1/2	10
37	17 - 5 3/4	25 1/2	75 1/2	1/2	1/4	3/4	10 3/4
38	17 - 5 3/4	25 1/2	75 5/8	1/4	1/2	1/2	8
39	17 - 8 1/8	26 3/10	76 3/4	5/16	1/4	3/8	5 1/2
40	17 - 6 3/8	25 1/2	76 1/4	5/16	1/4	3/4	8 3/4
41	17 - 7 3/8	25 5/8	76 5/8	1/4	3/8	1/4	9 1/2
42	17 - 6 1/2	25 1/2	76 1/2	1/4	0	1/4	10 1/4
43	17 - 6 7/8	25 5/8	76 7/8	1/4	1/4	1/4	9
44	17 - 6 1/2	25 1/2	77	0	3/8	1/4	1/2
45	17 - 6	25 5/8	77 1/4	1/8	1/4	5/8	3 1/2
46	17 - 6	25 1/2	77	3/8	1/8	0	5 1/4
47	17 - 6 1/4	25 5/8	77 3/4	3/8	1/4	1/4	3
48	17 - 5 1/2	25 5/8	77 3/8	1/4	1/2	3/8	6

POST FLIGHT(CONTINUED)

BRIDLE LEG	H - INCHES	
S/N 40	$91\frac{1}{4}$	$\frac{3}{4}$
S/N 41	$91\frac{3}{8}$	$\frac{3}{4}$
S/N 42	$91\frac{1}{4}$	$\frac{3}{4}$

VENT DIA.		
RADIAL	J - INCHES	
1/25	$42\frac{7}{8}$	
7/31	$42\frac{7}{8}$	
13/37	$42\frac{1}{4}$	
19/43	43-0	